DIGITAL ACCESS TO SCHOLARSHIP AT HARVARD
DASH.HARVARD.EDU

HARVARD LIBRARY
Office for Scholarly Communication

Identification and Analysis of a New Tumor and Metastasis Suppressor Gene, RASAL2

Citation

McLaughlin, Sara Koenig. 2013. Identification and Analysis of a New Tumor and Metastasis Suppressor Gene, RASAL2. Doctoral dissertation, Harvard University.

Permanent link

http://nrs.harvard.edu/urn-3:HUL.InstRepos:11156678

Terms of Use

This article was downloaded from Harvard University's DASH repository, and is made available under the terms and conditions applicable to Other Posted Material, as set forth at http://nrs.harvard.edu/urn-3:HUL.InstRepos:dash.current.terms-of-use#LAA

Share Your Story

The Harvard community has made this article openly available.
Please share how this access benefits you. Submit a story .

Accessibility

© 2013 – Sara Koenig McLaughlin
All rights reserved.

Identification and Analysis of a New Tumor and Metastasis Suppressor Gene, *RASAL2*

Abstract

RAS is one of the most commonly mutated genes in human cancer; its aberrant activation drives tumor cell proliferation and survival. However, *RAS* mutations are rare in some cancers, including breast cancer, even though the Ras pathway is hyperactivated, suggesting that alternative mechanisms deregulate Ras signaling in these settings. The RasGAPs are negative regulators of Ras and, as such, are poised to function as tumor suppressors whose loss might contribute to Ras pathway hyperactivation in cancer. However, the RasGAPs remain an understudied family of genes whose role in cancer has not been fully explored. In this Dissertation I identify a previously uncharacterized RasGAP, *RASAL2*, as the newest tumor suppressor in this gene family.

We find reports of *RASAL2* mutations in breast and other cancers, and determine that RASAL2 expression is lost or suppressed in an even higher fraction of breast cancer cell lines and tumors. We find that RASAL2 functions to suppress transformation and that its inactivation promotes transformation. Further, we determine that RASAL2 inactivation also promotes cell migration, invasion, and tumor progression, suggesting distinct roles for RASAL2 inactivation in tumor formation and progression. To study RASAL2 *in vivo*, we generate a *Rasal2* mutant mouse model. We cross *Rasal2* mutant mice to a breast cancer-prone strain and discover that in this context *Rasal2* loss potently increases metastasis. Additionally, we cross *Rasal2* mutant mice into a broad tumor-prone background, and find increased tumorigenesis and widespread metastasis in various tissues. Together these findings reveal RASAL2 as a tumor and metastasis suppressor.

We explore mechanisms of RASAL2 inactivation in breast cancer and implicate epigenetic and miRNA-mediated suppression. We find that RASAL2 inactivation cooperates

with estrogen to drive proliferation of estrogen receptor-positive breast cancer cell lines. Finally, we discover that the RasGAPs RASAL2 and DAB2IP interact, suggesting that RasGAPs may act in concert.

In summary we have identified a new tumor suppressor in the RasGAP gene family, elucidated the biological consequences of its inactivation, and explored its regulation and function. We believe that these studies highlight the importance of RasGAPs as tumor suppressors and open exciting avenues for future exploration.

Table of Contents

List of Figures

List of Tables

Acknowledgements

I first would like to thank my advisor, Karen Cichowski. Karen welcomed me into her laboratory and enabled the transition to her laboratory and the field of cancer biology to be smooth. I truly appreciate how deeply Karen cared about me as a student and as a person. She taught me to think and write as a scientist, was a great listener, and was a lot of fun. I am grateful that I ended up in her laboratory and had the privilege of spending five years learning from her and working with her. I also am thankful for Karen's full support of my decision to go to medical school.

I also would like to thank the Cichowski laboratory members whom I had the privilege of getting to know. You helped me grow scientifically, were incredibly collaborative and supportive, and became some of my closest friends. In particular I would like to thank Pablo Hollstein and Scott Jones for welcoming me into the laboratory, Junxia Min for scientific training, Jody Fromm and Masha Enos for being dear, supportive friends, and Clare Malone and Naomi Olsen for being superb rotation supervisees and becoming wonderful colleagues and friends. Lastly I would like to thank Pablo Hollstein, Clare Malone, Masha Enos, Becky Lock, Naomi Olsen, and Abigail Miller for critical reading of this Dissertation.

I would like to thank my Dissertation Advisory Committee, Drs. Steve Elledge, Carla Kim, Sandra McAllister, and Karl Münger, for excellent scientific guidance, and my Dissertation Defense Committee, Drs. Phillip Hinds, Andrea McClatchey, Karl Münger, and Alex Toker, for reviewing this Dissertation and carrying out my defense.

I would like to thank my husband John, who understands me better than anybody and who provided critical support throughout my time as a graduate student. As I learned about science, cancer biology, and myself, we in parallel grew up as adults and as a couple while greatly enjoying our time in Boston among amazing, educated, interesting people.

I also would like to thank my family, in particular my parents, my brother, and my in-laws, each of whom added much love, support, and fun to my life during graduate school. I am

particularly lucky that my father is a scientist and provided me not only with parental support but also with scientific guidance.

I would like to thank my many friends who supported me, cared about me, and were interested in my research, in particular Rachel Otto and Erin Tush McArdle, whose friendships are invaluable to me. I would like to thank Christine DeGennaro for countless walks to the New Research Building and discussions of research and life. I would like to thank Jennifer Lester and The Seraphim Singers for becoming a close family and adding healing, energizing, glorious music making to my life. And I would like to thank BodyScapes Fitness, in particular Dave Bergeron and Leoni Epiphaniou, for making the gym a place I felt at home and a place to which I could escape daily to get exercise and clear my mind.

I would like to thank Sarah Gaw for use of the scanner at the School of the Museum of Fine Arts, and Phillip Schwartz at Protein Biotechnologies for detailed discussions and supporting our proposal to collaborate. Finally, I would like to thank Nancy Andrews and the members of her laboratory who taught me the first things I learned in graduate school. The part of my research that we published is presented here as Appendix C.

Chapter 1

Introduction

This Dissertation focuses on the previously uncharacterized RasGAP gene, *RASAL2*, and how its inactivation promotes the Ras pathway and cancer. In this Introduction Chapter I discuss the Ras pathway in normal biology and cancer to provide context for my studies. My research primarily addresses *RASAL2* inactivation in breast cancer tumorigenesis and metastasis; therefore in this Chapter I also provide background on breast cancer and metastasis. Lastly, I discuss p53 and epigenetics, two important cancer-related topics relevant to the work in this Dissertation.

THE RAS PATHWAY

The Ras pathway is an essential cell signaling pathway through which cells respond to external stimuli and appropriately control growth and proliferation. There are over thirty *RAS* genes, which belong to the ~150-member Ras superfamily of small GTPases[1]. However, in this Dissertation I limit the discussion to the three main *RAS* genes with roles in cancer (which also were the founding members of the superfamily): *KRAS*, *HRAS*, and *NRAS*. Although initially identified for their transforming properties when mutated[2-6], it is now clear that *K*-, *H*-, and *N*-*RAS* have widespread roles in normal development, particularly in controlling cell growth, proliferation, and differentiation[7]. Interestingly, mouse modeling and cell culture studies, as well as differences among the Ras proteins, including expression pattern, subcellular localization, post-translational modification, and protein structure, support the notion that K-, H-, and N-Ras have both overlapping and distinct functions in normal biology[8-11].

Regulation of Ras activity

The Ras GTPases cycle between GTP-bound and GDP-bound states (Figure 1-1). When bound to GTP, Ras adopts an active conformation and binds downstream effector proteins with high affinity[12]. When bound to GDP, Ras is inactive; thus, Ras functions as a molecular switch that cycles between on and off states. Two families of regulatory proteins

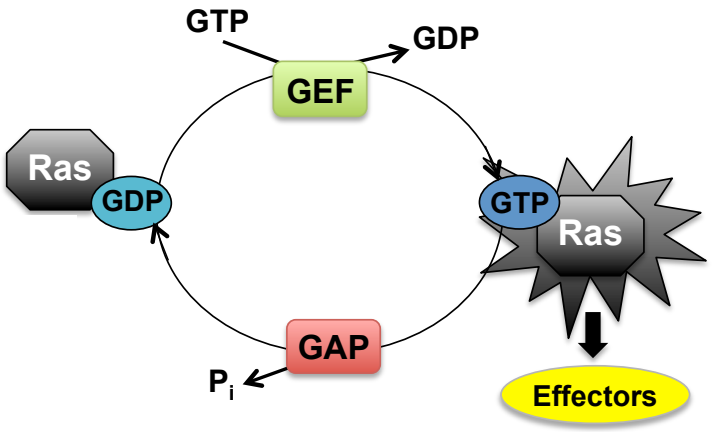

Figure 1-1: RasGTP – RasGDP cycle
Ras is active and signals to downstream effectors when GTP-bound. RasGAPs catalyze the hydrolysis of RasGTP to RasGDP, thereby inactivating Ras. RasGEFs catalyze the exchange of GDP for GTP, activating Ras. Figure adapted from[13].

accelerate the otherwise slow conversion of Ras between on and off states and, importantly, play central roles in controlling levels and duration of Ras activity (Figure 1-1): Ras proteins have intrinsic GTPase activity such that GTP bound to Ras will be hydrolyzed to GDP, and Ras inactivated[14]. In the cell, Ras GTPase activating proteins (RasGAPs) catalyze the hydrolysis of RasGTP, greatly accelerating this process[15,16]. By promoting GTP hydrolysis, RasGAPs promote Ras inactivation and thus are direct negative regulators of Ras signaling. The RasGAPs are a main focus of this Dissertation and will be discussed in detail below. Inactive Ras becomes activated when GTP replaces GDP. Ras guanine nucleotide exchange factors (RasGEFs) catalyze this intrinsically slow process by promoting the release of GDP from inactive Ras[17,18]. The cellular concentration of GTP is approximately 10-fold higher than that of cellular GDP, thus, following GDP release, Ras proteins bind GTP and become activated. By promoting the exchange of GDP for GTP, RasGEFs act as direct positive regulators of Ras signaling.

RasGEFs provide one link from external stimuli to Ras. Following growth factor /mitogen binding of receptors such as the EGFR family of receptor tyrosine kinases, receptor tyrosine kinases (RTKs) dimerize, trans- or auto-phosphorylate their intracellular tails, and become

activated[19]. Activated RTKs serve as docking sites for a number of adaptor proteins, including GRB2. These adaptor proteins recruit RasGEFs, such as SOS1, which then activate Ras by catalyzing the exchange of GDP for GTP, as described above[20-24]. Distinct RTKs utilize unique combinations of adaptor proteins and RasGEFs, thus activation of distinct RTKs can differentially drive the Ras pathway. The RasGAP neurofibromin (discussed below) provides another link between external stimuli and Ras. Growth factor or serum treatment triggers proteasomal degradation of neurofibromin. Neurofibromin destruction is required for maximal Ras activation following growth factor or serum treatment and controls the duration of the Ras signal, as neurofibromin re-expression is required to appropriately attenuate Ras pathway activation[25].

Ras downstream effector pathways

Ras mediates its effects via activation of downstream signaling pathways (Figure 1-2). A number of Ras effector pathways have been identified, via functional studies and the identification of a Ras binding domain in direct Ras effector proteins. The first identified Ras effector pathway was the mitogen-activated protein kinase (MAPK) pathway[26-29]. RasGTP activates the MAPK pathway by recruiting, binding, and promoting the activation of Raf (there are three human Raf proteins, ARaf, BRaf, and Raf1, encoded by *ARAF*, *BRAF*, and *RAF1*). Raf is a serine/threonine kinase that upon activation triggers a canonical kinase phosphorylation cascade. Raf phosphorylates and activates MEK serine/threonine kinase (encoded by *MAP2K1*, mitogen-activated protein kinase kinase 1), which in turn phosphorylates and activates ERK1 and 2 (extracellular signal-regulated kinases 1 and 2, encoded by *MAPK1* and 2, mitogen-activated protein kinases 1 and 2)[30]. ERK in turn activates a myriad of nuclear and cytosolic proteins from transcription factors (including STAT3, ETS family transcription factors, and c-JUN) and kinases (including RSK, MSK and MNK family kinases) to cytoskeletal proteins and receptors, and, via these effectors, drives cell cycle progression and cell survival[7,31]. Notably,

data suggest that the Raf/MEK/ERK pathway plays a key role in Ras-driven tumorigenesis, as discussed below.

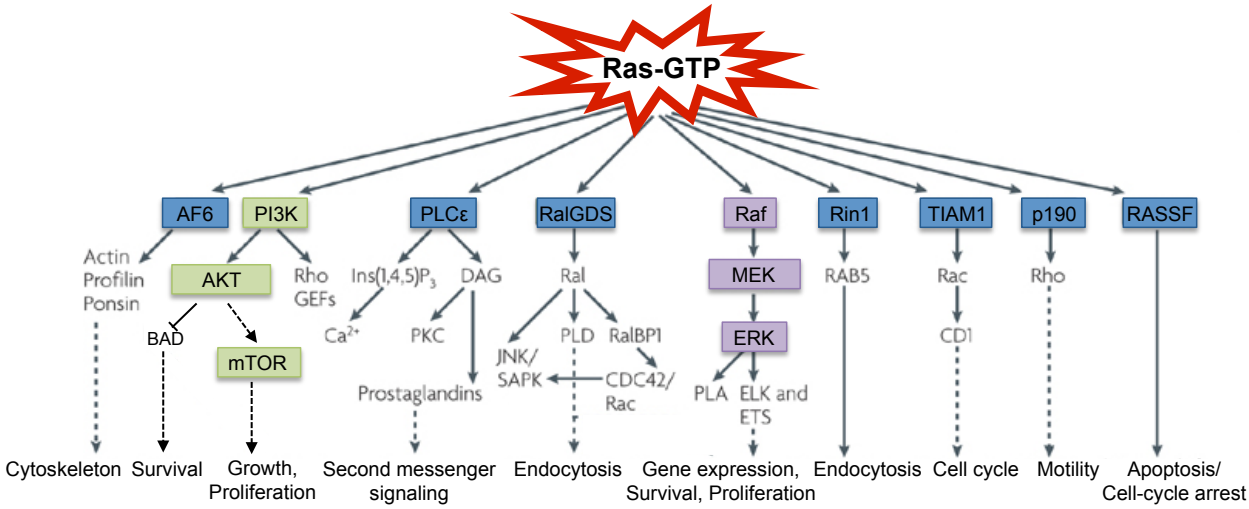

Figure 1-2: Ras effector pathways
When GTP-bound, Ras binds effector proteins and triggers numerous downstream pathways, as shown. PI3K and MAPK pathways are indicated in green and purple, respectively. Figure adapted from[32].

Ras also drives the phosphatidylinositol 3-kinase (PI3K) pathway (Figure 1-2), through direct binding to the p110α catalytic subunit of PI3K (class IA PI3Ks are composed of a catalytic subunit, p110, and a regulatory subunit, p85)[33]. PI3K drives signaling through the lipid second messenger phosphatidylinositol-3,4,5-triphosphate (PIP_3), which is generated from phosphatidylinositol-4,5-bisphosphate (PIP_2) through PI3K phosphorylation. The phosphatase PTEN can dephosphorylate PIP_3 and convert it back to PIP_2. As discussed below, both PI3K activation and PTEN loss commonly occur in cancer. PIP_3 recruits and promotes activation of the AKT serine/threonine kinases[34]. Among a number of activities, active AKT inhibits the tumor suppressor proteins TSC2 and TSC1. This leads to an accumulation of active Rheb (RhebGTP); RhebGTP activates mTOR, which in turn promotes translation of a set of proteins through two major effectors, ribosomal protein S6 (following phosphorylation by S6 kinase), and eukaryotic initiation factor 4E (via inhibition of 4EBP1)[35,36]. PI3K-AKT-mTOR signaling promotes cell growth and proliferation. PI3K-AKT signaling also regulates cell survival via AKT-

mediated inhibition of the pro-apoptotic protein BAD[37,38]. Ras-independent mechanisms also can activate PI3K signaling: activated receptor tyrosine kinases promote PI3K signaling via direct binding of the p85 regulatory subunit of PI3K and/or via adaptor proteins[36]. Further, it should be noted that both the Raf/MEK/ERK and PI3K/AKT pathways are immensely complex with multiple inputs, outputs, and feedback loops[35,39]. Only the basic components of the pathways as they relate to Ras-driven signaling are described here.

RasGTP also has been shown to stimulate additional effector pathways, including but not limited to the RalGDS, TIAM1/Rac, and PLCε pathways (Figure 1-2)[32,40-45]. The effects of Ras activation on vesicle trafficking, cytoskeletal organization, and calcium signaling have been attributed to activation of these pathways[7]. However, MAPK and PI3K, and to a lesser extent RalGDS, are thought to be the pathways that drive cancer, as discussed in the following section.

THE RAS PATHWAY IN CANCER

RAS is one of the most commonly mutated genes in human cancer; overall, *RAS* mutations are found in approximately 30% of human tumors[46]. Each of the predominant three *RAS* isoforms is commonly mutated in a number of tumor types, although the pattern of mutation varies between the *RAS* genes (Table 1-1). Overall *KRAS* mutations are most common (approximately 22%), followed by *NRAS* (8%), and *HRAS* (3%)[46]. Oncogenic *RAS* mutations prevent GTP hydrolysis, thus fixing Ras in its active conformation[47-51]. Most oncogenic *RAS* mutations involve amino acids 12, 13, or 61[52-54]. Amplification of wildtype *RAS* genes also occurs in some tumor types, including in breast and lung cancers[16,55-57]. Oncogenic *RAS* transforms immortalized cells in culture[58]. More recently, myriad mouse modeling studies have confirmed the potent oncogenicity of mutant *RAS*, both in tumorigenesis overall and in specific tumor types via conditional mouse models[59].

Table 1-1: Frequency of *RAS* mutations in human cancer

Tissue	*HRAS*	*KRAS*	*NRAS*
Adrenal gland	0.7%	0.5%	5.3%
Autonomic ganglia	0%	0.9%	1.9%
Biliary tract	0%	28.0%	2.4%
Bone	1.1%	0.6%	0.4%
Breast	0.5%	1.7%	0.9%
Central nervous system	0%	0.8%	0.6%
Cervix	7.6%	7.2%	1.3%
Endometrium	0.5%	14.9%	2.2%
Eye	0%	2.0%	1.2%
Haematopoietic and lymphoid tissue	0.3%	4.9%	9.9%
Kidney	0.1%	0.6%	0.4%
Large intestine	0.1%	34.2%	3.4%
Liver	0.3%	4.3%	2.1%
Lung	0.6%	16.2%	0.9%
Oesophagus	0.8%	2.5%	0%
Ovary	0%	12.4%	0.7%
Pancreas	0%	56.7%	0.8%
Pituitary	3.3%	0%	0%
Prostate	3.8%	5.9%	1.0%
Salivary gland	14.0%	3.5%	0%
Skin	6.4%	2.0%	15.5%
Small Intestine	0.0%	17.7%	0%
Soft tissue	4.3%	5.0%	4.2%
Stomach	2.1%	6.3%	1.0%
Testis	3.9%	3.8%	2.8%
Thymus	2.2%	2.2%	0%
Thyroid	3.7%	2.1%	6.4%
Upper aerodigestive tract	8.1%	2.5%	2.7%
Urinary tract	9.1%	4.7%	1.2%

Data from Catalogue of Somatic Mutations in Cancer (COSMIC) database[46].

The Ras pathway also is aberrantly activated in cancer via misregulation or mutation of upstream regulators of Ras (Table 1-2), such as receptor tyrosine kinases, which promote growth factor-independent Ras pathway activation and tumorigenesis. For example, the ERBB family receptor tyrosine kinase *EGFR* is frequently mutated or overexpressed in non-small cell lung cancer and most other epithelial cancers[60-64]. Hyperactivated EGFR stimulates Ras, MAPK,

and PI3K pathways; these pathways contribute to EGFR-driven tumorigenesis, as evidenced by the anti-tumor effects MAPK and PI3K inhibition has on these tumors[63]. Additionally, the ERBB family receptor tyrosine kinase *HER2 (ERBB2)* is frequently amplified in, and promotes, breast cancer[65], as will be discussed in more detail below. Mutations in *PDGFR* and *KIT* receptor tyrosine kinases also commonly occur in gastrointestinal stromal tumors (GISTs)[66]. Clearly, RTK activation contributes to Ras pathway activation across many tumor types; notably, many therapeutic strategies aim to target RTKs and/or the PI3K and MAPK effector pathways in these tumors[67].

Table 1-2: Ras pathway aberrations in human cancer

Gene	Aberration	Cancer Types
Receptor Tyrosine Kinases upstream of Ras		
HER2	Amplification	Breast
EGFR	Overexpression Mutation	most carcinomas GBM, NSCLC
PDGFR	Mutation	GIST
KIT	Mutation	GIST
Ras effector pathway components		
BRAF	Mutation	Melanoma; Colon
PIK3CA	Amplification Mutation	Head & Neck, SCLC, Cervical, Gastric, Esophageal Breast, Colon, Endometrial, GBM, Ovarian
AKT1	Amplification Mutation	Gastric Breast, Colon, SCLC
AKT2	Amplification Mutation	Head & Neck, Pancreatic, Ovarian, Breast Colon
PTEN	Mutation; Deletion; other	Breast, Prostate, Pancreatic, GBM, Melanoma
RasGAPs		
NF1	Mutation; Deletion Degradation	NSCLC, Melanoma, GBM, Neuroblastoma GBM
DAB2IP	Epigenetic Suppression	Prostate

Ras pathway aberrations that commonly occur in human cancer (data from sources indicated in text body).

As direct regulators of Ras, one might hypothesize that RasGEFs and RasGAPs could play oncogenic and tumor suppressive roles in human cancer, respectively. Germline mutations in the RasGEF *SOS1* cause the developmental disorder Noonan syndrome[68,69]. Noonan patients have an increased risk of developing juvenile myelomonocytic leukemia (JMML)[70]; however, to date there is no evidence of mutations in *SOS1* or other RasGEFs in sporadic tumors. In contrast, expanding evidence supports a role for RasGAPs as tumor suppressors inactivated in sporadic cancer, as discussed below.

Aberrant activation of Ras effector pathways, in particular the MAPK and PI3K pathways, frequently drives human cancer as well (Table 1-2). Activating *BRAF* mutations are found in approximately 60% of melanomas as well as in colorectal and other tumor types[71]. Amplification or mutation of *PIK3CA* (which encodes the p110α catalytic subunit of PI3K) and *AKT1* and *2* also occur in a variety of human cancers[46,72-82]. Further, *PTEN* is mutated, deleted, or inactivated via other mechanisms at a very high rate in human cancer[46,83-88]; in fact, after *p53*, *PTEN* is the most commonly inactivated human tumor suppressor gene[7]. Together with mouse model and cell culture functional studies (described elsewhere), these findings underscore the importance of the Ras pathway in cancer and emphasize the pro-tumorigenic roles of both the MAPK and PI3K effector pathways. In Chapter 2 of this Dissertation I discuss how Ras, MAPK, and PI3K signaling contribute to breast cancer tumorigenesis and metastasis following inactivation of the RasGAP *RASAL2*.

RAS GTPASE ACTIVATING PROTEINS

Ras GTPase Activating Proteins, or RasGAPs, are direct negative regulators of Ras[16]. There are fourteen RasGAPs in the human genome; each contains a region of RasGAP domain sequence homology[89]. RasGAPs catalyze the hydrolysis of RasGTP to RasGDP by increasing Ras's intrinsic GTPase activity 10^5-fold[15,90]. Structural analysis of the GAP domain (of p120RasGAP) bound to Ras revealed that a highly conserved arginine residue in the GAP

domain forms an arginine finger that interacts with Ras side-chain II. Through this interaction RasGAPs stabilize the GTP hydrolysis transition state and catalyze the reaction[91]. Notably, oncogenic mutations in *RAS* (such as at Glycine 12 and Glutamine 61) prevent RasGAP stabilization of the GTP hydrolysis reaction transition state[91]. These findings explain why RasGAPs are ineffective against mutant Ras (when Trahey and McCormick discovered p120RasGAP they noticed but could not explain how p120RasGAP affected the activity of wildtype but not mutant Ras[16]), and highlight the critical role that RasGAPs normally assume in attenuating Ras signaling.

It should be noted that the RasGAPs are a part of a larger group of GAPs for the Ras superfamily of small GTPase proteins. Nearly 200 proteins contain GAP domains and most GAP domain containing proteins likely possess catalytic activity[92]. The large number of GAP proteins in the human genome further emphasizes the importance of this class of regulatory proteins[92].

The fourteen human RasGAPs all contain a GAP homology domain but otherwise diverge significantly (Figure 1-3). The RasGAPs can be divided into subfamilies, grouping those with more similar overall homology and domain architecture. I will now discuss each RasGAP in turn, highlighting information that has informed our studies of the RasGAP *RASAL2*, which is the focus of this Dissertation.

NF1

NF1 is one of the most well characterized RasGAP genes, because germline loss of *NF1* causes an inherited cancer predisposition syndrome, as discussed below. The protein product of *NF1*, neurofibromin, plays an important role in normal Ras pathway regulation of cell cycle progression: growth factor stimulation triggers ubiquitin-mediated proteasomal degradation of neurofibromin, which leads to increased levels of RasGTP and drives entry into the G1 phase of the cell cycle[25]. *NF1* is an extremely large gene, comprising 60 exons and

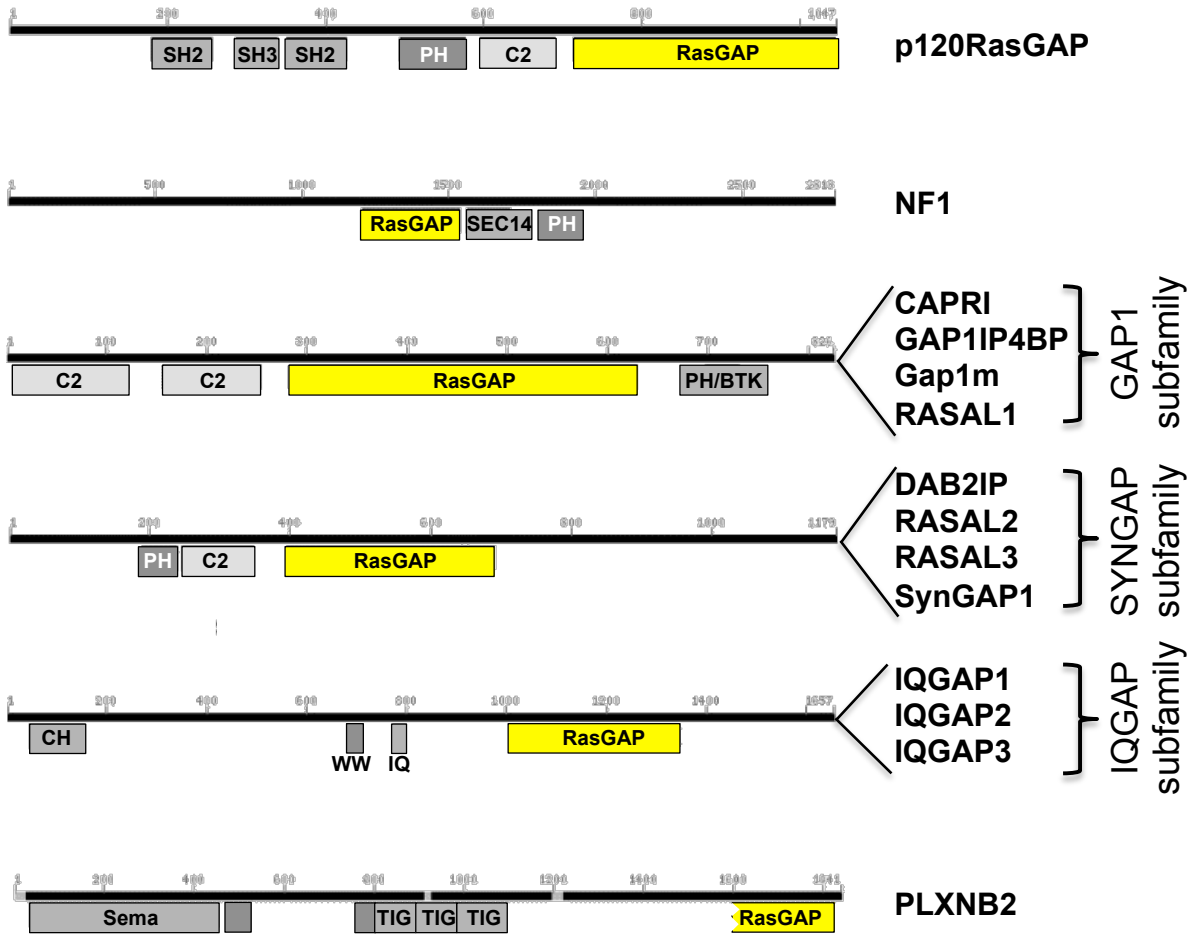

Figure 1-3: The human Ras GTPase Activating Proteins
The domain structures of the 14 human RasGAPs (GTPase Activating Proteins) are shown, grouped by subfamily. p120RasGAP: SH2 and SH3 (Src homology), PH (pleckstrin homology), C2 (C2 phospholipid/Ca^{2+} binding motif), and RasGAP domains. NF1: RasGAP, Sec14, and PH domains. GAP1 family: C2, RasGAP, and PH/BTK (PH/Bruton's Tyrosine Kinase) domains. SYNGAP family: PH, C2, and RasGAP domains. IQGAP family: CH (calponin homology, actin binding), WW (tryptophan), IQ (calmodulin binding), and RasGAP domains. PLXNB2: Sema (semaphorin binding), IPT/TIG (immunoglobulin-like fold), and RasGAP domains. Figure adapted from[89,93].

encoding a 2818-amino acid protein. Thus, the RasGAP domain of *NF1* occupies a small fraction (approximately 10%) of the total gene. *NF1* also contains a Sec14 homology domain, which is thought to facility lipid binding and localization to the cell membrane, and a pleckstrin homology (PH) domain[94]. It is currently unknown whether *NF1* contains additional regulatory or functional domains.

Germline loss of *NF1* via deletion or loss-of-function mutation underlies neurofibromatosis type 1 (NF1)[95,96], a familial tumor predisposition syndrome that affects 1 in 3500 individuals worldwide[97]. NF1 patients develop benign plexiform and dermal neurofibromas as well as malignant peripheral nerve sheath tumors (MPNSTs). MPNSTs are aggressive and generally inoperable as they often involve nerves. Radiation and chemotherapy are minimally effective and, in the absence of other therapeutic options, MPNSTs can become lethal within months. Therefore, much NF1-related research today focuses on finding a successful therapy for MPNSTs. NF1 patients also have an elevated risk of developing astrocytomas, myeloid leukemia, and pheochromocytomas. Additionally, NF1 patients display development abnormalities, including short stature and lower IQ, and develop a range of benign lesions, including café-au-lait spots (hyperpigmentation of the skin) and Lisch nodules (benign lesions of the iris)[97].

Malignant tumors from NF1 patients exhibit loss of heterozygosity of *NF1*, through somatic mutation or deletion, making *NF1* a canonical tumor suppressor gene that adheres to the Knudson's two-hit hypothesis of gene inactivation[98-100]. Consistent with neurofibromin's function as a RasGAP, tumors from NF1 patients have elevated Ras pathway activity, and aberrant Ras activity drives tumorigenesis[101,102]. Downstream of Ras, the PI3K-AKT-mTOR pathway is critical for MPNST growth: using a genetically engineered mouse model of MPNST development (cis deletion of *Nf1* and *Trp53*, which reside on the same chromosome), our laboratory showed that the mTOR inhibitor rapamycin induces a cytostatic response in MPNSTs[102,103]. Recently, work from our laboratory has shown that this cytostatic response can be converted to a cytotoxic response by combining rapamycin with IPI-504, an Hsp90 inhibitor and ER stress-inducing agent[104]. Notably, combined rapamycin and IPI-504 treatment induces tumor shrinkage not only in MPNSTs, but also more broadly among Ras pathway-driven tumor types, including in a *KRAS* mutant lung cancer model[104]. These findings suggest that many lessons learned studying the biology of RasGAP inactivation can be applied more broadly to

Ras-driven tumors, and that RasGAP inactivation provides a useful system in which to study Ras activation in a physiologically and biologically relevant setting.

Interestingly, neurofibromatosis type 1 patient mutations occur not only within the RasGAP domain of *NF1*, including mutation of the arginine finger crucial for GAP activity described above, but also throughout the gene[105,106]. This finding suggests that neurofibromin may have additional non-RasGAP functions, a hypothesis supported by unpublished data from our laboratory. As I discuss below and in Chapter 4 of this Dissertation, we hypothesize that many RasGAPs may have additional functions.

Recently, studies have shown that *NF1* also is inactivated somatically in sporadic cancer, including in melanoma[107-109], glioblastoma[110-112], non-small cell lung cancer[113], and neuroblastoma[114] (Table 1-2). In melanoma, functional studies have further shown that *NF1* loss cooperates with *BRAF* mutation to drive melanomagenesis, demonstrating a causal role for *NF1* loss[107]. We believe that the clear role neurofibromin inactivation plays in sporadic tumorigenesis points to a possible broader role for the RasGAP family as tumor suppressors inactivated in sporadic cancer. Interestingly, in glioblastoma, both mutation of the *NF1* gene and aberrant proteasomal degradation of the protein contribute to *NF1* inactivation[110]. As I discuss in Chapters 3 and 4 of this Dissertation, we hypothesize that multiple, some non-genetic, mechanisms often contribute to RasGAP gene inactivation in sporadic cancer.

DAB2IP

To date, other than *NF1*, the only RasGAP confirmed to be a human tumor suppressor gene is *DAB2IP*. *DAB2IP* falls in the SYNGAP subfamily of RasGAPs along with *SYNGAP1*, *RASAL3,* and *RASAL2*, each of which will be discussed below and the last of which is the focus of this Dissertation. Prior to recent work from our laboratory, there were hints that *DAB2IP* may be inactivated in sporadic cancer and therefore that it might be a tumor suppressor gene. A translocation disrupts *DAB2IP* in acute myeloid leukemia[115]. Additionally, studies suggested

that the *DAB2IP* promoter was hypermethylated in breast, lung, prostate and gastrointestinal cancer cell lines, and limited *in vitro* experiments suggested that the Polycomb group protein EZH2 might target *DAB2IP*, together suggesting that *DAB2IP* could be epigenetically silenced in cancer[116-120]. More recently, mutations in *DAB2IP* have been found in tumors from breast, central nervous system, cervix, endometrium, colon, lung, ovary, pancreas, prostate, and upper aerodigestive tract tissues[46].

A 2010 publication from our laboratory demonstrated a causal role for *DAB2IP* inactivation in prostate cancer tumorigenesis and metastasis[121]. I collaborated with the lead author on this study, and a reprint of this manuscript is included in this Dissertation as Appendix B. The key findings for our understanding of DAB2IP and more generally for RasGAPs in cancer are discussed here. Using an orthotopic xenograft prostate tumor model, our laboratory found that *DAB2IP* inactivation increased prostate cancer tumorigenesis and metastasis. Specifically, we found that, in prostate cancer cells, *DAB2IP* inactivation promoted both the Ras and NF-κB pathways, through two distinct domains. Moreover, we found that DAB2IP loss-mediated Ras activation drove primary tumorigenesis whereas the NF-κB signal was responsible for the metastatic phenotype. Thus, DAB2IP acts as a signaling scaffold and is a potent tumor and metastasis suppressor because of its ability to simultaneously regulate multiple critical signaling pathways. We hypothesize that other RasGAPs, particularly those that function as human tumor suppressors, also may act as signaling scaffolds and control multiple signaling pathways, a concept I will discuss further in Chapter 4 of this Dissertation.

Our laboratory determined that *DAB2IP* is inactivated in prostate cancer via epigenetic silencing, a possibility hinted to by earlier studies[118,120]. The Polycomb group protein EZH2 (discussed below) is overexpressed in prostate cancer[122]. We showed that EZH2 drives prostate cancer tumorigenesis and metastasis, that it suppresses *DAB2IP*, and that EZH2-mediated suppression of *DAB2IP* is important for the oncogenic effects of EZH2 in prostate cancer. These findings are noteworthy because they prove a causal role for EZH2 as a driver of

prostate cancer and because they show that epigenetic silencing of a RasGAP is a key mechanism of prostate tumorigenesis and metastasis. Epigenetic silencing of RasGAPs is a theme I will discuss further in Chapter 3 of this Dissertation. Lastly, our laboratory showed that DAB2IP expression is lost in human tumors, DAB2IP expression decreases with increasing tumor grade, and DAB2IP and EZH2 expression inversely correlate in human prostate cancer, further supporting the conclusion that DAB2IP loss plays a role in human prostate cancer development.

SynGAP1 and RASAL3

SYNGAP1 (Synaptic GAP 1) and *RASAL3* (RAS protein Activator Like 3) are the two RasGAPs that along with *RASAL2* and *DAB2IP* complete the SYNGAP subfamily of RasGAPs. The SYNGAP subfamily is defined by the presence of pleckstrin homology (PH) and C2 phospholipid/Ca^{2+} binding motif (C2) domains preceding the RasGAP domain. SynGAP1 expression is restricted to neurons[123,124]. SynGAP1 function also is restricted to neurons, where it affects synaptic strength and plasticity[125]. SynGAP1 is regulated by Ca^{2+}/calmodulin-dependent protein kinase II[126] and, interestingly, it exhibits both RasGAP and RapGAP activity, the latter of which is dependent on both its C2 and RasGAP domains[127,128]. *Syngap1* mutant mice display a range of behavioral and learning defects[129,130], and human mutation studies have linked *SYNGAP1* to autism-spectrum disorders and mental retardation[131,132]. SynGAP1, however, has not been linked to cancer.

RASAL3 is a newly identified and completely uncharacterized RasGAP. RASAL3 appears to be widely expressed, similar to RASAL2 and DAB2IP and unlike SynGAP1's tissue specific expression pattern. The final RasGAP in this subfamily, *RASAL2*, is the subject of this Dissertation and will be discussed below.

p120RasGAP

p120RasGAP (*RASA1*) was the initial human RasGAP identified[15,16]. N-terminal to its RasGAP domain, p120RasGAP contains SH2 and SH3 domains, which are thought to facilitate receptor tyrosine kinase binding and suggest a scaffolding role for p120RasGAP[133-137], as well as PH and C2 domains. Functional data suggest that p120RasGAP may help to remodel the actin cytoskeleton[138] and affect cell movement[139,140].

Rasa1 (p120RasGAP) null mice are embryonic lethal[141]. Lethality is attributed to vascular defects that result from defective endothelial cell organization. Mutations in *RASA1* have been linked to Parkes-Weber syndrome and capillary and arterial defects, further suggesting an important role for p120RasGAP in endothelial cell function[142-144]. Additionally, a recent publication showed that miRNA-mediated suppression of p120RasGAP in endothelial cells promoted neovascularization in tumors[145]. In epithelial cells, however, there is no evidence that p120RasGAP functions as a tumor suppressor.

RASAL1, CAPRI, Gap1m, and GAP1IP4BP

RASAL1, CAPRI (RASA4), GAP1M (RASA2), and *GAP1IP4BP (RASA3)* comprise the GAP1 family of RasGAPs. Each has tandem C2 domains, a RasGAP domain, and a PH/BTK domain. Interestingly, RASAL1, CAPRI, and GAP1IP4BP are dual-function Ras- and Rap-GAPs[146]. Furthermore, a recent study discovered that CAPRI can exist as a monomer or a homodimer and that its dimerization state determines whether it acts as a RasGAP or RapGAP[147]. RasGAP dimerization is a focus of Chapter 3 of this Dissertation, in which we study the heterodimerization of the RasGAPs RASAL2 and DAB2IP. CAPRI and RASAL1 are calcium-responsive RasGAPs, via their C2 domains (Gap1m and GAP1IP4BP are not)[148,149].

There have been suggestions in the literature that CAPRI and RASAL1 could potentially function as tumor suppressors, although to date no evidence shows that inactivation of these RasGAPs drives sporadic tumorigenesis. A 2005 *in vitro* RNAi screen for tumor suppressor genes that could transform immortalized mammary epithelial cells identified *CAPRI* as a

candidate tumor suppressor[150]. However, although *Rasa4* (Capri) knockout mice display immunological defects, no cancer related phenotype has been reported[151]. Publicly available databases suggest that *CAPRI* is very rarely mutated in sporadic cancer; two non-synonymous missense mutations in *CAPRI* have been reported (in lung and prostate cancer), and they do not reside within a known domain of the protein[46]. A second 2005 RNAi-based tumor suppressor screen (in immortalized human fibroblasts) indirectly identified *RASAL1* as a potential tumor suppressor gene. The transcription factor *PITX1* scored in the screen; follow-up analyses revealed that *RASAL1* is a transcriptional target of *PITX1* and that PITX1 exerts its tumor suppressive roles at least in part via up-regulation of *RASAL1*[152]. More recent studies have found that RASAL1 expression is low in cancer cell lines of a number of tumor types including gastric, colon, and liver cancers, that the *RASAL1* promoter is hypermethylated in tumor samples, and that ectopic RASAL1 exerts some tumor suppressive properties in cancer cell lines[153-156]. Non-synonymous missense mutations in *RASAL1* have been identified at a low frequency (1% overall) in tumors from a number of tissue types including lung, endometrium, and skin[46]. Although far from conclusive evidence identifying *RASAL1* or *CAPRI* inactivation as cancer driving, it seems plausible that future studies could reveal such a role; I return to this possibility in Chapter 4 of this Dissertation.

IQGAP1, 2, and 3

Three human RasGAPs fall into the IQGAP subfamily, *IQGAP1*, *IQGAP2*, and *IQGAP3*. The IQGAPs contain a calponin homology (CH) actin binding domain, a WW domain, and an IQ calmodulin-binding motif. IQGAPs only contain a C-terminal portion of the canonical RasGAP domain; the segment that the IQGAPs contain lacks an arginine finger and thus does not display active RasGAP activity[157,158]. A recent study found that IQGAPs could bind Ras through their truncated RasGAP domain and that acute inactivation of IQGAP3 led to decreased RasGTP levels whereas IQGAP3 expression enhanced MAPK pathway activity[159]. These

findings suggest that IQGAPs may have pro-proliferative effects and imply that IQGAPs could potentially have pro-tumorigenic roles in cancer, but are not likely to function as tumor suppressor genes.

PLXNB2

PLXNB2 contains an N-terminal Sema domain through which it serves as a receptor for semaphorins[160]. The majority of reported PLXNB2 functions relate to its binding of semaphorins, including roles in neuronal and kidney development and function[161-164]. Although *PLXNB2* contains a region of RasGAP domain homology, whether it is a functional RasGAP and what effects this activity might have remain unknown.

Clearly, the RasGAPs remain an understudied family of genes whose role in cancer has not been fully explored. The findings that *NF1* is lost not only in neurofibromatosis type 1, but also in sporadic cancer, and that *DAB2IP* is a prostate cancer tumor and metastasis suppressor, support our hypothesis that other RasGAPs may also function as tumor suppressors in sporadic cancer. In this Dissertation I identify the RasGAP *RASAL2* as the newest tumor suppressor in this gene family. Next, I discuss what was previously known about *RASAL2*.

RASAL2

The focus of this Dissertation is RASAL2 (RAS protein Activator Like 2), also called nGAP. *RASAL2* is in the SYNGAP subfamily of RasGAPs along with *SYNGAP1*, *DAB2IP*, and *RASAL3*, and, until this work, was one of the least studied of all RasGAP genes. The sole publication focused on RASAL2 cloned the gene and indirectly determined the protein to be a functional RasGAP by its ability to rescue a heat-shock phenotype in yeast lacking the yeast RasGAP Ira2[165].

The *RASAL2* gene is located at chromosome 1q24. Notably, the 1q chromosome arm often undergoes copy number gain in breast and other cancers[166,167]. How this copy number gain relates to *RASAL2* inactivation in cancer is an intriguing concept I discuss in Chapter 4 of this Dissertation. There are two main isoforms of human *RASAL2*. Isoform two is slightly longer than isoform one; it differs in its first few exons and hence has an entirely different proximal promoter region than isoform one (Figure 1-4A). Our unpublished findings suggest that isoform two is the predominantly expressed isoform (data not shown). Furthermore, the one main mouse *Rasal2* isoform is orthologous to human isoform two. Interestingly, the promoter of human *RASAL2* isoform two contains a highly CpG dinucleotide rich "CpG island", suggesting that this promoter could be subject to hypermethylation, a concept I address in Chapter 3 of this Dissertation. The *RASAL2* genomic locus also is predicted to contain a RASAL2 antisense RNA (*RASAL2 AS1*), but what biological function it may have remains unexplored (Figure 1-4A).

The *RASAL2* mRNA comprises 18 exons and yields an approximately 150-kilodalton protein (Figure 1-4B). The RASAL2 protein contains pleckstrin homology (PH) and C2 phospholipid/Ca^{2+} binding motif (C2) domains N-terminal to its RasGAP domain (Figure 1-4C). PH domains have been shown to facilitate a wide range of protein-protein interactions including binding phosphotyrosine- and polyproline-containing proteins, as well as interactions with phosphatidylinositol in membranes[168]; however, RASAL2 PH domain function and subcellular localization have not been explored. Additionally, whether the C2 domain of RASAL2 confers calcium responsiveness like is true for some but not all C2 domain containing RasGAPs remains unknown. Prior to this work, RASAL2 GAP activity had not been demonstrated in mammalian cells; however, as mentioned above, ectopic human RASAL2 had been shown to rescue a heat-shock phenotype in yeast lacking a yeast RasGAP, suggesting that RASAL2 is a functional RasGAP[165]. The PH, C2, and RasGAP domains comprise approximately half of the RASAL2 protein; it remains unknown whether RASAL2 contains additional functional domains

or motifs. In Chapter 3 of this Dissertation I identify and study a coiled-coil protein-protein interaction motif at the extreme C-terminus of RASAL2 (Figure 1-4C); this finding suggests that RASAL2 may have additional functions or at minimum additional regulatory domains.

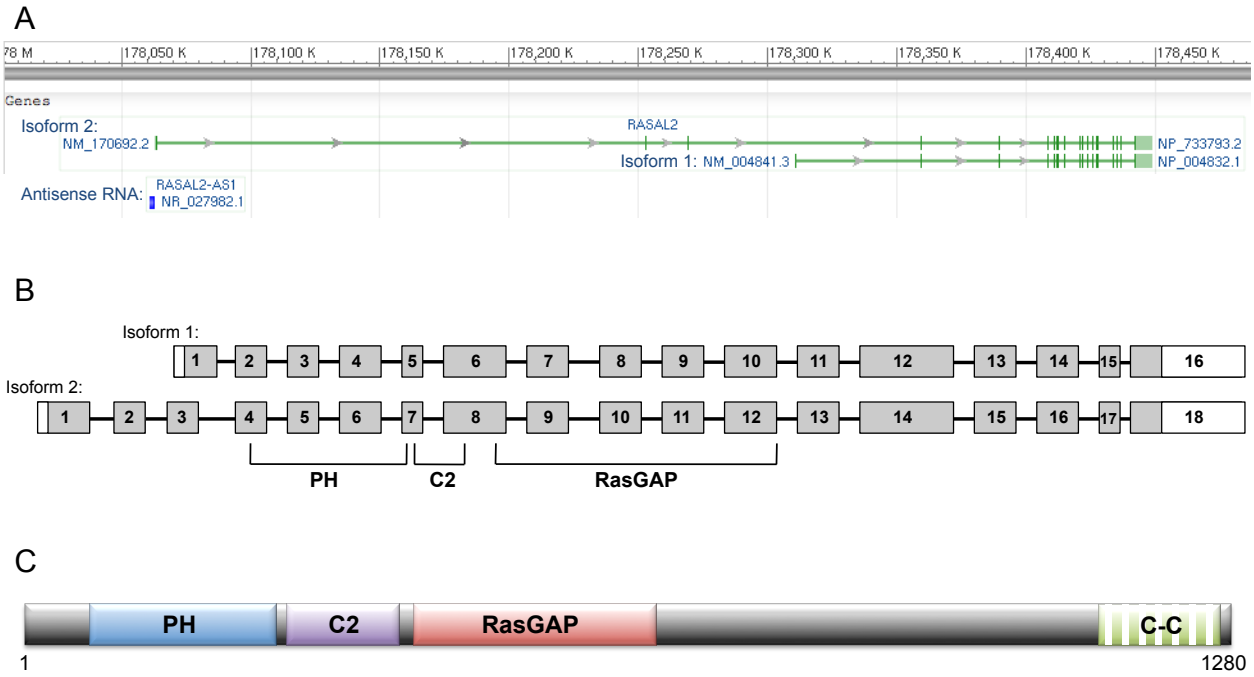

Figure 1-4: RASAL2
(A) *RASAL2* genomic locus on chromosome 1q. *RASAL2* isoforms 1 and 2 and *RASAL2* antisense RNA are indicated. Image from NCBI (http://www.ncbi.nlm.nih.gov/gene/9462).
(B) *RASAL2* mRNA. *RASAL2* isoform 1 (top) and 2 (bottom) mRNAs are 16 and 18 exons long, respectively, with identical final 15 exons. Un-shaded areas represent 5' and 3' UTRs. Exons encoding PH, C2, and RasGAP domains are indicated.
(C) The RASAL2 protein contains pleckstrin homology (PH), C2 phospholipid/Ca^{2+} binding (C2), and RasGAP domains. The putative coiled-coil domain (C-C) discussed in Chapters 1 and 3 of this Dissertation also is indicated. The 1280-amino acid long isoform 2 is shown (isoform 1 contains the same domains but is 1139 amino acids long).

RASAL2 is expressed in most tissues and developmental stages, indicating that it may function in multiple tissue types, unlike *SYNGAP1*, whose expression and function are restricted to neuronal tissues. A few publications have identified potential RASAL2-interacting proteins. One study searching for protein partners of NF-κB family members found RASAL2 to co-immunoprecipitate with the inhibitor of NF-κB, IκB-β, in HEK293 cells[169]. Additionally, a study of

14-3-3-binding proteins reported that RASAL2 interacts with 14-3-3 γ in HEK293 cells[170]. However, the validity and biological significance of these interactions remain unknown. Nevertheless, these putative interactions imply potential additional functions for RASAL2, a concept addressed in Chapter 4 of this Dissertation.

In summary, until the work presented in this Dissertation, *RASAL2* was a completely uncharacterized RasGAP gene with no link to human cancer. In the following chapters I present our findings, which show that *RASAL2* is a tumor and metastasis suppressor gene in breast and possibly other cancers, and which begin to uncover its biological functions and regulation.

THE MAMMARY GLAND

The mammary gland is the organ responsible for lactation in mammals (the presence of a mammary gland defines mammals and gives the group its name). The human mammary gland consists of a network of ducts that travel from the nipple to terminal ductal lobular units, which, interestingly, are where most breast cancers arise[171,172]. Of note, the mouse mammary gland consists of alveolar buds that form with each estrous cycle instead of terminal ductal lobular units, and contains less fibrous tissue and more adipocytes than the human gland[172]. However, despite these structural differences, data suggest that the mouse and human mammary glands have similar cellular hierarchies and functions, supporting the utility of mouse models of mammary gland development and disease[172].

The mammary gland contains a number of cell types (Figure 1-5A)[172]. Luminal epithelial cells surround mammary gland duct lumen and range from a single layer to a few layers thick, depending on the section of the ductal network. Myoepithelial cells surround the luminal epithelial cells and contract to push milk through the ducts. Finally, a basement membrane of cytoskeletal proteins surrounds the myoepithelial cell layer. Adipocytes, fibroblasts, and macrophages surround the duct. Although their precise location is not fully known, the vast expansion of the duct during puberty and pregnancy, along with other evidence, suggests that

mammary stem cells also reside within the mammary gland[173]. Mammary stem cells are thought to differentiate into the luminal and myoepithelial cell lineages[174]. Exactly what marks these cells remains an issue of debate and investigation. Mammary stem cells are believed to lack expression of estrogen receptor, progesterone receptor, and HER2.

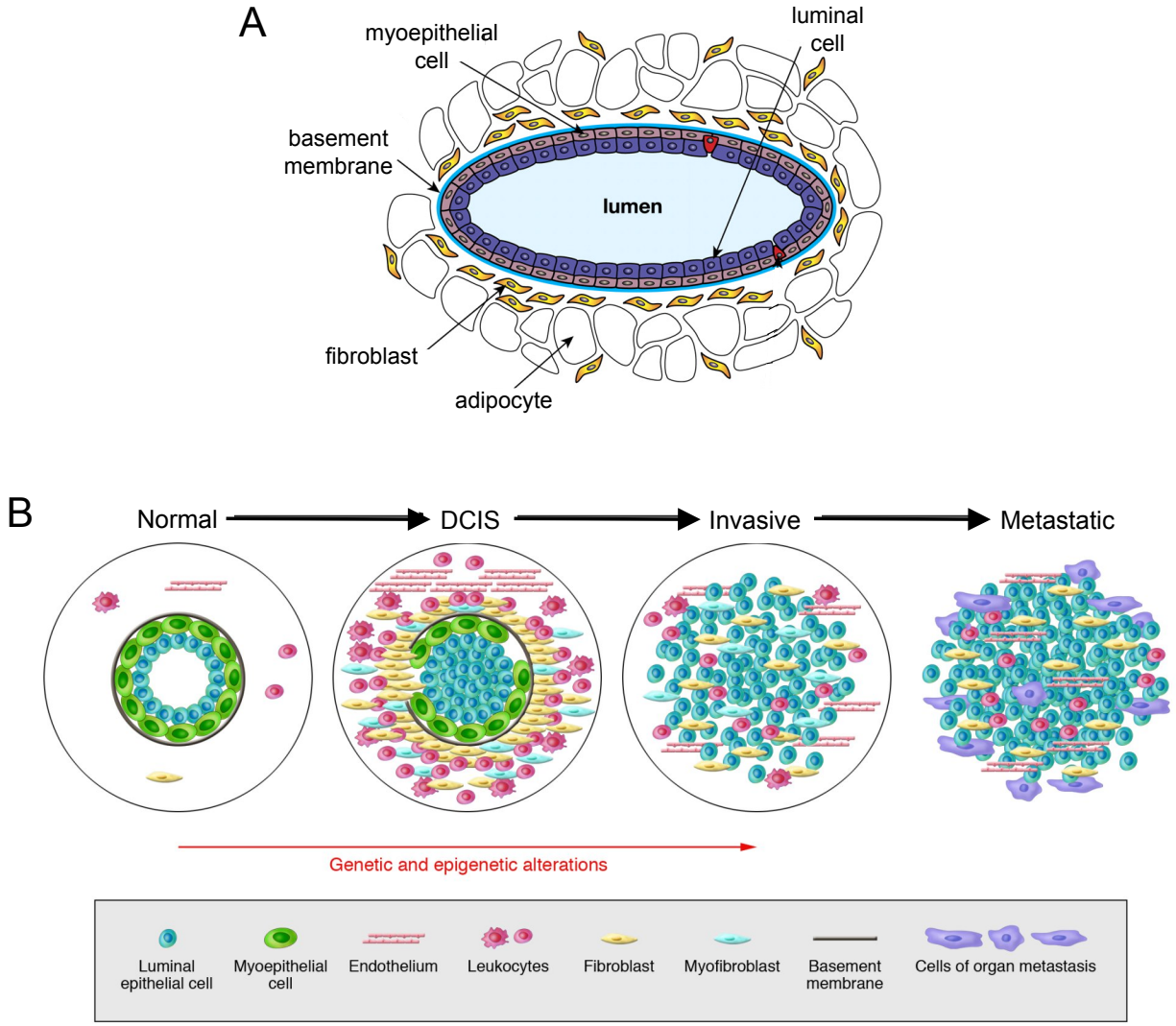

Figure 1-5: The mammary gland in normal biology and malignant progression
(A) The normal mammary gland comprises luminal epithelial cells that line the lumen of the ducts. Myoepithelial cells and basement membrane surround the luminal epithelial cells. The glad also contains adipocytes, fibroblasts, and macrophages (not shown). Figure adapted from[172].
(B) The stages of breast cancer progression: normal duct, ductal carcinoma *in situ* (DCIS), invasive carcinoma, and metastatic disease. Description of stages in text. Figure from[175].

Estrogen and the estrogen receptor

The primary hormone that controls mammary gland structure and function is estrogen, a steroid hormone that is synthesized from cholesterol via a series of enzymatic reactions. Estrogen is critical for sexual and reproductive function, but also plays a significant role elsewhere in the body, including in the cardiovascular, musculoskeletal, and immune systems[176,177].

Estrogen exerts its effects via binding the estrogen receptor (ER). There are two human estrogen receptors, ERα and ERβ, which are encoded by different genes (*ESR1* and *ESR2*), and which data suggest have different activities[178]. ERα is the predominant ER responsible for the canonical effects of estrogen and is the ER known to play a causal role in breast cancer; therefore, in this Dissertation I will not further discuss ERβ. ERα is expressed in reproductive organs as well as in other tissue types including muscle, bone, adrenal gland, pituitary gland, and spleen, as might be expected given its role in many organ systems. Within the mammary gland, ERα is expressed in many luminal mammary epithelial cells and is essential for mammary gland development: *Esr1* (ERα) knockout mice fail to fully develop mammary gland ductal trees[179-181].

ERα is a nuclear hormone receptor that in the absence of ligand resides in the cytoplasm and at the cell membrane[182]. Ligand binding induces a conformation change that leads to ERα dimerization and activation. Activated ERα dimers travel to the nucleus and bind target DNA at estrogen response elements, which typically are in non-promoter (enhancer) genomic regions. ERα regulates thousands of genes, the so-called ERα cistrome, and recruits a variety of co-factors to promote (or repress) transcription in a context-specific manner[183,184]. ERα also affects transcription through its interaction with other DNA-binding transcription factors, including NF-κB, AP1, and SP1[185]. ERα-driven transcription promotes cell growth and survival, and ERα-positive cells are dependent on its activity for these properties.

In addition to its canonical activity as a ligand-activated transcription factor, ERα can be activated in a ligand-independent manner: activated ERK and AKT have been shown to phosphorylate and activate ERα, leading to ERα-driven transcription[186-188]. Additionally, within minutes of estrogen stimulation, ERα elicits rapid "non-genomic" effects. These effects include activation of receptor tyrosine kinases (HER2, EGFR, IGF1R, SRC), eNOS, MAPK, and PI3K, which drive additional transcriptional programs[189-194]. The crosstalk between ERα and the MAPK and PI3K pathways is something I will discuss further in Chapters 3 and 4 of this Dissertation.

BREAST CANCER

Breast cancer is the most common cancer in women both worldwide and in the United States, where there were approximately 230,000 new cases in 2012 and 40,000 deaths[195]. Individuals with family members afflicted by the disease have an elevated risk, suggesting a genetic component. Mutations in the breast cancer predisposition genes *BRCA1, BRCA2*, and *TP53* account for less than one quarter of this elevated risk, pointing to additional contributions from other genes and pathways[175].

Breast cancer develops through a series of distinct stages, beginning with pre-malignant atypical ductal hyperplasia, or aberrant proliferation of cells in the mammary duct (Figure 1-5B)[175]. The first malignant stage of breast cancer is ductal carcinoma *in situ* (DCIS), which is characterized by ducts filled with abnormal-looking cells, but an intact myoepithelial layer and basement membrane. Loss of the myoepithelial layer and basement membrane marks and is thought to contribute to progression from DCIS to invasive carcinoma. Tumor cells that invade the stroma and travel to metastatic sites yield the most advanced stage, metastatic disease.

Breast cancer is a heterogeneous disease, both in terms of molecular underpinnings and clinical outcome. Histopathologically, breast cancers can be divided into a number of types,

including invasive ductal, invasive lobular, cribriform, mucinous, and medullary carcinomas[196]. Approximately 80% of tumors are invasive ductal carcinomas (IDC), a category comprised of tumors not otherwise specified to another histopathological group[196]. Therefore, it is not surprising that IDCs themselves are heterogeneous. Beginning in the early 2000s, a number of groups performed microarray analyses of primary IDCs[197-202]. Hierarchical clustering of primary tumor expression profiles revealed four major IDC subtypes: luminal A, luminal B, HER2-enriched, and basal-like (Table 1-3). The tumor subtypes have distinct prognoses (Figure 1-6)[201,203]; furthermore, our understanding of the biology underlying each subtype has led to separate treatment strategies, thus improving our management of the disease. I will now briefly discuss each subtype.

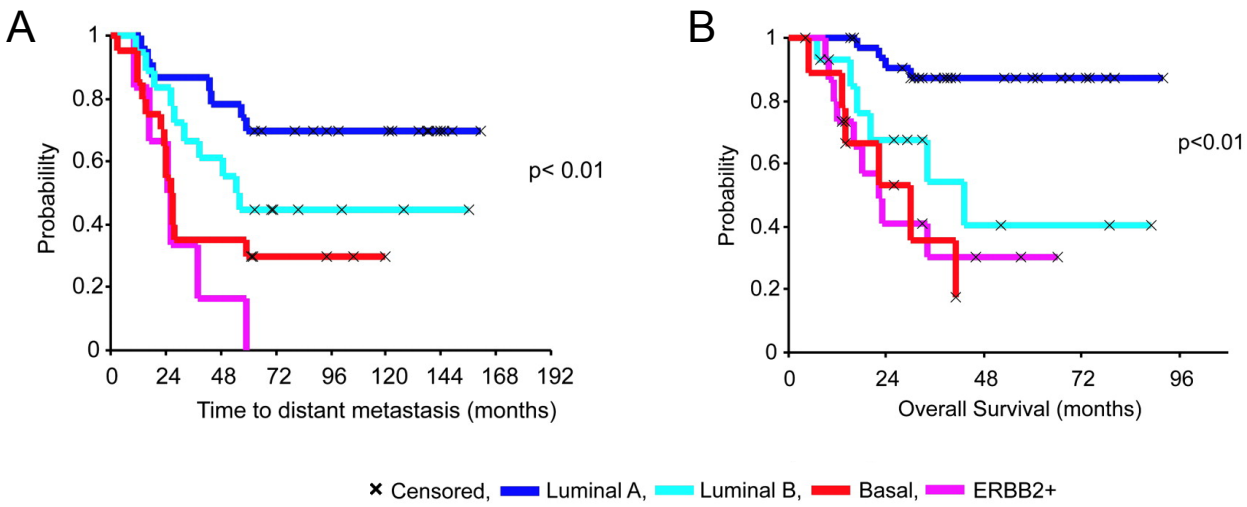

Figure 1-6: Outcomes of breast cancer subtypes
Kaplan-meier curves showing metastasis-free survival (A) and overall survival (B) in two different cohorts of breast cancer patients (A – van't Veer, B – Norway), divided by breast cancer subtype. dark blue: luminal A, light blue: luminal B, pink: HER2-enriched ("ERBB2"), red: basal-like. Breast cancer subtypes predict statistically significant differences in outcome. Figure adapted from[201].

Luminal breast cancers

Hierarchical clustering of primary breast tumor mRNA expression profiles clusters 70% of tumors into the "luminal" subtype, named because many of the highly-expressed genes in these tumors are expressed in normal luminal epithelial cells in the mammary gland[197,198].

Whether luminal tumors derive from normal luminal mammary epithelial cells, however, is a highly debated issue beyond the scope of this Dissertation. Luminal tumors typically express ERα and ERα-driven gene expression is thought to drive the mRNA expression signature that defines this group[197,203,204]. ERα-positive luminal tumors depend on ERα expression for growth. Further, human tumor and molecular biology data indicate that ERα activity plays a causal role in the development of ERα-positive breast tumors: sustained exposure to estrogen is a well-established cause of breast cancer (its carcinogenic properties have been appreciated for over a century), and estrogen exerts its effects via the estrogen receptor, in particular ERα[205]. As in the normal mammary gland, ERα in breast cancer cells regulates many genes[206,207]. Its control of *MYC* (Myc) and *CCND1* (Cyclin D1) in particular, however, are thought to contribute to breast tumorigenesis[183].

Table 1-3: Breast cancer subtypes

Subtype:	**Luminal A**	**Luminal B**	**HER2-enriched**	**Basal-like**
Percent of Cases	50-60%	10-20%	10-20%	10-20%
ER+/HER2- *	**87%**	**82%**	20%	10%
HER2+ *	7%	**15%**	**68%**	2%
TNBC *	2%	1%	9%	**80%**
mRNA expression *	High ER cluster; low proliferation	Lower ER cluster; high proliferation	HER2 amplicon signature; high proliferation	Basal signature; high proliferation
Therapy **	anti-estrogen (tamoxifen, aromatase inhib.)	anti-estrogen + chemo	anti-HER2 (trastuzumab, lapatinib) + chemo	chemo (+ PARP inhib.***)

Incidence, ER and HER2 status (ER-positivity, HER2-overexpression), mRNA signature, and therapeutic strategy for luminal A, luminal B, HER2-enriched, and basal-like breast cancer subtypes. *: Data from[56]. **: Data from[208]. ***: for *BRCA* mutant patients only.

The luminal tumor subtype itself is heterogeneous, and expression profiling sub-divides luminal tumors into A and B groups (Table 1-3). The majority of luminal tumors are type A and overall have the best prognosis of breast cancer subtypes, with 5-year survival rates of over eighty percent[198,201]. Luminal B tumors are more highly proliferative than luminal A tumors and have poorer prognoses[198,201]. They also often overexpress the HER2 receptor tyrosine kinase[203]. HER2-overexpressing luminal B tumors exhibit elevated ERα activity due to crosstalk

between the pathways; HER2 signaling is thought to promote ERα activity at least in part via ERK and AKT downstream of Ras[186-188].

For over a century, because of estrogen's causal role in tumorigenesis, physicians have attempted to treat breast cancers by counteracting the effects of estrogen signaling. Anti-estrogen therapy has progressed from ovary removal in the early 1900s to the 1970s, when physicians began treating patients with drugs that specifically block estrogen action[185]. In fact, anti-estrogen therapy was the first successful targeted therapy for cancer[209]. Today, anti-estrogen therapy remains the standard of care for patients with ERα-positive disease. Most patients are treated with tamoxifen, a Selective Estrogen Receptor Modulator that competitively binds ER and acts as an estrogen antagonist[210]. Aromatase inhibitors, which inhibit the final step in estrogen biosynthesis, are also used in the clinic. Luminal B tumors generally respond less well to anti-estrogen therapies, likely because of HER2-driven ERα pathway activity[211]. Patients with luminal B disease typically receive chemotherapy in addition to anti-estrogen therapy because of the poorer response to anti-ER therapies and because the greater proliferative index leads to a better response to chemotherapy.

Approximately one-third of women treated with the standard tamoxifen regimen relapse with endocrine resistant disease within 15 years[210]. Given that ~70% of breast cancers are ERα-positive, the patients that develop anti-ER-resistant tumors represent nearly one-quarter of all breast cancer cases[185]. Thus, much research has gone into identifying mechanisms of resistance to endocrine therapies, predicting which tumors will become resistant, and determining how to prevent resistance or treat resistant tumors. Acquired resistance to tamoxifen often occurs at long latency, which presents unique challenges for determining mechanisms of resistance in patients[185]. Current proposed mechanisms of acquired resistance fall into a few categories: alternative activation of ERα signaling, activation of receptor tyrosine kinase signaling pathways, and up-regulation of ERα transcriptional targets; each mechanism

would allow cells to promote proliferation and survival in an alternative or additional way than through ERα[185,208,212,213].

HER2-enriched breast cancers

Ten to twenty percent of breast cancers overexpress the receptor tyrosine kinase (RTK) HER2 (also called ERBB2), but are ERα-negative. These tumors group by molecular profile and comprise the "HER2-enriched" or "ERBB2" subtype (Table 1-3)[197,198]. HER2 overexpression not only defines the subtype, but also defines tumor biology, as these tumors are dependent on HER2 signaling. *HER2* amplification or transcriptional up-regulation drives overexpression (*HER2* mutations occur less frequently[214])[65,215]. HER2 is an ERBB family receptor tyrosine kinase. Generally, ligand binding of ERBB family RTKs triggers receptor dimerization, which in turn leads to activation of tyrosine kinase activity, phosphorylation, and downstream signal transduction[216]. Ligands have been identified for the other ERBB RTKs; however, after much searching, researchers concluded that there is no ligand for HER2 and that unlike the other ERBBs, HER2 remains in a conformation open for dimerization[217]. HER2 can dimerize with EGFR, ERBB3, or ERBB4. Activated ERBB dimers trigger many downstream signaling cascades, including the Ras pathway (via the GRB2 adaptor and the RasGEF SOS), the Jak/STAT pathway, and direct activation of PI3K[216,218]. HER2-induced Ras pathway activation in breast cancer will be discussed in more detail below.

HER2 tumors are aggressive and have a poor prognosis[198,201], although recent advances in targeted therapies have significantly improved patient outcomes[219]. Today, the most widely used anti-HER2 therapies are trastuzumab and lapatinib. Trastuzumab is a monoclonal antibody that binds the extracellular domain of HER2[220]; its mechanism of action remains unclear but may involve preventing dimerization with other ERBB family RTKs, antibody-dependent cellular cytotoxicity, or induction of cell cycle arrest or apoptosis, among a number of

proposed mechanisms[221,222]. Lapatinib is a reversible inhibitor of intracellular kinase activity of both HER2 and EGFR[223-225]. Although lapatinib has more potent anti-HER2 effects *in vitro*[226,227], trastuzumab has been more successful *in vivo*[228], perhaps because of the anti-tumor immune response it elicits. Both treatments are typically given in combination with chemotherapy. Many new targeted therapies are in clinical trials or pre-clinical development, including trastuzumab/lapatinib combination therapy (which seems to outperform either drug alone)[229], irreversible EGFR/HER2 inhibitors, and anti-HER2 antibodies tethered with toxins to deliver both the antibody and toxic agent specifically to HER2-overexpressing cells[208,219].

Although HER2 targeted therapies are highly successful, tumors typically relapse. Mechanisms of *de novo* and acquired resistance are thought to fall into a few broad categories[219]. Overexpression or dependence on other ERBB RTKs, including overexpression of EGFR and ERBB3, overexpression of TGFα (an EGFR ligand), and expression of a fragment of HER2 that prevents trastuzumab binding, can cause resistance. Second, increased signaling through pathways downstream of HER2 or other growth-promoting pathways may cause resistance, such as could occur via *PIK3CA* mutation or *PTEN* loss. However, to date there is a lack of patient data showing that this mechanism occurs in human tumors. Third, increased expression of ERα, via lapatinib-induced ERα transcription, can confer resistance (lapatinib treatment causes a decrease in phosphorylated AKT; as a result FOXO3 remains dephosphorylated and in the nucleus where it promotes ERα transcription)[230]. In Chapter 4 of this Dissertation I discuss the hypothesis that *RASAL2* inactivation may contribute to resistance to anti-HER2 and/or anti-estrogen therapies in breast cancer patients.

Basal-like breast cancers

Ten to twenty percent of breast cancers are categorized as “basal-like” because molecular profiling revealed that many highly expressed genes in these tumors are commonly

expressed in normal mammary myoepithelial cells[197,198]. Again, whether basal-like tumors originate from basal cells remains an open question, beyond the scope of this Dissertation[231]. The basal-like subtype of breast cancers is morphologically and clinically heterogeneous[232]. The majority of basal-like tumors lack expression of ERα and the progesterone receptor, and do not overexpress HER2 (Table 1-3). Therefore, they are often called "triple negative". Basal-like tumors also have a high rate of *TP53* mutations[56]. Due to the absence of therapeutic targets, basal-like disease is treated with chemotherapy[203]. Basal-like tumors have a poor prognosis and are highly proliferative. Likely due to their high proliferative index, tumors often respond well to chemotherapy, however, there is also a high rate of early relapse.

Individuals who inherit (or somatically acquire) mutations in the breast cancer predisposition genes *BRCA1* and *BRCA2* develop basal-like tumors[201,233]. A "targeted" therapy now exists for BRCA patients, taking advantage of the fact that BRCA1 and 2 are DNA repair proteins. Patients are given PARP inhibitors; PARP inhibition induces cell death in the context of *BRCA* mutations because double-stranded breaks arise that the cell cannot repair[208,232].

Mouse models of breast cancer

Many genetically engineered mouse models (GEMM) have been generated to study breast cancer[234], including GEMM that overexpress implicated breast cancer oncogenes, such as *MYC* or *HER2*, or lack implicated breast cancer tumor suppressor genes, such as *TP53* or *BRCA1*. These and other models have provided valuable *in vivo* insight into breast tumorigenesis. Many transgenic models utilize the Wap (whey acidic protein) or MMTV (mouse mammary tumor virus) promoters, which drive transcription primarily, but not exclusively, in the mammary gland. Wap and MMTV are hormonally regulated, so transgene expression levels increase with pregnancy and lactation. It also should be noted that different inbred mouse strains have vastly different susceptibilities to breast cancer, from highly prone FVB and BALB/c

strains to highly resistant C57BL6/J[235]. These and other factors significantly alter tumor phenotypes.

Most GEMM of luminal breast cancers are ERα-negative[236]. Recently, however, GEMM of ERα-positive disease have been generated, including mice that ectopically express ERα, aromatase (the enzyme that catalyzes the final step in estrogen biosynthesis), or AIB1 (an ERα co-activator) in the mammary epithelium[237].

HER2 mouse models of breast cancer

The first of many GEMM of *HER2*-driven breast cancer, published in 1988, consisted of MMTV-driven expression of a constitutively active mutant version of the rat *HER2*, called *Neu* (MMTV-*Neu*-NT)[238]. By three months of age, MMTV-*Neu*-NT mice develop multi-focal mammary tumors that involve the entire mammary gland. This model demonstrated the ability of HER2-driven signaling to induce mammary tumors in mice. However, *HER2* is rarely mutated in human breast tumors; typically it is amplified and overexpressed[239]. Therefore, a second *Neu* transgenic model was generated, also using the MMTV promoter, but ectopically expressing wildtype Neu (MMTV-*Neu*)[240]. MMTV-*Neu* animals develop focal mammary tumors at a longer latency (median seven months on an FVB background), and a fraction of tumor-bearing females develop lung metastases. Interestingly, tumors from MMTV-*Neu* mice are luminal-like (but ERα-negative). I utilize this GEMM to explore the role of *Rasal2* loss in breast cancer, as will be discussed in Chapter 2 of this Dissertation.

Models of breast cancer metastasis

Researchers have used a combination of cell culture, xenograft, and genetic mouse models to study mechanisms of breast cancer metastasis. In Chapter 2 of this Dissertation I utilize a xenograft model of progression from DCIS to invasive carcinoma. In this model,

injected cells form DCIS-like tumors that over time progress to invasive carcinoma[241,242]. A number of orthotopic xenograft systems exist in which tumor cells preferentially metastasize to one distal site, such as bone[243,244]. Xenograft models present certain advantages, such as the ease with which genetic manipulations can be made. Genetically engineered mouse models (GEMM) present a rigorous and complementary approach to study the biology of tumor progression and metastasis *in vivo*. Most metastatic breast cancer GEMM solely develop lung metastases[245]. Lymph node metastases also have been reported in a few instances, as well as liver metastases (in mammary-specific *Trp53* mutant mice)[245]. Human breast cancers frequently metastasize to the lung; however, they also commonly metastasize to many other organs (Figure 1-7)[196]. Clearly, the field is lacking GEMM of these metastases. In Chapter 2 of this Dissertation I report a new GEMM of breast cancer that metastasizes to the lung as well as to brain, kidney, gastrointestinal tract, and ovary, all organs to which human tumors metastasize but which to date have not been reported as metastatic sites in breast cancer GEMM.

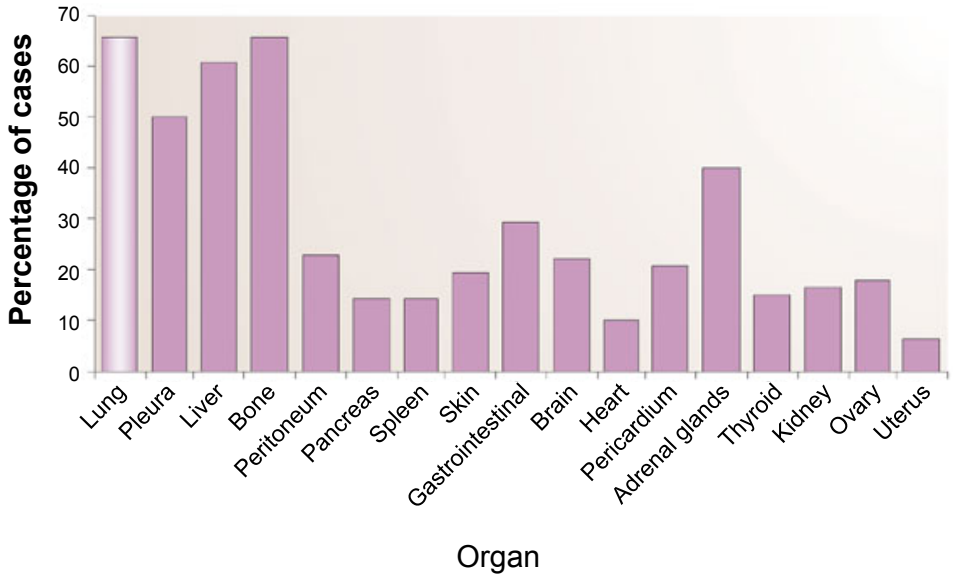

Figure 1-7: Sites of human breast cancer metastasis
Percentage of cases with metastasis to indicated sites. Figure adapted from[196].

MOLECULAR BIOLOGY OF METASTASIS

Cancer metastasis accounts for up to 90% of cancer deaths[246]. Thus, the imperative is high to better understand how metastasis occurs so that it can be prevented and effectively treated. It is now appreciated that metastasis involves a series of steps: tumor cells must invade the local microenvironment, intravasate into the bloodstream or lymphatic system, survive in circulation, extravasate into a distant organ, and survive and grow from a micrometastasis to a frank metastatic lesion[247]. In the field, researchers are working to identify properties of tumor cells that might allow the cells to undergo each of these steps. Researchers have demonstrated that the initial phases of the metastatic process require tumor cells to detach from adjacent cells, acquire motility, and invade through the surrounding stroma to the bloodstream or lymphatic system[247]. In Chapter 2 of this Dissertation I explore the contribution of *RASAL2* inactivation to the acquisition of these pro-metastatic properties in the context of breast cancer metastasis. Primary tumors of different organs preferentially metastasize to different sites; why this occurs is not known. Developing models of metastasis to biologically relevant organs should help to answer this question and may lead to better preventative and therapeutic strategies. As noted above, in Chapter 2 of this Dissertation I also develop a model of breast cancer metastasis that we expect will improve the field's understanding of the disease.

Breast cancer metastasis

Ten to fifteen percent of breast cancer patients develop metastatic disease within three years of diagnoses; many others develop metastases ten or more years later. The median survival of breast cancer patients with metastatic disease is only two to four years; thus there is a clear need to improve our understanding and treatment of metastatic breast cancer[203]. Metastatic breast cancer develops following the progression from ductal carcinoma *in situ* (DCIS) to invasive carcinoma and the invasion of tumor cells through the stroma into circulation[234]. Clinicians first can detect disseminated tumor cells in proximal lymph nodes, the

presence of which predicts increased risk for distant metastases[196]. Breast cancers most often metastasize to lung, bone, and liver, but frequently metastasize to many other sites as well (Figure 1-7)[196].

Breast cancer metastasis research efforts have implicated a number of genes and pathways in the metastatic process. First, the different breast cancer subtypes have different metastatic propensities and outcomes (Figure 1-6); however, it is not fully understood what genes drive these biological differences[203]. Expression profiling studies of primary tumors and paired metastases have identified poor prognosis or metastasis gene signatures[248], although again, whether the identified genes and pathways merely mark or also drive metastatic disease remains unclear. Some functional studies have implicated specific genes or pathways in driving breast cancer metastasis, such as the *MYC* oncogene. Linkage analyses identified *MYC* as a driver of a breast cancer poor prognosis (metastasis) signature, and the authors further found that acute inactivation of *MYC* suppressed invasion and metastasis in MDA-MB-231 cells[249].

Recent data also have pointed to a role for the tumor stroma and systemic microenvironment in progression and metastasis[250,251]. Studies have found genetic alterations in breast cancer myoepithelial cells, including alterations in secreted factors[250]. Functional studies also have shown that alterations in tumor stroma or systemic microenvironment can influence primary tumor progression[242,252,253]. Thus it will be important to continue to study both the primary tumor as well as to consider the role of the local and systemic microenvironments in progression.

The Ras pathway in metastasis

The contribution of the Ras pathway to primary tumor development is well established. In contrast, the role of Ras signaling in tumor progression and metastasis is less clear[254,255]. Oncogenic Ras can confer some pro-metastatic properties on cells *in vitro*: oncogenic Ras has been shown to increase cell motility through alterations in actin organization and polymerization,

up-regulate mesenchymal proteins associated with enhanced migratory potential, and decrease cell-cell adhesion and E-Cadherin expression[256-259]. Oncogenic Ras also has been shown to decrease cell attachment to extracellular matrix, enhance survival of cells detached from the extracellular matrix, and promote expression of extracellular matrix proteases, each of which could help cells invade surrounding normal tissue[260,261]. Further, oncogenic Ras-expressing NIH3T3 fibroblasts metastasize to the lung when injected into the tail vein of nude mice[262]. Many other published studies that discuss the Ras pathway and metastasis focus on the Ras pathway promoting metastasis in combination with other signaling pathways that themselves are better appreciated for roles in metastatic progression, such as the TGF-β pathway, thus making it difficult to draw conclusions about what contribution the Ras pathway itself may be making[263,264].

Focusing on clinical data, one would expect to see enrichment for *RAS* mutations or Ras pathway activity in metastatic tumors, a correlation between Ras pathway activity and increasing tumor stage, and/or the ability of Ras pathway activity to predict outcome, if the Ras pathway contributes to tumor metastasis. However, available clinical data show conflicting results, perhaps because of the methods used to call tumors *RAS* mutant or wildtype[265]. Furthermore, these studies focused on *RAS* mutations, and did not consider other mechanisms of Ras pathway activation. Clearly, many questions remain regarding whether and how the Ras pathway drives metastasis. As discussed below and in Chapter 2 of this Dissertation, our findings suggest that *RASAL2* inactivation activates the Ras pathway and promotes metastasis in breast and other tumor types.

THE RAS PATHWAY IN BREAST CANCER DEVELOPMENT AND METASTASIS

Although *RAS* is one of the most commonly mutated genes across all human cancers, *RAS* is rarely mutated in breast cancer: *RAS* mutations are found in only 3.2% of breast cancers (1.8% *KRAS*, 0.5% *HRAS*, 0.9% *NRAS*) (Table 1-4)[46]. Despite the dearth of *RAS* mutations,

the Ras pathway is frequently hyperactivated in breast cancer. Common activation of the Ras pathway in breast cancer first was noted in the late 1990s, when researchers looked in primary breast tumor samples and found elevated phospho-ERK levels and ERK activity in over 50% of tumors analyzed, as compared to normal mammary tissue[266-268]. Subsequently, von Lintig et al. directly assessed RasGTP levels, as well as phospho-ERK, and found both to be elevated in more than half of the tumor tissues analyzed[269]. More recently, Loboda et al. derived a Ras pathway gene signature (across tumor types) and found that this signature was high in 30% of breast cancer cell lines, of which very few were *RAS* mutant, and that phospho-ERK and phospho-MEK levels correlated with the Ras-ON signature[270].

Table 1-4: Ras pathway aberrations in breast cancer

Gene	Mutation	Amplification/Deletion
KRAS	1.8%	6% Amp*
NRAS	0.9%	
HRAS	0.5%	
NF1	1.8%	
HER2	1.2%	20-30% Amp
EGFR	0.8%	4% Amp*
PIK3CA	25.4%	
PTEN	5.0%	16% Del*
AKT1	4.0%	
PIK3R1	1.5%	
INPP4B	1.0%	17% Del*
BRAF	1.3%	6% Amp*

Common aberrations in *RAS* genes, upstream regulators, and downstream effectors in human breast cancers. Mutation frequencies as reported in the COSMIC database[46]. *: Data from[56]. Note, mutation, amplification, and deletions frequencies vary across breast cancer subtypes; overall frequencies are reported here.

Overexpression of oncogenic *RAS* transforms immortalized mammary epithelial cells and promotes anchorage-independent growth and xenograft tumor formation[271]. Mouse modeling studies further have shown that Ras can drive mammary tumorigenesis: animals with mammary-specific expression of an oncogenic *HRAS* transgene develop mammary tumors[272].

However, as *RAS* mutations are rare in breast cancer, overexpression of a *RAS* oncogene may not be an appropriate model to study Ras pathway driven breast tumorigenesis.

The mechanism of Ras pathway activation in breast cancer remains an unanswered question. Recent genomic studies have begun to identify some genetic alterations in tumors that would be expected to lead to Ras pathway activation or activation of downstream effector pathways (Table 1-4). Wildtype *KRAS* is amplified in approximately 6% of human breast cancers (typically basal-like tumors)[55,56]. Interestingly, *NF1* is mutated in 2% of tumors as well[56]. Amplification of *HER2 (ERBB2)* occurs in 20-30% of breast cancers (*HER2* mutations also are found, albeit infrequently); as a receptor tyrosine kinase upstream of Ras, *HER2* amplification would be expected to promote Ras pathway activity. The mouse model data presented in Chapter 2 of this Dissertation show that *RASAL2* loss and *HER2* gain cooperate in mammary tumorigenesis; in Chapter 4 of this Dissertation I explore the hypothesis that the positive HER2 signal might need loss of the negative RASAL2 signal to fully drive Ras pathway activation.

Downstream of Ras, mutations in MAPK and PI3K pathway members also have been identified in breast cancers (Table 1-4). *PIK3CA* (which encodes PI3K p110α subunit) is mutated in approximately 25% of breast cancers[46]. Mutations in *PTEN*, *AKT1*, *PIK3R1*, and *BRAF* also have been reported, although at frequencies of less than 5%[46,55,273]. Based on our current knowledge, it seems that additional, currently un-described mechanisms likely contribute to Ras pathway activation in breast cancer. In Chapter 2 of this Dissertation I show data supporting the hypothesis that *RASAL2* inactivation is a major mechanism by which the Ras pathway is activated in breast cancer.

The above studies focused on primary tumor development. The connection between the Ras pathway and breast cancer metastasis remains poorly explored and fully unanswered (as mentioned previously, the contribution of Ras to metastasis across tumor types also remains unclear). One of the initial studies that demonstrated MAPK pathway activation in breast tumors also noted trends of higher MAPK activity in lymph node positive breast cancers as compared to

node negative, and of higher MAPK activity in tumors from patients who relapsed versus those who did not[268]. These findings suggest that the Ras pathway may contribute to metastasis. Oncogenic *HRAS*-mediated transformation of an immortalized mammary epithelial cell population promotes lung metastasis from orthotopic xenograft tumors[274]. Additionally, the mammary tumors that develop in MMTV-*Ha-Ras* mice (described above) are locally invasive and occasionally metastasize to lung and liver[272]. However, these studies utilize overexpression of the *HRAS* oncogene, and thus do not recapitulate biologically relevant mechanisms of Ras pathway activation in breast cancer. Looking more generally, in the field, most xenograft studies investigating mechanisms of breast cancer metastasis utilize the metastatic MDA-MB-231 cells[275-277]. These cells harbor an oncogenic *KRAS* mutation; therefore, experiments using these cells are not designed to assess the contribution the Ras pathway may make to the metastatic process. Thus, it remains an open question to what extent the Ras pathway drives breast cancer metastasis. Our findings in Chapter 2 of this Dissertation suggest that Ras pathway activation, as mediated by loss of the RasGAP *RASAL2* in conjunction with *HER2* overexpression, potently drives breast cancer metastasis.

P53

TP53 is a widely-known tumor suppressor gene[278]. Under normal circumstances, ubiquitin-mediated proteasomal degradation keeps cellular levels of p53 protein low. Under conditions of damage or stress, however, the mechanisms that normally keep p53 levels low subside and p53 levels spike. p53 is a transcription factor, and accumulated p53 protein following stress or damage sets off the p53 transcriptional program, which can lead to cell cycle arrest, apoptosis, or senescence, depending on the context[279]. These responses comprise a central component of a cell's natural anti-cancer defense. In fact, p53 is the most commonly altered gene in human cancer. A variety of mechanisms, including mutation, deletion, and aberrant proteasomal degradation, disrupt p53 function in cancer[280-283]. Additionally, germline

mutation of *TP53* causes Li-Fraumeni syndrome, which is characterized by broad, early-onset tumorigenesis[284,285].

Trp53 mutant mice also are broadly tumor prone[286,287]. Genetic strain background alters the tumor phenotype that *Trp53* mutant mice develop[286]. On a mixed B6/129 background, *Trp53* homozygous mutant animals develop mostly lymphomas, but also sarcomas, and die at three to six months of age[287]. *Trp53* heterozygous mutant mice also are broadly tumor prone but their tumor spectrum differs from that of homozygotes[287,288]. p53 heterozygotes develop lymphomas, osteo- and other sarcomas, and, at a low incidence, carcinomas, including of the lung and mammary gland. p53 heterozygotes live ten to 24 months. Notably, their tumors rarely metastasize[289].

RAS mutations and p53 inactivation both occur at a high frequency in human cancers, and are found in overlapping sets of tumors. Numerous mouse models, including *Kras/Trp53*-driven non-small cell lung cancer and pancreatic cancer models[290,291], have demonstrated that Ras and p53 (loss-of-function) cooperate to promote tumorigenesis[59]. In the mouse genome, *Trp53* is located close to *Nf1* on the same chromosome. Cis deletion of *Trp53* and *Nf1* leads to the development of malignant peripheral nerve sheath tumors, the malignant tumor type neurofibromatosis type 1 patients develop (loss of heterozygosity of both *Trp53* and *Nf1* occurs in the tumors) [292,293]. This finding shows that loss of p53 also can cooperate with loss of a RasGAP to drive tumorigenesis. In Chapter 2 of this Dissertation I investigate the broad role of *RASAL2* loss in tumorigenesis and metastasis through the generation and analysis of *Trp53, Rasal2* compound mutant mice.

EPIGENETICS

Epigenetics is the study of heritable changes in gene expression that do not result from alterations in the DNA sequence. Multiple mechanisms of non-genetic gene regulation fall

under the category of epigenetics. However, here I will focus only on those that are relevant to this Dissertation, namely histone modification by Polycomb group proteins and DNA methylation.

Polycomb group protein-mediated gene silencing

Covalent modification of specific histone residues by chromatin modifying enzymes contributes to epigenetic regulation by altering the chromatin state and consequently the ability of transcription factors to access DNA[294,295]. Histone acetyltransferases acetylate lysine residues on histone proteins, a modification that generally opens chromatin, allows transcription factor access, and promotes gene expression. Histone acetyl marks can be removed by histone deacetylases. Additionally, histones lysine residues can be modified by methylation, carried out by histone methyltransferases, which attach one, two, or three methyl groups to a lysine, yielding a mono-, di-, or tri-methylated residue. Depending on the lysine residue, methylation marks can have activating or repressing effects on gene expression. For example, methylation of histone H3 lysines 4 and 36 positively regulates gene expression, whereas di- and tri-methylation of histone H3 lysine 27 has a repressive effect[296]. Histone methyl marks can be removed by histone demethylases. Additional histone modifications include ubiquitination and phosphorylation, which are attached to histone proteins by ubiquitin ligase enzymes and kinases, respectively[294].

Two multi-protein complexes carry out epigenetic silencing via histone modification, Polycomb Repressive Complexes (PRCs) 1 and 2. The PRCs first were identified for their roles in homeobox gene silencing during differentiation[297]. PRCs are essential for embryonic development and cell differentiation, and appear to play a role in the maintenance of stem cell-like states[298]. Today, it is well appreciated that aberrant PRC-mediated gene silencing plays a major role in cancer[299]; the cancer cell epigenome differs widely from that of normal cells and epigenetic changes alter expression of many genes that drive malignant transformation[295].

PRC2 contains three core component proteins: EZH2, EED, and SUZ12. Its catalytic member, EZH2, is a histone methyltransferase that tri-methylates histone H3 at lysine 27, suppressing gene expression. EZH2 is found to be overexpressed in many cancers, including breast and prostate, where its expression positively correlates with more advanced disease and poorer prognosis[122,300,301]. Thus, EZH2 is believed to play an oncogenic role in many tumor types. EZH2/PRC2 is thought to have many target genes; perhaps up to 10% of the genome in embryonic stem cells[302]. Identifying key direct targets, such as tumor suppressor genes whose suppression contributes to malignancy, is an important next step in our understanding of epigenetics and cancer. Recently, our laboratory showed that the RasGAP *DAB2IP* is a key EZH2 target in prostate cancer: *DAB2IP* suppression mediates many of the tumorigenic effects of EZH2[121].

In breast cancer, however, the role of EZH2 in tumor development and progression and its mechanism of action in driving these processes are not fully understood. As briefly mentioned above, EZH2 is overexpressed in breast tumors and higher expression correlates with more advanced disease, increased cellular proliferation, and other markers of aggressive disease[301,303]. Overexpression of EZH2 in immortalized mammary epithelial cells promotes anchorage-independent growth and invasion *in vitro*[300]. Mice genetically engineered to overexpress EZH2 in the mammary epithelium develop intraductal epithelial hyperplasia, albeit without a reported cancer phenotype[304]. Additionally, overexpression of EZH2 in a primary breast cancer cell population enriched for tumor initiating cells inhibits DNA repair and leads to an increased number of genomic aberrations, tumor initiating cell expansion, and increased self-renewal[305]. Clearly, although current data point to a functional role for EZH2 in breast cancer progression, the precise biological effects of EZH2 overexpression and what key target genes mediate its function have yet to be elucidated.

It is thought that PRC2-mediated histone lysine methylation promotes the recruitment of other chromatin modifying complexes, such as PRC1[298]. One core component of PRC1 is BMI1,

a ubiquitin ligase enzyme that ubiquitinates lysines on histone H2A which in turn are thought to contribute to gene silencing[306]. BMI1 is overexpressed in breast cancer cell lines and tumor samples and as such has been implicated as a breast cancer oncogene[307,308]. Additionally, BMI1 has been implicated as an oncogene in other tumor types such as head and neck squamous cell carcinoma[309]. Conflicting reports exist regarding a correlation between BMI1 overexpression and disease outcome in breast cancer[308,310]. Limited functional studies suggest that BMI1 may play a causal role in the disease: BMI1 can cooperate with oncogenic HRas to transform immortalized mammary epithelial cells (MCF10A), promote xenograft tumor growth, and enhance metastasis in a tail vein injection metastasis assay[311,312]. However, precisely how BMI1 contributes to breast cancer remains unclear. In Chapter 3 of this Dissertation I discuss our findings that identify *RASAL2* as a target of EZH2 and BMI1 in breast cancer.

DNA methylation

PRC2-mediated methylation of histone proteins also is thought to promote the recruitment of DNA methyltransferase enzymes to the chromatin (additional data also support a role for DNA methylation in Polycomb protein recruitment and histone modification) [295,299]. DNA methyltransferases primarily methylate cytosine residues within CpG dinucleotides of genomic DNA, often within regions of high CpG density (CpG islands) near the 5' end of genes[295]. DNA methylation is a repressive mark and is thought to induce a more permanent suppression of gene expression than that of histone modification. Normally, highly methylated DNA is restricted to heterochromatic regions of the genome that are not expressed. In cancer, however, methylation patterns are greatly altered; in fact DNA methylation alterations were the first epigenetic changes identified in cancer cells[313,314]. Studies have found that, in cancer cells, many previously methylated regions are hypomethylated, and many previously unmethylated regions are hypermethylated; both of these changes have been shown to contribute to tumorigenesis. For example, hypomethylation of repeat sequences in the genome increases

chromosome instability and promotes genomic rearrangement[315]. Aberrant hypermethylation has been found at many tumor suppressor gene promoters, such as *RB1*, where it prevents expression of the hypermethylated tumor suppressor gene and facilitates tumorigenesis[316]. In Chapter 3 of this Dissertation I explore whether the *RASAL2* promoter may be hypermethylated in breast cancer.

MicroRNA-mediated suppression of gene expression

MicroRNAs (miRNAs) are small non-coding RNAs that interact with target genes in a sequence specific manner and induce down-regulation of these targets via mRNA destruction and/or inhibition of protein translation[317]. (Whether miRNA mediated regulation of gene expression is an epigenetic mechanism is an item of debate beyond the scope of this Dissertation.) miRNA recognition sites typically reside within 3'-untranslated regions (3'UTRs) of genes and often are conserved, indicating their cross-species biological importance[318]. Today, miRNA misregulation occupies an increasingly large niche in cancer biology. For example, one of the earliest identified miRNAs, *let-7*, today is a well established tumor suppressor miRNA. *Let-7* expression is lost in lung and in other cancers[319,320]. Among many targets, let-7 has been show to target *RAS*, so its inactivation in cancer leads to Ras overexpression[321]. Conversely, miRNAs can act as oncogenes. For example, in breast cancer miR-10b is overexpressed and drives tumor progression and metastasis[322]. Not surprisingly, many oncogenic miRNAs act by targeting important tumor suppressor genes. For example, it recently was shown that the *PTEN* tumor suppressor gene is aberrantly suppressed in cancer by overexpressed miRNAs, including miR-22 and miR-26[86,87]. Similarly, we wanted to explore whether *RASAL2* is subject to aberrant miRNA-mediated suppression in cancer; I discuss our findings in Chapter 3 of this Dissertation.

OVERVIEW OF DISSERTATION

Cancer is the second leading cause of death after heart disease and arises when cells acquire genomic, genetic, epigenetic, and other aberrations and become able to proliferate uncontrollably and avoid cell death[323]. Understanding how cancer develops and progresses will enable us to prevent, detect, and treat the disease more effectively. In this Dissertation I hope to contribute to this massive undertaking through the identification and analysis of a new tumor and metastasis suppressor gene, *RASAL2*.

In Chapter 2 I identify *RASAL2* as a candidate tumor suppressor based on its ability to transform immortalized cells and by the presence of *RASAL2* mutations in human tumors. *RASAL2* is a RasGAP gene. Focusing on breast cancer, we show that RASAL2 inhibits Ras activity and that it functions as a tumor suppressor both *in vitro* and *in vivo*. We also show that *RASAL2* inactivation endows cells with migratory and invasive properties and accelerates the progression from ductal carcinoma *in situ* to invasive carcinoma in a xenograft breast cancer model. We generate a *Rasal2* mutant genetically engineered mouse model. We establish *Rasal2* mutant, mammary specific *Her2* transgenic compound mice and find a striking increase in breast cancer metastasis in these animals. Looking in primary human breast cancers we find loss of RASAL2 protein as compared to normal tissue, with a further decrease in metastatic samples. Finally, we generate *Rasal2*, *Trp53* double mutant compound mice, which exhibit increased tumorigenesis and widespread metastasis. We conclude that *RASAL2* is the newest tumor suppressor in the RasGAP family and that its inactivation contributes to primary tumorigenesis and more potently to metastasis.

In Chapter 3 I delve into the regulation and function of *RASAL2*. We investigate mechanisms of *RASAL2* inactivation in breast cancer and present data to support a potential role for both epigenetic silencing and miRNA-mediated suppression. We notice that *RASAL2* is frequently inactivated in ERα-positive breast cancer cell lines, and discover that *RASAL2* inactivation and estrogen cooperate to promote proliferation in these cells. Lastly, we find that

RASAL2 interacts with another tumor suppressor in the RasGAP family, DAB2IP, a finding that has broad implications for RASAL2 and DAB2IP function and for the RasGAP gene family overall.

In Appendix A I detail the *Rasal2* mutant genetically engineered mouse models I generated, including those analyzed in Chapter 2. In Appendix B I reprint a publication from our laboratory in which we identify *DAB2IP* as a prostate tumor and metastasis suppressor. Finally, in Appendix C I reprint a publication from Dr. Nancy Andrews' laboratory (where I spent one year of graduate school), in which collaborators and I discover that the transcription factor STAT5 regulates expression of the transferrin receptor and that hematopoietic-specific loss of *Stat5a/b* causes microcytic, hypochromic anemia in mice.

Page intentionally left blank

Chapter 2

The RasGAP Gene, *RASAL2*, Functions as a New Tumor and Metastasis Suppressor

The RasGAP Gene, *RASAL2*, Functions as a New Tumor and Metastasis Suppressor

Sara Koenig McLaughlin[1,2], Sarah Naomi Olsen[1,2], Benjamin Dake[3,4], Elgene Lim[2,5], Junxia Min[1,2], Charlotte Kuperwasser[3,4], and Karen Cichowski[1,2]

1: Genetics Division, Department of Medicine, Brigham and Women's Hospital, Boston, MA 02115

2: Harvard Medical School, Boston, MA 02115

3: Molecular Oncology Research Institute, Tufts Medical Center, Boston, MA 02111

4: Department of Anatomy and Cellular Biology, Tufts University School of Medicine, Boston, MA 02111

5: Division of Molecular and Cellular Oncology, Department of Medical Oncology, Dana-Farber Cancer Institute and Department of Medicine, Brigham and Women's Hospital, Boston, MA 02215

Author attributions

Sara Koenig McLaughlin: Performed all experiments not directly attributed to others and with KC planned the project and wrote the manuscript.

Sarah Naomi Olsen: Performed the experiments shown in Figure 2-4 panels A and C.

Benjamin Dake: Performed the experiment shown in Figure 2-3 panel C.

Elgene Lim: Performed the experiment shown in Figure 2-2 panel D.

Junxia Min: With SKM performed the experiment shown in Figure 2-1.

Charlotte Kuperwasser: Performed the analyses shown in Figure 2-9 panels E-H.

Karen Cichowski: Supervised and developed project and with SKM wrote the manuscript.

Figure 2-1 of this Chapter was published as supplemental data in the following manuscript:

An oncogene–tumor suppressor cascade drives metastatic prostate cancer by coordinately activating Ras and nuclear factor-κB.

Junxia Min, Alexander Zaslavsky, Giuseppe Fedele, Sara K McLaughlin, Elizabeth E Reczek, Thomas De Raedt, Isil Guney, David E Strochlic, Laura E MacConaill, Rameen Beroukhim, Roderick T Bronson, Sandra Ryeom, William C Hahn, Massimo Loda, and Karen Cichowski.

Nature Medicine 16, pp. 286-294 (2010).

The remainder of this Chapter has been submitted for publication as the following manuscript:

The RasGAP Gene, *RASAL2*, Functions as a New Tumor and Metastasis Suppressor

Sara Koenig McLaughlin, Sarah Naomi Olsen, Benjamin Dake, Elgene Lim, Roderick Terry Bronson, Thomas De Raedt, Rameen Beroukhim, Kornelia Polyak, Myles Brown, Charlotte Kuperwasser, and Karen Cichowski.

Submitted (2013).

Introduction

The Ras pathway is one of the most commonly deregulated pathways in human cancer[7]. Mutations in *RAS* genes occur in a variety of tumor types[32,324]; however the Ras pathway is also frequently activated as a consequence of alterations in upstream regulators and downstream effectors, underscoring the importance of this pathway in cancer[7].

Ras is negatively regulated by RasGAPs (Ras GTPase Activating Proteins), which catalyze the hydrolysis of Ras-GTP to Ras-GDP[89]. As such, RasGAPs are poised to function as potential tumor suppressors. Indeed, the *NF1* tumor suppressor encodes a RasGAP and is mutated in the familial cancer syndrome neurofibromatosis type 1[95,96]. *NF1* also is lost or suppressed in sporadic cancers, including glioblastoma[110-112], non-small cell lung cancer[113], neuroblastoma[114], and melanoma[107-109]. More recently the RasGAP gene, *DAB2IP*, has been shown to function as a potent tumor and metastasis suppressor in prostate cancer[121]. In total there are 14 RasGAP genes in the human genome[89]. All contain a RasGAP domain but exhibit little similarity elsewhere. It is currently unknown whether any of these other genes may also function as human tumor suppressors.

Breast cancer is the most common female cancer worldwide[325]. *K-, H-,* and *N-RAS* mutations are relatively rare in this tumor type and together have been detected in only ~3.2% of all breast lesions[46,326]. Nevertheless, the Ras/ERK pathway is hyperactivated in ≥50% of breast cancers and has been proposed to be involved in tumor progression and recurrence, suggesting that Ras may be more frequently activated by other mechanisms in these tumors[266,268,327]. In this study we identify a new RasGAP tumor suppressor in breast cancer. Through the analysis of human tumor samples, human xenografts, and genetically engineered mouse models we show that *RASAL2* loss plays a causal role in breast cancer development and metastasis. Additional mouse modeling studies reveal a broader potential role for *RASAL2* in other tumor types. Together these studies highlight the expanding role of RasGAP genes in cancer and reveal an important mechanism by which Ras becomes activated in breast tumors.

Results

The RasGAP gene, *RASAL2,* is a candidate tumor suppressor

We previously developed a cell-based screen to identify additional RasGAPs that might function as tumor suppressors[121]. Briefly, distinct shRNAs that recognize individual RasGAP genes were introduced into immortalized mouse embryonic fibroblasts (MEFs) and cells were evaluated for the ability to grow in soft agar. Three genes scored in this screen: *Nf1*, a well-documented tumor suppressor gene, *Dab2ip*, which we have since shown is a tumor suppressor in prostate cancer, and a third uncharacterized RasGAP, *Rasal2* (Figure 2-1)[121].

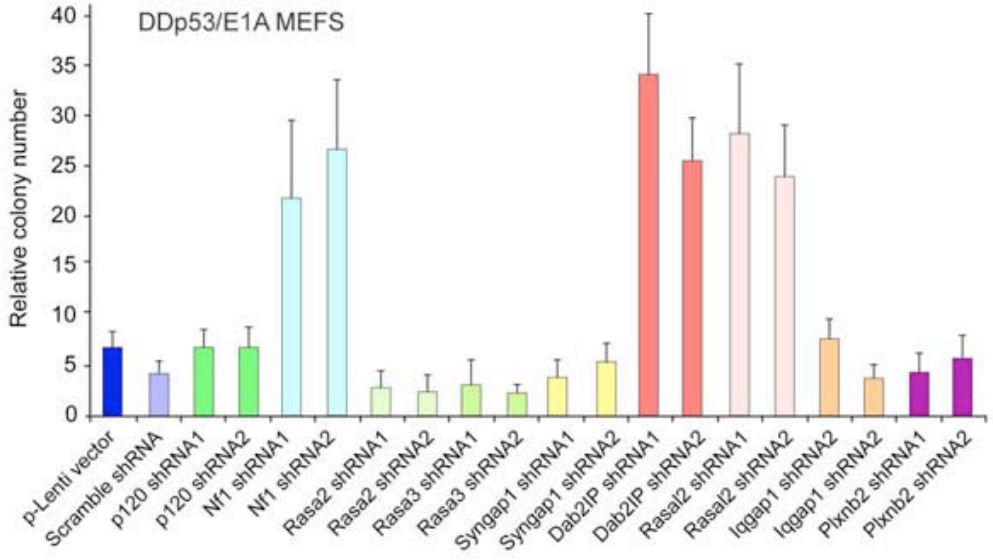

Figure 2-1. A screen for tumor suppressors in the RasGAP gene family
All available shRNA lentiviral constructs recognizing murine RasGAP genes were collected from The RNAi Consortium (Broad Institute, MIT) and introduced into MEFs expressing dominant-negative p53 and E1A. Cells were plated in soft agar to assess anchorage-independent growth. Macroscopic colonies were counted and reported as relative number of colonies ± SD.

Figure 2-2A demonstrates that distinct *Rasal2*-specific shRNA sequences promote colony growth in this assay and do so as well as *Nf1*-specific shRNAs. Upon identifying *RASAL2* as a candidate tumor suppressor, we searched publicly available databases and found mutations within the catalytic RasGAP domain in human breast cancers (Figure 2-2B and Table 2-1A)[328,329]. Current genomic mutation databases indicate that *RASAL2* is also mutated in several

Figure 2-2: *RASAL2* is a candidate tumor suppressor
(A) Left: Mouse embryonic fibroblasts (MEFs) immortalized with dominant negative p53 and adenoviral *E1A*-encoded protein were infected with lentiviral shRNAs targeting *Rasal2*, *Nf1*, or control, and plated in soft agar. Data are reported as relative number of colonies ± SEM. Inactivation of *Nf1* or *Rasal2* induced a statistically significant increase in anchorage-independent growth ($P \leq 0.0001$). Right: Western blot confirming knockdown.
(B) *RASAL2* mutations in human tumor samples[46]. Each triangle represents a non-synonymous mutation. Red triangles indicate breast cancer mutations.
(C) RASAL2 expression in a panel of human breast cancer cell lines in comparison to normal human mammary epithelial cells. Cell lines with very low or no RASAL2 are starred and bolded. Breast cancer subtypes are indicated (Lu: luminal, Ba: basal).
(D) Relative *RASAL2* expression in subsets of sorted human mammary epithelial cells[330]. MaSC: mammary stem cell-enriched (CD49hi EpCAM-). LP: luminal progenitor (CD49f+ EpCAM+). ML: mature luminal (CD49f- EpCAM+).
(E) Left: Western blot showing Ras-GTP and phospho-ERK (pERK) levels in MCF7 cells following expression of *LacZ* or *RASAL2* cDNA. Right: Western blot showing Ras-GTP and phospho-ERK (pERK) levels in MCF10A cells following shRNA-mediated inactivation of *RASAL2* or control (non-targeting “Scramble” shRNA).

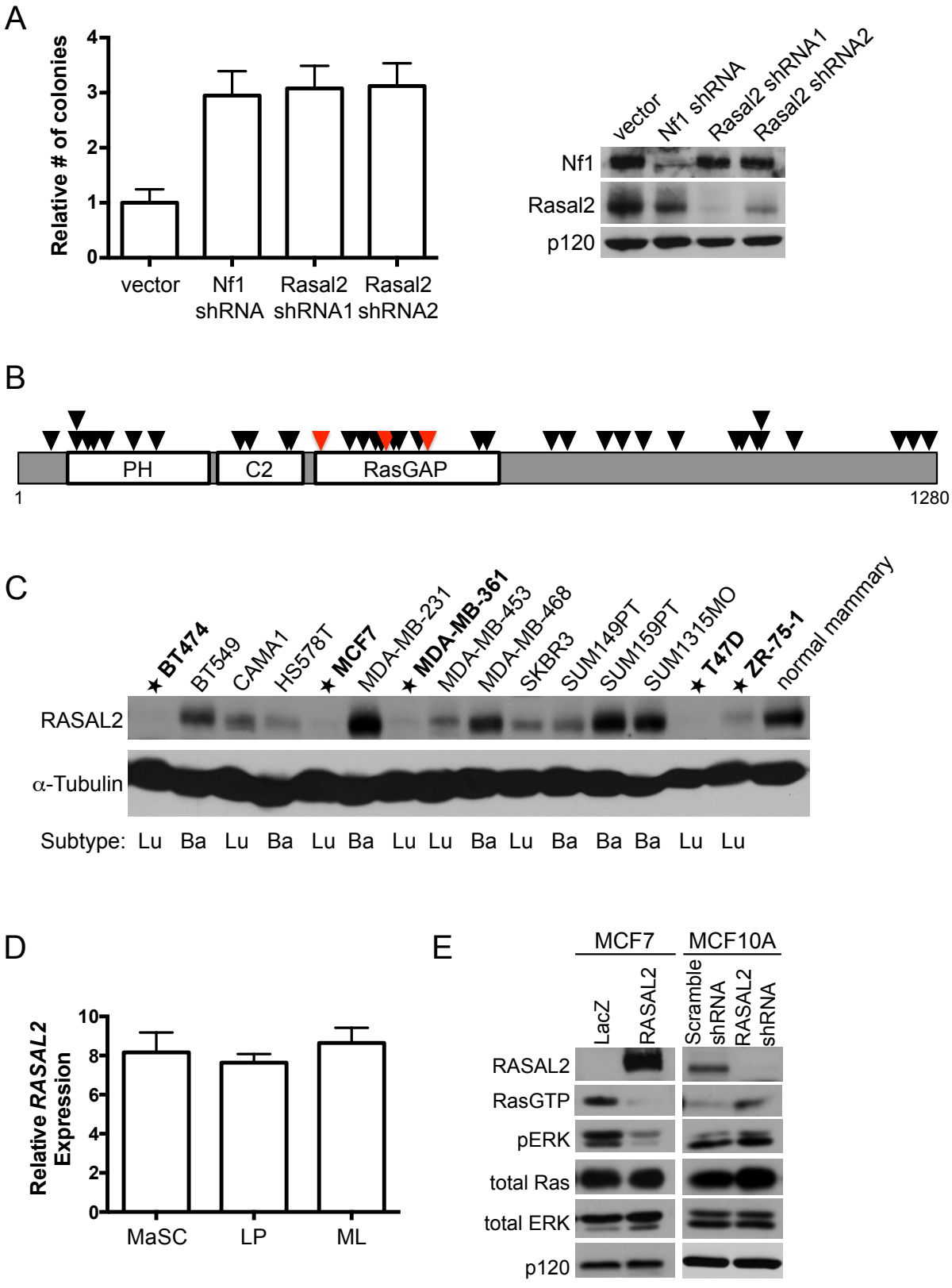

Figure 2-2 (Continued)

other cancers including colorectal, lung, and ovarian tumors (Figure 2-2B and Table 2-1B). In total 42 non-synonymous mutations have been detected in *RASAL2*, 31% of which reside in the catalytic RasGAP domain, many of which are predicted to be deleterious (Table 2-1B and Table 2-2). Because the mechanism by which Ras becomes activated in breast cancer is largely unknown, and because mutations in breast tumors were among the first to be identified, we began by investigating a potential role for *RASAL2* inactivation in breast cancer development.

Table 2-1: *RASAL2* mutations in human cancer

A

Cancer	Mutation	Domain	%	Reference
Breast Cancer	K417E	RasGAP	1.0	Shah
Breast Cancer	K567X	RasGAP	4.2	Sjöblom
Breast Cancer	E509D	RasGAP		

B

Cancer	Mutation Type	Domain	#	%
Lung: Adenocarcinoma, Small Cell Carcinoma, Squamous Cell Carcinoma	nonsense; missense	RasGAP; PH; unknown	16	3.8
Colorectal Carcinoma	missense	RasGAP; C2; unknown	8	1.3
Endometrioid Carcinoma	missense	unknown	3	1.5
Clear Cell Renal Cell Carcinoma	missense; frameshift	unknown	2	0.6
Ovarian Serous Carcinoma	nonsense; missense	RasGAP; unknown	2	0.3
Stomach Carcinoma	missense	unknown	1	10.0
Bile Duct Adenocarcinoma	missense	unknown	1	9.1
Bladder Carcinoma	missense	RasGAP	1	2.7
Hepatocellular Carcinoma	frameshift	C2	1	1.4
Head and Neck Squamous Cell Carcinoma	missense	PH	1	0.9
Prostate Adenocarcinoma	missense	PH	1	0.4
Chronic Lymphocytic Leukaemia-Small Lymphocytic Lymphoma	missense	unknown	1	0.2

(A) Non-synonymous *RASAL2* mutations in breast cancer samples[328,329]. %: percent of samples in study in which *RASAL2* mutations were identified.
(B) Non-synonymous *RASAL2* mutations in other tumor types. Data from COSMIC[46]. #: number of mutations. %: percent of total samples in which *RASAL2* mutations were identified.

Table 2-2: Human tumor mutations within the RasGAP domain of *RASAL2*

Mutation	Tissue
K417E	Breast
E509D	Breast
K567X	Breast
N457S	Colon
D477G	Colon
D494N	Colon
Y519N	Colon
S507F	Lung
G525W	Lung
L637V	Lung
A648S	Lung
E526D	Ovary
Q554H	Urinary Tract

Mutation: amino acid change. Tissue: tumor tissue type. Data from COSMIC[46].

Work from our laboratory and others have shown that the RasGAP genes *NF1* and *DAB2IP* are inactivated in cancer by genetic, epigenetic, and proteasomal mechanisms[110,116,121]. Moreover, in many instances the non-genetic mechanisms of inactivation of these tumor suppressors appear to be more prevalent than mutational events in sporadic tumors[107,110,121]. Therefore we began by examining RASAL2 protein expression in a panel of breast cancer cell lines. In comparison to normal mammary epithelial cells, RASAL2 was absent or minimally expressed in at least 5 out of 15 breast cancer cell lines, suggesting that RASAL2 may be frequently lost or suppressed in this tumor type (Figure 2-2C). Notably, RASAL2 levels were high in MDA-MB-231 and SUM159PT cells, which are known to harbor a mutation in *KRAS* and *HRAS*, respectively[331]. RASAL2 protein was frequently absent in cells derived from luminal cancers in this panel of lines. Cell sorting studies indicate that there are no inherent differences in *RASAL2* expression in any specific cell population within the mammary cell hierarchy: luminal progenitor, mature luminal, or mammary stem cell-enriched, indicating that the low RASAL2 levels associated with luminal cancer cell lines were not inherently associated with a pre-existing reduction in RASAL2 levels due to a specific cell of origin or cell fate, as has been

suggested for other genes (Figure 2-2D)[330]. When RASAL2 was reconstituted in MCF7 cells, which express little to no endogenous RASAL2, Ras-GTP and phospho-ERK levels were suppressed (Figure 2-2E). Conversely, acute inactivation of *RASAL2* via shRNA sequences in immortalized mammary epithelial cells (MCF10A) increased Ras-GTP and phospho-ERK levels (Figure 2-2E). These data confirm that RASAL2 is a functional RasGAP, and that its loss activates Ras in this tumor type.

RASAL2 functions as a tumor suppressor in breast cancer

We next investigated the biological consequences of reconstituting or suppressing *RASAL2* in breast cancer cell lines. When a *RASAL2* cDNA was introduced into human breast cancer cells that lack endogenous RASAL2, proliferation was largely unaffected (Figure 2-3A); however RASAL2 reconstitution significantly inhibited anchorage-independent colony growth (Figure 2-3B). Moreover, RASAL2 potently suppressed the growth of breast cancer xenografts *in vivo* (Figure 2-3C). Conversely, RNAi-mediated suppression of endogenous *RASAL2* in a breast cancer cell line that normally does not grow well as a xenograft promoted tumor growth *in vivo* (Figure 2-3D). Finally, the biological effects of *RASAL2* mutations identified in human breast cancer samples were evaluated. Two of the three mutants (K417E and K567X) failed to suppress anchorage-independent growth, demonstrating that these two mutations result in a clear loss-of-function (Figure 2-3E). The third mutation, which resulted in a more conservative amino acid change (E509D), still retained activity in this assay and therefore may not be pathogenic; however a number of additional non-conservative mutations have been detected in the RasGAP domain in other tumor types (Table 2-2). Together, these gain- and loss-of function-studies, mutational analysis, and expression studies suggest that RASAL2 can function as a tumor suppressor in the mammary epithelium and that its inactivation or loss can contribute to breast tumor development.

Figure 2-3. RASAL2 functions as a tumor suppressor in breast cancer
(A) Growth curves of MDA-MB-361 and MCF7 cells infected with *RASAL2* or *LacZ* control cDNA. Data points shown triplicate averages ± SD. There were no statistically significant differences in proliferation. Western blot on right confirms ectopic RASAL2 expression.
(B) Soft agar colony formation of MCF7, BT474, and MDA-MB-361 cells infected with *RASAL2* or *LacZ* control cDNA. Data show relative number of colonies ± SD. There was a statistically significant decrease in anchorage-independent growth upon ectopic RASAL2 expression (MCF7 and BT474 $P < 0.0001$; MDA-MB-361 $P = 0.002$). Western blots below confirm ectopic RASAL2 expression.
(C) Xenograft tumor formation of MDA-MB-361 cells infected with *RASAL2* or *LacZ* control cDNA and injected orthotopically into female NOD/SCID mice. Horizontal bar indicates mean tumor volume. There was a statistically significant decrease in tumor growth upon ectopic RASAL2 expression ($P < 0.0001$). Western blot on right confirms ectopic RASAL2 expression.
(D) Xenograft tumor formation of CAMA1 cells infected with shRNAs targeting *RASAL2* or non-targeting control shRNA and injected subcutaneously into female NOD/SCID mice. Horizontal bar indicates mean tumor volume. There was a statistically significant increase in tumor growth upon *RASAL2* inactivation ($P = 0.0007$). Western blot on right confirms RASAL2 knockdown.
(E) Soft agar colony formation of MCF7 cells infected with *LacZ*, *RASAL2*, or *RASAL2* mutant cDNA. Data show relative number of colonies ± SD. * indicates $P \leq 0.05$. Western blot on right confirms expression of constructs (probed with anti-HA antibody to recognize N-terminal HA tag).

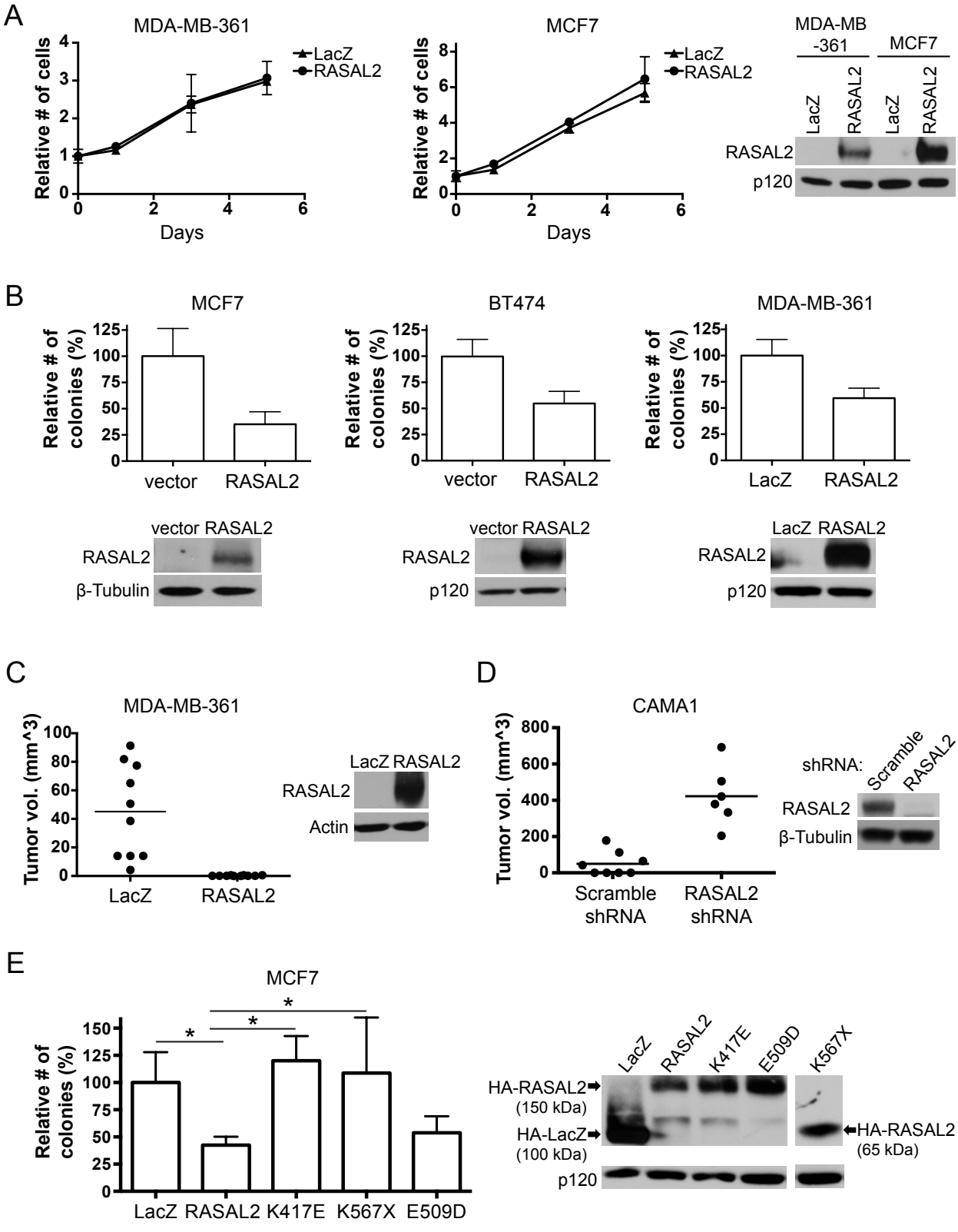

Figure 2-3 (Continued)

RASAL2 inactivation promotes migration, invasion, and tumor progression

To fully characterize the oncogenic effects of *RASAL2* loss we investigated whether *RASAL2* suppression might also promote migration, invasion, and tumor progression. We found that *RASAL2* suppression promoted the migration of MCF10A cells in a wound-healing assay (Figure 2-4A,B), and significantly enhanced invasion through Matrigel (Figure 2-4C, P = 0.002). Moreover, using a xenograft model of breast cancer progression that mimics the progression of ductal carcinoma *in situ* (DCIS) to invasive carcinoma[241,242], we found that *RASAL2* inactivation accelerated tumor progression, resulting in a rapid disruption of the myoepithelium and basement membrane, and the development of invasive adenocarcinoma (Figure 2-4D). Taken together these results suggest that *RASAL2* inactivation may also play a role in breast cancer progression.

Loss of *Rasal2* promotes metastasis and Ras activation in a genetically engineered mouse model of luminal breast cancer

As a rigorous and complementary means of investigating the biological consequences of *Rasal2* inactivation *in vivo* we generated genetically engineered mice that lack *Rasal2*. Mouse embryonic stem cells that contain a gene-trap cassette within the third intron of *Rasal2* were obtained from Toronto Centre for Phenogenomics (Figure 2-5A). These cells were used to generate gene-trap positive mice and appropriate integration as well as loss of Rasal2 expression were confirmed in mutant animals (Figure 2-5B,C). *Rasal2* -/- mice were viable and fertile and born at Mendelian ratios. We found that mutant animals did have a slightly shorter overall survival as compared to control animals (77.8 compared to 95.6 weeks; P = 0.007, Figure 2-6A). However there was no obvious difference in phenotype between wildtype and *Rasal2* -/- mice. A subset of animals from both cohorts developed tumors associated with old age. While *Rasal2* mutant mice developed these tumors earlier the tumor spectrum was similar to wildtype animals and they did not develop mammary lesions (Figure 2-6B). These results

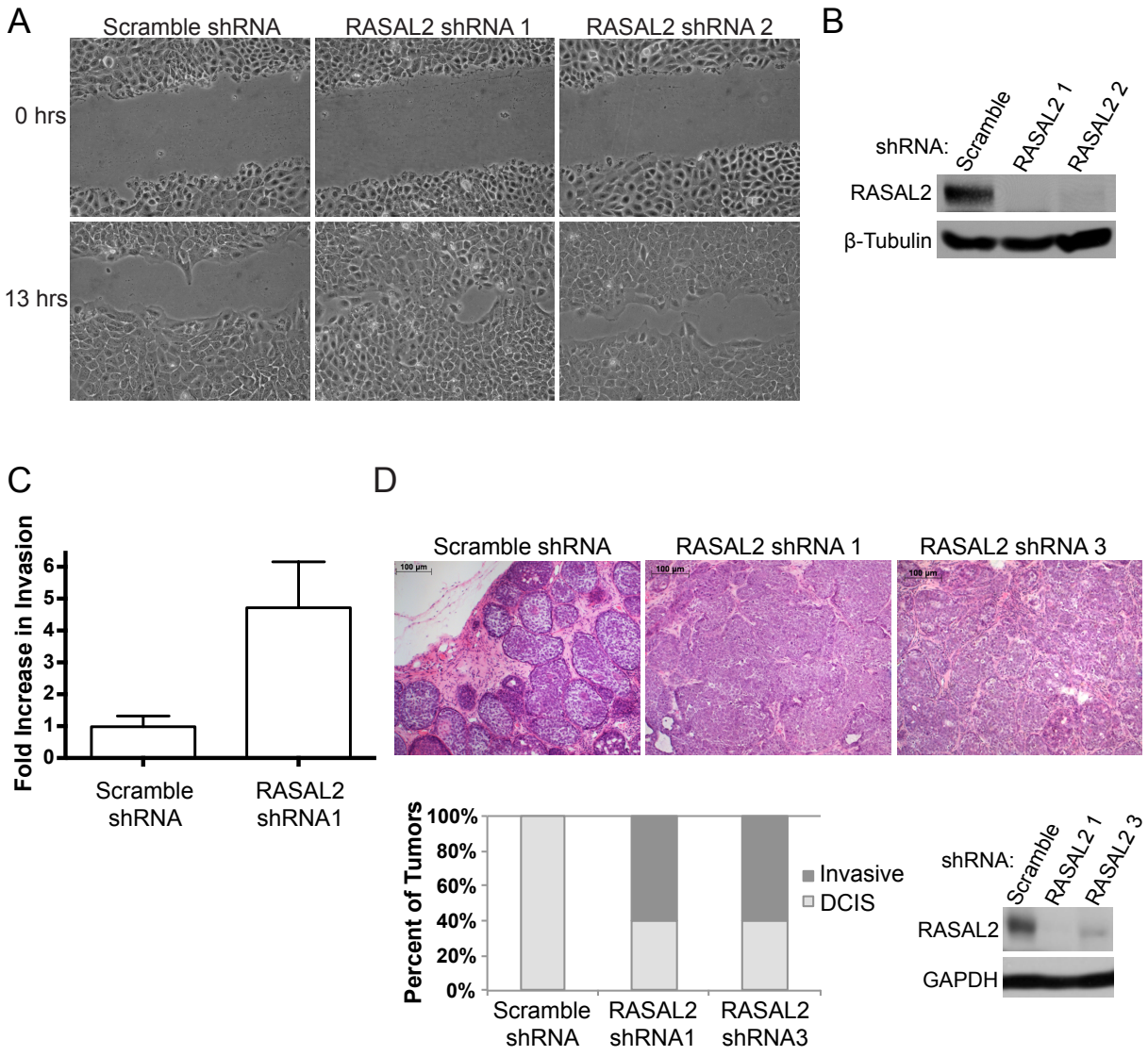

Figure 2-4. *RASAL2* inactivation promotes migration, invasion, and tumor progression
(A) Cell migration assay (wound healing). MCF10A cells infected with shRNAs targeting *RASAL2* or a non-targeting control were grown to confluence, scratched to create a wound, and imaged after indicated number of hours to monitor cell migration to close the wound. Representative images are shown.
(B) Western blot confirming RASAL2 knockdown in MCF10A cells used in (A) and (C).
(C) Transwell invasion assay. MCF10A cells infected with an shRNA targeting *RASAL2* or a non-targeting control were plated in triplicate on a Matrigel invasion chamber. Invasion was measured after 24 hours and reported as average ± SD (P = 0.002).
(D) Xenograft tumor progression. MCF10ADCIS cells were infected with shRNAs targeting *RASAL2* or a non-targeting control and injected subcutaneously into female nude mice. Top: Representative H&E images of xenograft tumors. Bottom left: Quantification of xenograft tumor progression. Bottom right: Western blot confirming RASAL2 knockdown.

Figure 2-5. Loss of *Rasal2* promotes metastasis and Ras activation in a genetically engineered mouse model of breast cancer

(A) Schematic of *Rasal2* genomic locus and pNMDi4 genetrap cassette. *Rasal2* comprises 18 exons (numbered). Un-shaded regions in exons 1 and 18 mark 5' and 3' UTRs, respectively. ATG indicates *Rasal2* translation start site. Known domains of Rasal2 are noted (PH, C2, and RasGAP). See Materials and Methods for detailed description of pNMDi4. The genetrap cassette targets the third intron of *Rasal2.*

(B) Genotyping of *Rasal2* mice to distinguish wildtype, heterozygous mutant (het), and homozygous mutant (hom).

(C) Western blot confirming loss of Rasal2 protein in genetrap animals (mammary gland tissue). wt: wildtype, het: heterozygous, hom: homozygous mutant.

(D) Top: Representative H&E images of primary mammary adenocarcinomas from *MMTVneu*; *Rasal2 +/+* and *MMTVneu*; *Rasal2 -/-* animals. Bottom: Representative H&E images of lung metastases from *MMTVneu*; *Rasal2 +/+* and *MMTVneu*; *Rasal2 -/-* animals. M indicates metastases.

(E) Lung metastasis burden in *MMTVneu*; *Rasal2 +/+* and *MMTVneu*; *Rasal2 -/-* animals. Lung metastasis incidence: percent of tumor-bearing females with lung metastases at sacrifice (P = 0.05; n=24 *MMTVneu*; *Rasal2 +/+*, n=23 *MMTVneu*; *Rasal2 -/-*). Average number of lung metastases per animal: counted per representative section of lungs for each tumor-bearing female (P = 0.04). Average metastasis burden per animal: average total area of metastasis in a representative section of lung for each tumor-bearing female (arbitrary units; P = 0.04).

(F) H&E images of metastases to brain (a), gut (b), ovary (c), and kidney (d) in compound tumor-bearing females. M indicates regions of metastasis.

(G) Western blot analysis of phospho-ERK (pERK) and phospho-AKT (pAKT) levels in primary mammary tumors from *MMTVneu*; *Rasal2 +/+* animals (numbers 1-9) and *MMTVneu*; *Rasal2 -/-* animals (numbers 10-18).

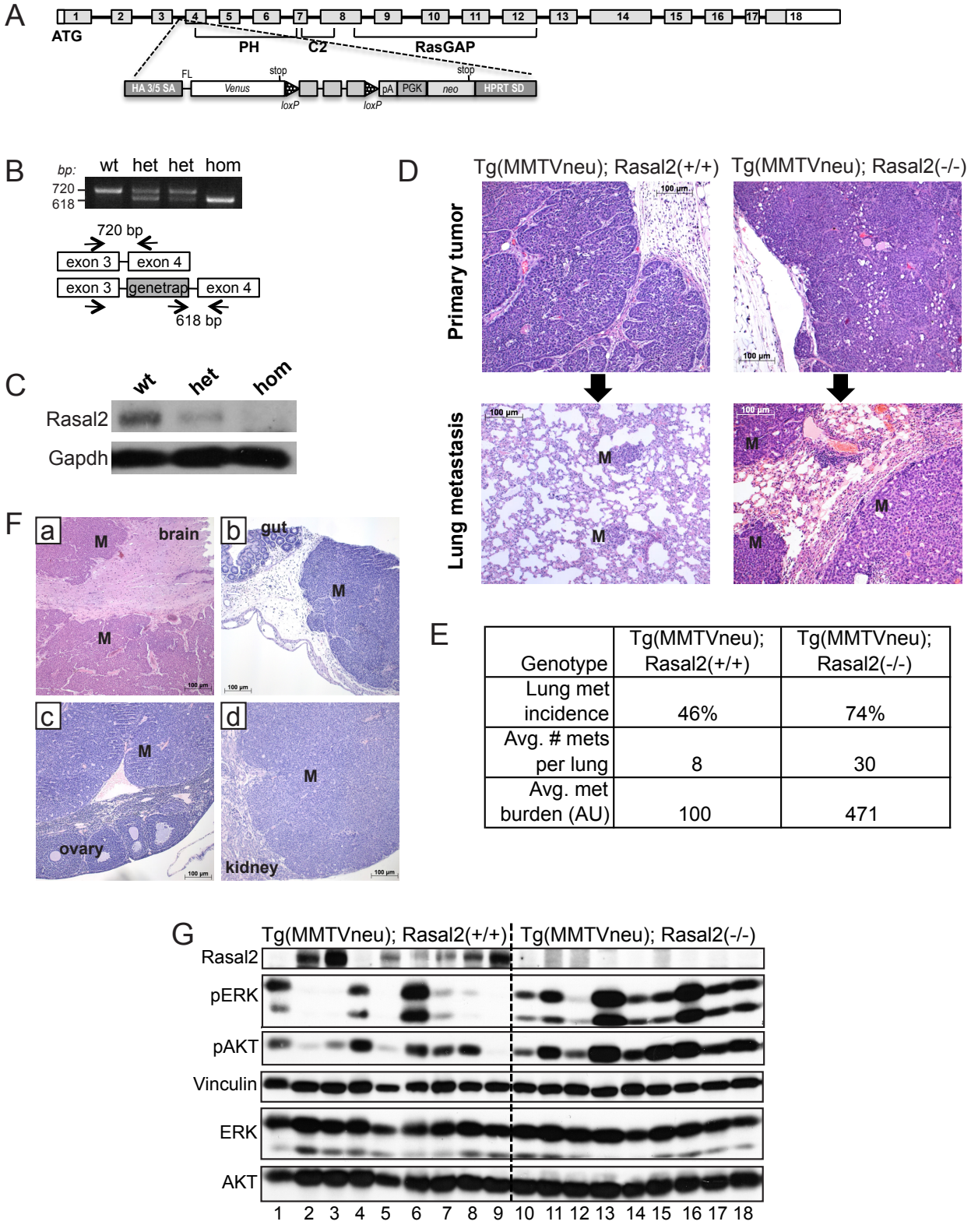

Genotype	Tg(MMTVneu); Rasal2(+/+)	Tg(MMTVneu); Rasal2(-/-)
Lung met incidence	46%	74%
Avg. # mets per lung	8	30
Avg. met burden (AU)	100	471

Figure 2-5 (Continued)

A

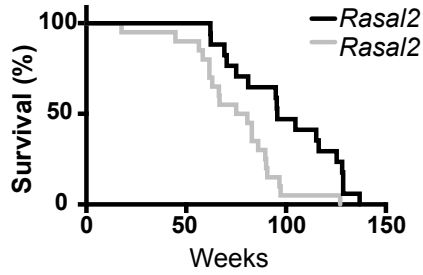

B

Genotype:	*Rasal2 +/+*	*Rasal2 +/-*	*Rasal2 -/-*
No Tumor	53%	55%	50%
Lung Adenoma	53%	0%	30%
Hepatocellular Carcinoma	18%	9%	15%
Histiocytic Sarcoma	12%	0%	0%
Lung Adenocarcinoma	6%	9%	5%
Lymphoma	6%	0%	0%
Stomach Adenoma	6%	0%	0%
Hepatoma	0%	18%	10%
Angiosarcoma	0%	27%	5%
Papilloma of the skin	0%	9%	0%
Bile Duct Adenoma	0%	9%	0%

Figure 2-6. Survival and phenotypes of *Rasal2* mutant mice
(A) Kaplan-Meier survival curves of *Rasal2 +/+* (n=17) and *Rasal2 -/-* (n=20) animals (P = 0.007).
(B) Phenotypes observed in *Rasal2 +/+* (n=17), *Rasal2 +/-* (n=11), and *Rasal2 -/-* (n=20) animals.

indicate that *Rasal2* loss is not sufficient to drive breast cancer in mice, but may play a more general role in enhancing the development of other spontaneous tumors.

To examine the effects of *RASAL2* loss on mammary tumorigenesis, we crossed *Rasal2 -/-* mice to animals that constitutively overexpress a wildtype *Her2 (Erbb2)* transgene in the mammary epithelium (*MMTVneu* mice)[240], which is a model of luminal breast cancers in mice[236]. Female *MMTVneu* mice have been reported to develop focal luminal mammary tumors and a fraction of tumor-bearing females develop lung metastases[240]. As expected, *MMTVneu* and *MMTVneu; Rasal2 -/-* compound mice developed mammary adenocarcinomas, and did so at a similar high frequency (Figure 2-5D, top panels, and Figure 2-7). Strikingly however, we found that *MMTVneu; Rasal2 -/-* mice developed substantially more metastases than *MMTVneu* animals. First, a higher fraction of compound mutant mice developed lung metastases (Figure 2-5E, 74% versus 46%, P = 0.05). Second, compound mutant mice developed more metastases per lung than *MMTVneu* animals (Figure 2-5E, 30 per mouse versus 8 per mouse, P = 0.04). Finally, the metastases were significantly larger in *MMTVneu; Rasal2 -/-* mice as

compared to *MMTVneu* mice (Figure 2-5E, $P = 0.04$). Interestingly, a subset of compound mutant mice also developed metastases to other organs, including brain, kidney, ovary, and gastrointestinal tract, something not observed in *MMTVneu* animals historically or in our cohort (Figure 2-5F). It should be noted that in most autochthonous mouse models of mammary adenocarcinoma, metastasis is typically limited to the lung and occasionally lymph nodes[245]. However, human breast cancers do frequently metastasize to the brain and these other distal sites, underscoring the significance of these observations and the potential utility of this mouse model[196]. Despite the dramatic increase in metastasis, no differences in primary tumor

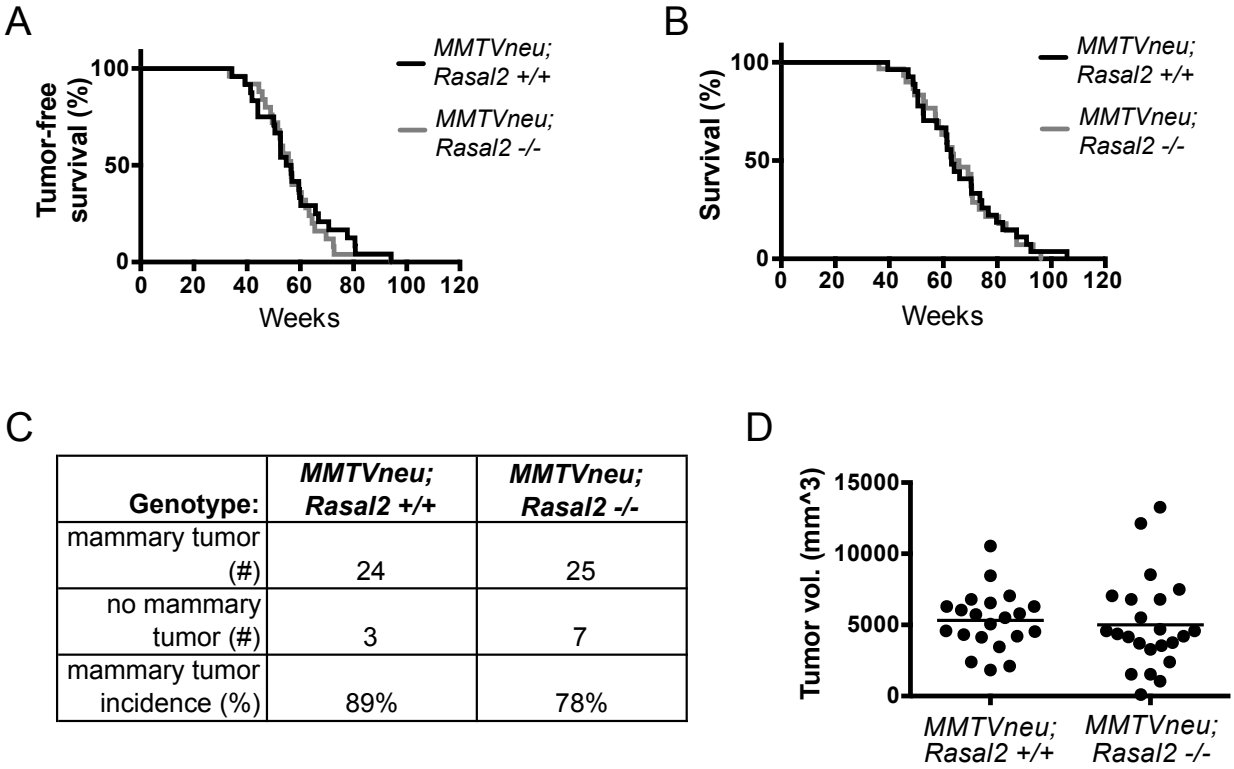

C

Genotype:	*MMTVneu; Rasal2 +/+*	*MMTVneu; Rasal2 -/-*
mammary tumor (#)	24	25
no mammary tumor (#)	3	7
mammary tumor incidence (%)	89%	78%

Figure 2-7: Tumor incidence and survival of *MMTVneu*; *Rasal2* compound mutant mice
(A) Kaplan-Meier curve showing tumor-free survival of *MMTVneu*; *Rasal2 +/+* (n=24) and *MMTVneu*; *Rasal2 -/-* (n=25) females. There is no difference in tumor-free survival ($P = 0.98$).
(B) Kaplan-Meier curve showing overall survival of *MMTVneu*; *Rasal2 +/+* (n=27) and *MMTVneu*; *Rasal2 -/-* (n=30) females. There is no difference in survival ($P = 0.90$).
(C) Mammary tumor incidence in *MMTVneu*; *Rasal2 +/+* and *MMTVneu*; *Rasal2 -/-* females. There is no difference in mammary tumor incidence ($P = 0.41$).
(D) Final mammary tumor volumes from tumor-bearing *MMTVneu*; *Rasal2 +/+* and *MMTVneu*; *Rasal2 -/-* females. Horizontal bars indicate mean tumor volume. There is no difference in tumor volume ($P = 0.41$).

incidence, growth rate, or tumor size were observed in *MMTVneu* versus *MMTVneu; Rasal2 -/-* mice, indicating that the differences in metastatic burden were not due to underlying differences in primary tumor onset or growth (Figure 2-7). Importantly, when we examined primary tumors from *MMTVneu; Rasal2 -/-* mice and *MMTVneu* animals, high levels of phospho-ERK and phospho-AKT were more consistently observed in *MMTVneu; Rasal2 -/-* lesions (Figure 2-5G). Moreover, we found that Rasal2 was spontaneously lost or suppressed in a subset of *MMTVneu* tumors and that this was accompanied by a substantial increase in phospho-ERK and phospho-AKT levels (Figure 2-5G). Finally, the primary tumor that spontaneously lost/suppressed Rasal2 and exhibited the most robust activation of the Ras pathway was a metastatic outlier within the *MMTVneu* cohort (Tumor 6, Figure 2-5G, and Figure 2-8). Taken together these findings indicate that *Rasal2* loss enhances Ras activity in mammary tumors and that its loss promotes tumor progression, invasion and metastasis in both autochthonous mouse models of breast cancer and human xenografts.

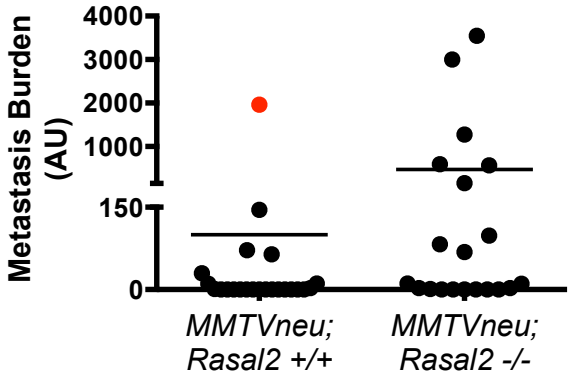

Figure 2-8. Metastasis burden in *MMTVneu* and *MMTVneu; Rasal2 -/-* mice
Metastasis burden in *MMTVneu; Rasal2 +/+* and *MMTVneu; Rasal2 -/-* tumor-bearing females. Metastasis burden measures total area of metastasis within a representative section of lung (arbitrary units, AU). Red data point: metastatic outlier within *MMTVneu; Rasal2 +/+* cohort (Figure 2-5G, animal 6). Horizontal lines: mean metastasis burden (*MMTVneu; Rasal2 +/+* = 100, *MMTVneu; Rasal2 -/-* = 471; *P* = 0.04).

RASAL2 in primary human breast cancers

Genomic analyses indicated that *RASAL2* mutations do occur in human breast cancer but are relatively rare (Table 2-1A)[46]. However, the two other known RasGAP tumor suppressors appear to be more frequently inactivated in cancer via multiple non-genetic mechanisms. To more accurately determine how frequently *RASAL2* is lost or suppressed in human breast cancers we directly examined RASAL2 protein levels in primary human tumors. Existing RASAL2 antibodies cannot be used for immunohistochemistry; therefore we obtained breast cancer arrays comprised of 55 sets of protein lysates (in triplicate) from matched primary breast tumors and adjacent normal mammary tissue taken from naïve patients[332,333]. These tumor samples have been histologically verified to contain at least 80% cancer cells and the normal tissue is cancer cell-free. We first validated our purified RASAL2 antibody in this assay and found that dot blots from RASAL2-expressing and non-expressing human breast cancer cell lines exhibited the expected pattern of expression (Figure 2-9A, top). *RASAL2*-specific shRNA sequences also successfully ablated expression in this assay (Figure 2-9A, bottom). Using the tumor arrays we found that RASAL2 expression was decreased by 75%-100% in 20% of human breast tumors as compared to adjacent normal mammary tissue (Figure 2-9B,C). These results confirm our finding in breast cancer cell lines, suggesting that RASAL2 expression is lost or suppressed in a significant fraction of human breast cancers at a frequency that is much greater than indicated by mutation analysis alone. More importantly, however, low RASAL2 protein levels were significantly associated with metastasis (Figure 2-9D; $P = 0.006$).

Because our cell line analysis showed that RASAL2 expression is low or undetectable in a subset of luminal breast cancer cell lines (Figure 2-2), and mouse modeling studies further demonstrated that *RASAL2* loss promotes the metastasis of luminal tumors, we wanted to evaluate *RASAL2* expression in the context of different breast cancer subtypes. Human breast cancers can be molecularly classified into distinct subtypes: basal-like, HER2-positive, luminal A, luminal B, and normal breast-like[197,198,334,335]. Notably, molecular subtype association analysis

Figure 2-9. RASAL2 expression is lost/low in primary human breast cancers and low levels are associated with metastasis and recurrence

(A) Test dot blot of RASAL2 antibody. RIPA whole cell extracts from human breast cancer cell lines with high or low RASAL2 expression (MDA-MB-231 "231" and T47D, respectively) (top) or MCF10ADCIS cells infected with control or *RASAL2*-targeting shRNAs (bottom) were spotted on a nitrocellulose membrane and probed with the RASAL2 antibody.

(B) Sample images from human breast tumor lysate array. Six sets of RASAL2 and total protein stains are shown. Each set contains triplicate spots of tumor lysate (right) and triplicate spots of paired normal tissue lysate (left).

(C) Tumor lysate microarray results. Each bar marks the change in RASAL2 expression in one tumor sample as compared to its matched normal control. RASAL2 levels in each spot were quantified, normalized to total protein in the same spot, and averaged among the triplicate, yielding the "normalized value". Fold change in RASAL2 expression was determined by taking the Log2 of the ratio of the normalized tumor value over the normalized control tissue value. Shaded bars indicate metastatic samples. RASAL2 expression decreased by 75%-100% in 20% of tumors on the array, as compared to matched normal controls.

(D) The decrease in RASAL2 protein expression in tumor versus normal in non-metastatic (Stages I, II, III) versus metastatic (Stage IV) tumors. Graph shows the Log2 fold change in RASAL2 expression in tumor versus normal. Data are reported as average ± 95% CI. P = 0.006.

(E) Heatmap of *RASAL2* gene expression as a function of robust molecular subtype predictor classification, which is based on patients classified in the same tumor subtype. Percentages of tumors with high, intermediate and low RASAL2 expression per molecular subtype are given in the gene expression table

(F) *RASAL2* expression table. For each breast cancer subtype, the number of samples and percentage of samples with low, intermediate, or high *RASAL2* mRNA expression are indicated.

(G) Kaplan-Meier curve showing recurrence-free survival of luminal B tumors with high or low *RASAL2* expression. logrank P = 0.013.

(H) Kaplan-Meier curve showing overall survival of luminal B tumors with high or low *RASAL2* expression. logrank P = 0.013.

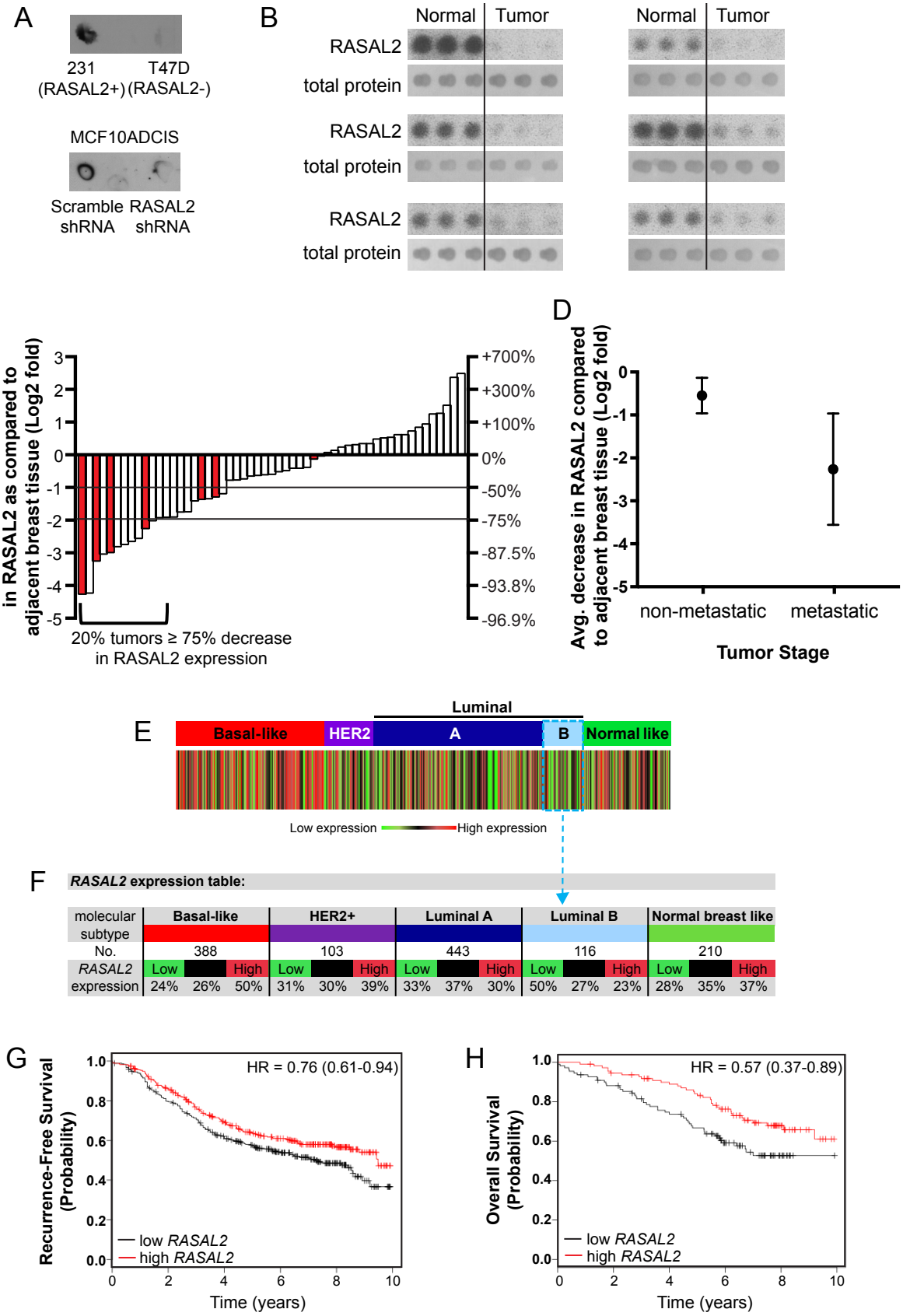

Figure 2-9 (Continued)

of transcriptional profiles from primary breast cancers revealed that RASAL2 expression was low in luminal B breast cancers; 50% of luminal B tumors expressed the lowest levels of *RASAL2*, consistent with a potential role for *RASAL2* loss in this subtype (Figure 2-9E,F). Moreover, low *RASAL2* expression was also associated with both increased tumor recurrence (Figure 2-9G, logrank $P = 0.0133$) and decreased overall survival (Figure 2-9H, logrank $P = 0.0131$) in patients with luminal B cancers. Taken altogether cellular, xenograft, mouse modeling, and human tumor studies suggest that *RASAL2* loss promotes breast cancer development and metastasis, and may play a particularly important role in the progression of luminal B tumors.

Rasal2 mutations promote tumor development and widespread metastasis in *p53* mutant mice

To determine whether *RASAL2* inactivation might also contribute to the development of other sporadic tumors, *Rasal2* -/- mice were crossed to mice mutant for p53, one of the most commonly inactivated tumor suppressors in human cancer[278,336]. *Trp53* mutant mice develop a spectrum of lymphomas and sarcomas and some carcinomas arise in heterozygotes[286,287]. In addition to the classical tumors observed in *Trp53* mutant mice, *Rasal2/Trp53* compound mutant mice developed several other lesions that were not found in *Trp53* mutant controls, historically or in our cohort (Figure 2-10A)[287,288]. Specifically, *Rasal2/Trp53* mutant mice developed hepatocellular carcinomas and other liver tumors, colonic adenomas, and oral and stomach tumors (Figure 2-10A). These findings are of particular interest because *RASAL2* mutations have been found in related human cancers, namely hepatocellular carcinoma, colorectal carcinoma, head and neck squamous cell carcinoma, and stomach cancer (Table 2-1B). Together, these data suggest that RASAL2 loss may play a broader role in the development of these tumor types.

Figure 2-10. *Rasal2, Trp53* compound mutant mice develop highly metastatic tumors
(A) Phenotypes in *Rasal2/Trp53* compound mutant mice. Pie charts display the array of phenotypes in each genotype. New phenotypes in *Rasal2* mutant compound mice are shown in color. n=21 *Rasal2 +/+; Trp53 -/-*, 18 *Rasal2 +/-; Trp53 -/-*, 31 *Rasal2 -/-; Trp53 -/-*, 16 *Rasal2 +/+; Trp53 +/-*, 21 *Rasal2 +/-; Trp53 +/-*, 21 *Rasal2 -/-; Trp53 +/-*.
(B) Percentage of metastatic solid tumors in *Rasal2 +/+, +/-,* and *-/-; Trp53 +/-* compound mice. Increased metastasis in compound animals is statistically significant ($P = 0.003$). The paucity of metastatic solid tumors in *Trp53 +/-* mice is supported by historical data on a similar strain background in which 3/44 animals (7%) developed metastases[289].
(C) Representative images of metastatic lesions (bottom) and their primary tumors (top). From left to right: mammary adenocarcinoma and lung metastasis, osteosarcoma and liver metastasis, hepatocellular carcinoma and lung metastasis, and lung adenocarcinoma and liver metastasis. M: metastasis, Lu: lung, Liv: liver.

A

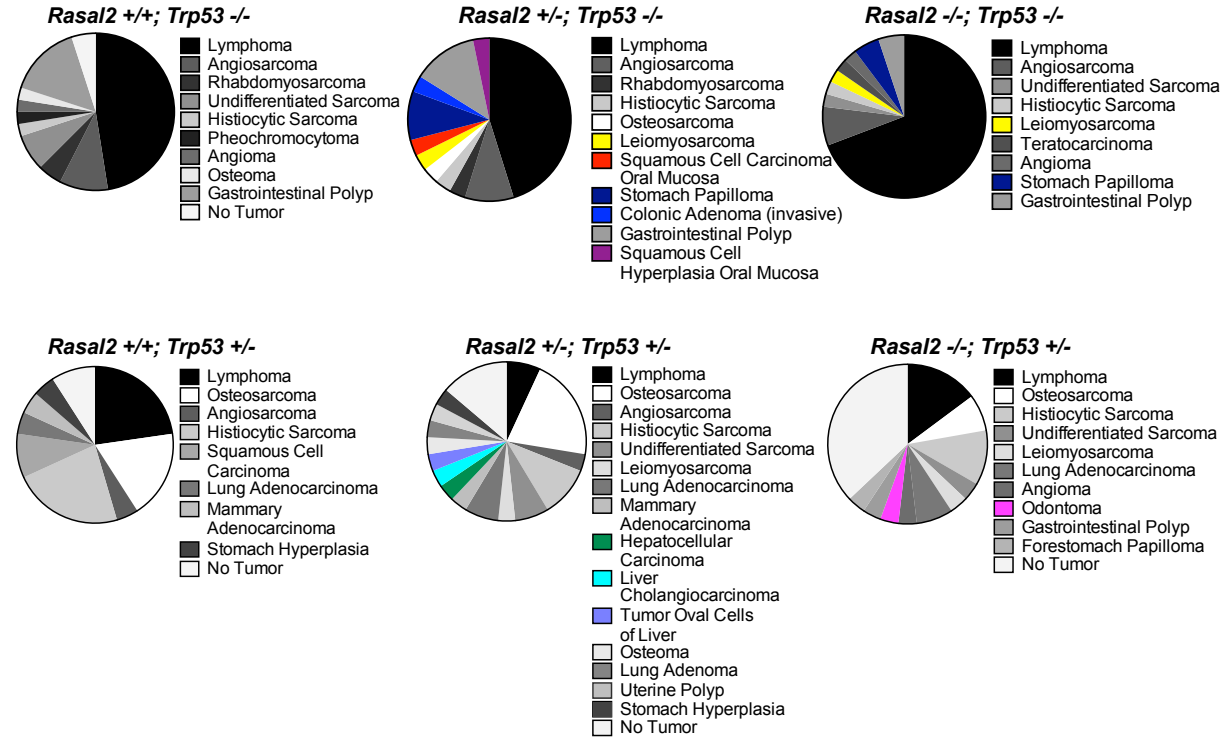

B

Genotype:	*Rasal2 +/+; Trp53 +/-*	*Rasal2 +/-; Trp53 +/-*	*Rasal2 -/-; Trp53 +/-*
Percentage of Solid Tumors with Metastases	18%	60%	83%

C

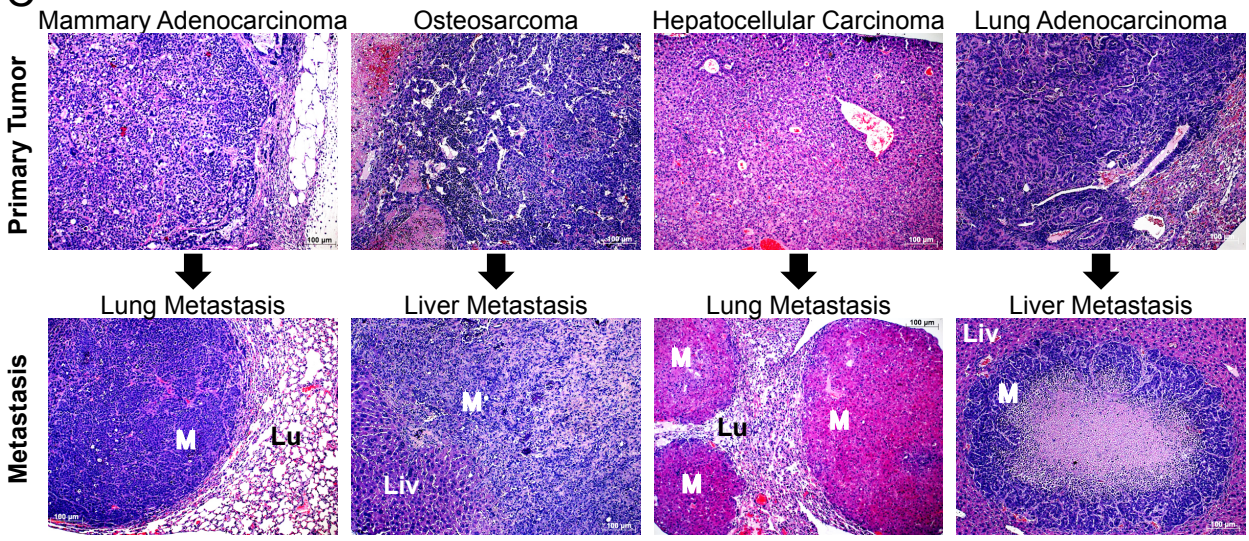

Figure 2-10 (Continued)

However the most striking phenotype in *Rasal2/Trp53* mutant mice was that *Rasal2* loss potently promoted metastasis. The *Trp53* -/- mice, either with or without functional Rasal2, typically died from the primary tumor, which was frequently lymphoma. Nevertheless 60% of the solid tumors that developed in *Rasal2 +/-; Trp53 +/-* mice and 83% of the solid tumors from *Rasal2 -/-; Trp53 +/-* mice were metastatic, as compared to 18% of tumors in *Trp53 +/-* mice (Figure 2-10B, $P = 0.003$). Specifically, *Rasal2/Trp53* mutant animals developed highly metastatic mammary adenocarcinomas, hepatocellular carcinomas, lung adenocarcinomas, and various sarcomas, again tumor types in which *RASAL2* mutations have been detected in humans (Figure 2-10C). Thus these findings further underscore the role of RASAL2 loss as a driver of metastasis and suggest that its inactivation may play a role in the progression of breast and other human cancers.

Discussion

The Ras pathway plays a well-established role in cancer[7]. However the primary mechanism(s) by which Ras becomes activated in breast cancers has remained elusive. Here we report that *RASAL2*, which encodes a previously uncharacterized RasGAP, functions as a tumor and metastasis suppressor in breast and other cancers. First, we have shown that loss-of-function mutations in *RASAL2* are found in human breast cancers and other tumor types. However, like other RasGAP genes *RASAL2* appears to be more frequently inactivated by non-genetic mechanisms and it is substantially repressed in at least 20% of primary human breast cancers. Second, *RASAL2* ablation promotes tumor growth and progression in two different human xenograft models, while *RASAL2* reconstitution suppresses breast tumor growth. Third, *RASAL2* mutations activate Ras and significantly promote metastasis in a genetically engineered mouse model of luminal mammary cancer. Fourth, *RASAL2* mutations cooperate with *p53* mutations in tumor development and promote the metastasis of several tumor types, including mammary tumors, in the mouse. Finally, RASAL2 is lost or suppressed in a significant

fraction of human breast cancers and low RASAL2 protein levels are associated with metastasis. Notably, the lowest *RASAL2* mRNA expression levels were most frequently observed in luminal B human breast cancers and also were associated with recurrence and reduced survival of patients with this tumor subtype. Collectively, these data suggest that RASAL2 loss plays a causal role in breast cancer pathogenesis, and may be particularly important for progression and metastasis.

It should be noted that while *RAS* mutations are rare in breast cancer, they do occur. Moreover amplifications of wildtype *RAS* are frequently observed in basal-like breast cancers, the most aggressive subtype of human breast cancer, underscoring the connection between Ras activation and breast cancer progression[55,56,270,337]. Our data suggest that overall *RASAL2* is suppressed or lost in at least 20% of human breast cancers. However expression analysis of different breast cancer subtypes suggests that *RASAL2* may play a particularly important role in the progression of luminal B tumors. The observation that *RASAL2* loss promotes metastasis in a mouse model of luminal tumors further supports this possibility. In this respect it is notable that luminal B tumors have poorer outcomes than luminal A tumors, however the mechanism(s) that drive the progression of these tumors are largely unknown. Our data suggest that RASAL2 loss/suppression may play a causal role in the progression of this subtype, although these observations do not preclude its potential involvement in other subtypes.

Finally while *RASAL2* is mutated in breast cancer and in other human tumors, it appears to be more commonly inactivated via non-mutational mechanisms. Notably, the other RasGAP tumor suppressors, *NF1* and *DAB2IP*, are also inactivated in cancer by both genetic and several non-genetic mechanisms[110,121]. Similarly, *PTEN* and *INPP4B*, two other tumor suppressors that negatively regulate an overlapping set of signals, are also suppressed by multiple mechanisms in cancer, some of which have not yet been elucidated[338-340]. As such, loss of PTEN protein expression, rather than mutational status or copy number, is often evaluated in clinical samples during clinical trials and for pathological staging[341,342]. The observation that *RASAL2* loss plays

a causal role in breast cancer progression and metastasis in animal models and that its expression is lowest in primary human tumors that ultimately progress or recur, suggests that *RASAL2* may ultimately be useful as a prognostic biomarker, in at least a subset of breast cancers, such as luminal B tumors. Regardless, these studies have identified a new gene involved in breast cancer progression and have revealed a mechanism by which Ras becomes activated in this disease.

Materials and Methods

Cell Culture and DNA Constructs

Mouse embryonic fibroblasts (MEFs) were isolated and immortalized with dominant-negative P53 and adenoviral *E1A*-encoded protein[102]. MCF7 and MCF10A cells were purchased from ATCC. BT549, HS578T, MDA-MB-231, MDA-MB-453, MDA-MB-468, SKBR3, T47D, and ZR-75-1 cells were obtained from Dr. William Hahn (Dana-Farber Cancer Institute). SUM149PT, SUM159PT, SUM1315MO, and BT474 cells were obtained from Dr. Frank McCormick (University of California San Francisco). MCF10A.DCIS cells were obtained from Dr. Kornelia Polyak (Dana-Farber Cancer Institute), MDA-MB-361 cells were obtained from Dr. Charlotte Kuperwasser (Tufts University), and CAMA1 cells were obtained from Dr. Marcia Haigis (Harvard Medical School). Cell lines were cultured according to published protocols.

Endogenous proteins were inactivated using short-hairpin RNAs (shRNAs) from The RNAi Consortium (Broad Institute, MIT) with the following target 21-mer sequences: NF1 shRNA (5'-TTATAAATAGCCTGGAAAAGG-3'), RASAL2 shRNA1 (5'-CCCTCGTGTTCTTGCTGATAT-3'), and RASAL2 shRNA2 (Figure 2-4 shRNA3) (5'-GCCTTCCACCTCTTCATAGTA-3'). A scrambled non-silencing shRNA was purchased from Addgene (5'-CCTAAGGTTAAGTCGCCCTCG-3')[343]. A *RASAL2*-targeting shRNA was cloned into the pLKO vector (Figure 2-4 shRNA2) (5'-ATGGAGTGCAATAGGACATTG-3'). The Mammalian Gene Collection fully sequenced human *RASAL2* cDNA was purchased from Open

Biosystems (cat. # MHS4426-99623118) and cloned it into the pHAGE-N-Flag-HA lentiviral expression vector (Dr. J. Wade Harper, Harvard Medical School) for expression in cell lines. The *RASAL2* cDNA was mutagenized using QuikChange II Site-Directed Mutagenesis kit, according to the manufacturer's instructions (Agilent). shRNA or cDNA vectors along with viral packaging plasmids delta 8.2 and VSVG were transfected into 293T cells using Fugene6 (Roche), following the manufacturer's instructions. Virus supernatant was harvested after 48 hours, filtered through a 0.45μm filter, and incubated on target cells for 6 hours at a 1:2-1:10 dilution with 8μg/ml polybrene. Infected cells were selected in 0.5-2.0μg/ml puromycin, as optimized for each cell line.

Proliferation Curves

150,000 cells were plated in triplicate in 6-well dishes. The following day cells were counted for day 0, and then triplicate sets of cells were counted on subsequent days as indicated.

Soft Agar and Xenograft Assays

Soft agar assays were plated in triplicate in 6-well dishes using the appropriate growth media for each cell line and SeaPlaque GTG low melting point agarose (Lonza). Plating conditions were as follows. MEFs: 10,000 cells, 0.5% agar base, 0.35% agar top. MCF7 cells: 5,000 cells, 0.5% agar base, 0.35% agar top. BT474 cells: 10,000 cells, 0.6% agar base, 0.35% agar top. MDA-MB-361 cells: 50,000 cells, 0.5% agar base, 0.35% agar top. Macroscopic colonies were counted after 2-6 weeks in 5 representative fields per well.

Female nude and NOD/SCID mice were purchased from Charles River Laboratories (cat. #s 088 and 394, respectively) for subcutaneous xenograft experiments. Cells were injected with matrigel (BD Biosciences cat. # 354234) as follows: MCF10A.DCIS ($1x10^5$ cells, 50% matrigel, nude mice), CAMA1 ($2x10^6$ cells, 50% matrigel, NOD/SCID mice). For mammary fat pad

orthotopic xenograft experiments, $1x10^6$ MDA-MB-361 cells were injected in 50% matrigel bilaterally into the 4^{th} mammary glands of female NOD/SCID mice (Jackson Laboratories). Tumor size was measured by caliper and tumor volume was calculated using the formula volume = (length x $width^2$) x π/6.

Migration and Invasion Assays

For migration assays, MCF10A cells were grown to 95-100% confluence and treated with mitomycin C to inhibit cell division. Wounds were generated with a pipette tip and images of wound healing (migration) were taken at indicated time intervals. For invasion assays, 100,000 MCF10A cells were plated per well on BioCoat Matrigel Invasion Chambers (BD cat. # 354480) and after 24 hours invaded cells were fixed, stained, and counted, following the manufacturer's instructions.

Rasal2 Mutant Mice

All animal procedures were approved by the Center for Animal and Comparative Medicine at Harvard Medical School in accordance with the NIH Guildlines for the Care and Use of Laboratory Animals and the Animal Welfare Act. A mouse embryonic stem cell line in which the pNMDi4 genetrap cassette targets *Rasal2* was purchased from the Toronto Centre for Phenogenomics / Canadian Mouse Mutant Repository (clone CMHD 463C12). The pNMDi4 genetrap cassette contains the following elements as depicted in Figure 3A: HA 3/5 SA (splice acceptor), FL (flexible linker), Venus (enhanced yellow fluorescent gene) with stop codon, loxP sites, pA (polyadenylation signal), PGK (promoter), neo (neomycin resistance gene) with stop codon, HPRT SD (splice donor). The neomycin resistance gene stop codon prevents translation of 3' exons. The presence of the genetrap cassette within the third intron of *Rasal2* was confirmed using cDNA PCR. The Brigham and Women's Hospital Transgenic Mouse Facility injected ES cells into blastocysts and implanted them into pseudo-pregnant recipients to

generate chimeric pups. Chimeras were crossed to Black 6 animals (C57BL/6-E, Charles River Laboratories cat. # 475) and pups were tested for presence of the genetrap. Two additional copies of the genetrap cassette elsewhere in the genome were discovered in the mouse ES cell line and genetrap mice. Genetrap-positive mice were crossed to wildtype animals and Southern blotting was used to identify pups that had the genetrap cassette only within the *Rasal2* locus (data not shown). These animals were used as founders for all cohorts and subsequent crosses.

Rasal2 Genotyping

Primers for PCR of the genetrap cassette were NMD.F (5'-CATGGTCCTGCTGGAGTTC-3') and NMD.R (5'-TGCCTTTAGACCTTTTTGTGG-3'). Total RNA was extracted from homogenized tails using QiaShredder and RNeasy kits (Qiagen), and cDNA was synthesized using qScript cDNA Synthesis Kit (Quanta), following the manufacturer's instructions. PCR was performed on cDNA with primers NeoL (5'-GCTATCAGGACATAGCGTTGGCTAC-3'), GT463C12_F3 (5'-TCGGATCCTTCTGGAGTCAG-3'), and GT463C12_R1 (5'-CTCTCTCGGAGGCAGAGCTA-3') to detect wild type (F3/R1) and mutant (NeoL/R1) transcripts.

Compound Mutant Mice

Rasal2 genetrap mice were crossed to FVB/N-Tg(MMTVneu)202Mul/J mice (Jackson Laboratories cat. # 002376)[240] or to B6.129S2-*Trp53*^{Tm1Tyj}/J mice (Jackson Laboratories cat. # 002101)[287] to generate the following compound strains for analysis: *MMTVneu; Rasal2 +/+*, *MMTVneu; Rasal2 +/-*, *MMTVneu; Rasal2 -/-*, *Trp53 +/-; Rasal2 +/+*, *Trp53 +/-; Rasal2 +/-*, *Trp53 +/-; Rasal2 -/-*, *Trp53 -/-; Rasal2 +/+*, *Trp53 -/-; Rasal2 +/-*, and *Trp53 -/-; Rasal2 -/-*. Genotyping of the neu transgene and *Trp53* was performed following published protocols. Cohorts of *Rasal2* mutant mice and controls were on a 129-enriched background (75%

129SvImJ, 25% C57BL6). Cohorts of *Trp53; Rasal2* compound mice and controls were on a mixed 129/B6 background (62.5% C57BL6, 37.5% 129SvImJ). Cohorts of *MMTVneu*; *Rasal2* compound mice and controls were on a background of 56% 129SvImJ, 25% FVB, and 19% C57BL6.

Protein Lysates and Western Blot Analyses

Protein extracts were isolated from cells or homogenized tissue in 1% SDS boiling lysis buffer. Ras-GTP levels were determined using a Ras Activation Assay kit, following the manufacturer's instructions (EMD Millipore). Protein lysates were quantified and separated on polyacrylamide gels. Western blots were probed following validated procedures using the following antibodies: Actin (Sigma cat. # A2066), phospho-AKT (Ser473, Cell Signaling cat. # 4060), AKT (Cell Signaling cat. # 9272), ER (Thermo cat. # R9101-SO), phospho-ERK (Thr202/Thr204, Cell Signaling cat. # 4370), ERK (Cell Signaling cat. # 9102), GAPDH (Cell Signaling cat. # 2118), HA (Covance cat. # MMS-101P), HER2 (Cell Signaling cat. # 2242), NF1 (UP69 C-terminal polyclonal antibody)[110], p120RasGAP (BD Transduction Laboratories cat. # 610040), Ras (Upstate cat. # 05-516), α-Tubulin (Sigma cat. # T5168), β-Tubulin (Sigma cat. # T4026), and Vinculin (Cell Signaling cat. # 4650). A peptide antigen (NP_773793 amino acids 1111-1130) was used to generate and affinity purify an anti-RASAL2 rabbit polyclonal antibody (Covance ImmunoTechnologies).

Tumor and Tissue Analysis

Tumors and tissues were fixed in buffered formalin, stored in 70% ethanol, paraffin embedded, and sectioned. Sections were stained with hematoxylin and eosin and analyzed by the rodent pathologist, Dr. Roderick Bronson.

Tumor Lysate Array Analysis

The RASAL2 antibody was tested for use on tumor lysate arrays by probing nitrocellulose membranes that had been spotted with 1μg/μl RIPA lysates from human breast cancer cell lines with high or low RASAL2 levels or from MCF10ADCIS cells infected with shRNA sequences targeting *RASAL2* or control.

Qualitative breast cancer tumor lysate arrays were purchased from Protein Biotechnologies (cat. # PMA2-001-L). Arrays were probed with the affinity purified RASAL2 antibody. Developed film was scanned and quantified using ImageJ software. Arrays were then stained with Colloidal Gold, scanned, and total protein was quantified using ImageJ. RASAL2 levels in each spot were normalized to the Colloidal Gold level in the same spot. Triplicate spots were then averaged, and the ratio between the tumor normalized triplicate and normal normalized triplicate was calculated and reported as a Log2 fold change value.

Molecular Subtype Association and Survival Analysis

Gene expression correlations targeted analysis was applied on published genomic data on patients classified in the same molecular subtype with the six molecular subtype predictors[201,334,335] using GenExMiner as previously described[344]. A gene expression map was determined by molecular subtype predictors (single sample predictors (SSPs) and/or subtype clustering models (SCMs)). A gene expression table was also provided for robust classifications, indicating for each subtype the proportion of patient with low, intermediate and high gene expression; gene expression values being split in order to form three equal groups.

Gene expression data and relapse free and overall survival information were analyzed as previously described[345]. Data were downloaded from GEO (Affymetrix HGU133A and HGU133+2 microarrays), EGA and TCGA. The background database integrates gene expression and clinical data simultaneously. To analyze the prognostic value of RASAL2, the patient samples are split into two groups according to median expression of RASAL2.

Page intentionally left blank

Chapter 3

Regulation and Function of the Tumor Suppressor Gene *RASAL2*

Regulation and Function of the Tumor Suppressor Gene *RASAL2*

Sara Koenig McLaughlin[1,2], Sarah Naomi Olsen[1,2], Marshall Thomas[2,3], Elgene Lim[2,4], and Karen Cichowski[1,2]

1: Genetics Division, Department of Medicine, Brigham and Women's Hospital, Boston, MA 02115

2: Harvard Medical School, Boston, MA 02115

3: Harvard Immune Disease Institute, Boston, MA 02115

4: Dana-Farber Cancer Institute, Boston, MA 02115

Author attributions

Sara Koenig McLaughlin: Planned all experiments and wrote the manuscript; performed all experiments not directly attributed to others.

Sarah Naomi Olsen: Performed the experiments shown in Figure 3-4 panels D and E.

Marshall Thomas: Performed the experiment shown in Figure 3-2 panel C.

Elgene Lim: Performed the analysis shown in Figure 3-3 panel B.

Karen Cichowski: Supervised and developed the project and edited the manuscript.

Introduction

In Chapter 2 of this Dissertation I identify *RASAL2* as a putative tumor suppressor RasGAP gene, and show *in vitro* and *in vivo* data that support a role for *RASAL2* inactivation in breast cancer development and metastasis. Additionally, I demonstrate that *RASAL2* inactivation promotes the development and progression of other sporadic tumor types. These findings raise a number of new questions as to the biology, regulation, and function of RASAL2. In this Chapter I present our current efforts at addressing these questions. These unpublished findings represent several avenues the laboratory could further explore. First, we investigate the mechanisms by which *RASAL2* is inactivated in breast cancer. Second, we assess whether *RASAL2* inactivation has an augmented effect on specific breast cancer subtypes. Finally, we determine that RASAL2 interacts with another RasGAP, DAB2IP, and consider the biological consequences of this interaction. We believe that the data presented in this Chapter represent the beginning of the next, exciting phase of RASAL2 exploration and will lead to a better understanding of the role of RasGAPs in cancer.

MECHANISMS OF RASAL2 INACTIVATION IN BREAST CANCER

Currently available data suggest that *RASAL2* is mutated in approximately 1-4% of breast cancers[46,328,329]. However, as shown in Chapter 2 of this Dissertation, we found that *RASAL2* expression is absent or low in at least 30% of breast cancer cell lines and is reduced by 75-100% in 20% of primary breast tumors samples. Therefore, we believe that the *RASAL2* mutation frequency underrepresents the actual number of cases in which *RASAL2* is inactivated in breast cancer, and that *RASAL2* is likely inactivated via additional mechanisms. *RASAL2* resides on chromosome 1q, a region of the genome that often undergoes copy number gain in breast and other cancers[166,167], and focal deletions of *RASAL2* have not been reported. Thus, we believe that genomic deletion of *RASAL2* does not contribute to its inactivation in cancer. Instead, we hypothesize that *RASAL2* inactivation might more commonly occur via non-genetic

mechanisms. A precedent exists for non-genetic mechanisms of RasGAP inactivation in cancer: both *NF1* and *DAB2IP* are commonly inactivated in cancer via non-genetic mechanisms, *NF1* by aberrant proteasomal degradation[110], and *DAB2IP* by epigenetic silencing[121]. In this Chapter I explore the roles of epigenetic silencing and miRNA suppression in *RASAL2* inactivation in breast cancer.

Epigenetic silencing

The Polycomb Repressive Complexes (PRCs) 1 and 2 are critical mediators of epigenetic gene regulation. PRCs 1 and 2 affect gene transcription by modifying chromatin-associated histones at specific genetic loci[299]. Multiple PRC members have been implicated as oncogenes in human cancer. The PRC2 member EZH2, a histone methyltransferase, is overexpressed in many tumor types, including breast and prostate cancer. In prostate cancer, EZH2 expression has been shown to increase with increasing tumor grade and stage[122]. Work from our laboratory demonstrated a causal role for EZH2 in driving both prostate primary tumor formation and metastasis[121]. Importantly, this study also revealed the RasGAP *DAB2IP* as a critical target of EZH2, and led us to hypothesize that epigenetics may more broadly contribute to RasGAP inactivation in cancer. Studies have reported that, in breast cancer, EZH2 is overexpressed and its overexpression correlates with more aggressive disease and poor prognosis[300,301,303]; however, key target genes of EZH2 have not yet been identified. In this Chapter we test the hypothesis that *RASAL2* is a target of EZH2 in breast cancer. We also investigate whether the PRC1 member BMI1 targets *RASAL2*, as BMI1 also has been implicated as a breast cancer oncogene[307,346]. Hypermethylation of promoter DNA can follow histone modification and induce a permanent suppression of target genes[295]. Therefore, in this Chapter we also explore whether the *RASAL2* promoter may be hypermethylated in breast cancer.

MicroRNA-mediated gene regulation

MicroRNAs (miRNAs) are small non-coding RNAs that down-regulate expression of target genes through inhibition of protein translation and/or degradation of mRNA[318]. It is becoming clear that miRNAs play an important role driving gene expression alterations that contribute to human cancer[317]. In this Chapter we explore whether miRNA-mediated suppression of *RASAL2* contributes to its inactivation in breast cancer. We identify a list of candidate miRNAs predicted to target *RASAL2* and perform experiments to functionally validate one candidate, miR-135b, a miRNA that had been implicated as an oncogene in breast and colon cancers due to its overexpression in these tumor types, but whose target genes and functional effects had not been explored[347,348].

RASAL2 AND ESTROGEN RECEPTOR POSITIVE BREAST CANCERS

Breast cancer is a heterogeneous disease, comprising distinct tumor types that can be grouped based on gene expression signatures[197,198]. Seventy percent of breast cancers belong to the luminal subtype; these tumors typically express the estrogen receptor alpha (ERα)[183,185]. ERα is a nuclear hormone receptor and is the major receptor for estrogen, the steroid hormone responsible for mammary gland development and function. Estrogen binding induces ERα dimerization and activation followed by nuclear translocation and activation of a vast transcriptional program that promotes cell growth and survival. ERα also elicits “non-genomic” responses within minutes of ligand binding that occur in the cytoplasm in the absence of gene transcription. These effects include activation of receptor tyrosine kinases, eNOS, PI3K, and MAPK[178].

For over a century it has been appreciated that extended exposure to estrogen plays a cause role in breast cancer; throughout this period physicians and scientists have made eliminating estrogens or ERα function a therapeutic strategy[185]. Since the 1970s, the standard

of care for patients with ERα-positive breast cancer has been targeted anti-estrogen therapy, typically tamoxifen, which acts as an estrogen antagonist, or an aromatase inhibitor, which inhibits the final step of estrogen biosynthesis[185]. These therapies are widely successful, at least initially, underscoring the central role estrogen and ERα play in driving these tumors. It is thought that both the canonical transcriptional effects of ERα, as well as its non-genomic effects, contribute to tumorigenesis[185].

Data suggest that significant crosstalk exists between ERα signaling and the Ras pathway. Upon estrogen stimulation, non-genomic activities of ERα include activation of the PI3K and MAPK Ras effector pathways[349]. Conversely, both AKT and ERK also have been shown to phosphorylate and activate ERα[186-188]. We hypothesized that, in ERα-positive tumors and cell lines, inactivation of the RasGAP *RASAL2* might enhance ERα signaling, such as via AKT and ERK, and thus confer a proliferative advantage upon ERα-positive breast cancer cells that had lost *RASAL2* expression. Interestingly, in Chapter 2 of this Dissertation we discovered that *RASAL2* expression is lost in many ERα positive breast cancer primary tumor samples and cell lines. Further, *RAS* mutations are rare in breast cancer and *KRAS* amplification occurs predominantly in basal-like tumors[55,56], so neither genetic alteration is likely to exist in ERα-positive tumors to generate a similar cooperative effect. In this Chapter we investigate the hypothesis that *RASAL2* inactivation and estrogen signaling cooperate to drive proliferation of ERα-positive luminal breast cancer cells.

RASGAP DIMERIZATION

There are fourteen RasGAPs in the human genome. Emerging data suggest that multiple RasGAPs may function as human tumor suppressors. It remains unknown whether RasGAPs play critical tumor suppressive roles in mutually exclusive settings, whether any RasGAPs might exhibit overlapping or redundant functions, and/or whether any RasGAPs might

cooperate within one cell or tissue type. Recent evidence of RasGAP dimerization suggests that at least the last of these three possibilities might occur. Dai et al. determined that the RasGAP CAPRI *(RASA4)* homodimerizes and that its status as a homodimer or monomer differentially affects its RasGAP and RapGAP activities[147]. Dai et al. also showed that CAPRI homodimerization occurs via a C-terminal coiled-coil domain, a finding we will return to below[147]. Additionally, p120RasGAP (*RASA1*) has been shown to dimerize with the RhoGAP DLC1 (Deleted in Liver Cancer 1), a tumor suppressor gene commonly deleted in liver cancer[350]. The authors determined that p120RasGAP-DLC1 dimerization occurs via the SH3 domains of p120RasGAP and the RhoGAP domain of DLC1; the authors' *in vitro* data further suggested that the interaction inhibits DLC1's RhoGAP activity[350].

The fourteen human RasGAPs share a GAP domain but otherwise differ widely; RasGAPs with similar overall domain architectures can be grouped into subfamilies. Two RasGAP genes recently identified as tumor suppressors, *RASAL2* and *DAB2IP*, fall in the same RasGAP subfamily. Interestingly, published and unpublished data implicate inactivation of both *RASAL2* and *DAB2IP* in some of the same tumor types, including in breast cancer. *RASAL2* inactivation in breast cancer has been discussed at length in this Dissertation; the *DAB2IP* promoter has been shown to be hypermethylated and protein levels suppressed in breast cancer cell lines[116]. Therefore we hypothesized that RASAL2 and DAB2IP might have overlapping functions or cooperate to carry out their functions. To begin addressing this possibility we chose to investigate whether RASAL2 and DAB2IP interact in mammary epithelial cells. These data are presented in this Chapter.

Results and Discussion

MECHANISMS OF RASAL2 INACTIVATION IN BREAST CANCER

Epigenetic silencing of *RASAL2*

To begin to investigate whether epigenetic silencing contributes to *RASAL2* inactivation in breast cancer, we assessed the effects of the Polycomb group proteins EZH2 and BMI1 on *RASAL2* expression. We ectopically expressed EZH2 or BMI1 in MCF10A cells and found that RASAL2 protein expression decreased by approximately 55% and 40%, respectively, showing that both EZH2 and BMI1 can suppress *RASAL2* in mammary epithelial cells (Figure 3-1A). To elucidate whether Polycomb proteins are responsible for the low expression of RASAL2 in breast cancer, we acutely inactivated *EZH2* or *BMI1* in a number of breast cancer cell lines with low RASAL2 levels. We found that inactivation of either *EZH2* or *BMI1* resulted in an increase in RASAL2 expression, further supporting our hypothesis that epigenetic silencing contributes to *RASAL2* inactivation in breast cancer (Figure 3-1B).

DNA methylation often follows histone modification and further suppresses gene expression. DNA methylation occurs at CpG islands, often near gene promoter regions. Notably, the *RASAL2* promoter contains a CpG island and thus could be subject to hypermethylation, which also may contribute to gene silencing (Figure 3-1C).

These data show that the Polycomb group proteins EZH2 and BMI1 can repress *RASAL2* expression, and that acute inactivation of either EZH2 or BMI1 can partially reverse this effect, suggesting that EZH2 and BMI1 may contribute to *RASAL2* inactivation in breast cancer. It would be interesting to follow these studies with more detailed biochemical analyses, and with biological studies to explore how central a role *RASAL2* inactivation plays in the oncogenic effects of EZH2 or BMI1 overexpression in breast cancer. We also found that the *RASAL2* promoter contains a CpG island and could be subject to DNA hypermethylation. It would be interesting to determine if the *RASAL2* promoter is hypermethylated in breast cancer tumor tissues and cell lines. Together these studies would deepen our understanding of epigenetic silencing of *RASAL2* in breast cancer, and more broadly how epigenetic regulators act as oncogenes through repression of tumor suppressors.

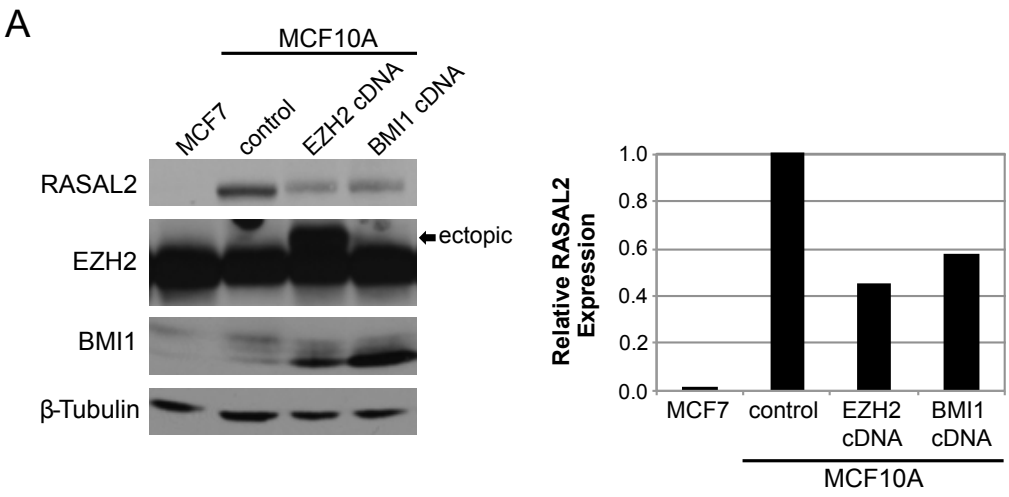

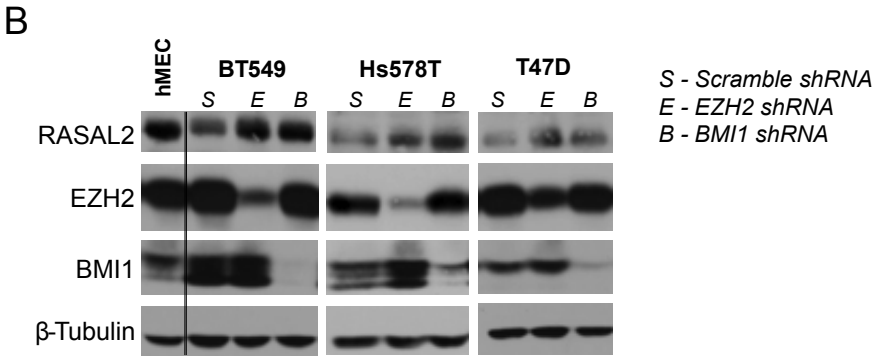

C

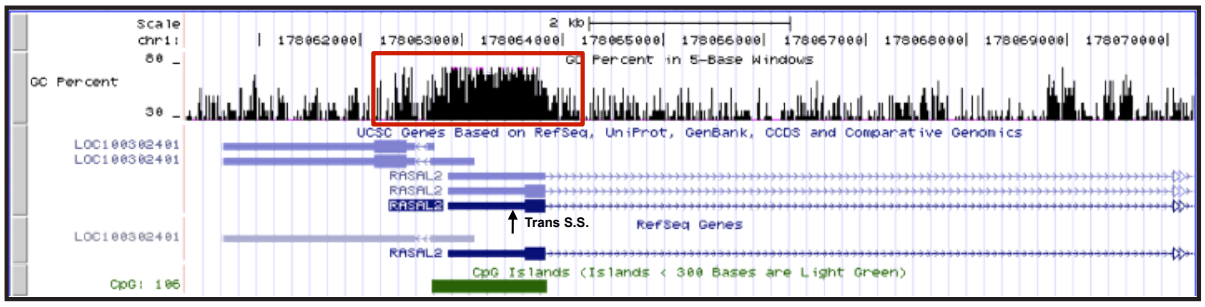

Figure 3-1: Epigenetic silencing of *RASAL2*

(A) Effect of ectopic EZH2 or BMI1 on RASAL2 expression. MCF10A cells were infected with *EZH2* or *BMI1* cDNA or a control; MCF7 cells are a negative control for RASAL2 expression. Western blot shows RASAL2 levels and confirms EZH2 and BMI1 ectopic expression; Arrow marks ectopic (tagged) EZH2. Graph quantifies RASAL2 levels in Western blot.

(B) Effect of *EZH2* or *BMI1* inactivation on RASAL2 expression. Western blot showing RASAL2 levels in BT549, Hs578T, and T47D breast cancer cell lines following acute inactivation of *EZH2* (E) or *BMI1* (B) as compared to a non-targeting "Scramble" shRNA (S). Human mammary epithelial cells (hMEC) are a positive control for RASAL2 expression. Western blot confirms EZH2 and BMI1 knockdown.

(C) *RASAL2* genomic locus (image from UCSC Genome Browser). Red box highlights a CpG-rich region (CpG island) in the *RASAL2* proximal promoter and exon 1. Trans S.S. indicates transcription start site.

However, Polycomb group proteins silence genes by inhibiting transcription; therefore we would expect to see changes in *RASAL2* mRNA expression in breast cancer samples in which *RASAL2* was silenced by this mechanism. We looked extensively at mRNA microarray expression databases (Oncomine, TCGA – The Cancer Genome Atlas), but did not see a decrease in *RASAL2* mRNA expression in breast cancer samples in these databases (nor an inverse correlation between *RASAL2* and *EZH2* or *BMI1*) (data not shown). Therefore we concluded that although epigenetics may play a role in *RASAL2* suppression, as of yet there is no definite link. Many possibilities exist that could explain why we do not see loss of *RASAL2* mRNA expression in publicly available databases. Importantly, as described in Chapter 2 of this Dissertation, we do see loss of RASAL2 protein in breast cancer primary tumors and cell lines. Therefore we chose to explore additional hypotheses of how RASAL2 might be inactivated and, based on the above observations, hypothesized that RASAL2 may be commonly inactivated in cancer via post-transcriptional (specifically post mRNA) mechanisms. We began to pursue this possibility by investigating miRNA-mediated suppression (data suggest that miRNAs may repress expression of target genes through mRNA degradation and suppression of protein translation[318]) and proteasomal degradation. We will next discuss miRNA-mediated suppression of *RASAL2* in breast cancer; in Chapter 4 of this Dissertation we discuss proteasomal degradation.

miRNA-mediated suppression of RASAL2

We used publicly available miRNA prediction algorithms to identify miRNAs predicted to target *RASAL2*, focusing on miRNAs that multiple algorithms predict to target *RASAL2* (to reduce the number of false positives) and on miRNAs that the prediction algorithm TargetScan ranks highly (our unpublished observations suggest that TargetScan predictions are most often accurate[351]) (Figure 3-2A). We then queried the literature to identify miRNAs implicated as breast cancer oncogenes. The intersection of these searches resulted in miRNA candidates

Figure 3-2: miRNA-mediated suppression of RASAL2
(A) Table of miRNAs predicted to target *RASAL2*. Number of miRNA prediction databases that predict each miRNA to target *RASAL2* is indicated. Databases searched were TargetScan, miRanda, PicTar, and microcosm. TargetScan Rank: where within the top 20 miRNAs predicted to target *RASAL2* each miRNA on this list falls. --: not ranked.
(B) Top: Western blot showing RASAL2 expression following transfection of a miR control or miR-135b mimic into MCF10A cells. Bottom: Quantification of Western blot results.
(C) Luciferase reporter system and results. Top: schematic of luciferase reporter construct in which the *RASAL2* 3'UTR follows the *Renilla luciferase* gene. Bottom: Results of luciferase assay, shown as the ratio of renilla to firefly (internal control) luciferase in cells transfected with a miR-135b mimic versus a miR mimic control. EV: empty vector 3'UTR. The *RASAL2* 3'UTR was subcloned into the luciferase reporter vector in two pieces, as diagrammed. Black horizontal bars mark predicted miR-135b consensus recognition sites. RASAL2-1: construct with the 5' half of the *RASAL2* 3'UTR (3 miR-135b consensus sites). RASAL2-2: construct with the 3' half of the *RASAL2* 3'UTR (2 miR-135b consensus sites).
(D) Top: Relative expression of miR-135b in a panel of breast cancer cell lines and normal mammary epithelial cells, as determined by quantitative real-time PCR. Data are shown as average ± SD. Bottom: Western blot showing RASAL2 expression in panel of breast cancer cell lines. Cell lines with relatively high miR-135b and low RASAL2 levels are circled (MCF7, MDA-MB-361).

A

miRNA	Number of Databases	TargetScan Rank
126*	3	--
135a	2	2
135b	2	2
490-3p	2	3
221	2	7
29c	2	9
125a	2	10
125b	2	10
145	2	14
16	2	20
195	2	20
17-3p	2	--

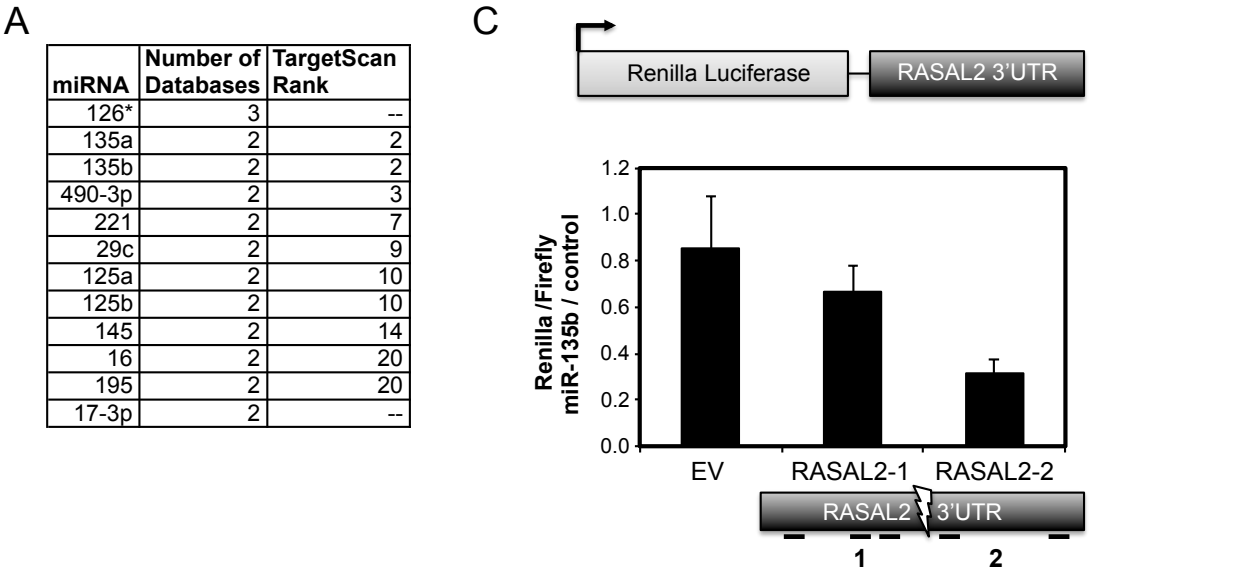

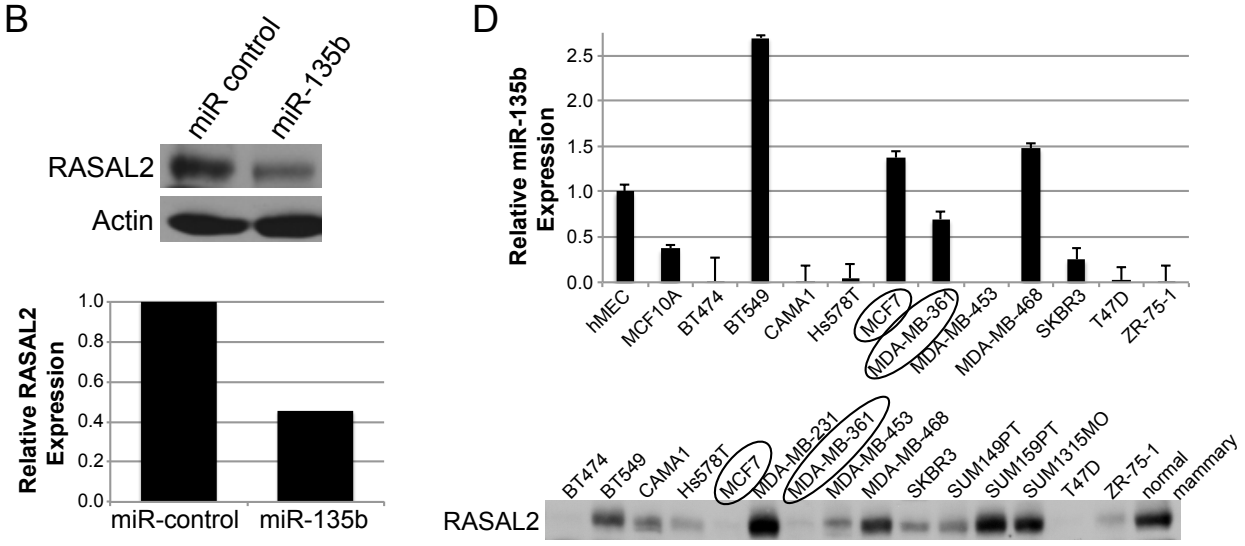

Figure 3-2 (Continued)

implicated as breast cancer oncogenes and predicted to target *RASAL2*. We hypothesized that some of these miRNAs may aberrantly down-regulate *RASAL2* in breast cancer, explaining at least in part how *RASAL2* is inactivated and how the miRNA(s) drive breast cancer. We first focused on miR-135b; miR-135b was predicted to target *RASAL2* by multiple prediction algorithms and TargetScan ranked it highly, and miR-135b had been linked to breast cancer but its important target genes were not known. We ectopically expressed a miR-135b or control miRNA mimic in MCF10A cells, and found that ectopic miR-135b decreased endogenous RASAL2 expression by over 50%, demonstrating that miR-135b can suppress *RASAL2* (Figure 3-2B).

We next wanted to confirm that miR-135b directly targets *RASAL2*. The *RASAL2* 3'UTR contains five predicted miR-135b target sites. We cloned the *RASAL2* 3'UTR, in two approximately 3kb pieces, into a luciferase reporter vector (Figure 3-2C). We transfected the luciferase-*RASAL2*-3'UTR construct (or a control 3'UTR construct) into HeLa cells along with either a miR-135b or control miRNA mimic. We assessed luciferase expression and found that miR-135b specifically decreased expression of luciferase from each luciferase-*RASAL2*-3'UTR construct (interestingly, the second half of the *RASAL2* 3'UTR had a more potent effect) (Figure 3-2C). Based on these data we concluded that miR-135b directly targets the *RASAL2* 3'UTR.

Having shown that miR-135b down-regulates *RASAL2* in mammary epithelial cells, we wanted to explore whether miR-135b contributes to *RASAL2* inactivation in breast cancer. To this end we assessed miR-135b expression in our panel of breast cancer cell lines to determine whether miR-135b and *RASAL2* expression levels inversely correlate overall or in a particular subset of samples. miR-135b expression was high in some cell lines with low RASAL2 (MCF7, MDA-MB-361), suggesting that in these lines miR-135b may contribute to *RASAL2* suppression (Figure 3-2D, circled). Overall, however, there was not a strong inverse correlation between miR-135b and RASAL2 expression. Thus, although miR-135b may contribute to *RASAL2* inactivation in some cases, at this point it is unclear the role it may play *in vivo*; to determine this

we would need tumor samples where we could assess miRNA and protein levels. It also would be interesting to pursue other putative *RASAL2*-targeting miRNAs and to identify which miRNAs might play significant roles in *RASAL2* inactivation in breast cancer.

Prior to the studies presented here, it was unknown how *RASAL2* was inactivated in breast cancer. In this Chapter we demonstrated a possible role for two non-genetic mechanisms. We believe that both mechanisms, and possibly others, may contribute to *RASAL2* inactivation in breast cancer. Precedent exists for tumor suppressor genes to be inactivated in cancer via multiple mechanisms. The RasGAP gene *NF1* is inactivated in glioblastoma via mutation, deletion, and aberrant proteasomal degradation[110], and the RasGAP gene *DAB2IP* is inactivated in prostate cancer via multiple, mainly non-genetic mechanisms [118,121]. Further, we believe that the biology of tumor evolution might promote multiple, particularly non-genetic mechanisms of gene inactivation. I explore these concepts in Chapter 4 of this Dissertation. Finally, we believe that understanding how *RASAL2* is inactivated in breast cancer will allow us to explore potential prognostic indicators or therapeutic avenues.

RASAL2 INACTIVATION COOPERATES WITH ESTROGEN SIGNALING

At least 20% of breast cancer tumor samples and cell lines we have interrogated express significantly reduced RASAL2 levels. Many of these tumors and cell lines are luminal and ERα-positive (Figure 3-3A and Chapter 2). We decided to investigate whether *RASAL2* inactivation might specifically contribute to the biology of ERα-positive breast tumors. However, we first wanted to address the possibility that low RASAL2 in luminal breast cancers simply reflects an absence of *RASAL2* expression in all luminal mammary epithelial cells (and not a specific inactivation of *RASAL2* in cancer). All normal mammary epithelial cell lines in culture are basal-like, so we were not able to look at RASAL2 protein expression in this manner.

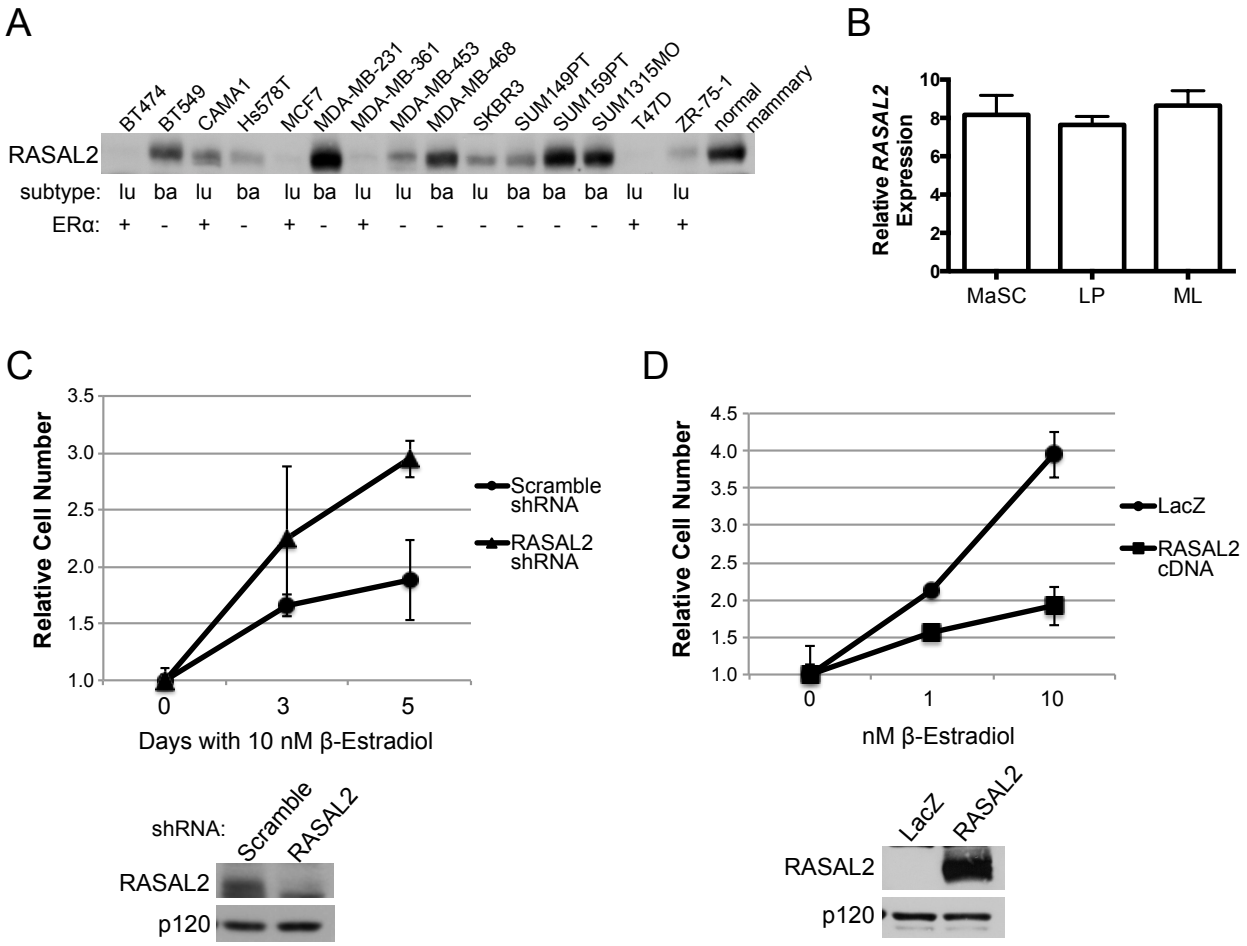

Figure 3-3: *RASAL2* inactivation cooperates with estrogen signaling
(A) RASAL2 expression, breast cancer subtype (lu – luminal, ba – basal), and ERα status in a panel of breast cancer cell lines.
(B) Relative *RASAL2* expression in subsets of sorted human mammary epithelial cells. MaSC: mammary stem cell-enriched (CD49hi EpCAM-). LP: luminal progenitor (CD49f+ EpCAM+). ML: mature luminal (CD49f- EpCAM+)[330].
(C) Growth curve of CAMA1 cells following acute inactivation of *RASAL2* or control (Scramble shRNA). Cells were plated, treated with 10nM β-estradiol, and counted on indicated days. Data are shown as relative cell number ± SD. Western blot below confirms RASAL2 knockdown.
(D) Growth curve of MCF7 cells following ectopic expression of *RASAL2* or *LacZ* cDNA. Cells were plated, treated with 0, 1, or 10nM β-estradiol, and counted on day 5. Data are shown as relative cell number ± SD. Western blot below confirms ectopic RASAL2 expression.

Instead, we assessed *RASAL2* mRNA expression in sorted human mammary epithelial cells and found similar levels of *RASAL2* in a mammary stem cell-enriched population of cells, luminal progenitor cells, and mature luminal cells (Figure 3-3B)[330]. These data suggest that *RASAL2* is expressed to a similar level in different types of mammary epithelial cells; thus we think it is unlikely that *RASAL2* is not expressed in luminal cells, and believe that this finding supports our hypothesis that instead *RASAL2* is inactivated in luminal mammary tumors.

We next asked whether *RASAL2* inactivation cooperates with ERα-driven signaling. We acutely inactivated *RASAL2* in CAMA1 cells (which are ERα-positive) and assessed estrogen-driven proliferation. Indeed, we found that *RASAL2* inactivation accelerated estrogen-driven proliferation (Figure 3-3C). We then ectopically expressed RASAL2 in MCF7 cells (which are ERα-positive and lack RASAL2) and found that ectopic RASAL2 interfered with estrogen-driven proliferation (Figure 3-3D). Notably, RASAL2 does not affect cell proliferation under normal growth conditions (Figure 2-3A). Together these data suggest that *RASAL2* inactivation enhances ERα-driven proliferation in breast cancer cells.

Within the last decade molecular profiling has divided breast cancers into distinct subtypes[197-199]. An important next step for the field is to understand the biology of each subtype and what drives them. What pathways are most important and how can we use this information to better design therapeutic strategies?

RASAL2 is a RasGAP, a negative regulator of Ras. We believe that *RASAL2* inactivation contributes broadly to breast cancer at least in part via its promotion of Ras signaling. Here we showed that *RASAL2* expression is low in many ERα-positive breast cancer cell lines and that *RASAL2* inactivation cooperates with estrogen to promote proliferation in these cells. This cooperation could occur via ERK and AKT phosphorylation and activation of ERα, events that have been shown to occur[186-188], which would lead to increased ERα-driven

transcription and proliferation. This also could occur via a novel mechanism, either downstream of Ras or independently. These findings imply that *RASAL2* inactivation may have a particularly potent impact in ERα-positive tumors due to the dual effects of *RASAL2* inactivation on the Ras pathway and ERα signaling. It would be very interesting to delve further into these possibilities, in part because of potential implications for resistance to endocrine therapy, a concept that will be discussed in more detail in Chapter 4 of this Dissertation.

THE RASGAPS RASAL2 AND DAB2IP INTERACT

The RasGAPs RASAL2 and DAB2IP share the same domain organization and thus are in the same RasGAP subfamily. We noticed that in addition to their homologous PH, C2, and RasGAP domains, the extreme C-termini of RASAL2 and DAB2IP are highly homologous (71%, Figure 3-4A). This region does not comprise a previously annotated domain, however, we discovered that it is predicted to form hydrophobic coiled-coils (Figure 3-4B). Interestingly, the RasGAP CAPRI homodimerizes via a similar C-terminal coiled-coil domain[147]. Thus, we hypothesized that the RasGAPs RASAL2 and DAB2IP might heterodimerize via their homologous C-terminal coiled-coil domains in mammary epithelial cells, and that this could be important for protein function. We immunoprecipitated endogenous RASAL2 from MCF10A cells and found that it co-immunoprecipitated endogenous DAB2IP, whereas control immunoprecipitations (p120RasGAP, pre-immune serum) did not (Figure 3-4C). The same immunoprecipitation performed on MCF10A cells in which *RASAL2* had been acutely inactivated largely failed to co-immunoprecipitate DAB2IP, showing that DAB2IP immunoprecipitates with RASAL2 and not non-specifically (Figure 3-4C). We performed a reciprocal co-immunoprecipitation and confirmed that endogenous DAB2IP pulls down endogenous RASAL2 (Figure 3-4D). Together these data show that endogenous RASAL2 and DAB2IP interact in mammary epithelial cells.

Figure 3-4: RASAL2 and DAB2IP interact
(A) Top: Schematic of RASAL2 and DAB2IP domain organization. Each contains a pleckstrin homology (PH) domain, a C2 domain, and a RasGAP domain, as indicated. DAB2IP also has a Period-like domain (Per). The extreme C-termini of RASAL2 and DAB2IP are highly homologous (checkered box). Bottom: Alignment of RASAL2 and DAB2IP extreme C-termini (http://www.ebi.ac.uk/Tools/msa/clustalw2/). * - identical amino acid, : - highly similar amino acid.
(B) Extreme C-termini of RASAL2 (and DAB2IP, data not shown) are predicated to form coiled-coils. Data from http://embnet.vital-it.ch/software/COILS_form.html
(C) Co-immunoprecipitation of RASAL2 and DAB2IP from MCF10A cells. Left: Western blot of co-immunoprecipitation. Top indicates antibody used for immunoprecipitation (IP), left indicates antibodies used to probe Western blot. Right: Western blot of whole cell extracts. Two right-most lanes of both IP (left panel) and whole cell extract (right panel) Western blots are from MCF10A cells infected with shRNAs targeting *RASAL2* (shR2) or control "Scrambled" shRNA (shScr).
(D) Reverse co-immunoprecipitation in MCF10A cells. IP antibody listed on top, Western blot antibody listed on left. RASAL2 and DAB2IP co-immunoprecipitate each other; p120RasGAP does not.
(E) Truncation of RASAL2 abolishes the RASAL2-DAB2IP interaction. N-terminal HA-tagged *LacZ*, *RASAL2* or *RASAL2* truncation mutant (Y1180X) cDNAs were expressed in MCF10A cells. Left: Western blots probed for HA and DAB2IP following immunoprecipitation with an HA antibody. Right: whole cell extracts confirming expression of constructs. endog: endogenous RASAL2; FL: full length (wildtype) cDNA; Y1180X: RASAL2 truncation mutant cDNA.

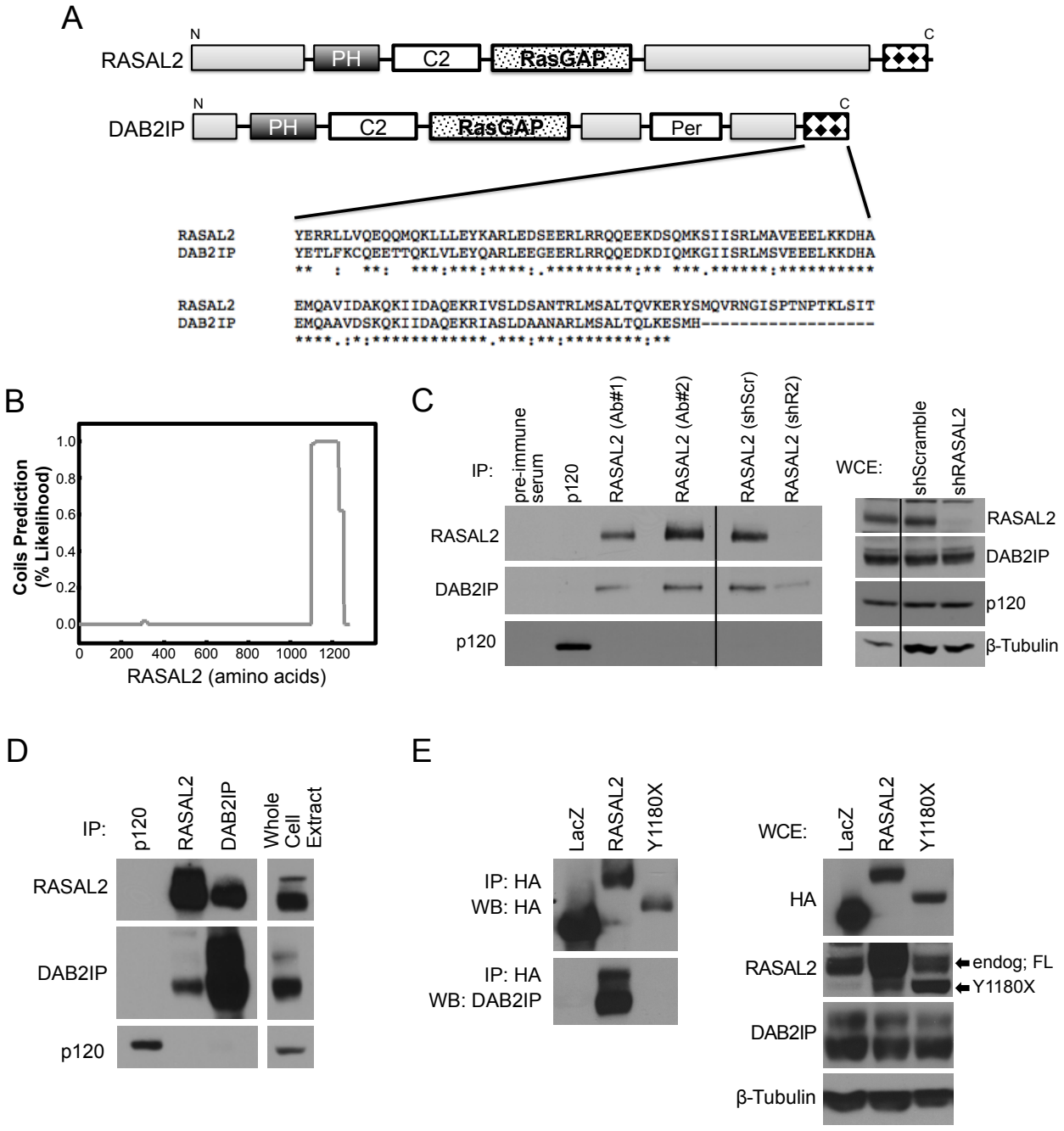

Figure 3-4 (Continued)

We next tested our hypothesis that dimerization occurs via the homologous C-terminal coiled-coil region. We generated a truncation mutant of *RASAL2* that terminates immediately preceding this region. We expressed wildtype or truncated *RASAL2* cDNAs in MCF10A cells and immunoprecipitated exogenous RASAL2 by its N-terminal HA tag. We found that while wildtype RASAL2 co-immunoprecipitated DAB2IP, the RASAL2 truncation completely abolished DAB2IP co-immunoprecipitation (Figure 3-4E). These data show that RASAL2 interacts with DAB2IP via its C-terminal hydrophobic coiled-coil domain.

Together, these data strongly suggest that RASAL2 and DAB2IP interact in mammary epithelial cells. To our knowledge this is the first example of RasGAP-RasGAP heterodimerization. This finding raises many exciting questions about RASAL2 and DAB2IP, with potential implications for the whole gene family.

With the knowledge that RASAL2 and DAB2IP interact, it would be interesting to explore the biochemistry of the interaction: What is the stoichiometry of the interaction? Does either protein also homodimerize? Under what conditions do they heterodimerize? It also would be very interesting and important to explore the biology of the interaction: Is the interaction necessary or sufficient for RasGAP activity? For tumor suppressor function? DAB2IP inhibits NF-κB as well as Ras[121]; might *RASAL2* inactivation also increases NF-κB signaling, perhaps through DAB2IP? Given the strong connection between *DAB2IP* inactivation and metastasis via NF-κB, the RASAL2-DAB2IP interaction suggests that RASAL2 loss might promote metastasis via DAB2IP and NF-κB. We return to this hypothesis in Chapter 4 of this Dissertation. Finally, in this Chapter we also identified the RASAL2-DAB2IP interaction domain. This will provide a useful tool to address the above-stated questions.

Increasing evidence indicates that the RasGAPs are an important class of human tumor suppressor genes. There are fourteen human RasGAP genes, many of which are expressed in

the majority of tissue types. One important question is if and how RasGAPs cooperate in their functions. In this Chapter we showed that the RasGAPs RASAL2 and DAB2IP do indeed interact. These findings have clear implications for RASAL2 and DAB2IP biology, as mentioned above, and imply a potential role for RasGAP dimerization throughout the gene family. It will be important to consider potential RasGAP-RasGAP interactions and their functional consequences as we expand our studies of RasGAPs in cancer.

Materials and Methods

Cell Culture

MCF7 and MCF10A cells were purchased from ATCC. BT549, Hs578T, and T47D cells were obtained from Dr. William Hahn (Dana-Farber Cancer Institute), and CAMA1 cells from Dr. Marcia Haigis (Harvard Medical School). Cell lines were cultured according to published protocols. For estrogen-driven proliferation assays, cells were cultured in phenol red-free media with charcoal/dextran-treated Fetal Bovine Serum (HyClone). Cells were plated in triplicate in 6-well plates and treated the following day with indicated concentrations of β-estradiol (Sigma) or ethanol for the indicated number of days.

DNA Constructs, Transfections, and Infections

Endogenous proteins were inactivated using short-hairpin RNAs (shRNAs) from The RNAi Consortium (Broad Institute, MIT) with the following target 21-mer sequences: RASAL2 5'-CCCTCGTGTTCTTGCTGATAT-3', EZH2 5'-TATTGCCTTCTCACCAGCTGC-3', and BMI1 5'-CGGAAAGTAAACAAAGACAAA-3'. A scrambled non-silencing shRNA was purchased from Addgene 5'-CCTAAGGTTAAGTCGCCCTCG-3' [343]. The Mammalian Gene Collection fully sequenced human *RASAL2* cDNA was purchased from Open Biosystems (cat. # MHS4426-99623118) and cloned into the pHAGE-N-Flag-HA lentiviral expression vector (Dr. J. Wade Harper, Harvard Medical School) for expression in cell lines. The *RASAL2* cDNA was

mutagenized using QuikChange II Site-Directed Mutagenesis kit, according to the manufacturer's instructions (Agilent). The *EZH2* cDNA was cloned into the pBabe-myc retroviral vector for expression in cell lines[121]. The *BMI1* cDNA was obtained from the Orfeome collection and cloned into the pBabe retroviral vector for expression in cell lines.

shRNA or cDNA vectors along with viral packaging plasmids delta 8.2 and VSVG were transfected into 293T cells using Fugene6 (Roche), following the manufacturer's instructions. Virus supernatant was harvested after 48 hours, filtered through a 0.45μm filter, and incubated on target cells for 6 hours at a 1:2-1:10 dilution with 8μg/ml polybrene. Infected cells were selected in 0.5-2.0μg/ml puromycin, as optimized for each cell line.

miRNAs mimics and U6 snRNA control were purchased from Dharmacon and transfected into MCF10A cells using Dharmafect 1 transfection reagent. Dharmafect 1 was incubated in OptiMEM and then incubated with 50nM miRNA mimic or U6 control. The miRNA/Dharmafect mixture was added to a suspension of MCF10A cells and plated at 400,000 cells per well in 6-well plates. Protein was harvested 48-72 hours post transfection.

Luciferase Assays

The psicheck-2 vector (Promega) was modified by replacing the SV40 promoter with the mouse PGK promoter using the BglII and NheI sites, in order to reduce *Renilla* mRNA expression to more physiological levels. The *RASAL2* 3'UTR was divided into two overlapping fragments, covering base pairs 1-2899 (RASAL2.1) and base pairs 2875-6268 (RASAL2.2) and amplified by RT-PCR, then cloned into the *Renilla* 3'UTR using the NotI and XhoI sites. The plasmids were co-transfected with miR-135b or control miRNA mimics into HeLa cells using Lipofectamine, and luciferase activity was tested 48 hours post transfection with the Dual-Luciferase Reporter Assay System (Promega) as per the manufacturer's instructions. *Renilla*

luminescence was normalized to an internal control (*Firefly*) and test transfections were normalized to the control mimic transfections.

TaqMan Analysis of miRNA Levels

Total RNA was isolated from breast cancer cell lines using Trizol reagent, following the manufacturer's instructions (Invitrogen). Reverse transcription and real-time PCR were carried out using TaqMan MicroRNA Reverse Transcription Kit and TaqMan MicroRNA Assays, according to the manufacturer's instructions (Applied Biosystems).

Immunoprecipitation, Protein Lysates, and Western Blot Analyses

For immunoprecipitations (IP), MCF10A cells were lysed in ice-cold CHAPS buffer with protease inhibitor tablets (Roche). Lysates were normalized and an aliquot removed for whole cell lysate analysis. Lysates were pre-cleared with protein A beads and incubated with pre-mixed IP antibody and protein A beads overnight at 4°C. Beads were pelleted and washed before separating by polyacrylamide gel electrophoresis.

Whole cell protein extracts were isolated from cells in 1% SDS boiling lysis buffer. Protein lysates were quantified and separated on polyacrylamide gels. Western blots were probed following validated procedures using the following antibodies: Actin (Sigma cat. # A2066), BMI1 (Millipore cat. # 05-637), DAB2IP (Abcam cat. # 87811), EZH2 (BD cat. # 612666), GAPDH (Cell Signaling cat. # 2118), HA (Covance cat. # MMS-101P), p120RasGAP (BD Transduction Laboratories cat. # 610040), and β-Tubulin (Sigma cat. # T4026). A peptide antigen (NP_773793 amino acids 1111-1130) was used to generate and affinity purify an anti-RASAL2 rabbit polyclonal antibody (Covance ImmunoTechnologies).

Page intentionally left blank

Chapter 4

Conclusion and Future Directions

Conclusion

The goal of this Dissertation was to elucidate whether any additional RasGAP genes function as tumor suppressors in sporadic cancer. Indeed, we discovered that a previously uncharacterized RasGAP gene, *RASAL2*, is a tumor and metastasis suppressor in breast and possibly other cancers. We identified *RASAL2* as a candidate tumor suppressor gene through a cell-based screen, and chose to focus on its role in breast cancer based on the lack of *RAS* mutations in this tumor type, the potential importance of the Ras pathway in breast cancer, and the presence of RasGAP domain mutations in *RASAL2* in breast tumors.

We confirmed that RASAL2 is a functional RasGAP and showed that it acts as a tumor suppressor: ectopic RASAL2 suppresses anchorage-independent growth *in vitro* and tumor formation *in vivo* and, conversely, inactivation of *RASAL2* promotes anchorage-independent growth *in vitro*, xenograft tumor formation *in vivo*, and tumorigenesis in *Rasal2*-null genetically engineered mouse models. We also discovered that inactivation of *RASAL2* promotes cell migration, invasion, tumor progression, and, strikingly, widespread metastasis in multiple genetically engineered mouse models, including a mammary tumor model. We found that *RASAL2* expression is lost in primary human breast tumors, with greatest loss in metastatic lesions, providing strong support that RASAL2 loss contributes to human breast cancer development and metastasis. Additionally, we discovered that the Ras pathway is hyperactivated in mammary tumors that lost *Rasal2* through genetic deletion or spontaneous loss; these findings suggest that RASAL2 loss activates the Ras pathway and represents one mechanism by which the pathway is activated in, and contributes to, breast tumorigenesis and metastasis.

Although mutations in *RASAL2* do occur at a low frequency in human breast tumors, our human tumor and cell line data suggest that *RASAL2* is inactivated more frequently than indicated by mutation analysis alone, implying that *RASAL2* may be inactivated more commonly by non-genetic mechanisms. Indeed, we found that both epigenetic silencing and miRNA-

mediated suppression may contribute to *RASAL2* inactivation in breast cancer. These findings support our broader hypothesis that tumor suppressor RasGAPs are commonly inactivated in human cancer via non-genetic mechanisms.

Finally, we discovered that RASAL2 interacts with another tumor suppressor RasGAP, DAB2IP, in mammary epithelial cells. This finding suggests that RASAL2 and DAB2IP may act in concert in their tumor and metastasis suppressor functions.

Together, our human tumor, mouse modeling, and cell culture data strongly support our conclusion that *RASAL2* is the newest tumor and metastasis suppressor in the RasGAP gene family. Our findings further provide support to what we view as three important, emerging concepts. First, that the Ras pathway plays a key role in breast tumorigenesis and metastasis, and becomes hyperactivated as a result of *RASAL2* inactivation. Second, that epigenetic and non-genetic repression of tumor suppressor genes is a common mechanism of their inactivation in cancer. And third, that multiple RasGAPs are human tumor suppressors and may function together to carry out their tumor suppressive activities.

Future Directions

Mechanisms of *RASAL2* inactivation in breast cancer

Currently available data suggest that *RASAL2* mutations occur in 1-4% of breast cancers[46,328,329]. However, as reported in Chapter 2 of this Dissertation, we found that RASAL2 protein is lost in at least 20% of breast cancer primary tumor tissues and cell lines. Thus, we believe that the *RASAL2* mutation rate underrepresents the frequency with which *RASAL2* is inactivated in breast cancer, and raises the question of how *RASAL2* is commonly inactivated. In Chapter 3 of this Dissertation we began to investigate two possible mechanisms of inactivation. First, we explored epigenetic silencing; we found that EZH2 and BMI1 can suppress *RASAL2* expression and that inactivation of EZH2 or BMI1 increases *RASAL2* expression. Among possible next steps, it would be important to determine whether EZH2 or

BMI1 can be found at the *RASAL2* promoter, and to determine whether re-expression of RASAL2 can rescue phenotypes induced by EZH2 or BMI1. However, as noted in Chapter 3 of this Dissertation, in contrast to our finding of RASAL2 protein loss in at least 20% of breast cancer samples, publicly available mRNA expression databases do not indicate loss of *RASAL2* mRNA in breast tumor samples as compared to normal mammary tissue. We would expect mRNA and protein levels to be suppressed by EZH2 or BMI1-mediated silencing; thus it remains unclear how significant a role Polycomb group protein mediated silencing may play in RASAL2 suppression in human tumors. We therefore began to explore additional possible mechanisms of *RASAL2* inactivation in breast cancer.

In Chapter 3 of this Dissertation we initiated an investigation into whether miRNAs might suppress *RASAL2* in breast cancer, and presented preliminary data on one miRNA, miR-135b. Many miRNAs are predicted to target *RASAL2* and have been implicated as breast cancer oncogenes; it would be important to functionally test more candidate miRNAs to more thoroughly explore how miRNA regulation contributes to *RASAL2* inactivation in breast cancer. Furthermore, it will be important to obtain human tissue samples in which we can assess expression levels of RASAL2 (protein) and miRNAs.

It also will be important to consider additional mechanisms of inactivation, in particular proteasomal degradation. The RasGAP neurofibromin is aberrantly degraded by the proteasome in glioblastoma[110]. Additionally, many other well-known tumor suppressor genes, including *TP53, PTEN,* and *CDKN1B* (p27), are inactivated in cancer partially via proteasomal degradation[88,280,352]. We hypothesize that RASAL2 also could be subject to aberrant proteasomal degradation in sporadic cancer. Our preliminary analysis in breast cancer cell lines indicates that proteasomal degradation may play a role in RASAL2 inactivation in some cases (data not shown), and warrants further investigation into this hypothesis.

The *RASAL2* gene is located on chromosome 1q (1q24). The 1q chromosome arm often undergoes copy number gain in breast and other cancers[166,167], and there is no evidence

of focal deletion of *RASAL2*. Thus, genomic loss is not likely to contribute to *RASAL2* inactivation in breast cancer. Further, the copy number gain of 1q raises an intriguing hypothesis. Perhaps in tumors cells with 1q gain, only cells that evolve a means to suppress or at least not overexpress *RASAL2* are able to grow and progress as a tumor. In order to test this hypothesis we would want to determine whether *RASAL2* is specifically suppressed or not overexpressed in tumors with 1q gain, for example in comparison to other genes on the 1q amplicon.

Our hypothesis of 1q copy number gain and subsequent suppression of *RASAL2* fits well with the potential mechanisms of inactivation suggested by our preliminary data (epigenetics, miRNAs, proteasomal destruction), and with our understanding of how tumor cells avoid or escape a phenomenon called oncogene induced senescence. Oncogene induced senescence is a natural tumor suppressive mechanism that exists within cells[353]. Upon expression of an oncogene, such as mutant Ras, cells undergo a burst of proliferation followed by an irreversible growth arrest[354]. Importantly, the signals that activate oncogene induced senescence are sensitive to levels of the oncogenic stimulus. For example, overexpression of oncogenic Ras in mammary epithelial cells triggers oncogene induced senescence, whereas low-level expression of the same oncogene does not trigger senescence and instead drives proliferation[355]. Thus, a gradual increase in Ras signaling as a result of a gradual suppression of *RASAL2*, such as in response to gradually increasing EZH2 levels (which data has shown occurs in breast and other tumors[122,300]), might allow the tumor to grow and evade oncogene induced senescence. It would be very interesting to explore this hypothesis. Notably, this hypothesis could be true whether or not *RASAL2* is specifically suppressed in tumors with 1q copy number gain, and vice versa.

Biochemical analysis of RASAL2

Before the work presented in this Dissertation, *RASAL2* was a completely uncharacterized gene beyond its indirectly determined activity as a RasGAP[165]. We have confirmed that RASAL2 is a functional RasGAP and have demonstrated its biological importance in suppressing tumorigenesis and metastasis. Many questions remain regarding RASAL2 structure and function, a more detailed understanding of which will aid our understanding of RASAL2 biology. We know that RASAL2 is a functional RasGAP, however, it will be important to determine which Ras isoform(s) RASAL2 most potently regulates. Our preliminary data suggest that RASAL2 may regulate both H- and K-Ras (data not shown). Data suggest that a number of RasGAPs (SYNGAP1, RASAL1, CAPRI, and GAP1IP4BP) also function as RapGAPs[127,146]. It would be interesting to explore whether RASAL2 also has activity against Rap.

RASAL2 contains pleckstrin homology (PH) and C2 domains. It would be informative to determine the function of these domains, in particular whether RASAL2 is a calcium-regulated RasGAP. Many RasGAPs contain C2 domains; some but not all C2-domain containing RasGAPs are calcium-sensitive[126,148,149]. It also will be important to determine RASAL2's subcellular localization, which may be determined in part by its PH domain; this may help answer questions about protein function and protein-protein interactions.

Finally, it would be interesting to investigate whether RASAL2 expression and function are cell cycle regulated. The RasGAP neurofibromin is cell cycle regulated via proteasomal degradation; neurofibromin destruction plays a key role in Ras pathway activation and entry into the G1 phase of the cell cycle[25]. It remains an open question whether RASAL2 (or any other RasGAP) also is regulated by the cell cycle.

Novel functions of RASAL2

In this Dissertation we showed that RASAL2 is a functional RasGAP. An exciting and as of yet unexplored possibility is that RASAL2 also possesses non-RasGAP activities.

Suggestions in the literature, our unpublished findings, and precedent from other RasGAPs all support this hypothesis. Two published large-scale co-immunoprecipitation/mass-spectrometry studies have identified putative RASAL2-interacting proteins. Bouwmeester et al. found RASAL2 to co-immunoprecipitate with the inhibitor of NF-κB, IκB-β[169]. We find this putative interaction especially intriguing because precedent exists for tumor suppressor RasGAPs to co-regulate the Ras and NF-κB pathways: DAB2IP suppresses both Ras and NF-κB and both functions are critical for the potent tumor suppressive effects of DAB2IP in the prostate[121]. It will be exciting to pursue Bouwmeester et al.'s finding, and if the interaction between RASAL2 and IκB-β is confirmed, to characterize the interaction and elucidate its biological effects. Second, Jin et al. reported that RASAL2 co-immunoprecipitates with 14-3-3 γ[170]. 14-3-3 proteins are abundant cellular proteins with diverse roles to facilitate protein-protein interactions, affect protein subcellular localization, and stabilize phospho-protein conformations[170]. The 14-3-3 γ-RASAL2 interaction was reported in HEK293 cells. We would want to determine whether these proteins interact in mammary epithelial cells, and to assess the impact of 14-3-3 γ binding on RASAL2 subcellular localization, other protein-protein interactions, and function.

A collaborator's unpublished findings suggest that RASAL2 also may interact with the proteins MCC and USHBP1[356]. MCC (mutated in colorectal cancer) and USHBP1 (Usher syndrome 1C binding protein 1, also called MCC2) are related proteins thought to have tumor suppressive functions in the colon, perhaps via negative regulation of the cell cycle[357,358]. Using a combination of proteomics and bioinformatics approaches, our collaborators sought to identify proteins that interacted with both MCC and USHBP1. One of their top hits was RASAL2, indicating that RASAL2 interacts with MCC and USHBP1, either together or separately. Surprisingly, another top hit was DAB2IP, suggesting that RASAL2 and DAB2IP may complex together with these proteins, or that RASAL2 and DAB2IP could substitute for each other in binding MCC and USHBP1. In light of our findings that RASAL2 and DAB2IP interact with each

other (Chapter 3), we hypothesize that a complex may form containing RASAL2, DAB2IP, MCC, and USHBP1. Whether this complex exists and what function it has are exciting questions waiting to be answered.

As a complementary means to interrogate novel functions of RASAL2, it could be revealing to take an unbiased approach, namely via microarray analysis and immunoprecipitation/mass-spectrometry. Microarray analyses comparing control and *RASAL2* knockdown cells would uncover signaling pathways altered upon *RASAL2* inactivation. We would expect to see up-regulation of the Ras pathway, but anticipate that other pathways might also be up- or down- regulated. In parallel we also could immunoprecipitate RASAL2 from cells (particularly from mammary epithelial cells where we know RASAL2 functions) and use mass spectrometry to identify novel RASAL2-interacting proteins, possibly confirm the above-mentioned putative RASAL2-interacting proteins, and point to potential signaling pathways that RASAL2 affects.

We anticipate that RASAL2 possesses non-RasGAP activities, and expect that the targeted and unbiased approaches described above will uncover new function(s). Importantly, a precedent exists for RasGAPs to act as signaling scaffolds, controlling multiple pathways. Our laboratory showed that the RasGAP DAB2IP negatively regulates both Ras and NF-κB signaling and that DAB2IP is a potent tumor and metastasis suppressor in the prostate because of its ability to critically regulate both pathways[121]. The *NF1* gene encodes a nearly 3000-amino acid protein, only 10% of which comprises annotated domains. However, neurofibromatosis type I patients present with mutations that span the *NF1* gene[105]. Together these data suggest that NF1 also has non-RasGAP functions, a hypothesis supported by our laboratory's unpublished findings. Notably, NF1 and DAB2IP are the only RasGAPs confirmed to be human tumor suppressors (before our identification of RASAL2). However, as detailed in Chapter 1 of this Dissertation, most of the 14 human RasGAPs possess catalytic GAP activity; why certain RasGAPs are tumor suppressors and others are not remains an open and very interesting

question. Many factors could contribute, including RasGAP expression pattern, subcellular localization, and target Ras protein(s). However, we hypothesize that another important factor may be whether a RasGAP gene possesses additional non-RasGAP activities such that it coordinately regulates Ras as well as another critical signaling pathway in the cell. We expect that future studies of RASAL2 and NF1 non-RasGAP functions as well as further characterization of other RasGAPs, will help test this hypothesis and elucidate what makes a RasGAP a tumor suppressor.

RASAL2-DAB2IP interaction and function

In this Dissertation we report for the first time that the RasGAPs RASAL2 and DAB2IP interact. This exciting finding raises many questions regarding how RASAL2 and DAB2IP each function, with implications for the RasGAP gene family as a whole; I will discuss a selection of these questions here. The most important next step in studying this interaction will be to investigate its biological consequences. Is the interaction necessary and/or sufficient for the tumor suppressive functions of each protein? Does heterodimerization impact the RasGAP activity of either RASAL2 or DAB2IP? DAB2IP also inhibits the NF-κB pathway, therefore it also will be important to assess whether heterodimerization impacts DAB2IP's effects on NF-κB signaling (and potentially on metastasis, as discussed further below). In this Dissertation we determined that RASAL2 and DAB2IP interact via a highly homologous coiled-coil region at the proteins' C-termini, and generated a truncation mutation in RASAL2 that abolishes heterodimerization. The heterodimerization mutant should prove to be a useful tool for future dissection of the biochemistry and biology of the interaction.

RASAL2 and DAB2IP both have been implicated as tumor suppressors in breast cancer (our work presented in this Dissertation – RASAL2, Dote et al. – DAB2IP[116]). This, in combination with knowledge of the RASAL2-DAB2IP interaction in mammary epithelial cells,

evokes many possible scenarios for how the proteins might function. Does loss of either RASAL2 or DAB2IP promote tumorigenesis? Metastasis? Is loss of both proteins required for either process? It will be exciting to answer these questions. Further, lessons learned regarding how RASAL2 and DAB2IP function together in breast cancer may be applicable to RASAL2 and DAB2IP in other tumor types, and possibly to other RasGAPs whose functions might be affected by heterodimerization.

Lastly, it also is important to note that future experiments assessing novel functions of RASAL2 (discussed above) will need to consider that novel functions may result from direct actions of RASAL2 or indirectly via RASAL2 binding to DAB2IP.

Signaling in *MMTVneu*; *Rasal2* compound mutant mice

Neu (HER2) is a receptor tyrosine kinase that signals through the Ras pathway. A very simplified model might suggest, therefore, that *HER2* overexpression and *RASAL2* loss might be redundant and together might have the same phenotype as either alteration individually. However, our mouse model data presented in Chapter 2 of this Dissertation clearly show that this is not true, as double mutant compound mice are subject to a significantly greater metastasis burden than *MMTVneu* controls. Many possibilities exist as to how *HER2* overexpression and *RASAL2* loss cooperate. First, both HER2 and RASAL2 likely have functions that are non-redundant. HER2 does signal through the MAPK and PI3K pathways; however, it also activates other downstream effectors, such as the Jak/STAT pathway[218]. Further, as discussed in this Chapter, we hypothesize that RASAL2 may have non-RasGAP activities, such as activating the NF-κB pathway. Second, even within the same signal cascade, we believe that *HER2* overexpression and *RASAL2* loss might cooperate. *HER2* overexpression drives signaling through the pathway; however, negative regulators of the pathway, such as RASAL2, still could lessen pathway throughput, and many studies have demonstrated that flux through the pathway affects biological outcome[359,360]. Thus, losing

RASAL2 might be necessary for HER2 to fully activate the MAPK and PI3K pathways. We expect that this may be particularly important for promoting metastasis, as *MMTVneu*; *Rasal2* compound mutant mice specifically develop a more severe metastatic phenotype.

Mechanism of metastasis potentiation upon *RASAL2* loss

The mouse models presented in this Dissertation revealed a striking increase in metastasis upon *Rasal2* loss. It would be interesting to determine the mechanism(s) by which *Rasal2* loss drives metastasis. The contribution of the Ras pathway to cancer metastasis remains an open question; moreover, RASAL2 may or may not have additional, non-RasGAP functions. Therefore, it will be very interesting to determine whether *RASAL2* inactivation drives metastasis through its activation of the Ras pathway and/or via other mechanisms. The NF-κB pathway is a known driver of metastasis[361]. One hypothesis is that *RASAL2* loss drives metastasis via activation of NF-κB, either directly such as via binding of IκB-β, or indirectly, via DAB2IP and its well-established regulation of NF-κB signaling[121].

If the Ras pathway contributes to metastasis following *Rasal2* loss, it would be interesting to determine which effector pathways downstream of Ras play a critical role in this process. Such insights would have potential therapeutic benefits as well. Ras itself is not currently druggable[32], but many drugs exist that target Ras effector pathways, such as rapamycin which inhibits mTOR (PI3K pathway), and PD-901 which inhibits MEK (MAPK pathway). It would be important to identify the downstream effectors that drive metastasis in order to design a therapeutic strategy to target the key pathway(s); notably, our laboratory has used this strategy successfully: our laboratory identified mTOR as the critical Ras effector pathway in MPNST development and used this knowledge to design what proved to be a successful therapeutic strategy of rapamycin treatment[102,103]. In this Dissertation I showed that *Rasal2* loss drives metastasis not only of breast tumors but also from numerous sporadic

tumors that *Trp53 +/-; Rasal2* compound mutant mice develop. It would be interesting to assess whether the same or different pathways drive metastasis in these settings.

RASAL2 loss and resistance to anti-estrogen or anti-HER2 therapies

Resistance to targeted therapy for breast cancer remains a major outstanding problem in the clinic. Nearly one-third of women who present with ERα-positive breast cancer and are treated with the standard five years of tamoxifen therapy relapse with endocrine-resistant disease[185]. Importantly, given the high fraction of breast cancers that are ERα-positive, patients with endocrine resistant disease represent nearly one-quarter of all breast cancer cases. Mechanisms of resistance are not well understood, but one proposed mechanism involves up-regulation of receptor tyrosine kinases or activation of the Ras, MAPK, and PI3K pathways[362]. Cell culture studies suggest that PI3K and MAPK signaling can confer resistance to endocrine therapy through ligand-independent activation of ERα (AKT and ERK each can phosphorylate and activate ERα and can do so in the absence of estrogen[186-188]) and/or through activation of canonical PI3K and MAPK transcriptional targets that promote proliferation and survival independently of ERα[185,363]. However, whether these proposed mechanisms cause resistance in patients remains unclear[185]. Given that *RASAL2* inactivation stimulates the MAPK and PI3K pathways, and that *RASAL2* inactivation contributes to ERα-driven proliferation (perhaps via AKT or ERK-mediated phosphorylation of ERα, or via a novel mechanism) as shown in Chapter 3 of this Dissertation, we hypothesize that *RASAL2* inactivation in ERα-positive breast cancers may be a mechanism by which endocrine resistance develops. It would be exciting to explore this possibility; clarifying mechanisms of endocrine resistance that occur in women with ERα-positive breast cancer could help suggest ways to treat endocrine resistant disease more effectively.

HER2-overexpressing breast cancers are aggressive and have poor prognoses[203]. Anti-HER2 targeted therapies currently used in the clinic include trastuzumab, a monoclonal antibody that binds HER2[220-222], and lapatinib, an dual EGFR/HER2 kinase inhibitor[223-225]. Although tumors generally respond well to these therapies, the majority of tumors relapse within one year of treatment, and 15% are *de novo* resistant[364,365]. Proposed mechanisms of resistance to anti-HER2 breast cancer therapy include signaling through other ERBB receptor tyrosine kinases and alternative mechanisms that activate signaling pathways downstream of HER2[208,219]. (ERα expression and signaling is another major proposed mechanism of resistance.) In particular, studies have implicated Ras, MAPK, and PI3K signaling in anti-HER2 resistance. The PI3K pathway has been shown to confer resistance to both lapatinib and trastuzumab, and it has been proposed (but not proven) that the PI3K pathway may become activated in human tumors via *PIK3CA* mutation or *PTEN* loss[366-368]. Further, unpublished data from a collaborator demonstrated that oncogenic Ras confers resistance to lapatinib in *HER2*-overexpressing breast cancer cell lines[369]. Oncogenic Ras also confers resistance to anti-EGFR therapies in a number of tumors types[370]. Based on these findings, the dearth of *RAS* mutations in breast cancer, and the role that we believe *RASAL2* inactivation plays in this tumor type, we hypothesize that *RASAL2* inactivation may be a mechanism by which *HER2*-overexpressing breast cancers acquire resistance or are *de novo* resistant to anti-HER2 therapies. Notably, our *MMTVneu*; *Rasal2 -/-* mouse model provides a unique tool to study HER2 resistance and to test this hypothesis. Finally, it is important to mention that mechanisms of resistance to anti-HER2 therapies could differ depending on the specific therapy[227].

RASAL2 inactivation in other sporadic cancers

The majority of the work presented in this Dissertation focuses on *RASAL2* inactivation in breast cancer. However, our data suggest that *RASAL2* inactivation might also contribute to other sporadic cancers. First, *RASAL2* mutations have been found in a number of tumor types,

including lung, liver, ovarian, and head and neck cancers. Second, in the context of *Trp53* homozygous or heterozygous loss, *Rasal2* loss promotes the development and metastasis of a range of tumor types. Notably, many of the tumor types observed in *Trp53*/*Rasal2* double mutant compound mice also are tumor types in which *RASAL2* mutations have been found in human tumor samples (head and neck, colon, liver). Thus, in would be interesting to expand our studies of RASAL2 to these tumor types, via additional mouse crosses, the generation of a conditional *Rasal2* knockout mouse model, and cell and xenograft studies similar to those we have performed for our analyses of RASAL2 in breast cancer. Furthermore, many of the breast cancer-related future directions described in this Chapter may be applicable to RASAL2 in other tumor types as well, such as differential effects on primary tumorigenesis versus metastasis and the interaction of RASAL2 and DAB2IP.

Additional tumor suppressor RasGAP genes

The work presented in this Dissertation highlights the RasGAPs as an expanding class of human tumor suppressor genes. In addition to the future studies described above which will deepen our understanding of *RASAL2*, the newest tumor suppressor in the RasGAP gene family, it also could be interesting to broaden our studies and explore whether there are additional tumor suppressors within the family. Our initial screen for tumor suppressors in the RasGAP gene family identified three genes, *NF1*, *DAB2IP*, and *RASAL2*, each of which we now know is indeed a tumor suppressor[121]. It is possible, however, that additional RasGAPs also may have tumor suppressive roles in sporadic cancer. In particular, suggestions in the literature point to *RASAL1* and *CAPRI* as possible tumor suppressor genes[150,152]. Perhaps notably, our screen was unable to assess the transforming properties of *RASAL1* or *CAPRI* inactivation: *RASAL1* is not expressed in the cells in which we conducted our screen, so our negative result was uninformative. Additionally, shRNAs targeting *CAPRI* were not available at the time we performed the screen so we were unable to include *CAPRI* in the experiment. Therefore, future

research efforts to identify additional RasGAP tumor suppressor genes might want to focus first on these two RasGAPs.

All together, we believe that the Future Directions described here layered atop the findings presented in this Dissertation will expand and develop our understanding of RasGAPs as tumor suppressor genes inactivated in sporadic cancer, the Ras pathway in primary tumorigenesis and metastasis, mechanisms of breast cancer primary tumorigenesis and metastasis, and mechanisms of resistance in breast cancer patients; and ultimately, we hope, improve outcomes for cancer patients.

References

1. Colicelli, J. Human RAS superfamily proteins and related GTPases. *Sci. STKE* **2004**, RE13 (2004).

2. Kirsten, W. H. & Mayer, L. A. Malignant lymphomas of extrathymic origin induced in rats by murine erythroblastosis virus. *J Natl Cancer Inst* **43**, 735–746 (1969).

3. HARVEY, J. J. AN UNIDENTIFIED VIRUS WHICH CAUSES THE RAPID PRODUCTION OF TUMOURS IN MICE. *Nature* **204**, 1104–1105 (1964).

4. Perucho, M. *et al.* Human-tumor-derived cell lines contain common and different transforming genes. *Cell* **27**, 467–476 (1981).

5. Krontiris, T. G. & Cooper, G. M. Transforming activity of human tumor DNAs. *Proc Natl Acad Sci USA* **78**, 1181–1184 (1981).

6. Shih, C., Padhy, L. C., Murray, M. & Weinberg, R. A. Transforming genes of carcinomas and neuroblastomas introduced into mouse fibroblasts. *Nature* **290**, 261–264 (1981).

7. Downward, J. Targeting RAS signalling pathways in cancer therapy. *Nat Rev Cancer* **3**, 11–22 (2003).

8. Hancock, J. F. Ras proteins: different signals from different locations. *Nat Rev Mol Cell Biol* **4**, 373–384 (2003).

9. Johnson, L. *et al.* K-ras is an essential gene in the mouse with partial functional overlap with N-ras. *Genes Dev* **11**, 2468–2481 (1997).

10. Koera, K. *et al.* K-ras is essential for the development of the mouse embryo. *Oncology* **15**, 1151–1159 (1997).

11. Esteban, L. M. *et al.* Targeted genomic disruption of H-ras and N-ras, individually or in combination, reveals the dispensability of both loci for mouse growth and development. *Mol Cell Biol* **21**, 1444–1452 (2001).

12. Herrmann, C., Horn, G., Spaargaren, M. & Wittinghofer, A. Differential interaction of the ras family GTP-binding proteins H-Ras, Rap1A, and R-Ras with the putative effector molecules Raf kinase and Ral-guanine nucleotide exchange factor. *J Biol Chem* **271**, 6794–6800 (1996).

13. Bernards, A. & Settleman, J. GAP control: regulating the regulators of small GTPases. *Trends Cell Biol* **14**, 377–385 (2004).

14. Neal, S. E., Eccleston, J. F., Hall, A. & Webb, M. R. Kinetic analysis of the hydrolysis of GTP by p21N-ras. The basal GTPase mechanism. *J Biol Chem* **263**, 19718–19722 (1988).

15. Gibbs, J. B., Schaber, M. D., Allard, W. J., Sigal, I. S. & Scolnick, E. M. Purification of ras GTPase activating protein from bovine brain. *Proc Natl Acad Sci USA* **85**, 5026–5030

(1988).

16. Trahey, M. & McCormick, F. A cytoplasmic protein stimulates normal N-ras p21 GTPase, but does not affect oncogenic mutants. *Science* **238**, 542–545 (1987).

17. Chardin, P. *et al.* Human Sos1: a guanine nucleotide exchange factor for Ras that binds to GRB2. *Science* **260**, 1338–1343 (1993).

18. Bowtell, D., Fu, P., Simon, M. & Senior, P. Identification of murine homologues of the Drosophila son of sevenless gene: potential activators of ras. *Proc Natl Acad Sci USA* **89**, 6511–6515 (1992).

19. Schlessinger, J. Cell signaling by receptor tyrosine kinases. *Cell* **103**, 211–225 (2000).

20. Gale, N. W., Kaplan, S., Lowenstein, E. J., Schlessinger, J. & Bar-Sagi, D. Grb2 mediates the EGF-dependent activation of guanine nucleotide exchange on Ras. *Nature* **363**, 88–92 (1993).

21. Li, N. *et al.* Guanine-nucleotide-releasing factor hSos1 binds to Grb2 and links receptor tyrosine kinases to Ras signalling. *Nature* **363**, 85–88 (1993).

22. Rozakis-Adcock, M., Fernley, R., Wade, J., Pawson, T. & Bowtell, D. The SH2 and SH3 domains of mammalian Grb2 couple the EGF receptor to the Ras activator mSos1. *Nature* **363**, 83–85 (1993).

23. Egan, S. E. *et al.* Association of Sos Ras exchange protein with Grb2 is implicated in tyrosine kinase signal transduction and transformation. *Nature* **363**, 45–51 (1993).

24. Buday, L. & Downward, J. Epidermal growth factor regulates p21ras through the formation of a complex of receptor, Grb2 adapter protein, and Sos nucleotide exchange factor. *Cell* **73**, 611–620 (1993).

25. Cichowski, K., Santiago, S., Jardim, M., Johnson, B. W. & Jacks, T. Dynamic regulation of the Ras pathway via proteolysis of the NF1 tumor suppressor. *Genes Dev* **17**, 449–454 (2003).

26. Moodie, S. A., Willumsen, B. M., Weber, M. J. & Wolfman, A. Complexes of Ras.GTP with Raf-1 and mitogen-activated protein kinase kinase. *Science* **260**, 1658–1661 (1993).

27. Warne, P. H., Viciana, P. R. & Downward, J. Direct interaction of Ras and the amino-terminal region of Raf-1 in vitro. *Nature* **364**, 352–355 (1993).

28. Zhang, X. F. *et al.* Normal and oncogenic p21ras proteins bind to the amino-terminal regulatory domain of c-Raf-1. *Nature* **364**, 308–313 (1993).

29. Vojtek, A. B., Hollenberg, S. M. & Cooper, J. A. Mammalian Ras interacts directly with the serine/threonine kinase Raf. *Cell* **74**, 205–214 (1993).

30. Kolch, W. Coordinating ERK/MAPK signalling through scaffolds and inhibitors. *Nat Rev*

Mol Cell Biol **6**, 827–837 (2005).

31. Roux, P. P. & Blenis, J. ERK and p38 MAPK-activated protein kinases: a family of protein kinases with diverse biological functions. *Microbiol. Mol. Biol. Rev.* **68**, 320–344 (2004).

32. Karnoub, A. E. & Weinberg, R. A. Ras oncogenes: split personalities. *Nat Rev Mol Cell Biol* **9**, 517–531 (2008).

33. Rodriguez-Viciana, P. *et al.* Phosphatidylinositol-3-OH kinase as a direct target of Ras. *Nature* **370**, 527–532 (1994).

34. Franke, T. F., Kaplan, D. R., Cantley, L. C. & Toker, A. Direct regulation of the Akt proto-oncogene product by phosphatidylinositol-3,4-bisphosphate. *Science* **275**, 665–668 (1997).

35. Manning, B. D. & Cantley, L. C. AKT/PKB signaling: navigating downstream. *Cell* **129**, 1261–1274 (2007).

36. Shaw, R. J. & Cantley, L. C. Ras, PI(3)K and mTOR signalling controls tumour cell growth. *Nature* **441**, 424–430 (2006).

37. Datta, S. R. *et al.* Akt phosphorylation of BAD couples survival signals to the cell-intrinsic death machinery. *Cell* **91**, 231–241 (1997).

38. del Peso, L., González-García, M., Page, C., Herrera, R. & Nuñez, G. Interleukin-3-induced phosphorylation of BAD through the protein kinase Akt. *Science* **278**, 687–689 (1997).

39. Mendoza, M. C., Er, E. E. & Blenis, J. The Ras-ERK and PI3K-mTOR pathways: cross-talk and compensation. *Trends Biochem. Sci.* **36**, 320–328 (2011).

40. Hofer, F., Fields, S., Schneider, C. & Martin, G. S. Activated Ras interacts with the Ral guanine nucleotide dissociation stimulator. *Proc Natl Acad Sci USA* **91**, 11089–11093 (1994).

41. Kikuchi, A., Demo, S. D., Ye, Z. H., Chen, Y. W. & Williams, L. T. ralGDS family members interact with the effector loop of ras p21. *Mol Cell Biol* **14**, 7483–7491 (1994).

42. Spaargaren, M. & Bischoff, J. R. Identification of the guanine nucleotide dissociation stimulator for Ral as a putative effector molecule of R-ras, H-ras, K-ras, and Rap. *Proc Natl Acad Sci USA* **91**, 12609–12613 (1994).

43. Kelley, G. G., Reks, S. E., Ondrako, J. M. & Smrcka, A. V. Phospholipase C(epsilon): a novel Ras effector. *EMBO J* **20**, 743–754 (2001).

44. Song, C. *et al.* Regulation of a novel human phospholipase C, PLCepsilon, through membrane targeting by Ras. *J Biol Chem* **276**, 2752–2757 (2001).

45. Lambert, J. M. *et al.* Tiam1 mediates Ras activation of Rac by a PI(3)K-independent mechanism. *Nat Cell Biol* **4**, 621–625 (2002).

46. Bamford, S. *et al.* The COSMIC (Catalogue of Somatic Mutations in Cancer) database and website. *Br J Cancer* **91**, 355–358 (2004).

47. McGrath, J. P., Capon, D. J., Goeddel, D. V. & Levinson, A. D. Comparative biochemical properties of normal and activated human ras p21 protein. *Nature* **310**, 644–649 (1984).

48. Gibbs, J. B., Sigal, I. S., Poe, M. & Scolnick, E. M. Intrinsic GTPase activity distinguishes normal and oncogenic ras p21 molecules. *Proc Natl Acad Sci USA* **81**, 5704–5708 (1984).

49. Sweet, R. W. *et al.* The product of ras is a GTPase and the T24 oncogenic mutant is deficient in this activity. *Nature* **311**, 273–275 (1984).

50. Clark, R., Wong, G., Arnheim, N., Nitecki, D. & McCormick, F. Antibodies specific for amino acid 12 of the ras oncogene product inhibit GTP binding. *Proc Natl Acad Sci USA* **82**, 5280–5284 (1985).

51. Der, C. J., Finkel, T. & Cooper, G. M. Biological and biochemical properties of human rasH genes mutated at codon 61. *Cell* **44**, 167–176 (1986).

52. Tabin, C. J. *et al.* Mechanism of activation of a human oncogene. *Nature* **300**, 143–149 (1982).

53. Reddy, E. P., Reynolds, R. K., Santos, E. & Barbacid, M. A point mutation is responsible for the acquisition of transforming properties by the T24 human bladder carcinoma oncogene. *Nature* **300**, 149–152 (1982).

54. Taparowsky, E. *et al.* Activation of the T24 bladder carcinoma transforming gene is linked to a single amino acid change. *Nature* **300**, 762–765 (1982).

55. Curtis, C. *et al.* The genomic and transcriptomic architecture of 2,000 breast tumours reveals novel subgroups. *Nature* **486**, 346–352 (2012).

56. Cancer Genome Atlas Network Comprehensive molecular portraits of human breast tumours. *Nature* **490**, 61–70 (2012).

57. Wagner, P. L. *et al.* In situ evidence of KRAS amplification and association with increased p21 levels in non-small cell lung carcinoma. *Am. J. Clin. Pathol.* **132**, 500–505 (2009).

58. Hahn, W. C. *et al.* Creation of human tumour cells with defined genetic elements. *Nature* **400**, 464–468 (1999).

59. Karreth, F. A. & Tuveson, D. A. Modelling oncogenic Ras/Raf signalling in the mouse. *Curr. Opin. Genet. Dev.* **19**, 4–11 (2009).

60. Sauter, G., Maeda, T., Waldman, F. M., Davis, R. L. & Feuerstein, B. G. Patterns of epidermal growth factor receptor amplification in malignant gliomas. *Am J Pathol* **148**, 1047–1053 (1996).

61. Narita, Y. *et al.* Mutant epidermal growth factor receptor signaling down-regulates p27

through activation of the phosphatidylinositol 3-kinase/Akt pathway in glioblastomas. *Cancer Res* **62**, 6764–6769 (2002).

62. Arteaga, C. L. EGF receptor mutations in lung cancer: from humans to mice and maybe back to humans. *Cancer Cell* **9**, 421–423 (2006).

63. Mendelsohn, J. & Baselga, J. The EGF receptor family as targets for cancer therapy. *Oncology* **19**, 6550–6565 (2000).

64. Kuan, C. T., Wikstrand, C. J. & Bigner, D. D. EGF mutant receptor vIII as a molecular target in cancer therapy. *Endocr Relat Cancer* **8**, 83–96 (2001).

65. Moasser, M. M. The oncogene HER2: its signaling and transforming functions and its role in human cancer pathogenesis. *Oncology* **26**, 6469–6487 (2007).

66. Tornillo, L. & Terracciano, L. M. An update on molecular genetics of gastrointestinal stromal tumours. *J. Clin. Pathol.* **59**, 557–563 (2006).

67. Hynes, N. E. & MacDonald, G. ErbB receptors and signaling pathways in cancer. *Current Opinion in Cell Biology* **21**, 177–184 (2009).

68. Roberts, A. E. *et al.* Germline gain-of-function mutations in SOS1 cause Noonan syndrome. *Nat Genet* **39**, 70–74 (2007).

69. Tartaglia, M. *et al.* Gain-of-function SOS1 mutations cause a distinctive form of Noonan syndrome. *Nat Genet* **39**, 75–79 (2007).

70. Schubbert, S., Shannon, K. & Bollag, G. Hyperactive Ras in developmental disorders and cancer. *Nat Rev Cancer* **7**, 295–308 (2007).

71. Davies, H. *et al.* Mutations of the BRAF gene in human cancer. *Nature* **417**, 949–954 (2002).

72. Pedrero, J. M. G. *et al.* Frequent genetic and biochemical alterations of the PI 3-K/AKT/PTEN pathway in head and neck squamous cell carcinoma. *Int. J. Cancer* **114**, 242–248 (2005).

73. Björkqvist, A. M. *et al.* DNA gains in 3q occur frequently in squamous cell carcinoma of the lung, but not in adenocarcinoma. *Genes Chromosomes Cancer* **22**, 79–82 (1998).

74. Ma, Y. Y. *et al.* PIK3CA as an oncogene in cervical cancer. *Oncology* **19**, 2739–2744 (2000).

75. Byun, D.-S. *et al.* Frequent monoallelic deletion of PTEN and its reciprocal associatioin with PIK3CA amplification in gastric carcinoma. *Int. J. Cancer* **104**, 318–327 (2003).

76. Miller, C. T. *et al.* Gene amplification in esophageal adenocarcinomas and Barrett's with high-grade dysplasia. *Clin Cancer Res* **9**, 4819–4825 (2003).

77. Staal, S. P. Molecular cloning of the akt oncogene and its human homologues AKT1 and AKT2: amplification of AKT1 in a primary human gastric adenocarcinoma. *Proc Natl Acad Sci USA* **84**, 5034–5037 (1987).

78. Carpten, J. D. *et al.* A transforming mutation in the pleckstrin homology domain of AKT1 in cancer. *Nature* **448**, 439–444 (2007).

79. Ruggeri, B. A., Huang, L., Wood, M., Cheng, J. Q. & Testa, J. R. Amplification and overexpression of the AKT2 oncogene in a subset of human pancreatic ductal adenocarcinomas. *Mol. Carcinog.* **21**, 81–86 (1998).

80. Cheng, J. Q. *et al.* Amplification of AKT2 in human pancreatic cells and inhibition of AKT2 expression and tumorigenicity by antisense RNA. *Proc Natl Acad Sci USA* **93**, 3636–3641 (1996).

81. Bellacosa, A. *et al.* Molecular alterations of the AKT2 oncogene in ovarian and breast carcinomas. *Int. J. Cancer* **64**, 280–285 (1995).

82. Parsons, D. W. *et al.* Colorectal cancer: mutations in a signalling pathway. *Nature* **436**, 792 (2005).

83. Ali, I. U., Schriml, L. M. & Dean, M. Mutational spectra of PTEN/MMAC1 gene: a tumor suppressor with lipid phosphatase activity. *J Natl Cancer Inst* **91**, 1922–1932 (1999).

84. Chalhoub, N. & Baker, S. J. PTEN and the PI3-kinase pathway in cancer. *Annu. Rev. Pathol. Mech. Dis.* **4**, 127–150 (2009).

85. Teresi, R. E., Planchon, S. M., Waite, K. A. & Eng, C. Regulation of the PTEN promoter by statins and SREBP. *Hum. Mol. Genet.* **17**, 919–928 (2008).

86. Huse, J. T. *et al.* The PTEN-regulating microRNA miR-26a is amplified in high-grade glioma and facilitates gliomagenesis in vivo. *Genes Dev* **23**, 1327–1337 (2009).

87. Poliseno, L. *et al.* Identification of the miR-106b~25 microRNA cluster as a proto-oncogenic PTEN-targeting intron that cooperates with its host gene MCM7 in transformation. *Sci Signal* **3**, ra29 (2010).

88. Wang, X. *et al.* NEDD4-1 is a proto-oncogenic ubiquitin ligase for PTEN. *Cell* **128**, 129–139 (2007).

89. Bernards, A. GAPs galore! A survey of putative Ras superfamily GTPase activating proteins in man and Drosophila. *Biochim Biophys Acta* **1603**, 47–82 (2003).

90. Gideon, P. *et al.* Mutational and kinetic analyses of the GTPase-activating protein (GAP)-p21 interaction: the C-terminal domain of GAP is not sufficient for full activity. *Mol Cell Biol* **12**, 2050–2056 (1992).

91. Scheffzek, K., Lautwein, A., Scherer, A., Franken, S. & Wittinghofer, A. Crystallization and preliminary X-ray crystallographic study of the Ras-GTPase-activating domain of human

p120GAP. *Proteins* **27**, 315–318 (1997).

92. Bernards, A. & Settleman, J. GAPs in growth factor signalling. *Growth Factors* **23**, 143–149 (2005).

93. Marchler-Bauer, A. *et al.* CDD: a Conserved Domain Database for the functional annotation of proteins. *Nucleic Acids Res* **39**, D225–9 (2011).

94. Welti, S., Fraterman, S., D'Angelo, I., Wilm, M. & Scheffzek, K. The sec14 homology module of neurofibromin binds cellular glycerophospholipids: mass spectrometry and structure of a lipid complex. *J. Mol. Biol.* **366**, 551–562 (2007).

95. Cawthon, R. M. *et al.* A major segment of the neurofibromatosis type 1 gene: cDNA sequence, genomic structure, and point mutations. *Cell* **62**, 193–201 (1990).

96. Martin, G. A. *et al.* The GAP-related domain of the neurofibromatosis type 1 gene product interacts with ras p21. *Cell* **63**, 843–849 (1990).

97. Riccardi, V. M. *Neurofibromatosis: Phenotype, Natural History, and Pathogenesis, Second Edition*. (The Johns Hopkins University Press, 1992).

98. Xu, W. *et al.* Loss of NF1 alleles in phaeochromocytomas from patients with type I neurofibromatosis. *Genes Chromosomes Cancer* **4**, 337–342 (1992).

99. Legius, E., Marchuk, D. A., Collins, F. S. & Glover, T. W. Somatic deletion of the neurofibromatosis type 1 gene in a neurofibrosarcoma supports a tumour suppressor gene hypothesis. *Nat Genet* **3**, 122–126 (1993).

100. Shannon, K. M. *et al.* Loss of the normal NF1 allele from the bone marrow of children with type 1 neurofibromatosis and malignant myeloid disorders. *N Engl J Med* **330**, 597–601 (1994).

101. DeClue, J. E. *et al.* Abnormal regulation of mammalian p21ras contributes to malignant tumor growth in von Recklinghausen (type 1) neurofibromatosis. *Cell* **69**, 265–273 (1992).

102. Johannessen, C. M. *et al.* The NF1 tumor suppressor critically regulates TSC2 and mTOR. *Proc Natl Acad Sci USA* **102**, 8573–8578 (2005).

103. Johannessen, C. M. *et al.* TORC1 is essential for NF1-associated malignancies. *Curr Biol* **18**, 56–62 (2008).

104. De Raedt, T. *et al.* Exploiting cancer cell vulnerabilities to develop a combination therapy for ras-driven tumors. *Cancer Cell* **20**, 400–413 (2011).

105. Messiaen, L. M. *et al.* Exhaustive mutation analysis of the NF1 gene allows identification of 95% of mutations and reveals a high frequency of unusual splicing defects. *Hum. Mutat.* **15**, 541–555 (2000).

106. Klose, A. *et al.* Selective disactivation of neurofibromin GAP activity in neurofibromatosis

type 1. *Hum. Mol. Genet.* **7**, 1261–1268 (1998).

107. Maertens, O. *et al.* Elucidating distinct roles for NF1 in melanomagenesis. *Cancer Discov* (2012).doi:10.1158/2159-8290.CD-12-0313

108. Dahlman, K. B. *et al.* BRAF(L597) mutations in melanoma are associated with sensitivity to MEK inhibitors. *Cancer Discov* **2**, 791–797 (2012).

109. Krauthammer, M. *et al.* Exome sequencing identifies recurrent somatic RAC1 mutations in melanoma. *Nat Genet* **44**, 1006–1014 (2012).

110. McGillicuddy, L. T. *et al.* Proteasomal and genetic inactivation of the NF1 tumor suppressor in gliomagenesis. *Cancer Cell* **16**, 44–54 (2009).

111. Parsons, D. W. *et al.* An integrated genomic analysis of human glioblastoma multiforme. *Science* **321**, 1807–1812 (2008).

112. Cancer Genome Atlas Research Network Comprehensive genomic characterization defines human glioblastoma genes and core pathways. *Nature* **455**, 1061–1068 (2008).

113. Ding, L. *et al.* Somatic mutations affect key pathways in lung adenocarcinoma. *Nature* **455**, 1069–1075 (2008).

114. Hölzel, M. *et al.* NF1 is a tumor suppressor in neuroblastoma that determines retinoic acid response and disease outcome. *Cell* **142**, 218–229 (2010).

115. Bergh, von, A. R. M. *et al.* Identification of a novel RAS GTPase-activating protein (RASGAP) gene at 9q34 as an MLL fusion partner in a patient with de novo acute myeloid leukemia. *Genes Chromosomes Cancer* **39**, 324–334 (2004).

116. Dote, H. *et al.* Aberrant promoter methylation in human DAB2 interactive protein (hDAB2IP) gene in breast cancer. *Clin Cancer Res* **10**, 2082–2089 (2004).

117. Dote, H. *et al.* Aberrant promoter methylation in human DAB2 interactive protein (hDAB2IP) gene in gastrointestinal tumour. *Br J Cancer* **92**, 1117–1125 (2005).

118. Chen, H., Toyooka, S., Gazdar, A. F. & Hsieh, J.-T. Epigenetic Regulation of a Novel Tumor Suppressor Gene (hDAB2IP) in Prostate Cancer Cell Lines. *Journal of Biological Chemistry* **278**, 3121–3130 (2003).

119. Yano, M. *et al.* Aberrant promoter methylation of human DAB2 interactive protein (hDAB2IP) gene in lung cancers. *Int. J. Cancer* **113**, 59–66 (2005).

120. Chen, H., Tu, S.-W. & Hsieh, J.-T. Down-regulation of human DAB2IP gene expression mediated by polycomb Ezh2 complex and histone deacetylase in prostate cancer. *J Biol Chem* **280**, 22437–22444 (2005).

121. Min, J. *et al.* An oncogene-tumor suppressor cascade drives metastatic prostate cancer by coordinately activating Ras and nuclear factor-kappaB. *Nat Med* **16**, 286–294 (2010).

122. Varambally, S. *et al.* The polycomb group protein EZH2 is involved in progression of prostate cancer. *Nature* **419**, 624–629 (2002).

123. Chen, H. J., Rojas-Soto, M., Oguni, A. & Kennedy, M. B. A synaptic Ras-GTPase activating protein (p135 SynGAP) inhibited by CaM kinase II. *Neuron* **20**, 895–904 (1998).

124. Kim, J. H., Liao, D., Lau, L. F. & Huganir, R. L. SynGAP: a synaptic RasGAP that associates with the PSD-95/SAP90 protein family. *Neuron* **20**, 683–691 (1998).

125. Kim, J. H., Lee, H.-K., Takamiya, K. & Huganir, R. L. The role of synaptic GTPase-activating protein in neuronal development and synaptic plasticity. *J. Neurosci.* **23**, 1119–1124 (2003).

126. Oh, J. S., Manzerra, P. & Kennedy, M. B. Regulation of the neuron-specific Ras GTPase-activating protein, synGAP, by Ca2+/calmodulin-dependent protein kinase II. *J Biol Chem* **279**, 17980–17988 (2004).

127. Krapivinsky, G., Medina, I., Krapivinsky, L., Gapon, S. & Clapham, D. E. SynGAP-MUPP1-CaMKII synaptic complexes regulate p38 MAP kinase activity and NMDA receptor-dependent synaptic AMPA receptor potentiation. *Neuron* **43**, 563–574 (2004).

128. Pena, V. *et al.* The C2 domain of SynGAP is essential for stimulation of the Rap GTPase reaction. *EMBO Rep.* **9**, 350–355 (2008).

129. Muhia, M., Yee, B. K., Feldon, J., Markopoulos, F. & Knuesel, I. Disruption of hippocampus-regulated behavioural and cognitive processes by heterozygous constitutive deletion of SynGAP. *Eur. J. Neurosci.* **31**, 529–543 (2010).

130. Muhia, M. *et al.* Molecular and behavioral changes associated with adult hippocampus-specific SynGAP1 knockout. *Learn. Mem.* **19**, 268–281 (2012).

131. Hamdan, F. F. *et al.* Mutations in SYNGAP1 in autosomal nonsyndromic mental retardation. *N Engl J Med* **360**, 599–605 (2009).

132. Pinto, D. *et al.* Functional impact of global rare copy number variation in autism spectrum disorders. *Nature* **466**, 368–372 (2010).

133. Liu, B. A. *et al.* SRC Homology 2 Domain Binding Sites in Insulin, IGF-1 and FGF receptor mediated signaling networks reveal an extensive potential interactome. *Cell Communication and Signaling* **10**, 1–1 (2012).

134. Gigoux, V., L'Hoste, S., Raynaud, F., Camonis, J. & Garbay, C. Identification of Aurora kinases as RasGAP Src homology 3 domain-binding proteins. *J Biol Chem* **277**, 23742–23746 (2002).

135. Liu, Y. F., Deth, R. C. & Devys, D. SH3 domain-dependent association of huntingtin with epidermal growth factor receptor signaling complexes. *J Biol Chem* **272**, 8121–8124 (1997).

136. Lock, P., Casagranda, F. & Dunn, A. R. Independent SH2-binding sites mediate interaction of Dok-related protein with RasGTPase-activating protein and Nck. *J Biol Chem* **274**, 22775–22784 (1999).

137. Sánchez-Margalet, V. & Najib, S. Sam68 is a docking protein linking GAP and PI3K in insulin receptor signaling. *Mol. Cell. Endocrinol.* **183**, 113–121 (2001).

138. McGlade, J. *et al.* The N-terminal region of GAP regulates cytoskeletal structure and cell adhesion. *EMBO J* **12**, 3073–3081 (1993).

139. Kulkarni, S. V., Gish, G., van der Geer, P., Henkemeyer, M. & Pawson, T. Role of p120 Ras-GAP in directed cell movement. *J Cell Biol* **149**, 457–470 (2000).

140. Tomar, A., Lim, S.-T., Lim, Y. & Schlaepfer, D. D. A FAK-p120RasGAP-p190RhoGAP complex regulates polarity in migrating cells. *J. Cell. Sci.* **122**, 1852–1862 (2009).

141. Henkemeyer, M. *et al.* Vascular system defects and neuronal apoptosis in mice lacking ras GTPase-activating protein. *Nature* **377**, 695–701 (1995).

142. Boon, L. M., Mulliken, J. B. & Vikkula, M. RASA1: variable phenotype with capillary and arteriovenous malformations. *Curr. Opin. Genet. Dev.* **15**, 265–269 (2005).

143. Eerola, I. *et al.* Capillary malformation-arteriovenous malformation, a new clinical and genetic disorder caused by RASA1 mutations. *Am. J. Hum. Genet.* **73**, 1240–1249 (2003).

144. Hershkovitz, D., Bercovich, D., Sprecher, E. & Lapidot, M. RASA1 mutations may cause hereditary capillary malformations without arteriovenous malformations. *Br. J. Dermatol.* **158**, 1035–1040 (2008).

145. Anand, S. *et al.* MicroRNA-132–mediated loss of p120RasGAP activates the endothelium to facilitate pathological angiogenesis. *Nat Med* **16**, 909–914 (2010).

146. Kupzig, S. GAP1 Family Members Constitute Bifunctional Ras and Rap GTPase-activating Proteins. *Journal of Biological Chemistry* **281**, 9891–9900 (2006).

147. Dai, Y. *et al.* Ca2+-dependent monomer and dimer formation switches capri between RasGAP and RapGAP activities. *J Biol Chem* (2011).doi:10.1074/jbc.M110.201301

148. Lockyer, P. J., Kupzig, S. & Cullen, P. J. CAPRI regulates Ca(2+)-dependent inactivation of the Ras-MAPK pathway. *Curr Biol* **11**, 981–986 (2001).

149. Walker, S. A. *et al.* Identification of a Ras GTPase-activating protein regulated by receptor-mediated Ca2+ oscillations. *EMBO J* **23**, 1749–1760 (2004).

150. Westbrook, T. F. *et al.* A genetic screen for candidate tumor suppressors identifies REST. *Cell* **121**, 837–848 (2005).

151. Zhang, J., Guo, J., Dzhagalov, I. & He, Y.-W. An essential function for the calcium-promoted Ras inactivator in Fcgamma receptor-mediated phagocytosis. *Nat. Immunol.* **6**,

911–919 (2005).

152. Kolfschoten, I. G. M. *et al.* A genetic screen identifies PITX1 as a suppressor of RAS activity and tumorigenicity. *Cell* **121**, 849–858 (2005).

153. Jin, H. *et al.* Epigenetic silencing of a Ca(2+)-regulated Ras GTPase-activating protein RASAL defines a new mechanism of Ras activation in human cancers. *Proc Natl Acad Sci USA* **104**, 12353–12358 (2007).

154. Ohta, M. *et al.* Decreased expression of the RAS-GTPase activating protein RASAL1 is associated with colorectal tumor progression. *Gastroenterology* **136**, 206–216 (2009).

155. Seto, M. *et al.* Reduced expression of RAS protein activator like-1 in gastric cancer. *Int. J. Cancer* **128**, 1293–1302 (2011).

156. Calvisi, D. F. *et al.* Inactivation of Ras GTPase-activating proteins promotes unrestrained activity of wild-type Ras in human liver cancer. *J. Hepatol.* **54**, 311–319 (2011).

157. Hart, M. J., Callow, M. G., Souza, B. & Polakis, P. IQGAP1, a calmodulin-binding protein with a rasGAP-related domain, is a potential effector for cdc42Hs. *EMBO J* **15**, 2997–3005 (1996).

158. Brill, S. *et al.* The Ras GTPase-activating-protein-related human protein IQGAP2 harbors a potential actin binding domain and interacts with calmodulin and Rho family GTPases. *Mol Cell Biol* **16**, 4869–4878 (1996).

159. Nojima, H. *et al.* IQGAP3 regulates cell proliferation through the Ras/ERK signalling cascade. *Nat Cell Biol* **10**, 971–978 (2008).

160. Tamagnone, L. *et al.* Plexins are a large family of receptors for transmembrane, secreted, and GPI-anchored semaphorins in vertebrates. *Cell* **99**, 71–80 (1999).

161. Deng, S. *et al.* Plexin-B2, but not Plexin-B1, critically modulates neuronal migration and patterning of the developing nervous system in vivo. *J. Neurosci.* **27**, 6333–6347 (2007).

162. Friedel, R. H. *et al.* Plexin-B2 controls the development of cerebellar granule cells. *J. Neurosci.* **27**, 3921–3932 (2007).

163. Saha, B., Ypsilanti, A. R., Boutin, C., Cremer, H. & Chédotal, A. Plexin-B2 regulates the proliferation and migration of neuroblasts in the postnatal and adult subventricular zone. *J. Neurosci.* **32**, 16892–16905 (2012).

164. Perälä, N. *et al.* Sema4C-Plexin B2 signalling modulates ureteric branching in developing kidney. *Differentiation* **81**, 81–91 (2011).

165. Noto, S. *et al.* A novel human RasGAP-like gene that maps within the prostate cancer susceptibility locus at chromosome 1q25. *FEBS Lett* **441**, 127–131 (1998).

166. Struski, S., Doco-Fenzy, M. & Cornillet-Lefebvre, P. Compilation of published comparative

genomic hybridization studies. *Cancer Genet. Cytogenet.* **135**, 63–90 (2002).

167. Courjal, F. & Theillet, C. Comparative genomic hybridization analysis of breast tumors with predetermined profiles of DNA amplification. *Cancer Res* **57**, 4368–4377 (1997).

168. Scheffzek, K. & Welti, S. Pleckstrin homology (PH) like domains - versatile modules in protein-protein interaction platforms. *FEBS Lett* **586**, 2662–2673 (2012).

169. Bouwmeester, T. *et al.* A physical and functional map of the human TNF-alpha/NF-kappa B signal transduction pathway. *Nat Cell Biol* **6**, 97–105 (2004).

170. Jin, J. *et al.* Proteomic, functional, and domain-based analysis of in vivo 14-3-3 binding proteins involved in cytoskeletal regulation and cellular organization. *Curr Biol* **14**, 1436–1450 (2004).

171. Wellings, S. R. & Jensen, H. M. On the origin and progression of ductal carcinoma in the human breast. *J Natl Cancer Inst* **50**, 1111–1118 (1973).

172. Visvader, J. E. Keeping abreast of the mammary epithelial hierarchy and breast tumorigenesis. *Genes Dev* **23**, 2563–2577 (2009).

173. Raouf, A., Sun, Y., Chatterjee, S. & Basak, P. The biology of human breast epithelial progenitors. *Semin. Cell Dev. Biol.* **23**, 606–612 (2012).

174. Jeselsohn, R. *et al.* Cyclin D1 kinase activity is required for the self-renewal of mammary stem and progenitor cells that are targets of MMTV-ErbB2 tumorigenesis. *Cancer Cell* **17**, 65–76 (2010).

175. Polyak, K. Breast cancer: origins and evolution. *J Clin Invest* **117**, 3155–3163 (2007).

176. Heldring, N. *et al.* Estrogen receptors: how do they signal and what are their targets. *Physiol Rev* **87**, 905–931 (2007).

177. Gustafsson, J.-Å. What pharmacologists can learn from recent advances in estrogen signalling. *Trends Pharmacol. Sci.* **24**, 479–485 (2003).

178. Thomas, C. & Gustafsson, J.-Å. The different roles of ER subtypes in cancer biology and therapy. *Nat Rev Cancer* **11**, 597–608 (2011).

179. Korach, K. S. Insights from the study of animals lacking functional estrogen receptor. *Science* **266**, 1524–1527 (1994).

180. Bocchinfuso, W. P. & Korach, K. S. Mammary gland development and tumorigenesis in estrogen receptor knockout mice. *J Mammary Gland Biol Neoplasia* **2**, 323–334 (1997).

181. Feng, Y., Manka, D., Wagner, K.-U. & Khan, S. A. Estrogen receptor-alpha expression in the mammary epithelium is required for ductal and alveolar morphogenesis in mice. *Proc Natl Acad Sci USA* **104**, 14718–14723 (2007).

182. Deroo, B. J. & Korach, K. S. Estrogen receptors and human disease. *J Clin Invest* **116**, 561–570 (2006).

183. Lupien, M. & Brown, M. Cistromics of hormone-dependent cancer. *Endocr Relat Cancer* **16**, 381–389 (2009).

184. Carroll, J. S. & Brown, M. Estrogen receptor target gene: an evolving concept. *Mol Endocrinol* **20**, 1707–1714 (2006).

185. Musgrove, E. A. & Sutherland, R. L. Biological determinants of endocrine resistance in breast cancer. *Nat Rev Cancer* **9**, 631–643 (2009).

186. Kato, S. *et al.* Activation of the estrogen receptor through phosphorylation by mitogen-activated protein kinase. *Science* **270**, 1491–1494 (1995).

187. Bunone, G., Briand, P. A., Miksicek, R. J. & Picard, D. Activation of the unliganded estrogen receptor by EGF involves the MAP kinase pathway and direct phosphorylation. *EMBO J* **15**, 2174–2183 (1996).

188. Campbell, R. A. *et al.* Phosphatidylinositol 3-kinase/AKT-mediated activation of estrogen receptor alpha: a new model for anti-estrogen resistance. *J Biol Chem* **276**, 9817–9824 (2001).

189. Björnström, L. & Sjöberg, M. Mechanisms of estrogen receptor signaling: convergence of genomic and nongenomic actions on target genes. *Mol Endocrinol* **19**, 833–842 (2005).

190. Chambliss, K. L. *et al.* Estrogen receptor alpha and endothelial nitric oxide synthase are organized into a functional signaling module in caveolae. *Circ. Res.* **87**, E44–52 (2000).

191. Kousteni, S. *et al.* Nongenotropic, sex-nonspecific signaling through the estrogen or androgen receptors: dissociation from transcriptional activity. *Cell* **104**, 719–730 (2001).

192. Kahlert, S. *et al.* Estrogen receptor alpha rapidly activates the IGF-1 receptor pathway. *J Biol Chem* **275**, 18447–18453 (2000).

193. Shupnik, M. A. Crosstalk between steroid receptors and the c-Src-receptor tyrosine kinase pathways: implications for cell proliferation. *Oncology* **23**, 7979–7989 (2004).

194. Song, R. X.-D. *et al.* Linkage of rapid estrogen action to MAPK activation by ERalpha-Shc association and Shc pathway activation. *Mol Endocrinol* **16**, 116–127 (2002).

195. Siegel, R., Naishadham, D. & Jemal, A. Cancer statistics, 2012. *CA Cancer J Clin* **62**, 10–29 (2012).

196. Weigelt, B., Peterse, J. L. & van t Veer, L. J. Breast cancer metastasis: markers and models. *Nat Rev Cancer* **5**, 591–602 (2005).

197. Perou, C. M. *et al.* Molecular portraits of human breast tumours. *Nature* **406**, 747–752 (2000).

198. Sørlie, T. *et al.* Gene expression patterns of breast carcinomas distinguish tumor subclasses with clinical implications. *Proc Natl Acad Sci USA* **98**, 10869–10874 (2001).

199. van t Veer, L. J. *et al.* Gene expression profiling predicts clinical outcome of breast cancer. *Nature* **415**, 530–536 (2002).

200. van de Vijver, M. J. *et al.* A gene-expression signature as a predictor of survival in breast cancer. *N Engl J Med* **347**, 1999–2009 (2002).

201. Sorlie, T. *et al.* Repeated observation of breast tumor subtypes in independent gene expression data sets. *Proc Natl Acad Sci USA* **100**, 8418–8423 (2003).

202. Sotiriou, C. *et al.* Breast cancer classification and prognosis based on gene expression profiles from a population-based study. *Proc Natl Acad Sci USA* **100**, 10393–10398 (2003).

203. Eroles, P., Bosch, A., Pérez-Fidalgo, J. A. & Lluch, A. Molecular biology in breast cancer: intrinsic subtypes and signaling pathways. *Cancer Treat. Rev.* **38**, 698–707 (2012).

204. West, M. *et al.* Predicting the clinical status of human breast cancer by using gene expression profiles. *Proc Natl Acad Sci USA* **98**, 11462–11467 (2001).

205. Hankinson, S. E., Colditz, G. A. & Willett, W. C. Towards an integrated model for breast cancer etiology: the lifelong interplay of genes, lifestyle, and hormones. *Breast Cancer Res* **6**, 213–218 (2004).

206. Hah, N. *et al.* A Rapid, Extensive, and Transient Transcriptional Response to Estrogen Signaling in Breast Cancer Cells. *Cell* **145**, 622–634 (2011).

207. Lupien, M. *et al.* Coactivator function defines the active estrogen receptor alpha cistrome. *Mol Cell Biol* **29**, 3413–3423 (2009).

208. Higgins, M. J. & Baselga, J. Targeted therapies for breast cancer. *J Clin Invest* **121**, 3797–3803 (2011).

209. Jensen, E. V. & Jordan, V. C. The estrogen receptor: a model for molecular medicine. *Clin Cancer Res* **9**, 1980–1989 (2003).

210. Lim, E., Metzger-Filho, O. & Winer, E. P. The Natural History of Homone Receptor-Positive Breast Cancer. *Oncology* 688–701 (2012).

211. Nahta, R. & O'Regan, R. M. Therapeutic implications of estrogen receptor signaling in HER2-positive breast cancers. *Breast Cancer Res Treat* **135**, 39–48 (2012).

212. Fox, E. M., Arteaga, C. L. & Miller, T. W. Abrogating endocrine resistance by targeting ERα and PI3K in breast cancer. *Front Oncol* **2**, 145 (2012).

213. Miller, T. W., Balko, J. M. & Arteaga, C. L. Phosphatidylinositol 3-kinase and antiestrogen resistance in breast cancer. *J Clin Oncol* **29**, 4452–4461 (2011).

214. Bose, R. *et al.* Activating HER2 Mutations in HER2 Gene Amplification Negative Breast Cancer. *Cancer Discov* **3**, 224–237 (2013).

215. Ross, J. S. *et al.* The HER-2 receptor and breast cancer: ten years of targeted anti-HER-2 therapy and personalized medicine. *Oncologist* **14**, 320–368 (2009).

216. Citri, A. & Yarden, Y. EGF-ERBB signalling: towards the systems level. *Nat Rev Mol Cell Biol* **7**, 505–516 (2006).

217. Graus-Porta, D., Beerli, R. R., Daly, J. M. & Hynes, N. E. ErbB-2, the preferred heterodimerization partner of all ErbB receptors, is a mediator of lateral signaling. *EMBO J* **16**, 1647–1655 (1997).

218. Hynes, N. E. & Lane, H. A. ERBB receptors and cancer: the complexity of targeted inhibitors. *Nat Rev Cancer* **5**, 341–354 (2005).

219. Arteaga, C. L. *et al.* Treatment of HER2-positive breast cancer: current status and future perspectives. *Nature Publishing Group* **9**, 16–32 (2011).

220. Hudis, C. A. Trastuzumab--mechanism of action and use in clinical practice. *N Engl J Med* **357**, 39–51 (2007).

221. Baselga, J., Albanell, J., Molina, M. A. & Arribas, J. Mechanism of action of trastuzumab and scientific update. *Semin. Oncol.* **28**, 4–11 (2001).

222. Spector, N. L. & Blackwell, K. L. Understanding the mechanisms behind trastuzumab therapy for human epidermal growth factor receptor 2-positive breast cancer. *J Clin Oncol* **27**, 5838–5847 (2009).

223. Spector, N. L. *et al.* Study of the biologic effects of lapatinib, a reversible inhibitor of ErbB1 and ErbB2 tyrosine kinases, on tumor growth and survival pathways in patients with advanced malignancies. *J Clin Oncol* **23**, 2502–2512 (2005).

224. Xia, W. *et al.* Anti-tumor activity of GW572016: a dual tyrosine kinase inhibitor blocks EGF activation of EGFR/erbB2 and downstream Erk1/2 and AKT pathways. *Oncology* **21**, 6255–6263 (2002).

225. Konecny, G. E. *et al.* Activity of the dual kinase inhibitor lapatinib (GW572016) against HER-2-overexpressing and trastuzumab-treated breast cancer cells. *Cancer Res* **66**, 1630–1639 (2006).

226. Scaltriti, M. *et al.* Expression of p95HER2, a truncated form of the HER2 receptor, and response to anti-HER2 therapies in breast cancer. *JNCI Journal of the National Cancer Institute* **99**, 628–638 (2007).

227. Wang, Y.-C. *et al.* Different mechanisms for resistance to trastuzumab versus lapatinib in HER2-positive breast cancers--role of estrogen receptor and HER2 reactivation. *Breast Cancer Res* **13**, R121 (2011).

228. MD, P. M. U. *et al.* Lapatinib versus trastuzumab in combination with neoadjuvant anthracycline-taxane-based chemotherapy (GeparQuinto, GBG 44): a randomised phase 3 trial. *Lancet Oncology* **13**, 135–144 (2012).

229. Blackwell, K. L. *et al.* Overall survival benefit with lapatinib in combination with trastuzumab for patients with human epidermal growth factor receptor 2-positive metastatic breast cancer: final results from the EGF104900 Study. *J Clin Oncol* **30**, 2585–2592 (2012).

230. Xia, W. *et al.* A model of acquired autoresistance to a potent ErbB2 tyrosine kinase inhibitor and a therapeutic strategy to prevent its onset in breast cancer. *Proc Natl Acad Sci USA* **103**, 7795–7800 (2006).

231. Gusterson, B. Do 'basal-like' breast cancers really exist? *Nat Rev Cancer* **9**, 128–134 (2009).

232. Duffy, M. J., McGowan, P. M. & Crown, J. Targeted therapy for triple-negative breast cancer: where are we? *Int. J. Cancer* **131**, 2471–2477 (2012).

233. Foulkes, W. D. *et al.* Germline BRCA1 mutations and a basal epithelial phenotype in breast cancer. *JNCI Journal of the National Cancer Institute* **95**, 1482–1485 (2003).

234. Vargo-Gogola, T. & Rosen, J. M. Modelling breast cancer: one size does not fit all. *Nat Rev Cancer* **7**, 659–672 (2007).

235. Caligiuri, I., Rizzolio, F., Boffo, S., Giordano, A. & Toffoli, G. Critical choices for modeling breast cancer in transgenic mouse models. *J. Cell. Physiol.* **227**, 2988–2991 (2012).

236. Herschkowitz, J. I. *et al.* Identification of conserved gene expression features between murine mammary carcinoma models and human breast tumors. *Genome Biol* **8**, R76 (2007).

237. Kirma, N. B. & Tekmal, R. R. Transgenic mouse models of hormonal mammary carcinogenesis: advantages and limitations. *J. Steroid Biochem. Mol. Biol.* **131**, 76–82 (2012).

238. Muller, W. J., Sinn, E., Pattengale, P. K., Wallace, R. & Leder, P. Single-step induction of mammary adenocarcinoma in transgenic mice bearing the activated c-neu oncogene. *Cell* **54**, 105–115 (1988).

239. Ursini-Siegel, J., Schade, B., Cardiff, R. D. & Muller, W. J. Insights from transgenic mouse models of ERBB2-induced breast cancer. *Nat Rev Cancer* **7**, 389–397 (2007).

240. Guy, C. T. *et al.* Expression of the neu protooncogene in the mammary epithelium of transgenic mice induces metastatic disease. *Proc Natl Acad Sci USA* **89**, 10578–10582 (1992).

241. Miller, F. R., Santner, S. J., Tait, L. & Dawson, P. J. MCF10DCIS.com xenograft model of human comedo ductal carcinoma in situ. *J Natl Cancer Inst* **92**, 1185–1186 (2000).

242. Hu, M. *et al.* Regulation of in situ to invasive breast carcinoma transition. *Cancer Cell* **13**, 394–406 (2008).

243. Kuperwasser, C. *et al.* A mouse model of human breast cancer metastasis to human bone. *Cancer Res* **65**, 6130–6138 (2005).

244. Welm, A. L. *et al.* The macrophage-stimulating protein pathway promotes metastasis in a mouse model for breast cancer and predicts poor prognosis in humans. *Proc Natl Acad Sci USA* **104**, 7570–7575 (2007).

245. Kim, I. S. & Baek, S. H. Mouse models for breast cancer metastasis. *Biochem. Biophys. Res. Commun.* **394**, 443–447 (2010).

246. Chaffer, C. L. & Weinberg, R. A. A perspective on cancer cell metastasis. *Science* **331**, 1559–1564 (2011).

247. Valastyan, S. & Weinberg, R. A. Tumor metastasis: molecular insights and evolving paradigms. *Cell* **147**, 275–292 (2011).

248. Blanco, M. A. & Kang, Y. Signaling pathways in breast cancer metastasis - novel insights from functional genomics. *Breast Cancer Res* **13**, 206 (2011).

249. Wolfer, A. *et al.* MYC regulation of a 'poor-prognosis' metastatic cancer cell state. *PNAS* **107**, 3698–3703 (2010).

250. Place, A. E., Jin Huh, S. & Polyak, K. The microenvironment in breast cancer progression: biology and implications for treatment. *Breast Cancer Res* **13**, 227 (2011).

251. McAllister, S. S. & Weinberg, R. A. Tumor-host interactions: a far-reaching relationship. *J Clin Oncol* **28**, 4022–4028 (2010).

252. Karnoub, A. E. *et al.* Mesenchymal stem cells within tumour stroma promote breast cancer metastasis. *Nature* **449**, 557–563 (2007).

253. McAllister, S. S. *et al.* Systemic endocrine instigation of indolent tumor growth requires osteopontin. *Cell* **133**, 994–1005 (2008).

254. Giehl, K. Oncogenic Ras in tumour progression and metastasis. *Biol. Chem.* **386**, 193–205 (2005).

255. Campbell, P. M. & Der, C. J. Oncogenic Ras and its role in tumor cell invasion and metastasis. *Semin Cancer Biol* **14**, 105–114 (2004).

256. Yan, Z. *et al.* Oncogenic c-Ki-ras but not oncogenic c-Ha-ras up-regulates CEA expression and disrupts basolateral polarity in colon epithelial cells. *J Biol Chem* **272**, 27902–27907 (1997).

257. Schmidt, C. R. *et al.* E-cadherin is regulated by the transcriptional repressor SLUG during Ras-mediated transformation of intestinal epithelial cells. *Surgery* **138**, 306–312 (2005).

258. De Corte, V. *et al.* Gelsolin-induced epithelial cell invasion is dependent on Ras-Rac signaling. *EMBO J* **21**, 6781–6790 (2002).

259. Shin, S., Dimitri, C. A., Yoon, S.-O., Dowdle, W. & Blenis, J. ERK2 but not ERK1 induces epithelial-to-mesenchymal transformation via DEF motif-dependent signaling events. *Mol Cell* **38**, 114–127 (2010).

260. Ballin, M., Gomez, D. E., Sinha, C. C. & Thorgeirsson, U. P. Ras oncogene mediated induction of a 92 kDa metalloproteinase; strong correlation with the malignant phenotype. *Biochem. Biophys. Res. Commun.* **154**, 832–838 (1988).

261. Reginato, M. J. *et al.* Integrins and EGFR coordinately regulate the pro-apoptotic protein Bim to prevent anoikis. *Nat Cell Biol* **5**, 733–740 (2003).

262. Webb, C. P., Van Aelst, L., Wigler, M. H. & Vande Woude, G. F. Signaling pathways in Ras-mediated tumorigenicity and metastasis. *Proc Natl Acad Sci USA* **95**, 8773–8778 (1998).

263. Fujimoto, K., Sheng, H., Shao, J. & Beauchamp, R. D. Transforming growth factor-beta1 promotes invasiveness after cellular transformation with activated Ras in intestinal epithelial cells. *Exp. Cell Res.* **266**, 239–249 (2001).

264. Horiguchi, K. *et al.* Role of Ras signaling in the induction of snail by transforming growth factor-beta. *J Biol Chem* **284**, 245–253 (2009).

265. Smakman, N., Borel Rinkes, I. H. M., Voest, E. E. & Kranenburg, O. Control of colorectal metastasis formation by K-Ras. *Biochim Biophys Acta* **1756**, 103–114 (2005).

266. Sivaraman, V. S., Wang, H., Nuovo, G. J. & Malbon, C. C. Hyperexpression of mitogen-activated protein kinase in human breast cancer. *J Clin Invest* **99**, 1478–1483 (1997).

267. Salh, B. *et al.* Investigation of the Mek-MAP kinase-Rsk pathway in human breast cancer. *Anticancer Res.* **19**, 731–740 (1999).

268. Mueller, H. *et al.* Potential prognostic value of mitogen-activated protein kinase activity for disease-free survival of primary breast cancer patients. *Int. J. Cancer* **89**, 384–388 (2000).

269. Lintig, von, F. C. *et al.* Ras activation in human breast cancer. *Breast Cancer Res Treat* **62**, 51–62 (2000).

270. Loboda, A. *et al.* A gene expression signature of RAS pathway dependence predicts response to PI3K and RAS pathway inhibitors and expands the population of RAS pathway activated tumors. *BMC Med Genomics* **3**, 26 (2010).

271. Elenbaas, B. *et al.* Human breast cancer cells generated by oncogenic transformation of primary mammary epithelial cells. *Genes Dev* **15**, 50–65 (2001).

272. Sinn, E. *et al.* Coexpression of MMTV/v-Ha-ras and MMTV/c-myc genes in transgenic mice: synergistic action of oncogenes in vivo. *Cell* **49**, 465–475 (1987).

273. Stephens, P. J. *et al.* The landscape of cancer genes and mutational processes in breast cancer. *Nature* **486**, 400–404 (2012).

274. Ince, T. A. *et al.* Transformation of different human breast epithelial cell types leads to distinct tumor phenotypes. *Cancer Cell* **12**, 160–170 (2007).

275. Minn, A. J. *et al.* Distinct organ-specific metastatic potential of individual breast cancer cells and primary tumors. *J Clin Invest* **115**, 44–55 (2005).

276. Minn, A. J. *et al.* Genes that mediate breast cancer metastasis to lung. *Nature* **436**, 518–524 (2005).

277. Bos, P. D. *et al.* Genes that mediate breast cancer metastasis to the brain. *Nature* **459**, 1005–1009 (2009).

278. Levine, A. J. & Oren, M. The first 30 years of p53: growing ever more complex. 1–10 (2009).doi:10.1038/nrc2723

279. Junttila, M. R. & Evan, G. I. p53--a Jack of all trades but master of none. *Nat Rev Cancer* **9**, 821–829 (2009).

280. Honda, R., Tanaka, H. & Yasuda, H. Oncoprotein MDM2 is a ubiquitin ligase E3 for tumor suppressor p53. *FEBS Lett* **420**, 25–27 (1997).

281. Hollstein, M., Sidransky, D., Vogelstein, B. & Harris, C. C. p53 mutations in human cancers. *Science* **253**, 49–53 (1991).

282. Levine, A. J., Momand, J. & Finlay, C. A. The p53 tumour suppressor gene. *Nature* **351**, 453–456 (1991).

283. Baker, S. J. *et al.* Chromosome 17 deletions and p53 gene mutations in colorectal carcinomas. *Science* **244**, 217–221 (1989).

284. Malkin, D. *et al.* Germ line p53 mutations in a familial syndrome of breast cancer, sarcomas, and other neoplasms. *Science* **250**, 1233–1238 (1990).

285. Srivastava, S., Zou, Z. Q., Pirollo, K., Blattner, W. & Chang, E. H. Germ-line transmission of a mutated p53 gene in a cancer-prone family with Li-Fraumeni syndrome. *Nature* **348**, 747–749 (1990).

286. Donehower, L. A. *et al.* Mice deficient for p53 are developmentally normal but susceptible to spontaneous tumours. *Nature* **356**, 215–221 (1992).

287. Jacks, T. *et al.* Tumor spectrum analysis in p53-mutant mice. *Curr Biol* **4**, 1–7 (1994).

288. Lawler, J. *et al.* Thrombospondin-1 gene expression affects survival and tumor spectrum of p53-deficient mice. *Am J Pathol* **159**, 1949–1956 (2001).

289. Taverna, D., Ullman-Culleré, M., Rayburn, H., Bronson, R. T. & Hynes, R. O. A test of the

role of alpha5 integrin/fibronectin interactions in tumorigenesis. *Cancer Res* **58**, 848–853 (1998).

290. Jackson, E. L. *et al.* The differential effects of mutant p53 alleles on advanced murine lung cancer. *Cancer Res* **65**, 10280–10288 (2005).

291. Hingorani, S. R. *et al.* Trp53R172H and KrasG12D cooperate to promote chromosomal instability and widely metastatic pancreatic ductal adenocarcinoma in mice. *Cancer Cell* **7**, 469–483 (2005).

292. Cichowski, K. *et al.* Mouse models of tumor development in neurofibromatosis type 1. *Science* **286**, 2172–2176 (1999).

293. Vogel, K. S. *et al.* Mouse tumor model for neurofibromatosis type 1. *Science* **286**, 2176–2179 (1999).

294. Cheung, P., Allis, C. D. & Sassone-Corsi, P. Signaling to chromatin through histone modifications. *Cell* **103**, 263–271 (2000).

295. Portela, A. & Esteller, M. Epigenetic modifications and human disease. *Nat Biotechnol* **28**, 1057–1068 (2010).

296. Baylin, S. B. & Jones, P. A. A decade of exploring the cancer epigenome - biological and translational implications. *Nat Rev Cancer* **11**, 726–734 (2011).

297. Ringrose, L. & Paro, R. Epigenetic regulation of cellular memory by the Polycomb and Trithorax group proteins. *Annu. Rev. Genet.* **38**, 413–443 (2004).

298. Sparmann, A. & van Lohuizen, M. Polycomb silencers control cell fate, development and cancer. *Nat Rev Cancer* **6**, 846–856 (2006).

299. Bracken, A. P. & Helin, K. Polycomb group proteins: navigators of lineage pathways led astray in cancer. *Nat Rev Cancer* **9**, 773–784 (2009).

300. Kleer, C. G. *et al.* EZH2 is a marker of aggressive breast cancer and promotes neoplastic transformation of breast epithelial cells. *Proc Natl Acad Sci USA* **100**, 11606–11611 (2003).

301. Collett, K. *et al.* Expression of enhancer of zeste homologue 2 is significantly associated with increased tumor cell proliferation and is a marker of aggressive breast cancer. *Clin Cancer Res* **12**, 1168–1174 (2006).

302. Margueron, R. & Reinberg, D. The Polycomb complex PRC2 and its mark in life. *Nature* **469**, 343–349 (2011).

303. Bachmann, I. M. *et al.* EZH2 expression is associated with high proliferation rate and aggressive tumor subgroups in cutaneous melanoma and cancers of the endometrium, prostate, and breast. *J Clin Oncol* **24**, 268–273 (2006).

304. Li, X. *et al.* Targeted overexpression of EZH2 in the mammary gland disrupts ductal

morphogenesis and causes epithelial hyperplasia. *Am J Pathol* **175**, 1246–1254 (2009).

305. Chang, C.-J. *et al.* EZH2 promotes expansion of breast tumor initiating cells through activation of RAF1-β-catenin signaling. *Cancer Cell* **19**, 86–100 (2011).

306. Cao, R., Tsukada, Y.-I. & Zhang, Y. Role of Bmi-1 and Ring1A in H2A ubiquitylation and Hox gene silencing. *Mol Cell* **20**, 845–854 (2005).

307. Dimri, G. P. *et al.* The Bmi-1 oncogene induces telomerase activity and immortalizes human mammary epithelial cells. *Cancer Res* **62**, 4736–4745 (2002).

308. Kim, J. H. *et al.* Overexpression of Bmi-1 oncoprotein correlates with axillary lymph node metastases in invasive ductal breast cancer. *Breast* **13**, 383–388 (2004).

309. Prince, M. E. *et al.* Identification of a subpopulation of cells with cancer stem cell properties in head and neck squamous cell carcinoma. *Proc Natl Acad Sci USA* **104**, 973–978 (2007).

310. Choi, Y. J. *et al.* Expression of Bmi-1 protein in tumor tissues is associated with favorable prognosis in breast cancer patients. *Breast Cancer Res Treat* **113**, 83–93 (2009).

311. Datta, S. *et al.* Bmi-1 cooperates with H-Ras to transform human mammary epithelial cells via dysregulation of multiple growth-regulatory pathways. *Cancer Res* **67**, 10286–10295 (2007).

312. Hoenerhoff, M. J. *et al.* BMI1 cooperates with H-RAS to induce an aggressive breast cancer phenotype with brain metastases. *Oncology* **28**, 3022–3032 (2009).

313. Feinberg, A. P. & Vogelstein, B. Hypomethylation distinguishes genes of some human cancers from their normal counterparts. *Nature* **301**, 89–92 (1983).

314. Riggs, A. D. & Jones, P. A. 5-methylcytosine, gene regulation, and cancer. *Adv. Cancer Res.* **40**, 1–30 (1983).

315. Eden, A., Gaudet, F., Waghmare, A. & Jaenisch, R. Chromosomal instability and tumors promoted by DNA hypomethylation. *Science* **300**, 455 (2003).

316. Greger, V., Passarge, E., Höpping, W., Messmer, E. & Horsthemke, B. Epigenetic changes may contribute to the formation and spontaneous regression of retinoblastoma. *Hum. Genet.* **83**, 155–158 (1989).

317. Ventura, A. & Jacks, T. MicroRNAs and cancer: short RNAs go a long way. *Cell* **136**, 586–591 (2009).

318. Bartel, D. P. MicroRNAs: target recognition and regulatory functions. *Cell* **136**, 215–233 (2009).

319. Calin, G. A. *et al.* Human microRNA genes are frequently located at fragile sites and genomic regions involved in cancers. *Proc Natl Acad Sci USA* **101**, 2999–3004 (2004).

320. Takamizawa, J. *et al.* Reduced expression of the let-7 microRNAs in human lung cancers in association with shortened postoperative survival. *Cancer Res* **64**, 3753–3756 (2004).

321. Johnson, S. M. *et al.* RAS is regulated by the let-7 microRNA family. *Cell* **120**, 635–647 (2005).

322. Ma, L., Teruya-Feldstein, J. & Weinberg, R. A. Tumour invasion and metastasis initiated by microRNA-10b in breast cancer. *Nature* **449**, 682–688 (2007).

323. Hanahan, D. & Weinberg, R. A. Hallmarks of cancer: the next generation. *Cell* **144**, 646–674 (2011).

324. Pylayeva-Gupta, Y., Grabocka, E. & Bar-Sagi, D. RAS oncogenes: weaving a tumorigenic web. *Nat Rev Cancer* **11**, 761–774 (2011).

325. Kamangar, F., Dores, G. M. & Anderson, W. F. Patterns of cancer incidence, mortality, and prevalence across five continents: defining priorities to reduce cancer disparities in different geographic regions of the world. *J Clin Oncol* **24**, 2137–2150 (2006).

326. *The Sanger Institute Catalogue Of Somatic Mutations In Cancer http://www.sanger.ac.uk/cosmic*. (Wellcome Trust Sanger Institute).at <http://www.sanger.ac.uk/cosmic >

327. Lintig, von, F. C. *et al.* Ras activation in human breast cancer. *Breast Cancer Res Treat* **62**, 51–62 (2000).

328. Sjöblom, T. *et al.* The consensus coding sequences of human breast and colorectal cancers. *Science* **314**, 268–274 (2006).

329. Shah, S. P. *et al.* The clonal and mutational evolution spectrum of primary triple-negative breast cancers. *Nature* **486**, 395–399 (2012).

330. Lim, E. *et al.* Aberrant luminal progenitors as the candidate target population for basal tumor development in BRCA1 mutation carriers. *Nat Med* **15**, 907–913 (2009).

331. Hollestelle, A., Elstrodt, F., Nagel, J. H. A., Kallemeijn, W. W. & Schutte, M. Phosphatidylinositol-3-OH kinase or RAS pathway mutations in human breast cancer cell lines. *Mol Cancer Res* **5**, 195–201 (2007).

332. Seo, Y. H. & Carroll, K. S. Profiling protein thiol oxidation in tumor cells using sulfenic acid-specific antibodies. *PNAS* **106**, 16163–16168 (2009).

333. Mueller, C., Liotta, L. A. & Espina, V. Reverse phase protein microarrays advance to use in clinical trials. *Molecular Oncology* **4**, 461–481 (2010).

334. Hu, Z. *et al.* The molecular portraits of breast tumors are conserved across microarray platforms. *BMC Genomics* **7**, 96 (2006).

335. Parker, J. S. *et al.* Supervised risk predictor of breast cancer based on intrinsic subtypes. *J*

Clin Oncol **27**, 1160–1167 (2009).

336. Vousden, K. H. & Lane, D. P. p53 in health and disease. *Nat Rev Mol Cell Biol* **8**, 275–283 (2007).

337. Bild, A. H. *et al.* Oncogenic pathway signatures in human cancers as a guide to targeted therapies. *Nature* **439**, 353–357 (2006).

338. Song, M. S., Salmena, L. & Pandolfi, P. P. The functions and regulation of the PTEN tumour suppressor. *Nat Rev Mol Cell Biol* **13**, 283–296 (2012).

339. Gewinner, C. *et al.* Evidence that inositol polyphosphate 4-phosphatase type II is a tumor suppressor that inhibits PI3K signaling. *Cancer Cell* **16**, 115–125 (2009).

340. Fedele, C. G. *et al.* Inositol polyphosphate 4-phosphatase II regulates PI3K/Akt signaling and is lost in human basal-like breast cancers. *PNAS* **107**, 22231–22236 (2010).

341. McMenamin, M. E. *et al.* Loss of PTEN expression in paraffin-embedded primary prostate cancer correlates with high Gleason score and advanced stage. *Cancer Res* **59**, 4291–4296 (1999).

342. Thomas, G. V. *et al.* Antibody-based profiling of the phosphoinositide 3-kinase pathway in clinical prostate cancer. *Clin Cancer Res* **10**, 8351–8356 (2004).

343. Sarbassov, D. D., Guertin, D. A., Ali, S. M. & Sabatini, D. M. Phosphorylation and regulation of Akt/PKB by the rictor-mTOR complex. *Science* **307**, 1098–1101 (2005).

344. Jézéquel, P. *et al.* bc-GenExMiner: an easy-to-use online platform for gene prognostic analyses in breast cancer. *Breast Cancer Res Treat* **131**, 765–775 (2012).

345. Győrffy, B. *et al.* An online survival analysis tool to rapidly assess the effect of 22,277 genes on breast cancer prognosis using microarray data of 1,809 patients. *Breast Cancer Res Treat* **123**, 725–731 (2010).

346. Lessard, J. & Sauvageau, G. Bmi-1 determines the proliferative capacity of normal and leukaemic stem cells. *Nature* **423**, 255–260 (2003).

347. Blenkiron, C. *et al.* MicroRNA expression profiling of human breast cancer identifies new markers of tumor subtype. *Genome Biol* **8**, R214 (2007).

348. Bandrés, E. *et al.* Identification by Real-time PCR of 13 mature microRNAs differentially expressed in colorectal cancer and non-tumoral tissues. *Mol Cancer* **5**, 29 (2006).

349. Keshamouni, V. G., Mattingly, R. R. & Reddy, K. B. Mechanism of 17-beta-estradiol-induced Erk1/2 activation in breast cancer cells. A role for HER2 AND PKC-delta. *J Biol Chem* **277**, 22558–22565 (2002).

350. Yang, X.-Y. *et al.* p120Ras-GAP binds the DLC1 Rho-GAP tumor suppressor protein and inhibits its RhoA GTPase and growth-suppressing activities. *Oncology* **28**, 1401–1409

(2009).

351. Thomas, M. P. & Lieberman, J. miRNA target prediction. (2012).

352. Pagano, M. *et al.* Role of the ubiquitin-proteasome pathway in regulating abundance of the cyclin-dependent kinase inhibitor p27. *Science* **269**, 682–685 (1995).

353. Courtois-Cox, S., Jones, S. L. & Cichowski, K. Many roads lead to oncogene-induced senescence. *Oncology* **27**, 2801–2809 (2008).

354. Serrano, M., Lin, A. W., McCurrach, M. E., Beach, D. & Lowe, S. W. Oncogenic ras provokes premature cell senescence associated with accumulation of p53 and p16INK4a. *Cell* **88**, 593–602 (1997).

355. Sarkisian, C. J. *et al.* Dose-dependent oncogene-induced senescence in vivo and its evasion during mammary tumorigenesis. *Nat Cell Biol* **9**, 493–505 (2007).

356. Gingras, A.-C. MCC and USHBP1 binding partners. (2010).

357. Fukuyama, R. *et al.* Mutated in colorectal cancer, a putative tumor suppressor for serrated colorectal cancer, selectively represses beta-catenin-dependent transcription. *Oncology* **27**, 6044–6055 (2008).

358. Ishikawa, S. *et al.* Interaction of MCC2, a novel homologue of MCC tumor suppressor, with PDZ-domain Protein AIE-75. *Gene* **267**, 101–110 (2001).

359. Murphy, L. O. & Blenis, J. MAPK signal specificity: the right place at the right time. *Trends Biochem. Sci.* **31**, 268–275 (2006).

360. Yuan, T. L. & Cantley, L. C. PI3K pathway alterations in cancer: variations on a theme. *Oncology* **27**, 5497–5510 (2008).

361. Naugler, W. E. & Karin, M. NF-kappaB and cancer-identifying targets and mechanisms. *Curr. Opin. Genet. Dev.* **18**, 19–26 (2008).

362. Arpino, G., Wiechmann, L., Osborne, C. K. & Schiff, R. Crosstalk between the estrogen receptor and the HER tyrosine kinase receptor family: molecular mechanism and clinical implications for endocrine therapy resistance. *Endocr Rev* **29**, 217–233 (2008).

363. Kurokawa, H. *et al.* Inhibition of HER2/neu (erbB-2) and mitogen-activated protein kinases enhances tamoxifen action against HER2-overexpressing, tamoxifen-resistant breast cancer cells. *Cancer Res* **60**, 5887–5894 (2000).

364. Bedard, P. L., Cardoso, F. & Piccart-Gebhart, M. J. Stemming Resistance to HER-2 Targeted Therapy. *J Mammary Gland Biol Neoplasia* **14**, 55–66 (2009).

365. Moy, B. & Goss, P. E. Lapatinib: current status and future directions in breast cancer. *Oncologist* **11**, 1047–1057 (2006).

366. Eichhorn, P. J. A. *et al.* Phosphatidylinositol 3-Kinase Hyperactivation Results in Lapatinib Resistance that Is Reversed by the mTOR/Phosphatidylinositol 3-Kinase Inhibitor NVP-BEZ235. *Cancer Res* **68**, 9221–9230 (2008).

367. Berns, K. *et al.* A functional genetic approach identifies the PI3K pathway as a major determinant of trastuzumab resistance in breast cancer. *Cancer Cell* **12**, 395–402 (2007).

368. Serra, V. *et al.* NVP-BEZ235, a dual PI3K/mTOR inhibitor, prevents PI3K signaling and inhibits the growth of cancer cells with activating PI3K mutations. *Cancer Res* **68**, 8022–8030 (2008).

369. Moody, S. E. Lapatinib resistance. (2012).

370. Kasper, S. *et al.* Oncogenic RAS simultaneously protects against anti-EGFR antibody-dependent cellular cytotoxicity and EGFR signaling blockade. *Oncology* (2012).doi:10.1038/onc.2012.302

Appendix A

Generation of *Rasal2* Mutant Genetically Engineered Mouse Models

In this Appendix I detail the methods used to generate *Rasal2* mutant genetically engineered mouse models.

Generation of the *Rasal2* genetically engineered mouse model described in Chapter 2

As noted in Chapter 2 of this Dissertation, we generated *Rasal2* mutant mice using a genetrap targeting strategy. We purchased a mouse embryonic stem (ES) cell line in which the pNMDi4 genetrap cassette targets the third intron of *Rasal2*, which importantly is upstream of all known domains (Toronto Centre for Phenogenomics / Canadian Mouse Mutant Repository embryonic stem cell clone CMHD 463C12) (Figure 2-5A). We confirmed the presence of the genetrap cassette within the third intron of *Rasal2* using PCR from cDNA (Figure 2-5B). The Brigham and Women's Hospital Transgenic Mouse Facility injected the ES cells into blastocysts and implanted them into pseudo-pregnant recipients to generate chimeric pups. We crossed chimeras to wildtype Black 6 animals (C57BL/6-E, Charles River Laboratories cat. # 475) and tested agouti pups (those whose chimeric parent-derived germ cell was genetrap ES cell line based) for presence of the genetrap. We noticed that too high a fraction of agouti pups were genetrap-positive. We would expect 50% of agouti pups to be genetrap positive: 50% of ES cell derived germ cells should be genetrap positive since the parental ES cell line should be monoallelic for the genetrap. However, 100% of agouti pups (13/13) were genetrap positive. We hypothesized that this resulted from the presence of multiple insertions of the genetrap cassette within the genome of the original mouse ES cell line.

To determine the number of genetrap copies in the mouse ES cell line and F1 pups, we performed Southern blot analyses of genomic DNA, probing for the genetrap cassette. We found that the ES cell line had three copies of the genetrap cassette, and that F1 pups had two or three of these copies (Figure A-1A). These findings suggested that the ES cell line has two extra copies of the genetrap. We outcrossed F1 pups to wildtype mice and performed Southern blot analyses of genomic DNA from pups. By cross referencing the Southern blot results with

cDNA PCR analyses that tested for the presence of the genetrap cassette within the *Rasal2* locus, we identified animals with the genetrap cassette only within the *Rasal2* locus (Figure A-1B). These animals were used as founders for all cohorts described in this Dissertation.

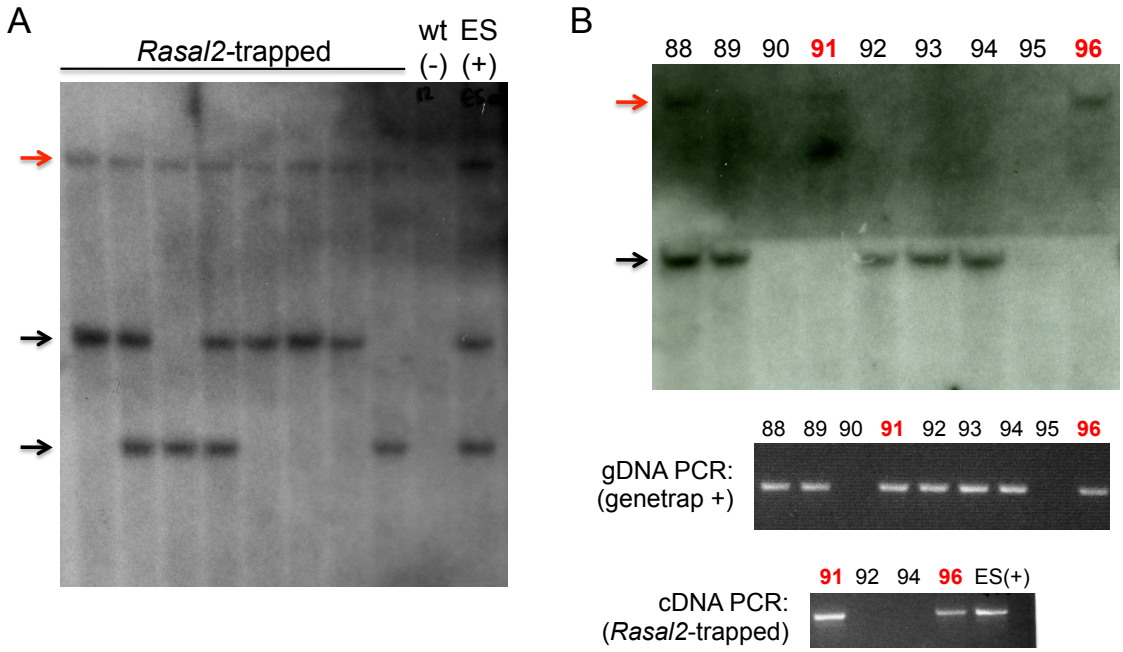

Figure A-1: Southern blot analysis of genetrap-positive mice
(A) Southern blot probed for genetrap cassette. Mouse embryonic stem cell line genomic DNA has 3 copies of the genetrap cassette (ES, far right lane). Genomic DNA from wildtype mice is a negative control and has no bands (wt, next to right most lane). Each other lane has genomic DNA from a mouse that has the genetrap cassette at least within the *Rasal2* locus, as determined by PCR of cDNA. The top band is present in all lanes, and therefore must be the band that recognizes the genetrap cassette in the *Rasal2* locus (red arrow). Black arrows indicate copies of the genetrap elsewhere in the genome.
(B) Confirmation of Southern blot results. Top panel: Southern blot for genetrap cassette. Red arrow indicates copy of the genetrap cassette within the *Rasal2* locus. Animals 91 and 96 have this band and no other bands. Middle panel: genomic DNA (gDNA) PCR is positive in all animals that have any copy of the genetrap cassette. All animals with a band on the Southern blot are gDNA PCR positive. Bottom panel: cDNA PCR for the genetrap cassette within the *Rasal2* locus. Animals 91 and 96 are positive, whereas 92 and 94 are negative (92 and 94 have the genetrap cassette within a different locus). Animals 91 and 96 were among those used to generate all cohorts and crosses.

Backcrossing *Rasal2* genetrap mice onto a pure background

The *Rasal2* genetrap animals described above and in Chapter 2 are on a 129-enriched background of 75% 129S1/SvImJ (129) and 25% C57BL6/J. We backcrossed the *Rasal2* genetrap line onto a pure 129 background through ten generations of backcrossing genetrap-

positive animals to wildtype 129S1/SvImJ animals and selecting genetrap-positive pups at each generation (Table A-1).

Table A-1: Genetically engineered mouse model backcrossing

Generation	129 contribution
F1	50.00%
N2	75.00%
N3	87.50%
N4	93.75%
N5	96.88%
N6	98.44%
N7	99.22%
N8	99.61%
N9	99.81%
N10	99.90%

Percent contribution of destination 129 genome to animals at each generation. Ten generations of backcrossing produces animals on a pure 129 background.

Generation of a second *Rasal2* genetrap mouse line

We obtained from the Texas Institute for Genomic Medicine a second mouse ES cell line with a genetrap cassette targeting *Rasal2*, mouse ES cell line IST11848D8 (Figure A-2A). The genetrap cassette is localized within intron 1 of *Rasal2* (Figure A-2B). We generated genetrap-positive animals, bred them onto a 129-enriched background, and generated a cohort of mice, which we have maintained within the laboratory but which we have not used for analyses described in this Dissertation.

A

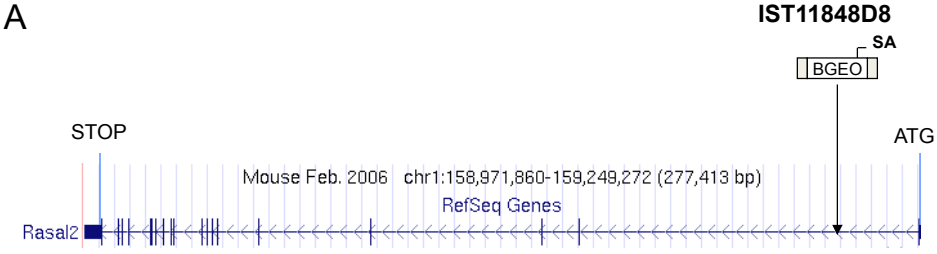

B

5'TAGAATCATACAATATTTATCTTTTTATATTTAGGTTATTTCCCTCTGTAAAATGTTTTCAGGGTTT
ATTCATATTGAAGCAAGTATCTAATTCTAGTCATTATAAGACTGAATAATATTCCTTTGTATGCGTT
GGTCATAATTTTTTAGACATTGATTTTCTGGTGAATGCTTTGGGTATTAACACTTTTTGGCTCTTG
TACGTCTTGCTGCTATCAAATTTGGTACACAAATAATCTTTCAATCCTTG*CTTGGAGTTTTTGGG
GGTATACCCAGGAGTAGAATTGCTGGGTCATATATTTTATTTTACTTTATTTTATTTTATTTATTT
TTTTTTTTTGGTTTTTCACACAGGGTTTCTCTGTGTAGCCCTAGCTGTCCTGGAACACACTCTGT
AGACCAGGCTGCCCTCGAACTCAGAAATCAGCCTGCCTCTGCCTCCCAAGTGCAAGGCATGC
GCCACCACTGCCCGACTCATATAATTTATTTTTAAGAGA-3'

Figure A-2: Second *Rasal2* genetrap line (A) Mouse ES genetrap cell line IST11848D8 targets intron 1 of *Rasal2*. (B) Precise location of the genetrap cassette as determined by the Texas Institute of Genomic Medicine. Asterisk indicates site of genetrap insertion.

Appendix B

Reprint: **An oncogene-tumor suppressor cascade drives metastatic prostate cancer by coordinately regulating Ras and nuclear factor-κB**

This Appendix consists of the following publication, in which I performed the experiments shown in Figure 4B and C, and, with Junxia Min, performed the shRNA screen described in the publication (Supplementary Figure 1) and shown as Figure 2-1 of this Dissertation.

An oncogene–tumor suppressor cascade drives metastatic prostate cancer by coordinately activating Ras and nuclear factor-κB.

Junxia Min, Alexander Zaslavsky, Giuseppe Fedele, Sara K McLaughlin, Elizabeth E Reczek, Thomas De Raedt, Isil Guney, David E Strochlic, Laura E MacConaill, Rameen Beroukhim, Roderick T Bronson, Sandra Ryeom, William C Hahn, Massimo Loda, and Karen Cichowski. *Nature Medicine* 16, pp. 286-294 (2010).

nature medicine

An oncogene–tumor suppressor cascade drives metastatic prostate cancer by coordinately activating Ras and nuclear factor-κB

Junxia Min[1,2], Alexander Zaslavsky[3], Giuseppe Fedele[2,4], Sara K McLaughlin[1,2], Elizabeth E Reczek[1,2], Thomas De Raedt[1,2], Isil Guney[2,4], David E Strochlic[2,4], Laura E MacConaill[5], Rameen Beroukhim[2,4,6,7], Roderick T Bronson[2], Sandra Ryeom[3], William C Hahn[2,4,5,7], Massimo Loda[2,4,7–9] & Karen Cichowski[1,2,10]

Metastasis is responsible for the majority of prostate cancer–related deaths; however, little is known about the molecular mechanisms that underlie this process. Here we identify an oncogene–tumor suppressor cascade that promotes prostate cancer growth and metastasis by coordinately activating the small GTPase Ras and nuclear factor-κB (NF-κB). Specifically, we show that loss of the Ras GTPase-activating protein (RasGAP) gene *DAB2IP* induces metastatic prostate cancer in an orthotopic mouse tumor model. Notably, DAB2IP functions as a signaling scaffold that coordinately regulates Ras and NF-κB through distinct domains to promote tumor growth and metastasis, respectively. *DAB2IP* is suppressed in human prostate cancer, where its expression inversely correlates with tumor grade and predicts prognosis. Moreover, we report that epigenetic silencing of *DAB2IP* is a key mechanism by which the polycomb-group protein histone-lysine *N*-methyltransferase EZH2 activates Ras and NF-κB and triggers metastasis. These studies define the mechanism by which two major pathways can be simultaneously activated in metastatic prostate cancer and establish EZH2 as a driver of metastasis.

Although early detection has reduced mortality from prostate cancer, there is no curative treatment for advanced disease[1]. Consequently, one in 30 men is expected to die from metastatic prostate cancer[1,2]. Nevertheless, our current understanding of the mechanisms that drive progression and metastasis is limited. Hyperactivation of Ras effector pathways (the extracellular signal-regulated kinase (ERK) and AKT kinase pathways) have been proposed to promote prostate cancer progression[3–6]. However, whereas AKT is activated by loss of the gene encoding phosphatase and tensin homolog, it is unclear how ERK is activated in this tumor type. *KRAS* and *BRAF* mutations are present in a subset of tumors from Japanese and Korean individuals, but are rare in American and European populations[7–9].

Ras is regulated positively by guanine nucleotide exchange factors (GEFs) and negatively by GAPs[10,11]. It is unknown whether GEFs have a role in cancer; however, one RasGAP, neurofibromin (encoded by *NF1*), is a known tumor suppressor[12–15]. Notably, there are 14 human RasGAPs, few of which have been studied in detail. Therefore, we investigated whether other RasGAP genes might also function as tumor suppressors. Here we identify a new tumor and metastasis suppressor within this gene family, define the mechanism by which its loss promotes metastatic prostate cancer and demonstrate that its epigenetic suppression is a key mechanism by which the polycomb-group protein EZH2 triggers metastasis.

RESULTS

DAB2IP suppression drives transformation

To identify tumor suppressors within the RasGAP family, we performed a cell-based screen, originally designed to quantify transformation caused by *NF1* loss[16]. As shown previously[16], *NF1* ablation promoted anchorage-independent growth (**Fig. 1a**). However, suppression of another RasGAP, *DAB2IP*, induced colonies that were larger than *NF1*-deficient colonies (**Fig. 1b**). Of note, transformation was not generally promoted by the loss of most RasGAPs, including p120RasGAP (**Fig. 1a** and **Supplementary Fig. 1**).

We then investigated whether there was evidence linking *DAB2IP* loss to human cancer. *DAB2IP* expression seems to be selectively suppressed in AML cell lines and in one case was disrupted by a translocation[17]. *DAB2IP* has also been reported to be epigenetically suppressed in advanced lung, breast and gastrointestinal tumors[18–20]. It is among the list of genes repressed by EZH2 in prostate cancer cell lines, a polycomb-group protein thought to promote advanced prostate cancer[21,22]. Nevertheless, the potential tumorigenic consequences of *DAB2IP* loss have not been investigated.

Given the proposed importance of the Ras-ERK pathway in prostate cancer progression and the lack of a mechanism by which it becomes activated[3–5,14], we explored a role for *DAB2IP* loss in this process.

[1]Genetics Division, Department of Medicine, Brigham and Women's Hospital, Boston, Massachusetts, USA. [2]Harvard Medical School, Boston, Massachusetts, USA. [3]Department of Cancer Biology, Abramson Family Cancer Research Institute, University of Pennsylvania School of Medicine, Philadelphia, Pennsylvania, USA. [4]Department of Medical Oncology, [5]Center for Cancer Genome Discovery and [6]Department of Cancer Biology, Dana-Farber Cancer Institute, Boston, Massachusetts, USA. [7]Broad Institute of Harvard and Massachusetts Institute of Technology, Cambridge, Massachusetts, USA. [8]Department of Pathology, Brigham and Women's Hospital, Boston, Massachusetts, USA. [9]Center for Molecular Oncologic Pathology, Dana-Farber Cancer Institute, Boston, Massachusetts, USA. [10]Ludwig Center at Dana-Farber/Harvard Cancer Center, Boston, Massachusetts, USA. Correspondence should be addressed to K.C. (kcichowski@rics.bwh.harvard.edu).

Received 21 September 2009; accepted 15 January 2010; published online 14 February 2010; doi:10.1038/nm.2100

Primary human prostate epithelial cells (PrECs) are immortalized by introducing Simian virus 40 (SV40) large T (LgT) and small t proteins and androgen receptor, but these cells are unable to form anchorage-independent colonies[23]. However, the addition of H-Ras^{V12} promotes colony growth and adenocarcinoma when such cells are injected into mice[23]. *DAB2IP* ablation also promoted colony growth, indicating that *DAB2IP* loss transforms human prostate cells (**Fig. 1c**). Notably, *DAB2IP* loss also triggered Ras, ERK and AKT activation (**Fig. 1d**). These phenotypes were reversed by rescuing cells with a *DAB2IP* complementary DNA (**Fig. 1e**,**f**).

DAB2IP loss promotes metastatic prostate cancer

When we orthotopically injected immortalized PrECs into mouse prostates, well-circumscribed, benign growths in the prostate developed (**Fig. 1g**), as previously described[23]. The lesions had a low proliferative index, showed considerable apoptosis and regressed (9 of 15 regressed completely) (**Fig. 1g** and **Supplementary Fig. 2a**,**b**). However, mice injected with PrECs expressing oncogenic H-Ras^{V12} (15 of 15) or *DAB2IP*-specific short hairpin RNAs (15 of 15), developed prostate adenocarcinomas that expressed cytokeratin-8, prostate-specific antigen (PSA) and little tumor protein p63, similar to high-grade human tumors (**Fig. 1g**,**h**). H-Ras^{V12}–expressing and *DAB2IP*-deficient tumors were highly proliferative, showed little apoptosis and grew with similar kinetics and to a similar maximum size (**Fig. 1g**,**i**,**j** and **Supplementary Fig. 2b**,**c**). Mice injected with *DAB2IP*-reconstituted cells were similar to controls; most lesions regressed in 45 d, were small in size, or both (**Fig. 1g** and **Supplementary Fig. 2c**).

However, whereas H-Ras^{V12}-driven tumors remained noninvasive and never disseminated, all *DAB2IP*-deficient tumors were invasive and metastatic (**Fig. 2** and **Supplementary Fig. 2d**). These tumors invaded the hip, lumbar muscle and bladder (**Fig. 2b**)[24]. We observed metastases starting at 45 d after injection in liver, proximal and distal lymph nodes,

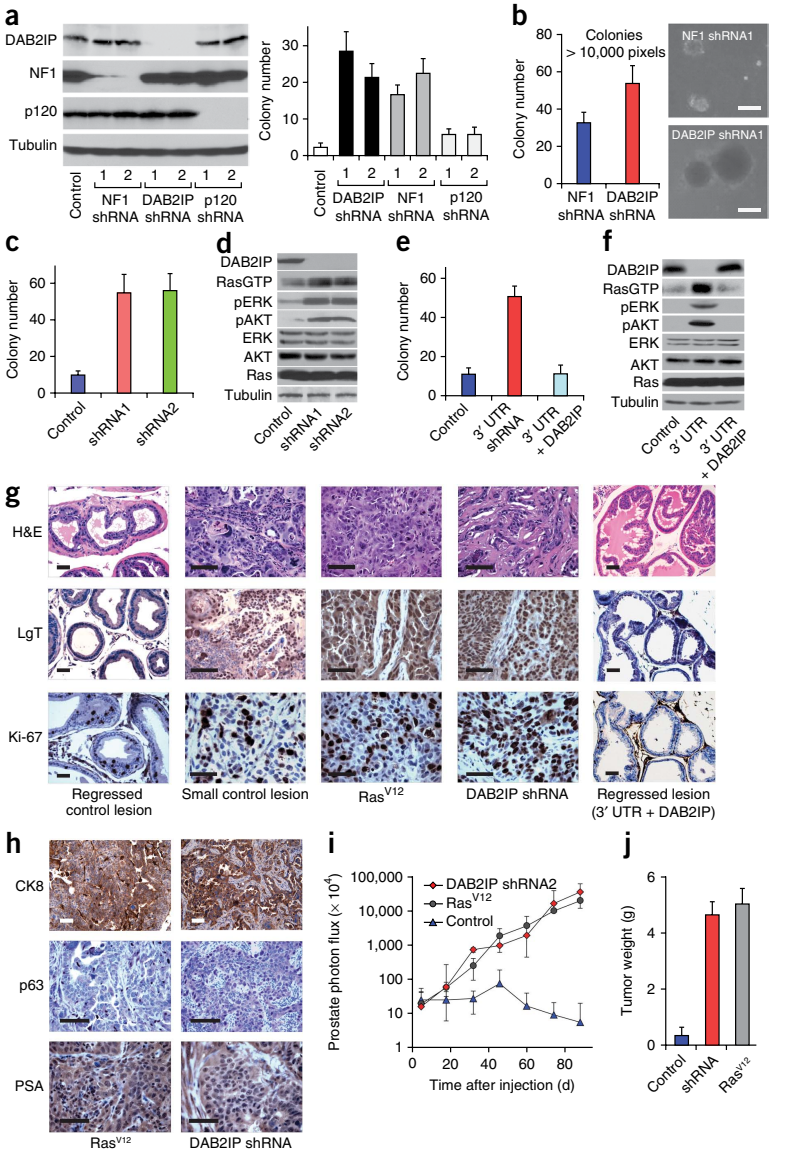

Figure 1 DAB2IP suppression induces prostate tumor development. (**a**) Left, immunoblots showing expression of NF1, DAB2IP and p120 RasGAP in mouse embryonic fibroblasts (MEFs) expressing the adenoviral E1A protein and a dominant-negative p53, after lentiviral expression of shRNAs targeting each protein. Right, colony formation in soft agar (right). Significance determined by Student's *t* test ($P = 3.7 \times 10^{-8}$ (DAB2IP shRNA1 versus control); $P = 8.6 \times 10^{-9}$ (DAB2IP shRNA2 versus control)). (**b**) Relative size of colonies resulting from loss of *Dab2ip* versus *Nf1*. A significant difference in colony size conferred by *Nf1* versus *Dab2ip* loss was determined by Student's *t* test ($P = 0.046$). $n = 3$. Scale bars, 1 mm. (**c**) Colony formation of immortalized PrEC cells infected with lentiviruses expressing *DAB2IP*-specific shRNA sequences. $n = 3$. Error bars refer to s.d. (**d**) Immunoblots of cells from **c** to assess DAB2IP knockdown and activation of Ras, ERK and AKT, as described in the Online Methods. (**e**) Colony growth induced by *DAB2IP* suppression with an shRNA directed to the 3′ untranslated region (UTR), or rescued with wild-type DAB2IP. (**f**) Immunoblots of cells in **e** to assess DAB2IP expression and activation of Ras, ERK and AKT. (**g**) Histological micrographs of tumors resulting from orthotopic injection of PrECs. Ki67 staining shows the proliferative index (quantified in **Supplementary Fig. 2**). The first column of images represents prostate tissue from a mouse in which a control lesion had regressed. The second column of images is from a small control lesion. The last column is from a prostate in which a 'rescued' lesion had regressed. (**h**) Immunohistochemical staining of H-Ras^{V12}–expressing and DAB2IP-deficient tumors with antibodies to cytokeratin-8 (CK8), p63 and PSA. (**i**) Volume of orthotopic tumors over time, calculated by Xenogen imaging. A Student's *t* test was used to compare the growth rates of H-Ras^{V12}–expressing and DAB2IP-deficient tumors ($P = 0.13$). $n = 10$ each. (**j**) Final weight of orthotopic tumors at H-Ras^{V12}–expressing and DAB2IP-deficient tumors (Student's *t* test ($P = 0.34$)). $n = 5$ each. All scale bars, 200 μm. Error bars refer to s.d.

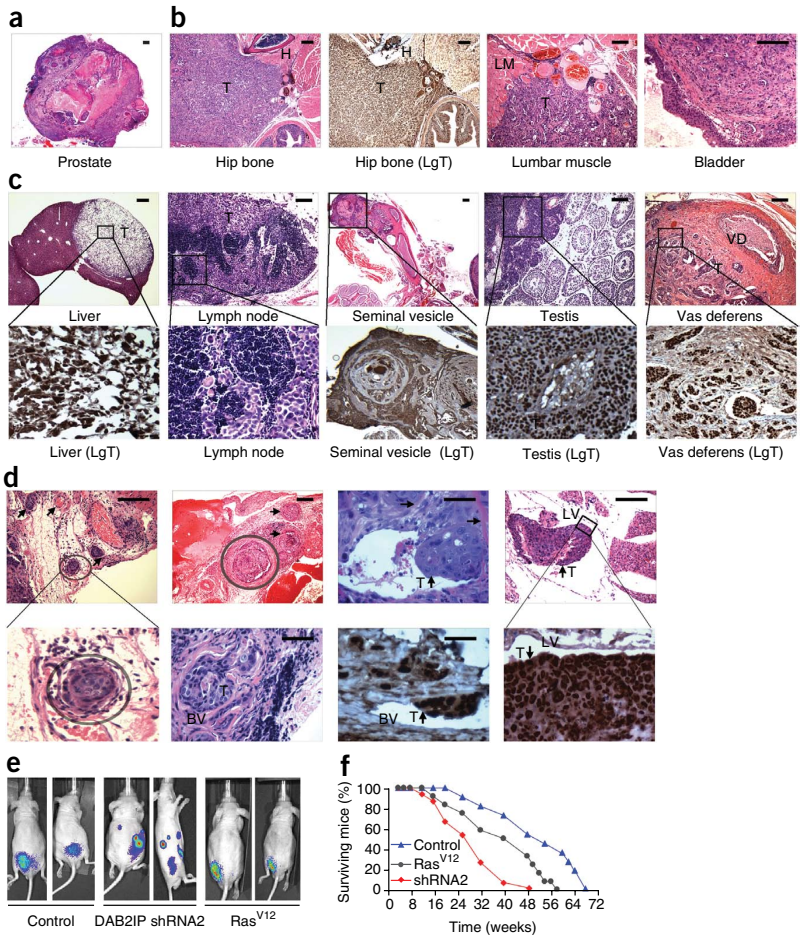

Figure 2 DAB2IP loss, but not H-Ras^{V12} expression, promotes invasion and widespread metastasis. (**a**) Histological micrographs of primary tumors from mice injected with H-Ras^{V12}-expressing PrEC cells. Scale bar, 5 mm. (**b**) Histological micrographs of primary tumors from mice injected with *DAB2IP*-deficient PrEC cells. Immunohistochemistry with an LgT-specific antibody is shown in the second image. Scale bar, 5 mm, except for lumbar muscle and bladder (scale bar, 1 mm). T, tumor; H, hipbone; LM, lumbar muscle. (**c**) Histological micrographs of metastases from mice injected with DAB2IP-deficient PrEC cells. Immunohistochemistry with an LgT-specific antibody on an adjacent section is shown at a higher power below each metastasis, with the exception of the lymph node, where H&E staining is shown. Scale bars: liver and seminal vesicle, 5 mm; lymph node, testis and vas deferens (VD), 1 nm. The first image in the top row was enlarged by 8.5-fold, the second image in the top row was enlarged by 4.5-fold, the third and fourth images in the top row were enlarged by 3.8-fold, and the fifth image in the top row was enlarged by 6.2-fold in Photoshop; all enlarged images are shown directly below the originals. (**d**) H&E-stained sections of tissues containing tumor cells (T) within blood vessels (BV and arrows) and lymphatic vessels (LV). When specified by lines, higher magnification images are shown. LgT antigen, which marks injected tumor cells, was expressed in cells found within both BV and LV (last two images, bottom row). Scale bars: first, second and fourth images in top row, 1 mm; third image in top row and second and third images on bottom row: 200 µm. The first panel in the top row was enlarged by 4.8-fold and the fourth image in the top row was enlarged by 6.2-fold in Photoshop; the enlarged images are shown directly below the originals. (**e**) Xenogen images of mice orthotopically injected with luciferase-expressing control, DAB2IP-deficient or H-Ras^{V12}-expressing cells. (**f**) Survival curves of mice with DAB2IP-deficient versus H-Ras^{V12}-expressing tumors.

seminal vesicles, testes and vas deferens (**Fig. 2c** and **Supplementary Fig. 2d**). The metastases were derived from PrECs, as confirmed by SV40 LgT antigen immunostaining and sequenome-based single nucleotide polymorphism genotyping (**Fig. 2c**,**d** and **Supplementary Fig. 3a**), and we never observed metastases from cells rescued with *DAB2IP*. We could readily detect DAB2IP-deficient tumor cells throughout the lymphatic and blood vessels, implicating both vessel systems in metastasis (**Fig. 2d**). Mice also developed thromboemboli, a life-threatening complication observed in a subset of individuals with prostate cancer (**Supplementary Fig. 3b**)[25]. The metastatic potential of these tumors can be best appreciated by Xenogen imaging (**Fig. 2e**). Mice harboring *DAB2IP*-deficient tumors showed reduced survival compared to those with H-Ras^{V12}–expressing tumors (**Fig. 2f**; $P = 0.03$, Mann-Whitney U test). Thus, *DAB2IP* suppression promotes prostate tumorigenesis and uniquely triggers metastasis.

RasGAP activity partially underlies DAB2IP function

Because DAB2IP is a RasGAP, we investigated whether aberrant Ras activation was responsible for these phenotypes. We expanded our analysis to include metastatic human prostate cancer cells in which *DAB2IP* is epigenetically silenced (PC-3 cells), to more directly assess the effects of *DAB2IP* loss in human cancer[21]. PC-3 and *DAB2IP*-deficient PrEC cells were reconstituted with wild-type *DAB2IP* or a GAP activity–deficient point mutant. Wild-type DAB2IP had subtle effects on the proliferation of these cell lines *in vitro*, indicating that the re-introduction of physiological amounts of DAB2IP does not, by itself, induce a growth arrest (**Supplementary Fig. 4**). DAB2IP proteins were equivalently expressed and recapitulated endogenous expression (**Fig. 3a**,**b**). Wild-type DAB2IP reduced Ras-GTP, phosphorylated ERK (pERK) and pAKT amounts, whereas the catalytically inactive RasGAP mutant (DAB2IP-R289L) did not suppress these effectors (**Fig. 3b**).

Mice injected with PC-3 cells developed metastatic prostate cancer (**Fig. 3c–e**). Wild-type DAB2IP significantly suppressed tumor development (**Fig. 3d**; $P = 3 \times 10^{-8}$, Mann-Whitney *U* test) and metastasis (**Fig. 3c**,**e**); however, DAB2IP-R289L was unable to suppress tumor growth, indicating that RasGAP activity is essential for its tumor-suppressive function (**Fig. 3c**,**d**; $P = 0.71$). Nevertheless, this mutant partially suppressed metastasis; only three of six mice developed metastases, and those that did had fewer metastases than mice injected with PC-3 cells lacking DAB2IP (**Fig. 3e**; $P = 0.0083$). We confirmed these findings with PrECs (**Fig. 3f**,**g**). These results suggest that other regions of DAB2IP harbor metastasis-suppressing activity.

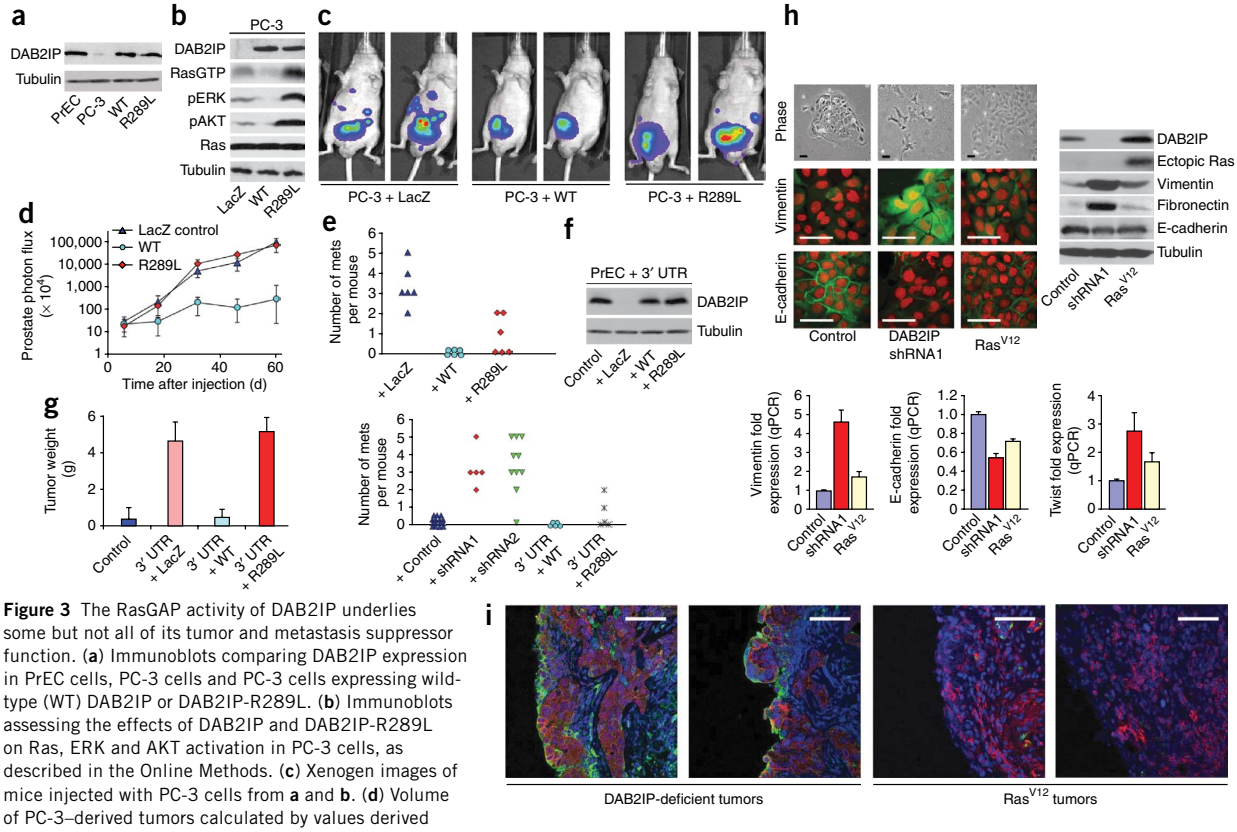

Figure 3 The RasGAP activity of DAB2IP underlies some but not all of its tumor and metastasis suppressor function. (**a**) Immunoblots comparing DAB2IP expression in PrEC cells, PC-3 cells and PC-3 cells expressing wild-type (WT) DAB2IP or DAB2IP-R289L. (**b**) Immunoblots assessing the effects of DAB2IP and DAB2IP-R289L on Ras, ERK and AKT activation in PC-3 cells, as described in the Online Methods. (**c**) Xenogen images of mice injected with PC-3 cells from **a** and **b**. (**d**) Volume of PC-3–derived tumors calculated by values derived from Xenogen images. (**e**) Dot plot depicting the number of metastases per mouse in mice injected with PC-3 cells expressing wild-type DAB2IP or DAB2IP-R289L. (**f**) DAB2IP immunoblot corresponding to **e**. (**g**) Left, bar graph showing final weight of tumors from PrECs. Right, dot plot depicting the number of metastases per mouse in mice injected with PrEC cells expressing *DAB2IP*-specific shRNAs 1 or 2 alone or with wild-type DAB2IP or DAB2IP-R289L. A Mann-Whitney *U* test ($P = 0.0030$) was used to illustrate a significant difference between the number of metastases that developed in mice injected with control PC-3 cells (expressing a LacZ contol) versus PC-3 cells expressing DAB2IP-R289L. (**h**) Left, phase-contrast images (top), immunofluorescence staining of the mesenchymal marker vimentin (middle) and immunofluorescence staining of the epithelial marker E-cadherin (bottom) of immortalized PrEC cells expressing a lentiviral vector control, a *DAB2IP*-specific shRNA or an activated Ras variant. Right, expression of DAB2IP, ectopic Ras, fibronectin, vimentin and E-cadherin, as detected by immunoblotting. Bottom, real-time PCR quantification of vimentin, E-cadherin and twist expression in response to DAB2IP loss or an activated Ras variant. (**i**) Confocal images of immunofluorescence staining of vimentin (green) and E-cadherin (red) in DAB2IP-deficient or H-Ras^{V12}-expressing tumors. All scale bars, 100 μm. Error bars reflect s.d.

DAB2IP regulates epithelial-to-mesenchymal transition

Notably, *DAB2IP* ablation in PrECs also induced an epithelial-to-mesenchymal transition (EMT), a dynamic cellular process thought to underlie metastasis by promoting invasion, intravasation and extravasation[26–28]. *DAB2IP* loss promoted an increase in the expression of the mesenchymal markers vimentin, twist and fibronectin and a concomitant reduction in the expression of membrane-bound E-cadherin (**Fig. 3h** and **Supplementary Fig. 5**)[29]. *DAB2IP* suppression also enhanced invasion (**Supplementary Fig. 5a**). EMT occurred synchronously within 96 h and was not caused by the outgrowth of a specialized subset of cells (**Supplementary Fig. 6**). In contrast, H-Ras^{V12} was a much weaker regulator of EMT (**Fig. 3h**).

We also observed EMT *in vivo*, as indicated by vimentin expression, which we observed in cells at the edge of these highly metastatic lesions (**Fig. 3i**). We observed this expression pattern in every tumor examined ($n = 12$), and the vimentin was present in tumor cells, not stroma, as the antibody that we used exclusively recognizes human protein. Similar findings have been described in a metastatic breast cancer model and support the hypothesis that environmental cues contribute to EMT and metastasis[28,30]. H-Ras^{V12}-expressing tumors never showed evidence of EMT (**Fig. 3i**), supporting the hypothesis that distinct effects of *DAB2IP* loss on EMT underlie metastasis.

DAB2IP loss promotes metastasis via NF-κB

Although Ras can promote EMT in some settings, a plethora of signals regulates this transition[27]. Of note, DAB2IP, in addition to its RasGAP activity, can suppress NF-κB in endothelial cells through a direct interaction with TRAF2, via a region distinct from the RasGAP domain[31]. Notably, NF-κB has a crucial role in EMT, and many EMT-associated genes, including *TWIST1*, are NF-κB targets[32]. NF-κB also promotes tumor progression and metastasis in other model systems[33]. Thus, we asked whether *DAB2IP* loss triggers EMT and metastasis by activating NF-κB.

Ectopic DAB2IP expression suppresses NF-κB in endothelial cells, but it was unknown whether *DAB2IP* loss would activate NF-κB in prostate cells[31]. DAB2IP ablation activated NF-κB (**Fig. 4a**) and increased expression of NF-κB transcriptional targets in PrECs

(**Fig. 4b**)[34]. Conversely, DAB2IP reconstitution suppressed NF-κB and target genes in PC-3 cells (**Fig. 4a**,**c**). A point mutant in the period-like domain of DAB2IP that prevents TRAF2 binding (S604A) is defective in suppressing NF-κB activity in endothelial cells[31]. DAB2IP-S604A did not effectively inhibit NF-κB, but it still suppressed Ras (**Supplementary Fig. 7a**,**b**). This mutant was also defective in suppressing invasion and EMT, suggesting that NF-κB mediates these phenotypes in response to *DAB2IP* loss (**Supplementary Fig. 7**). We confirmed this hypothesis by introducing a dominant-negative inhibitor of κBα protein, referred to as the IκBα super repressor (IκBαSR), which suppressed NF-κB activity, invasion and EMT in both model systems (**Supplementary Fig. 5** and data not shown). However, consistent with the notion that Ras feeds into the NF-κB pathway[35], the DAB2IP double mutant (R289L and S604A) was more defective in suppressing invasion, EMT and NF-κB, illustrating cooperativity between these two domains and downstream signals (**Supplementary Fig. 7**).

Notably, the DAB2IP-S604A mutant, which effectively suppressed Ras but not NF-κB, inhibited primary tumor growth, supporting the conclusion that Ras has a key role in tumor initiation (**Fig. 4d**–**g**; $P = 1.65 \times 10^{-7}$, Mann-Whitney U test). However, although the tumors were small, five of ten mice developed metastases, suggesting that aberrant NF-κB activity promoted dissemination (**Fig. 4f**,**g**). Accordingly, the IκBαSR had no effect on primary tumor development (**Fig. 4e**,**g**) but significantly suppressed metastasis (**Fig. 4f**,**g**; $P = 0.005$). The DAB2IP double mutant (R289L and S604A) did not suppress primary tumor development ($P = 0.48$) or metastasis ($P = 0.31$) (**Fig. 4e**–**g**). We observed similar results in the PrEC model (**Fig. 4h**,**i**).

We conclude that *DAB2IP* loss induces the activation of Ras and NF-κB in prostate cancer. Ras is essential in primary tumor growth, whereas NF-κB drives metastasis. Notably, we found that whereas both H-Ras^{V12} expression and *DAB2IP* loss activated ERK and

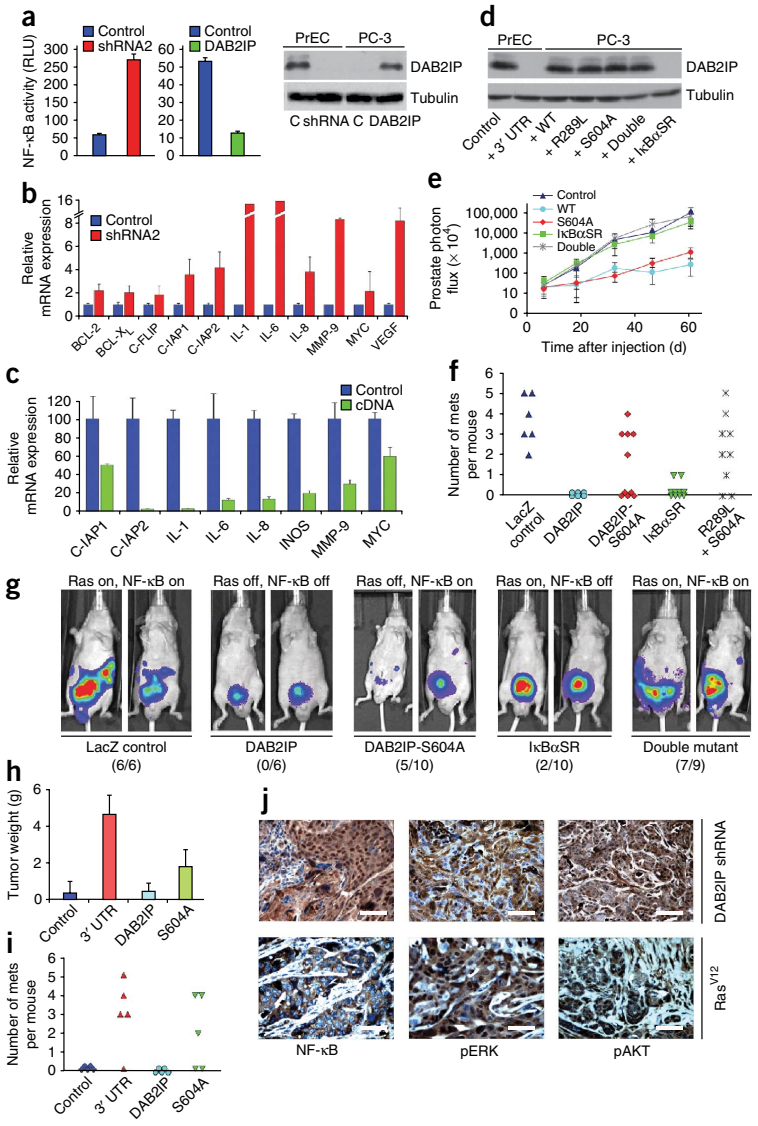

Figure 4 *DAB2IP* loss promotes tumorigenesis and metastasis via concomitant effects on Ras and NF-κB. (**a**) Left, NF-κB activity reported as relative light units (RLU) in response to DAB2IP suppression in PrEC cells. Middle, NF-κB activity in response to DAB2IP reconstitution in PC-3 cells. Right, DAB2IP immunoblot. Control (C) represents a control lentiviral shRNA or control cDNA plasmid where appropriate. (**b**) Expression of NF-κB targets as determined by quantitative PCR (qPCR) in PrEC cells with and without the DAB2IP shRNA even in the absence of the NF-κB–activating factor, tumor necrosis factor-α. BCL-2, B cell lymphoma-2; BCL-X_L, BCL2-like-1; C-FLIP, CASP8 and FADD-like apoptosis regulator; C-IAP1, baculoviral IAP repeat-containing-2; C-IAP2, baculoviral IAP repeat-containing-3; IL-1, interleukin-1; IL-6, interleukin-6; IL-8, interleukin-8; MMP-9, matrix metallopeptidase-9; MYC, v-myc myelocytomatosis viral oncogene homolog; VEGF, vascular endothelial growth factor; INOS, inducible nitric oxide synthase. (**c**) Expression of the same NF-κB targets as determined by qPCR in PC-3 cells with and without the DAB2IP cDNA, in the presence of tumor necrosis factor-α. (**d**) DAB2IP immunoblots of reconstituted PC-3 cells. Double DAB2IP mutant, R289L + S604A. IKBαSR expression is shown in **Supplementary Figure 7b**. (**e**) Tumor volumes derived from PC-3 cells calculated from Xenogen images. (**f**) A dot plot depicting the number of metastases detected in each mouse injected with PC-3 cells. (**g**) Xenogen images of mice injected with PC-3 cells from **d**–**f**. The Ras and NF-κB status noted above each image summarizes the biochemical effects of the expressed mutants. The numbers below the images represent the number of mice that developed metastases over the number of mice injected. (**h**) Final weight of tumors derived from control PrEC cells, PrEC cells with the 3′ UTR shRNA (3′ UTR cells), 3′ UTR cells reconstituted with DAB2IP or the S604A mutant. Expression of proteins was determined to be equivalent (data not shown). (**i**) A dot plot depicting the number of metastases detected in each mouse injected with the PrEC cells in **h**. (**j**) Immunohistochemistry with antibodies that recognize NF-κB, pERK and pAKT in DAB2IP-deficient and H-Ras^{V12}–expressing tumors. Scale bars, 200 μm. Error bars reflect s.d.

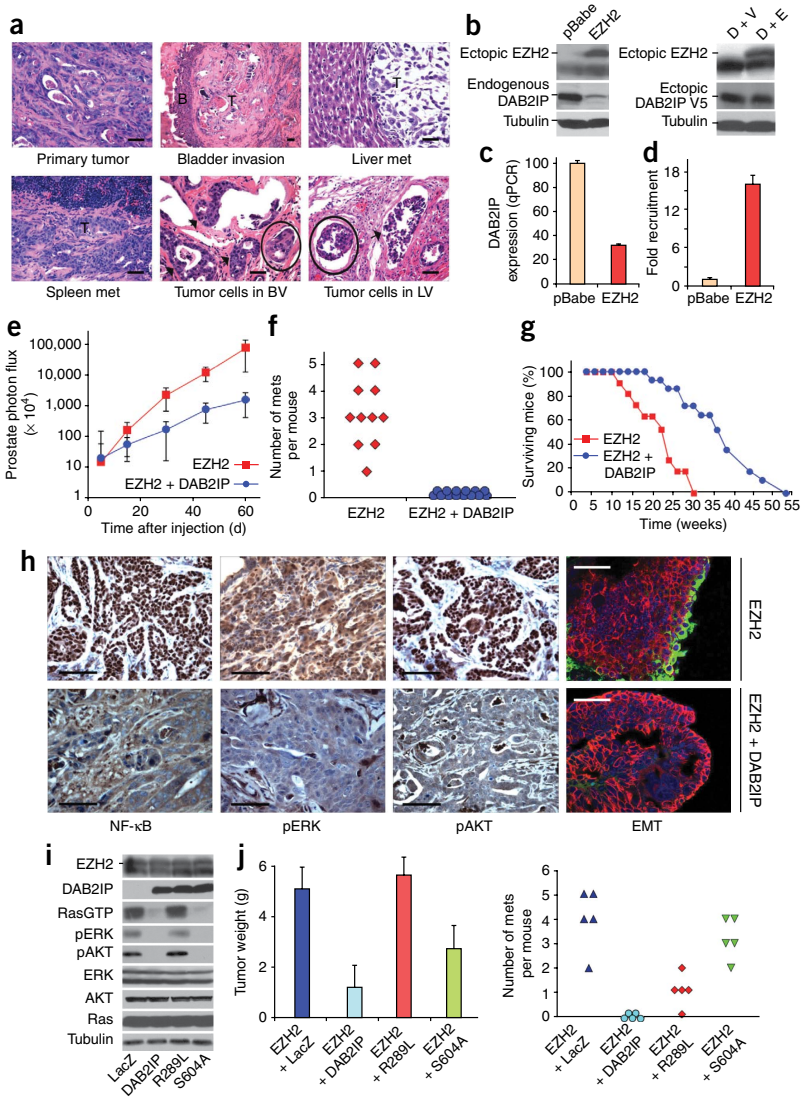

Figure 5 EZH2 promotes tumorigenesis and metastasis via suppression of *DAB2IP*. (**a**) Histological images of tumors and metastases from orthotopic injection of EZH2-expressing PrEC cells. Tumor cells observed within lymphatic vessels (LV) and blood vessels (BV) are circled. Metastasis data for all mice is in **Supplementary Table 1**. (**b**) Left, DAB2IP immunoblots of immortalized PrEC cells expressing a vector control or EZH2. The top band is EZH2. Right, immunoblots of cells in **b** reconstituted with ectopic DAB2IP with a V5 epitope tag. (**c**) Suppression of endogenous DAB2IP mRNA expression in response to EZH2, as determined by real-time PCR. pBabe seves as a control vector. (**d**) ChIP of EZH2 bound to the *DAB2IP* promoter. (**e**) Tumor volume calculated from Xenogen images of mice injected with cells expressing EZH2 or EZH2 and DAB2IP. (**f**) A dot plot depicting the number of metastases detected in each mouse injected with EZH2-expressing or EZH2- and DAB2IP-expressing PrEC cells. (**g**) Survival curves of mice orthotopically injected with iEZH2-expressing or EZH2- and DAB2IP-expressing PrEC cells. (**h**) Immunohistochemistry of EZH2-expressing or EZH2- and DAB2IP-expressing PrEC-derived tumors, using pERK–specific, pAKT–specific and NF-κB (p50) antibodies. On the left are confocal immunofluorescence images of EZH2-expressing or EZH2- and DAB2IP-expressing PrEC-derived tumors, using human vimentin-specific (green) and E-cadherin-specific (red) antibodies. (**i**) Immunoblots assessing the effects of EZH2 and DAB2IP reconstitution on Ras, ERK and AKT activation in PrEC cells, as described in the Online Methods. (**j**) Final weight of tumors and number of metastases detected in mice injected with the cells shown in **i**. All scale bars, 200 μm, except for confocal images, where scale bars are 100 μm. Error bars represent s.d.

AKT in prostate tumors, NF-κB was activated exclusively in *DAB2IP*-deficient tumors, as indicated by the nuclear rather than cytoplasmic staining of NF-κB in these cells, supporting the conclusion that DAB2IP has distinct effects on NF-κB (**Fig. 4j** and **Supplementary Fig. 8a**). Accordingly, we also observed an enhanced inflammatory response in *DAB2IP*-deficient tumors (**Supplementary Fig. 8b**). These observations challenge the concept that Ras and NF-κB exist in a simple linear pathway in this tumor type.

DAB2IP is a major EZH2 target

Thus far, our data identify a signaling cascade that drives metastatic disease and provide a tractable model system to interrogate the involvement of other genes in metastasis. Another gene implicated in metastatic prostate cancer is *EZH2*, which encodes the histone methyltransferase component of the polycomb-repressive complex-2 and regulates epigenetic gene silencing[36]. *EZH2* is overexpressed in many tumor types, and its expression correlates with tumor grade[36]. *EZH2* was also identified as the most differentially upregulated gene in metastatic prostate cancer[37]; however, EZH2 has never been shown to drive metastasis, thus a causal role for EZH2 in this process remains to be established.

Over 250 polycomb-repressive complex-2 targets have been identified, including *DAB2IP* (refs. 22,38,39). Therefore, we asked whether EZH2 could induce metastatic prostate cancer and investigated the potential contribution of *DAB2IP* silencing in EZH2-driven phenotypes. Notably, ectopic EZH2 expression promoted invasive prostate adenocarcinoma and metastasis to proximal and distal lymph nodes, liver and spleen (**Fig. 5a** and **Supplementary Table 1**). Like *DAB2IP*-deficient tumors, EZH2-driven tumors were detectable in lymphatic and blood vessels, and mice with these tumors developed thromboemboli (**Fig. 5a**).

The observation that EZH2 overexpression phenocopies *DAB2IP* loss suggested that *DAB2IP* might be a key target of EZH2 in metastatic prostate cancer. EZH2 suppressed DAB2IP protein and messenger RNA expression in PrECs (**Fig. 5b**,**c**), as previously observed in other cell lines[21]. Chromatin immunoprecipitation (ChIP) indicated that EZH2 bound the *DAB2IP* promoter (**Fig. 5d**), indicating a direct transcriptional suppression of *DAB2IP* by EZH2. When we reconstituted EZH2-expressing cells with endogenous levels of DAB2IP, tumor growth was suppressed, and in 2 of 14 cases the tumors eventually regressed (**Fig. 5e**; $P = 4 \times 10^{-12}$). Moreover, whereas we

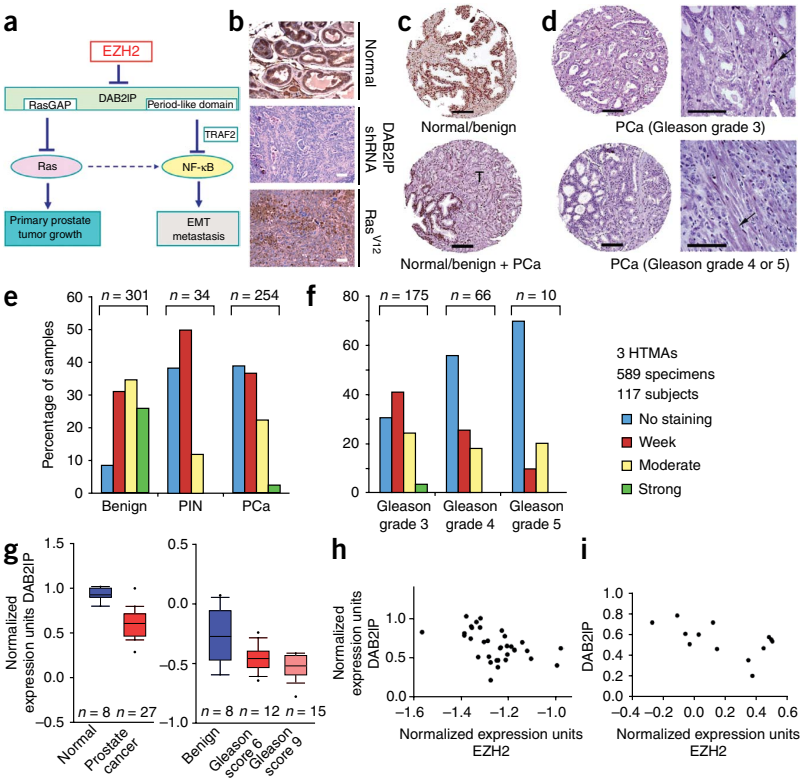

Figure 6 DAB2IP is suppressed in human prostate cancer. (**a**) Model of how EZH2 regulates DAB2IP, Ras and NF-κB to promote tumor development and metastasis. (**b**) DAB2IP immunohistochemical staining of normal mouse prostate, DAB2IP-deficient PrEC-derived tumors and Ras-driven tumors. (**c**) Top, immunohistochemical staining with a DAB2IP-specific antibody in normal human prostate epithelium. Bottom, immunohistochemical DAB2IP staining in normal human tissue and adjacent tumor tissue (T) within the same biopsy. PCa, prostate cancer. (**d**) Immunohistochemical staining of human tissue maicroarrays (HTMAs) with a DAB2IP-specific antibody in human prostate cancer tissues. Right, high-power magnification of images at left. Arrows depict stromal cells. (**e**) Histogram of DAB2IP protein expression in prostate intraepithelial neoplasia (PIN) and in prostate cancer compared to the benign prostate tissue (prostate cancer (PCa) versus benign prostate tissue, $P = 1.8 \times 10^{-27}$). (**f**) Histogram comparing DAB2IP expression and Gleason grade (not score), evaluated as the most prevalent pattern on each individual core (Gleason grade 5 versus Gleason grade 3 tumors, $P = 0.001$). Because the tissue sections on the arrays are relatively small, they were assigned a Gleason grade (1–5), rather than a Gleason score (1–10), the latter of which represents the combined total of the two most prevalent grades in an entire tumor. As such, Grade 4 and 5 tumors are high-grade tumors. (**g**) Box plots of DAB2IP mRNA expression data in prostate cancer compared to normal tissue ($P = 2.0 \times 10^{-7}$) and in high grade tumors as opposed to low grade and benign tissue ($P = 0.003$). (**h**,**i**) Expression of *DAB2IP* levels versus EZH2 levels in individual tumors and metastatic lesions using two different data sets described in text. All scale bars, 400 μm. Error bars represent s.d.

detected metastases in mice with EZH2-driven tumors within 8–12 weeks, DAB2IP prevented metastasis, even in mice surviving 1 year (**Fig. 5f**). Accordingly, mice injected with DAB2IP-expressing cells survived longer than those injected with cells expressing EZH2 alone (**Fig. 5g**; $P = 2.3 \times 10^{-4}$, Yates correction).

EZH2 also activated Ras, ERK, AKT and NF-κB, whereas DAB2IP reconstitution substantially suppressed activation (**Fig. 5h**,**i**). Moreover, like *DAB2IP*-deficient tumors, metastatic EZH2-expressing lesions also underwent EMT at the invasive edge, which was prevented by DAB2IP reconstitution (**Fig. 5h**). We also observed EMT *in vitro* (**Supplementary Fig. 9**). Finally, GAP domain (R289L) and period-like domain (S604A) mutants of DAB2IP had the same effects in EZH2-expressing cells as compared to DAB2IP-deficient PrEC and PC-3 cells on Ras signaling (**Fig. 5i**) and primary tumor growth and metastasis (**Fig. 5j**). Thus EZH2 activates Ras and NF-κB by epigenetically suppressing DAB2IP, providing the molecular mechanism by which an epigenetic regulator activates these two major signaling pathways (**Fig. 6a**).

DAB2IP is inactivated in human prostate cancer

DAB2IP deletions have not been reported in human tumors; however, our data suggested that epigenetic suppression might represent a key mechanism of *DAB2IP* loss in human prostate cancer. Although *DAB2IP* has been shown to be a target of EZH2 in a few prostate cancer cell lines[21], its expression has not been examined in human tumors. We confirmed the specificity of the DAB2IP-specific antibody (**Fig. 6b**) and performed immunohistochemical analysis on tissue microarrays containing 589 specimens from 117 individuals with prostate cancer. Normal basal and secretory cells expressed high amounts of DAB2IP (**Fig. 6c–f**). By contrast, the majority of prostatic intraepithelial neoplasias and adenocarcinomas showed weak or no DAB2IP expression, which was often restricted to stroma in these biopsies (**Fig. 6c–f**; Kruskal-Wallis test, $P = 1.8 \times 10^{-27}$). The low expression of DAB2IP can be appreciated in sections containing both normal and cancerous tissue (**Fig. 6c**). Notably, DAB2IP expression inversely correlated with Gleason grade (**Fig. 6f**; Kruskal-Wallis, $P = 0.001$). Finally, among 81 subjects for whom clinical information was available, we found that DAB2IP expression was significantly lower in subjects with a poor prognosis, as measured by a shorter time to elevated blood concentrations of PSA (univariate Cox regression analysis: hazard ratio, 0.51; 95% confidence interval, 0.2–0.9; $P = 0.03$). Taken together, these results support a causal role for *DAB2IP* loss in human prostate cancer progression.

To investigate whether *DAB2IP* suppression in prostate cancer is caused by EZH2-mediated transcriptional silencing, we examined *DAB2IP* and *EZH2* expression in Oncomine data sets[40]. Consistent with the results of our immunohistochemical analyses, *DAB2IP* mRNA levels were lower in prostate cancer compared to normal prostate tissue and decreased with increasing tumor grade (**Fig. 6g**; Student's *t* test $r = 7.181$, $P = 2 \times 10^{-7}$). We confirmed these results with three additional datasets[40–43]. By comparing *DAB2IP* and *EZH2* in individual tumors and metastases, we also found that *DAB2IP* levels inversely correlated with *EZH2* levels (**Fig. 6h**; Spearman $R = -0.5386$, *P* value (two-tailed) = 0.0010 (ref. 40); **Fig. 6i**; Spearman $R = -0.5604$,

P value (two-tailed) = 0.0463)[37]. Analysis of the distribution of *R* values from these data indicated that *DAB2IP* ranks in the top 4.5% of inversely correlated genes, as compared to *EZH2* (**Supplementary Fig. 10**). Collectively, these observations demonstrate that EZH2 and DAB2IP exist in a linear pathway that, when deregulated, promotes metastatic prostate cancer.

DISCUSSION

If detected early, prostate cancer is curable; however, there are no effective therapies for metastatic disease. The current treatment for recurrent prostate cancer is surgical or medical castration. However, patients ultimately relapse and develop androgen-independent, metastatic tumors[44]. Therefore there is a considerable gap in our understanding of the mechanisms that underlie prostate cancer progression, metastasis and the development of effective therapies.

This knowledge deficit is, in part, due to the lack of tractable model systems. Genetically engineered mouse models have helped define genes involved in tumor initiation and aspects of tumor progression; however, few models develop metastases, and, in those that do, it is unclear which genes drive this transition[45,46]. Thus, orthotopic models represent a platform that can be used in a more high-throughput fashion for gene discovery, in particular for metastasis, which requires numerous prerequisite alterations. In this study we have identified *DAB2IP* as a regulator of metastatic prostate cancer. To our knowledge, no other gene has been shown to have a direct causal role in driving prostate cancer metastasis, underscoring the importance of this finding and the utility of this model.

These studies also provide insight into mechanisms that regulate tumor initiation versus metastasis. Specifically, *DAB2IP* loss promotes primary tumor growth by activating Ras and drives metastasis through NF-κB, serving as a signaling scaffold to coordinately regulate these two prominent oncogenic pathways (**Fig. 6a**). Although Ras and NF-κB are known to be activated in advanced prostate cancer, the genetic alterations that confer activation are largely unknown[3–6,47]. Our findings reveal a molecular mechanism by which these two pathways can be activated in prostate cancer.

In some settings, Ras can promote NF-κB activation via its effects on the Ras-related protein RalB and the TANK-binding kinase-1 (refs. 47,48); however, here we report that Ras is not sufficient to stimulate NF-κB in prostate tumors. Although these observations seem contradictory, a mutation in the GAP domain of DAB2IP enhances the effects of a mutation in the period-like domain (on NF-κB activity), consistent with a cooperative role for Ras in this pathway. NF-κB is regulated by the integrated output of many signals, which may be differentially limiting in different tumor types. The data presented here suggest that DAB2IP is a crucial guardian of the NF-κB pathway in prostate tissue.

Finally, these studies suggest that epigenetic suppression of *DAB2IP* by EZH2 is a major mechanism of its inactivation in human prostate cancer. Of note, although EZH2 is highly expressed in advanced and metastatic prostate cancer[37], it has never been shown to induce metastasis, leading to the unresolved question of whether EZH2 upregulation is a marker or driver of metastasis[49]. Our studies establish a causal role for EZH2 in driving metastasis and identify *DAB2IP* as a key target in this process among numerous target genes, although certainly others may contribute. These observations have major therapeutic implications. Because EZH2 is an enzyme, it has been proposed to be a potential therapeutic target[36]. Our data underscore the utility of developing EZH2 inhibitors, as such agents might suppress both Ras and NF-κB—proteins that have proven difficult to target directly—in prostate cancer. These findings also support the possibility that such inhibitors might affect primary tumors and metastatic lesions.

METHODS

Methods and any associated references are available in the online version of the paper at http://www.nature.com/naturemedicine/.

Note: Supplementary information is available on the Nature Medicine website.

ACKNOWLEDGMENTS

The PMMP-luc-neo retroviral luciferase construct was generously provided by A.L. Kung and M. Chheda (Dana-Farber Cancer Institute (DFCI)). pRL-TK was a gift from J. Boehm (Broad Institute). We thank D. Barbie (DFCI), J. Boehm for NF-κB target primers and R. Chen (DFCI) for IκBαSR and G. Evan for helpful discussions. This grant was supported by in part by the US Department of Defense (PC074048) and the Ludwig Center at Dana-Farber/Harvard Cancer Center.

AUTHOR CONTRIBUTIONS

J.M., A.Z., S.K.M., E.E.R., I.G. and D.E.S. performed *in vitro* and *in vivo* experiments. G.F., R.T.B. and M.L. analyzed and interpreted the immunohistochemistry and histology experiments. G.F. performed analysis on tissue microarrays. T.D.R. performed statistical analysis. L.E.M. and R.B. performed Sequenome analysis. S.R., W.C.H. and M.L. provided scientific advice and helpful comments on manuscript. J.M. and K.C. conceptualized experiments, prepared figures and drafted the manuscript.

COMPETING INTERESTS STATEMENT

The authors declare no competing financial interests.

Published online at http://www.nature.com/naturemedicine/.
Reprints and permissions information is available online at http://npg.nature.com/reprintsandpermissions/.

1. Nelson, W.G., De Marzo, A.M. & Isaacs, W.B. Prostate cancer. *N. Engl. J. Med.* **349**, 366–381 (2003).
2. Jemal, A. *et al.* Cancer statistics, 2008. *CA Cancer J. Clin.* **58**, 71–96 (2008).
3. Jeong, J.H. *et al.* BRAF activation initiates but does not maintain invasive prostate adenocarcinoma. *PLoS One* **3**, e3949 (2008).
4. Shen, M.M. & Abate-Shen, C. Pten inactivation and the emergence of androgen-independent prostate cancer. *Cancer Res.* **67**, 6535–6538 (2007).
5. Gioeli, D., Mandell, J.W., Petroni, G.R., Frierson, H.F. Jr. & Weber, M.J. Activation of mitogen-activated protein kinase associated with prostate cancer progression. *Cancer Res.* **59**, 279–284 (1999).
6. Malik, S.N. *et al.* Immunohistochemical demonstration of phospho-Akt in high Gleason grade prostate cancer. *Clin. Cancer Res.* **8**, 1168–1171 (2002).
7. Carter, B.S., Epstein, J.I. & Isaacs, W.B. ras gene mutations in human prostate cancer. *Cancer Res.* **50**, 6830–6832 (1990).
8. Gumerlock, P.H., Poonamallee, U.R., Meyers, F.J. & deVere White, R.W. Activated ras alleles in human carcinoma of the prostate are rare. *Cancer Res.* **51**, 1632–1637 (1991).
9. Cho, N.Y. *et al.* BRAF and KRAS mutations in prostatic adenocarcinoma. *Int. J. Cancer* **119**, 1858–1862 (2006).
10. Bernards, A. & Settleman, J. GEFs in growth factor signaling. *Growth Factors* **25**, 355–361 (2007).
11. Bernards, A. & Settleman, J. GAPs in growth factor signaling. *Growth Factors* **23**, 143–149 (2005).
12. Riccardi, V.M. *Neurofibromatosis: Phenotype, Natural History and Pathogenesis.* Ch. 3 (The Johns Hopkins University Press, Baltimore, 1992).
13. Ding, L. *et al.* Somatic mutations affect key pathways in lung adenocarcinoma. *Nature* **455**, 1069–1075 (2008).
14. Cancer Genome Atlas Research Network. Comprehensive genomic characterization defines human glioblastoma genes and core pathways. *Nature* **455**, 1061–1068 (2008).
15. McGillicuddy, L.T. *et al.* Proteasomal and genetic inactivation of the NF1 tumor suppressor in gliomagenesis. *Cancer Cell* **16**, 44–54 (2009).
16. Johannessen, C.M. *et al.* The NF1 tumor suppressor critically regulates TSC2 and mTOR. *Proc. Natl. Acad. Sci. USA* **102**, 8573–8578 (2005).
17. von Bergh, A.R. *et al.* Identification of a novel RAS GTPase–activating protein (RASGAP) gene at 9q34 as an MLL fusion partner in a patient with *de novo* acute myeloid leukemia. *Genes Chromosom. Cancer* **39**, 324–334 (2004).
18. Dote, H. *et al.* Aberrant promoter methylation in human DAB2 interactive protein (hDAB2IP) gene in breast cancer. *Clin. Cancer Res.* **10**, 2082–2089 (2004).
19. Dote, H. *et al.* Aberrant promoter methylation in human DAB2 interactive protein (hDAB2IP) gene in gastrointestinal tumour. *Br. J. Cancer* **92**, 1117–1125 (2005).
20. Yano, M. *et al.* Aberrant promoter methylation of human DAB2 interactive protein (hDAB2IP) gene in lung cancers. *Int. J. Cancer* **113**, 59–66 (2005).

21. Chen, H., Tu, S.W. & Hsieh, J.T. Down-regulation of human *DAB2IP* gene expression mediated by polycomb Ezh2 complex and histone deacetylase in prostate cancer. *J. Biol. Chem.* **280**, 22437–22444 (2005).
22. Ke, X.S. *et al.* Genome-wide profiling of histone h3 lysine 4 and lysine 27 trimethylation reveals an epigenetic signature in prostate carcinogenesis. *PLoS One* **4**, e4687 (2009).
23. Berger, R. *et al.* Androgen-induced differentiation and tumorigenicity of human prostate epithelial cells. *Cancer Res.* **64**, 8867–8875 (2004).
24. Arai, Y. *et al.* Radical prostatectomy for clinically localized prostate cancer: local tumor extension and prognosis. *Int. J. Urol.* **3**, 373–378 (1996).
25. Sørensen, H.T., Mellemkjaer, L., Olsen, J.H. & Baron, J.A. Prognosis of cancers associated with venous thromboembolism. *N. Engl. J. Med.* **343**, 1846–1850 (2000).
26. Scheel, C., Onder, T., Karnoub, A. & Weinberg, R.A. Adaptation versus selection: the origins of metastatic behavior. *Cancer Res.* **67**, 11476–11479, discussion 11479–11480 (2007).
27. Thiery, J.P. Epithelial-mesenchymal transitions in tumour progression. *Nat. Rev. Cancer* **2**, 442–454 (2002).
28. Weinberg, R.A. *The Biology of Cancer.* (Garland Science, New York, 2007).
29. Yang, J. *et al.* Twist, a master regulator of morphogenesis, plays an essential role in tumor metastasis. *Cell* **117**, 927–939 (2004).
30. Joyce, J.A. & Pollard, J.W. Microenvironmental regulation of metastasis. *Nat. Rev. Cancer* **9**, 239–252 (2009).
31. Zhang, H. *et al.* AIP1/DAB2IP, a novel member of the Ras-GAP family, transduces TRAF2-induced ASK1-JNK activation. *J. Biol. Chem.* **279**, 44955–44965 (2004).
32. Huber, M.A., Beug, H. & Wirth, T. Epithelial-mesenchymal transition: NF-κB takes center stage. *Cell Cycle* **3**, 1477–1480 (2004).
33. Naugler, W.E. & Karin, M. NF-κB and cancer-identifying targets and mechanisms. *Curr. Opin. Genet. Dev.* **18**, 19–26 (2008).
34. Hayden, M.S. & Ghosh, S. Shared principles in NF-κB signaling. *Cell* **132**, 344–362 (2008).
35. Mayo, M.W. *et al.* Requirement of NF-κB activation to suppress p53-independent apoptosis induced by oncogenic Ras. *Science* **278**, 1812–1815 (1997).
36. Simon, J.A. & Lange, C.A. Roles of the EZH2 histone methyltransferase in cancer epigenetics. *Mutat. Res.* **647**, 21–29 (2008).
37. Varambally, S. *et al.* The polycomb group protein EZH2 is involved in progression of prostate cancer. *Nature* **419**, 624–629 (2002).
38. Yu, J. *et al.* A polycomb repression signature in metastatic prostate cancer predicts cancer outcome. *Cancer Res.* **67**, 10657–10663 (2007).
39. Kondo, Y. *et al.* Gene silencing in cancer by histone H3 lysine 27 trimethylation independent of promoter DNA methylation. *Nat. Genet.* **40**, 741–750 (2008).
40. Vanaja, D.K., Cheville, J.C., Iturria, S.J. & Young, C.Y. Transcriptional silencing of zinc finger protein 185 identified by expression profiling is associated with prostate cancer progression. *Cancer Res.* **63**, 3877–3882 (2003).
41. Lapointe, J. *et al.* Gene expression profiling identifies clinically relevant subtypes of prostate cancer. *Proc. Natl. Acad. Sci. USA* **101**, 811–816 (2004).
42. Tomlins, S.A., Rubin, M.A. & Chinnaiyan, A.M. Integrative biology of prostate cancer progression. *Annu. Rev. Pathol.* **1**, 243–271 (2006).
43. Luo, J.H. *et al.* Gene expression analysis of prostate cancers. *Mol. Carcinog.* **33**, 25–35 (2002).
44. Daskivich, T.J. & Oh, W.K. Recent progress in hormonal therapy for advanced prostate cancer. *Curr. Opin. Urol.* **16**, 173–178 (2006).
45. Abate-Shen, C. & Shen, M.M. Mouse models of prostate carcinogenesis. *Trends Genet.* **18**, S1–S5 (2002).
46. Wang, S. *et al.* Prostate-specific deletion of the murine Pten tumor suppressor gene leads to metastatic prostate cancer. *Cancer Cell* **4**, 209–221 (2003).
47. Henry, D.O. *et al.* Ral GTPases contribute to regulation of cyclin D1 through activation of NF-kappaB. *Mol. Cell. Biol.* **20**, 8084–8092 (2000).
48. Barbie, D.A. *et al.* Systematic RNA interference reveals that oncogenic KRAS-driven cancers require TBK1. *Nature* **462**, 108–112 (2009).
49. Sellers, W.R. & Loda, M. The EZH2 polycomb transcriptional repressor—a marker or mover of metastatic prostate cancer? *Cancer Cell* **2**, 349–350 (2002).

ONLINE METHODS

Cell culture. We established MEFs and immortalized PrECs expressing the adenoviral *E1A*-encoded protein and a dominant-negative p53 as previously described[16,23]. We obtained PrECs from Loza and grew them in defined prostate epithelial cells growth medium as previously described[23]. We obtained PC-3 cells from American Type Culture Collection and cultured them according to the suppliers' instructions.

Plasmids and retroviral and lentiviral infections. We obtained lentiviral pLKO shRNAs specific for the genes encoding DAB2IP2IP, NF1 and p120RasGAP from the Broad Institute RNAi consortium. The sequences for each siRNA set are as follows: DAB2IP shRNA 1: sense 5′-GCACATCACTAACCACTACCT-3′ and antisense 5′-AGGTAGTGGTTAGTGATGTGC-3′; DAB2IP shRNA 2: sense 5′-GTAATGTAACTATCTCACCTA-3′ and antisense 5′-TAGGTGAGATAGTT ACATTAC-3′; NF1 shRNA 1: sense 5′-CAACAACTTCAATGCAGTCTT-3′ and antisense 5′-AAGACTGCATTGAAGTTGTTG-3′; NF1 shRNA 2: sense 5′-TTATA AATAGCCTGGAAAAGG-3′ and antisense 5′-CCTTTTCCAGGCTATTTATAA; p120RasGAP shRNA 1: sense 5′-GCTGCCTAACTTATCCATCTT-3′ and antisense 5′-AAAAAGCTGCCTAACTTATCC-3′; p120RasGAP shRNA 2: sense 5′-CCCTACATGGAAGGTGTCAAT-3′ and antisense 5′-TAAAAACCCTACAT GGAAGGTG-3′; EZH2 shRNA 1: sense 5′-CGGAAATCTTAAACCAAGAAT-3′ and antisense 5′-CAAAAACGGAAATCTTAAAC-3′; EZH2 shRNA 2: sense 5′-TATTGCCTTCTCACCAGCTGC-3′ and antisense 5′-CAAAAATATTGCC TTCTCACC-3′. We assessed knockdown was assessed by western blotting or qPCR, as noted. We performed retroviral and lentiviral infections as previously described[16,23]. We amplified full-length DAB2IP cDNA by RT-PCR, cloned it into pLenti4/V5-DEST vector (Invitrogen) and verified the sequence. We cloned the EZH2 cDNA into pBabe-myc retroviral vector. We used the PMMP-luc-neo retroviral luciferase construct to monitor tumor growth in live mice[48].

Soft agar assay. We performed soft agar assays with MEFs or PrEC cells as previously described[16]. We analyzed colony size by ImageJ (US National Institutes of Health).

Nuclear factor-κB reporter assays. We seeded 2×10^4 cells in triplicate in 24-well plates. After 18 h, we transfected 100 ng of pNF-κB–luciferase (BD Bioscience) or pISRE-luciferase (Stratagene) plus 25 ng *Renilla* luciferase–encoding plasmid (pRL-TK) in triplicate wells with Fugene6 (Roche). We measured luciferase activity followed by *Renilla* luciferase activity 36 h after transfection with the Dual Luciferase Reporter Assay Kit (Promega). All data were normalized as relative luciferase light units / *Renilla* luciferase light units.

Chromatin immunoprecipitation assay. We performed the ChIP assay as described previously[50] with the ChIP Assay Kit (Upstate).

Immunoblotting and immunofluorescence. We generated a DAB2IP-specific monoclonal antibody against the last 120 C-terminal amino acids and named it WF17.1 (Dana-Farber Cancer Institute core facility). We used a hybridoma supernatant at a dilution of 1:6. We also used antibodies to the following proteins: NF1 (Santa Cruz, SC-67D), p120RasGAP (Transduction Laboratories), tubulin (Sigma), pERK(Ser473), pAKT, total ERK and total AKT (all ERK and AKT antibodies, Cell Signaling Technologies), E-cadherin (Santa Cruz), human vimentin (DakoCytomation) and EZH2 (monoclonal from BD, polyclonal from Invitrogen). We used Alexa Fluor 488 conjugated to mouse or rabbit secondary antibodies (Molecular Probes) for immunofluorescence. We performed confocal imaging with Zeiss LSM410 confocal microscopy systems.

Quantitative real-time PCR. We isolated total RNA with Trizol (Invitrogen). We obtained probes for specific genes from Applied Biosystems. We performed quantitative real-time PCR with iscript (Applied Biosystems). We performed each reaction in triplicate and normalized values to glyceraldehyde 3-phosphate dehydrogenase.

Orthotopic implantation. We obtained athymic male nude mice (*nu/nu*; 6 weeks old) from Jackson Laboratory. Mouse handling and experimental procedures were approved by the Center for Animal and Comparative Medicine in Harvard Medical School in accordance with the US National Institutes of Health Guidelines for the Care and Use of Laboratory Animals and the Animal Welfare Act. We carried out orthotopic implantations as previously described[23]. Briefly, we injected a suspension of cells (5×10^5 cells per 10 μl) in 50 μl of a 1:1 mixture of PBS and Matrigel (BD Biosciences) into the prostate.

Immunohistochemistry and tissue microarrays. We counted 500 cells from five different fields and scored the percentage of Ki67-positive cells among DAPI-positive cells. We collected human prostate tissue samples with approval from the Brigham and Women's Hospital Institutional Review Board and with informed subject consent for construction of tissue microarrays. We reassessed the Gleason grade on each individual core to ensure accuracy for these small tissue sections. We used a standard avidin-biotin complex immunohistochemical protocol to evaluate DAB2IP protein expression (1 in 6 DAB2IP antibody dilution overnight at 4 °C). We scanned tissue microarray slides with the Automated Imaging System Ariol SL-50 (Applied Imaging) and imported images into software for Tissue MicroArrays (TMAJ), a Web-based software program for the management of tissue microarray data. We evaluated immunostaining blinded to clinicopathological information and scored the stains as negative (0), weak (1), moderate (2) or strong (3). We used the average value from replicate cores for correlation with clinical outcome. We used univariate Cox regression analysis to assess the ability of DAB2IP expression to predict time to PSA failure, defined as a PSA concentration in the serum greater than 0.2 ng ml^{-1} after radical prostatectomy.

Gene expression analysis. We retrieved gene expression data discussed in this study from the Oncomine cancer microarray database.

Xenogen imaging. We imaged mice with an IVIS-100 CCD camera (Xenogen). For anatomical localization, we generated a pseudocolor image representing light intensity (blue, least intense; red, most intense) in LivingImage and superimposed it over the grayscale reference image.

Statistical analyses. If data were normally distributed, we used the Student's *t* test. Otherwise, we used the Mann-Whitney *U* test. We performed all analyses with the SYSTAT 12 software package. Specific tests are noted in the text and figure legends.

50. Chen, H., Toyooka, S., Gazdar, A.F. & Hsieh, J.T. Epigenetic regulation of a novel tumor suppressor gene (hDAB2IP) in prostate cancer cell lines. *J. Biol. Chem.* **278**, 3121–3130 (2003).

Appendix C

Reprint: **Hematopoietic-specific Stat5-null mice display microcytic hypochromic anemia associated with reduced transferrin receptor gene expression**

This Appendix consists of the following publication, which resulted from research during my year in Nancy Andrews' laboratory, in collaboration with Bing-Mei Zhu and Lothar Hennighausen at the National Institutes of Health. I helped to design and carry out experiments, analyze the results, and write the manuscript.

Hematopoietic-specific Stat5-null mice display microcytic hypochromic anemia associated with reduced transferrin receptor gene expression.

Bing-Mei Zhu*, Sara K. McLaughlin*, Risu Na, Jie Liu, Yongzhi Cui, Cyril Martin, Akiko Kimura, Gertraud W. Robinson, Nancy C. Andrews and Lothar Hennighausen

Blood 112, pp. 2071-2080 (2008).

* Indicates equal authorship.

Hematopoietic-specific Stat5-null mice display microcytic hypochromic anemia associated with reduced transferrin receptor gene expression

*Bing-Mei Zhu,[1] *Sara K. McLaughlin,[2] Risu Na,[1] Jie Liu,[3] Yongzhi Cui,[1] Cyril Martin,[1] Akiko Kimura,[1] Gertraud W. Robinson,[1] Nancy C. Andrews,[2] and Lothar Hennighausen[1]

[1]Laboratory of Genetics and Physiology, National Institute of Diabetes and Digestive and Kidney Diseases (NIDDKD), National Institutes of Health (NIH), Bethesda, MD; [2]Children's Hospital Boston and Harvard Medical School, Boston, MA; and [3]ImmunoTechnology Section, Vaccine Research Center, National Institute of Allergy and Infectious Diseases (NIAID), NIH, Bethesda, MD

Iron is essential for all cells but is toxic in excess, so iron absorption and distribution are tightly regulated. Serum iron is bound to transferrin and enters erythroid cells primarily via receptor-mediated endocytosis of the transferrin receptor (Tfr1). Tfr1 is essential for developing erythrocytes and reduced Tfr1 expression is associated with anemia. The transcription factors STAT5A/B are activated by many cytokines, including erythropoietin. *Stat5a/b*$^{-/-}$ mice are severely anemic and die perinatally, but no link has been made to iron homeostasis. To study the function of STAT5A/B in vivo, we deleted the floxed *Stat5a/b* locus in hematopoietic cells with a Tie2-Cre transgene. These mice exhibited microcytic, hypochromic anemia, as did lethally irradiated mice that received a transplant of *Stat5a/b*$^{-/-}$ fetal liver cells. Flow cytometry and RNA analyses of erythroid cells from mutant mice revealed a 50% reduction in *Tfr1* mRNA and protein. We detected STAT5A/B binding sites in the first intron of the *Tfr1* gene and found that expression of constitutively active STAT5A in an erythroid cell line increased Tfr1 levels. Chromatin immunoprecipitation experiments confirmed the binding of STAT5A/B to these sites. We conclude that STAT5A/B is an important regulator of iron update in erythroid progenitor cells via its control of *Tfr1* transcription. (Blood. 2008;112:2071-2080)

Introduction

Iron is an essential metal, used primarily by erythrocytes for hemoglobin synthesis. Intracellular iron levels must be controlled because iron can participate in redox reactions leading to the generation of damaging free radicals. Since there is no mechanism for regulated iron excretion, iron intake and distribution are tightly regulated. Serum iron circulates bound to transferrin and is taken up by cells via receptor-mediated endocytosis as iron-bound transferrin binds the transferrin receptor (Tfr1).[1] Mice lacking Tfr1 display severe anemia and die before embryonic day 12.5 (E12.5), thus supporting its critical role in erythropoiesis.[2] *Tfr1*$^{+/-}$ mice survive to adulthood but have microcytic, hypochromic erythrocytes, which are most likely due to a reduction of cell surface Tfr1 leading to iron-deficient erythropoiesis.[2]

Hepcidin, a secreted peptide hormone produced primarily by hepatocytes, is a key regulator of iron homeostasis. Hepcidin binds the iron exporter ferroportin, causing its internalization and degradation. Dietary iron enters circulation by traversing intestinal epithelial cells, exiting through ferroportin. Similarly, tissue macrophages that have phagocytosed senescent red blood cells release iron back into circulation through ferroportin. Therefore, hepcidin binding to ferroportin prevents dietary iron uptake and the release of iron from tissue macrophages. Hepcidin production responds to iron stores and erythroid demand and thereby balances iron release into the serum.[3]

STAT5A and STAT5B are transcription factors that are activated by numerous cytokines, including erythropoietin (Epo).[4-6] Upon binding of Epo to its receptor (EpoR), the receptor-associated tyrosine kinase Jak2 activates STAT5A/B, which in turn regulates erythropoiesis.[7-10] However, the molecular understanding of this process remains fragmented. Mice from which the entire *Stat5a/b* locus has been deleted (*Stat5a/b*$^{-/-}$ mice) display severe anemia and die perinatally,[8] precluding definitive analysis of the role of STAT5A/B in erythropoiesis in vivo. In particular, the perinatal lethality has prevented studies of the role of STAT5A/B in iron homeostasis.

To address the function of STAT5A/B in erythropoiesis in vivo, we deleted the *Stat5a/b* locus in hematopoietic stem cells (HSCs) through the use of mice that carried the *Stat5a/b* locus flanked by loxP sites and also a Tie2-Cre (TC) transgene[11,12] (*Stat5a/b*$^{f/f;\ TC}$), which is known to be active in HSCs. *Stat5a/b*$^{f/f;\ TC}$ neonates and adult mice displayed microcytic, hypochromic anemia and liver iron deposition. Here we analyze the molecular basis of the microcytic, hypochromic anemia and link STAT5A/B to transcriptional regulation of *Tfr1*.

Methods

Mice and genotype analysis

Stat5a/b$^{-/-}$ mice were generated using Cre-mediated recombination.[8] *Stat5a/b*$^{fl/fl}$ mice[8] were bred with mice carrying the Tie2-Cre transgene.[11,12] Genotyping was performed by polymerase chain reaction (PCR) as

Submitted December 5, 2007; accepted May 1, 2008. Prepublished online as *Blood* First Edition paper, June 13, 2008; DOI 10.1182/blood-2007-12-127480.

*B.-M.Z. and S.K.M. contributed equally to this work.

An Inside *Blood* analysis of this article appears at the front of this issue.

The online version of this article contains a data supplement.

The publication costs of this article were defrayed in part by page charge payment. Therefore, and solely to indicate this fact, this article is hereby marked "advertisement" in accordance with 18 USC section 1734.

described.[8,12] The *Stat5a/b* floxed allele was amplified with primers 5′-AGCAGCAACCAGAGGACTAC-3′ and 5′-TACCCGCTTCCATTGCTCAG-3′. Primers specific for the recombined *Stat5a/b* allele were 5′-AGCAGCAACCAGAGGACTAC-3′ and 5′-CCCATTATCACCTTCTTTACAG-3′. Tie2-Cre primers were 5′-CGCATAACCAGTGAAACAGCATTGC-3′ and 5′-CCCTGTGCTCAGACAGAAATGAGA-3′. Wild-type recipient mice (6- to 8-week-old B6.SJL-CD45.1 mice) were purchased from The Jackson Laboratory (Bar Harbor, ME). Animals were handled and housed in accordance with the guidelines of the National Institutes of Health (NIH, Bethesda, MD) Animal Care and Use Committee.

RNA isolation from erythroid cells and quantitative real-time PCR analysis of *Stat5* deletion efficiency and Tfr1 and DMT1 expression

Ter119-positive and -negative cells were isolated from fetal liver or adult bone marrow and spleen using magnetic positive selection with anti-Ter119 microBeads (Miltenyi Biotec, Auburn, CA) according to the manufacturer's instructions. RNA was extracted and purified using an RNeasy Plus mini kit (Qiagen, Valencia, CA). Total RNA (0.5 μg) was reverse transcribed into cDNA using the Superscript III First-strand synthesis Supermix (Invitrogen, Frederick, MD). Taqman real-time quantification of mRNA transcript levels was performed using mouse-specific FAM STAT5a primer Mm00839861_m1, Tfr1 primer Mm00441941_ml, DMT1 primer Mm00435363_ml (Applied Biosystems, Foster City, CA), and VIC β-actin primers for normalization. The assay was run on a 7900 HT fast real-time PCR system (Applied Biosystems) and analyzed with SDS2.3 Software (Applied Biosystems).

Complete blood count

Neonates and adult mice were bled from the mandibular vein into 1.5-mL microcentrifuge tubes through heparinized capillary hematocrit tubes (Drummond Scientific, Broomall, PA). Complete blood count (CBC) was measured by HEMAVET multispecies hematology system-HV950FS (Drew Scientific, Dallas, TX) per the manufacturer's instructions.

Giemsa staining

Blood smears were made using peripheral blood from the mouse mandibular vein. Slides were fixed in 100% methanol for 30 minutes, rinsed in water, and stained with freshly made 10% Giemsa for 30 minutes. The right femur was isolated from E18.5 embryos, fixed in neutral buffered formalin (Fisher Scientific, Pittsburgh, PA) at 4°C overnight, dehydrated, and embedded in paraffin. Tissue blocks were sectioned at 5 μm. Bone sections were deparaffinized and stained with freshly made 10% Giemsa for 30 minutes.

Images were captured on an Olympus (Tokyo, Japan) BX51 light microscope equipped with Plan 10×/0.25, Plan-NEOFLUAR 20×/0.50, and UPlan Fl 60×/1.25 Oil Iris lenses and a Nikon (Tokyo, Japan) digital still DXM 1200 camera using ACT-1 (version 2.6.3.0) software. Captured images were processed by Adobe Photoshop (version 9) and Illustrator (version 10) software (Adobe Systems, San Jose, CA).

Tissue iron analyses

Liver and spleen samples were digested in acid and tissue non–heme iron was determined as described previously.[13]

Serum iron analyses

Serum was separated from whole blood that had been collected by retro-orbital bleed in microtainer serum separator tubes (Becton Dickinson, Franklin Lakes, NJ) and stored at − 20°C. Serum iron and unsaturated iron binding capacity (UIBC) were determined using the Serum Iron/UIBC kit (ThermoDMA, Louisville, CO) according to the manufacturer's instructions.

Perls Prussian blue iron staining

Liver tissues were fixed in neutral buffered formalin (Fisher Scientific) at 4°C overnight, dehydrated, and embedded in paraffin. Tissue blocks were sectioned at 5 μm. Liver sections were deparaffinized and hydrated in distilled water, and incubated in stock potassium ferrocyanide solution for 5 minutes and in working potassium ferrocyanide–hydrochloric acid solution for 20 minutes. Sections were rinsed in distilled water and counterstained in nuclear fast red solution for 5 minutes. Sections were washed in running water and dehydrated in 95% and 100% alcohol, cleared in xylene, and then mounted with Permount (Fisher Scientific).

RNA isolation and quantitative real-time PCR analysis of hepcidin levels

Total RNA was isolated from liver tissue that had been snap-frozen at − 80°C and stored in RNALater (Qiagen). Livers were homogenized in RNA STAT-60 (Leedo Medical Laboratories, Houston, TX). RNA was extracted according to the manufacturer's instructions. Total RNA was treated with DNase I (Roche, Indianapolis, IN) to remove trace DNA, and cDNA was synthesized using the iScript cDNA Synthesis Kit (Bio-Rad, Hercules, CA), according to the manufacturer's instructions. Real-time quantification of mRNA transcript levels was performed using the iQ SYBR Green Supermix (Bio-Rad), according to the manufacturer's instructions. Hepcidin *(Hamp1)* mRNA was amplified using primers mHamp1-F 5′-CTGAGCAGCACCACCTATCTC-3′ and mHamp1-R 5′-TGGCTCTAGGCTATGTTTTGC-3′. β-Actin *(Actb)* mRNA was amplified as an internal control using primers mbact F 5′-ACCCACACTGTGCCCATCTA-3′ and mbact R 5′-CACGCTCGGTCAGGATCTTC-3′.[14] Standard curves for hepcidin and β-actin were generated from dilutions of cDNA made from liver in parallel to other experimental samples. Samples were run in triplicate and results were reported as the ratio of the mean values for hepcidin to β-actin.

Flow cytometry

Fetal livers were mechanically dissociated in phosphate-buffered saline with 0.5% bovine serum albumin (PBS/0.5% BSA) through a 40-μm strainer and resuspended in PBS/0.5% BSA. Cells were incubated with a phycoerythrin (PE)–conjugated α-Ter119 antibody, FITC-conjugated α-CD71 (Tfr1) antibody, and 7-AAD (7-amino-actinomycin D) for 15 minutes at room temperature. Blood from fetuses, neonates, or adults was collected and stained with a PE-conjugated α-CD71 antibody for 15 minutes at room temperature. After washing with PBS/0.5% BSA, cells were stained with Reti-COUNT (thiazole orange) reagent (BD Biosciences, San Diego, CA) for 30 minutes at room temperature followed directly by fluorescence-activated cell sorting (FACS) analysis. Constitutively active STAT5A-transfected MEL cells were stained with PE-conjugated α-phospho-STAT5A (Y694) or PE-conjugated α-CD71 antibodies for 15 minutes at room temperature. Cells were washed with PBS/0.5% BSA and FACS analysis was performed. All antibodies were purchased from BD Pharmingen (San Diego, CA) and antibody titers were determined before experiments. FACS analyses were carried out using FACSCalibur (BD Biosciences). Data analyses were performed using FlowJo (TreeStar, Eugene, OR).

Microarray analysis

Isolated Ter119-positive fetal liver cells from 3 to 5 E14.5 embryos of the same genotype were combined, and total RNA was extracted using TRIzol reagent (Life Technologies, Bethesda, MD) with 2 additional ethanol precipitations. RNA quality was verified using an Agilent Bioanalyzer (Agilent Technologies, Palo Alto, CA). Microarray analyses were performed using Affymetrix Mouse Genome 430 2.0 array GeneChips (Affymetrix, Santa Clara, CA). Microarray signals were analyzed using the Affymetrix RMA algorithm. Up- and down-regulated genes were selected based on *P* values less than .05 and fold changes of more than 1.5 or less than 1.5 as assessed by ANOVA using Partek Pro software (Partek, St Louis, MO). Microarray data have been deposited in Gene Expression Omnibus (GEO) under accession number GSE11777.[15]

Table 1. Hematologic indices of neonate and adult mice

	RBC, 10^9/L	Hb, g/L	HCT	MCV, fl	MCH, pg	RDW, %
Adults						
Control	9600 ± 300	141 ± 3	4.95 ± 0.07	51.9 ± 1.2	15.2 ± 0.3	19.1 ± 0.2
Stat5a/b$^{f/f}$	6600 ± 500*	84 ± 5*	2.86 ± 0.19*	47.4 ± 0.9*	13.9 ± 0.3*	23.2 ± 1.4*
Neonates						
Control	4500 ± 400	133 ± 14	4.73 ± 0.35	112.4 ± 2.6	30.1 ± 0.8	20.7 ± 0.3
Stat5a/b$^{f/f}$	2600 ± 200*	67 ± 5*	2.55 ± 0.21*	100.1 ± 3.8*	26.6 ± 1.1*	28.8 ± 1.1*
Stat5a/b$^{-/-}$	1900 ± 600*	36 ± 10*	1.6 ± 0.03*	84.8 ± 1.6*	19.2 ± 0.3*	19.6 ± 0.8

RBC indicates red blood cell count; Hb, hemoglobin; HCT, hematocrit; MCV, mean corpuscular volume; MCH, mean corpuscular hemoglobin; and RDW, red blood cell distribution width.

*$P < .05$ compared with control. n = 10 adults and n = 20 neonates for each group.

Retrovirus production and transfection with constitutively active STAT5A

Recombinant mouse stem cell virus (MSCV) vectors expressing STAT5A (R20, constitutively active mouse STAT5A), in which STAT5A was mutated at the N-terminus and amino acids 1 to 136 were deleted, and green fluorescent protein (GFP) were gifts from Dr Richard Moriggl (Vienna, Austria). The MEL cell line was maintained in Dulbecco modified Eagle medium (DMEM) with 10% FBS, penicillin, and streptomycin. MEL cells that express constitutively active mouse STAT5A were established by transfecting MEL cells with STAT5A/GFP retroviral vectors. MSCV-GFP–transfected MEL cells were set as control. MEL cells were transfected with the cell line Optimization Nucleofector kit (Amaxa, Gaithersburg, MD). Nucleofector Solution L (Amaxa) in combination with program A-20 was used in transfection. Four to 5 hours after transfection, 1.5% DMSO was added to the medium. The cultures were maintained at 37°C with 5% CO_2. After 72 hours, the MSCV-STAT5A-GFP– and MSCV-GFP–transfected MEL cells were collected, and activated STAT5A and Tfr1 expression levels were analyzed by FACS.

Chromatin immunoprecipitation assay

Chromatin immunoprecipitation (ChIP) assays were performed as previously described[16] using the Upstate Biotechnology ChIP kit (Temecula, CA). STAT5A/GFP- or GFP-transfected MEL cells were sorted by BD FACSAria Flow Cytometer (BD Biosciences) and were cross-linked immediately using 1% formaldehyde (Protocol Formalin; Fisher Scientific). Cell lysates were sonicated and immunoprecipitated with an α-Stat5 antibody (R&D Systems, Minneapolis, MN) or rabbit serum as a control (Upstate Biotechnology). Immunoprecipitated DNA was eluted and amplified by real-time PCR using a 7900 HT fast real-time PCR system (Applied Biosystems) and analyzed using SDS2.3 Software (Applied Biosystems). Sequence-specific primers and probes used for amplification of the putative STAT binding sites (GAS sites) within the *Tfr1* gene were as follows: GAS 1: 5′-CATGGTAGGATCTCAGTTCATGGC-3′ and 5′-CAGGTTACTGAAGGCTTACGATGG-3′; GAS 2: 5′-CTCCCAAGTGCTAGGATTAAAGGC-3′ and 5′-GACTGGATGCTGAATAGAGGTGGG-3′; GAS 3: 5′-GCTCTAGCGATTGGGTCTGTTTC-3′ and 5′-GCCTCTTGCCTCCCAAGTACTAG-3′. Sequence primers outside the GAS sites were as follows: 5′-AGTGTCACGGACATTTAGAGGGG-3′ and 5′-CAGCGTTCAGACCTATTCTGCC-3′. As a positive control, primers that detect the binding site for STAT5A/B on the *IGF-1* gene were designed based on the sequences in rat.[17] The sequence primers were 5′-GCATATGTCTCTGAAAGGGGTGA-3′ and 5′-GGCACAAGCTAGCCGATGGTTAG-3′, which detect 2 GAS sites in intron 2. All Ct values were normalized to the values from primers outside the *Tfr1* GAS sites (2 kb away from GAS 3 site) (ΔCt), and then ΔCt values were normalized to rabbit serum (ΔΔCt). The results (2^ ΔΔCt) were expressed as fold enrichment relative to GFP control.

Apoptosis assay

Spleens were taken from 8- to 10-week-old *Stat5a/b$^{f/f;\ TC}$* mice or littermate control mice and were resuspended in PBS/0.5% BSA. Ter119-positive cells were separated using magnetic positive selection with anti-Ter119 microBeads (Miltenyi Biotec) according to the manufacturer's instructions. An aliquot of the Ter119-positive cells were stained with annexin V–PE apoptosis detection kit I (BD Pharmingen) following the manufacturer's instructions and then incubated with an APC-conjugated α-Ter119 antibody (BD Pharmingen) for 15 minutes at room temperature. FACS analysis was performed as described in "Flow cytometry." The splenic Ter119-positive cells were cultured for 24 hours in IMDM with 15% FBS, 1% BSA, 200 μg/mL holo transferrin, 10 μg/mL recombinant human insulin, 2 mM L-glutamine, 10^{-4} M β-mercaptoethanol, and 5 U erythropoietin and then subjected to FACS analysis for apoptosis at the indicated time points.

Transplantation

Embryonic day-14.5 (E14) fetal liver cells were harvested from *Stat5a/b$^{-/-}$* fetuses or control littermates and dispersed with a 21-gauge needle. The cells were resuspended in phosphate-buffered saline containing 2% fetal bovine serum. Cells (1×10^6) were injected via the lateral tail vein into recipient mice that were lethally irradiated with 11Gγ 4 to 5 hours before injection. FACS analysis was used to determine the reconstitution of donor cells. PerCP-Cy5.5–conjugated CD45.2 was used as donor cell marker; and PE-conjugated CD45.1 was used as recipient cell marker. Mice were killed 5 months after transplantation and analyzed.

Results

Deletion of the *Stat5a/b* locus in the germ line and hematopoietic cells

Stat5a/b$^{+/-}$ mice[8] were generated through the deletion of the *Stat5a/b* locus flanked by loxP sites by an MMTV-Cre transgene, which is active in the female germ line.[18] The *Stat5a/b* locus was selectively deleted in hematopoietic cells in mice carrying 2 floxed *Stat5a/b* alleles and a Tie2-Cre transgene[11] (*Stat5a/b$^{f/f;\ TC}$* mice). Quantitative real-time PCR confirmed the deletion of the *Stat5a/b* locus in *Stat5a/b$^{f/f;\ TC}$* mice, and *Stat5a/b* mRNA levels in fetal Ter119-positive and -negative cells were reduced by more than 90% (data not shown).

Stat5a/b$^{+/-}$ males and females were mated, and from the more than 2000 mice weaned only 9 were *Stat5a/b$^{-/-}$*. Prior to parturition, *Stat5a/b$^{-/-}$* fetuses were present in a normal Mendelian ratio, suggesting that *Stat5a/b$^{-/-}$* mice died perinatally. Newborn *Stat5a/b$^{-/-}$* mice were anemic with hematocrits of approximately 1.6 (16%; Table 1) and died of unknown cause within hours after delivery. In contrast, *Stat5a/b$^{f/f;\ TC}$* mice were born at the expected Mendelian ratio. *Stat5a/b$^{f/f;\ TC}$* neonates had hematocrits of approximately 2.5 (25%) compared with 4.7 (47%) in controls, and hematocrits in adult mutant mice remained low at 2.9 (29%; Table 1). Both red cell size (mean corpuscular volume) and hemoglobin content (MCH) were significantly reduced in *Stat5a/b$^{-/-}$* and *Stat5$^{f/f;\ TC}$* neonates as well as in adult *Stat5a/b$^{f/f;\ TC}$* mice (Table 1),

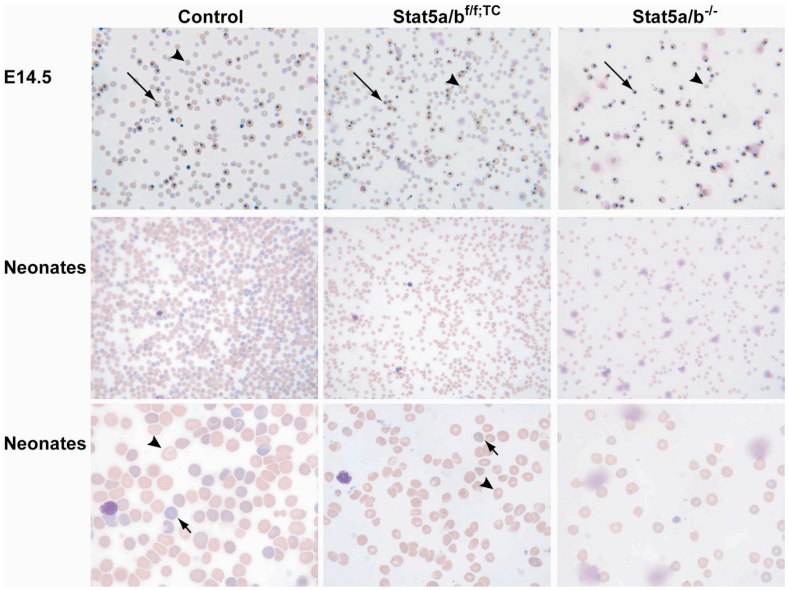

Figure 1. Peripheral blood smears from control, *Stat5a/b*$^{f/f;\,TC}$, and *Stat5a/b*$^{-/-}$ E14.5 embryos and neonates, subjected to Giemsa staining. Peripheral blood smears revealed microcytosis, anisocytosis, and hypochromia in *Stat5a/b* mutant mice, suggestive of iron deficiency. An increase in nucleated erythroblasts (long →) and reticulocytes (short →) further indicates stressed erythropoiesis in mutant mice. ➤ indicates mature red blood cells. Original magnifications: top and middle panels, ×200; bottom panel, ×600.

demonstrating that loss of STAT5A/B results in microcytic, hypochromic anemia. Increased red cell distribution width (RDW) in *Stat5a/b*$^{f/f;\,TC}$ neonates and adult mice was suggestive of iron deficiency. *Stat5a/b*$^{-/-}$ neonates were severely anemic, although their RDWs were not elevated, most likely due to a complete inability to produce normal cells. Consistent with the measured parameters, peripheral blood smears of *Stat5a/b*$^{f/f;\,TC}$ embryos and neonates subjected to Giemsa staining (Figure 1) showed microcytosis, anisocytosis, poikilocytosis, and hypochromia. The number of mature red blood cells was greatly reduced in *Stat5a/b*$^{f/f;\,TC}$ fetuses and neonates compared with wild-type controls, and a higher ratio of nucleated erythroid cells was observed (Figure 1). The morphology of bone marrow from *Stat5a/b*$^{f/f;\,TC}$ mice established the presence of red cell hypoplasia (Figure S1, available on the *Blood* website; see the Supplemental Materials link at the top of the online article). These findings all are consistent with a defect in delivery of iron to developing erythroblasts.

To determine whether phenotypic differences observed in *Stat5a/b*$^{-/-}$ and *Stat5a/b*$^{f/f;\,TC}$ mice compared with controls are autonomous to the hematopoietic lineage or due to changes in other tissues potentially affected by the loss of STAT5A/B, we transplanted *Stat5a/b*$^{-/-}$ fetal liver cells (CD45.2) into lethally irradiated hosts (CD45.1). Five months after transplantation, mice that received a transplant of control fetal liver cells had hematocrits of 3.8 (38%), whereas mice that received a transplant of *Stat5a/b*$^{-/-}$ cells had hematocrits of 2.6 (26%; Table 2). Both MCV and MCH were reduced in mice that received a transplant of *Stat5a/b*$^{-/-}$ cells. These data support our conclusion that loss of STAT5A/B in hematopoietic cells alone is sufficient to cause microcytic, hypochromic anemia. In lysed peripheral blood from mice that received a transplant of control cells, 95% of cells were CD45.2 (donor derived). In contrast, only 63% of these cells from mice that received a transplant of *Stat5a/b*$^{-/-}$ cells were C45.2, suggesting that surviving control recipient cells had a competitive advantage over *Stat5a/b*$^{-/-}$ cells (data not shown).

Analysis of tissue and serum iron

Microcytic, hypochromic anemia is commonly caused by insufficient iron available to developing erythrocytes. To determine whether *Stat5a/b* mutant mice had a defect in iron metabolism, tissue and serum non–heme iron levels were analyzed. We measured non–heme iron content in liver tissue from *Stat5a/b*$^{f/f;\,TC}$ and wild-type adult mice and *Stat5a/b*$^{f/f;\,TC}$ and wild-type neonates and found that the livers of *Stat5a/b*$^{f/f;\,TC}$ mice were iron loaded compared with wild-type controls (Figure 2A). In addition, Prussian blue iron staining of liver sections revealed periportal hepatocyte iron staining in *Stat5a/b*$^{f/f;\,TC}$ livers but not in controls (Figure 2E). There was no significant difference in spleen non–heme iron content by tissue iron assay or Prussian blue staining (data not shown). Serum iron levels (Figure 2B) and transferrin saturation (Figure 2C) were elevated in *Stat5a/b*$^{f/f;\,TC}$ mice compared with controls. These data demonstrate that *Stat5a/b*$^{f/f;\,TC}$ mice have sufficient or excess total body iron, suggesting that the anemia is not caused by overall iron insufficiency. Therefore, the anemia is likely caused by an inability of the erythrocytes to assimilate iron. To confirm cell autonomy, we analyzed iron parameters in lethally irradiated control mice that had received a transplant of control or

Table 2. Hematologic indices of mice that received a transplant of *Stat5a/b*$^{-/-}$ or control fetal liver cells

	RBC, 10^9/L	Hb, g/L	HCT	MCV, fl	MCH, pg	RDW, %
Control	8800 ± 200	120 ± 3	3.83 ± 0.08	43.6 ± 0.2	13.7 ± 0.1	17.1 ± 0.2
Stat5a/b$^{-/-}$	6100 ± 300*	82 ± 5*	2.63 ± 0.13*	41.9 ± 0.6*	12.9 ± 0.3*	17.3 ± 0.5

The mice were analyzed 5 months after transplantation.

RBC indicates red blood cell count; Hb, hemoglobin; HCT, hematocrit; MCV, mean corpuscular volume; MCH, mean corpuscular hemoglobin; and RDW, red blood cell distribution width.

*$P < .05$ compared with control. n = 5 in each group.

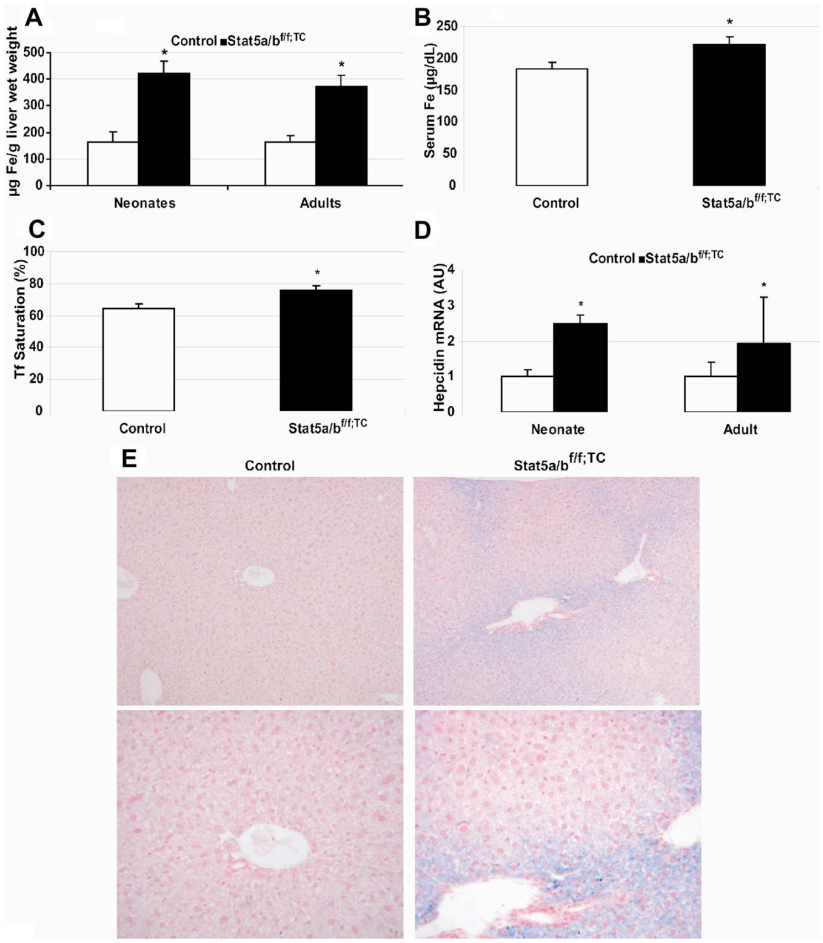

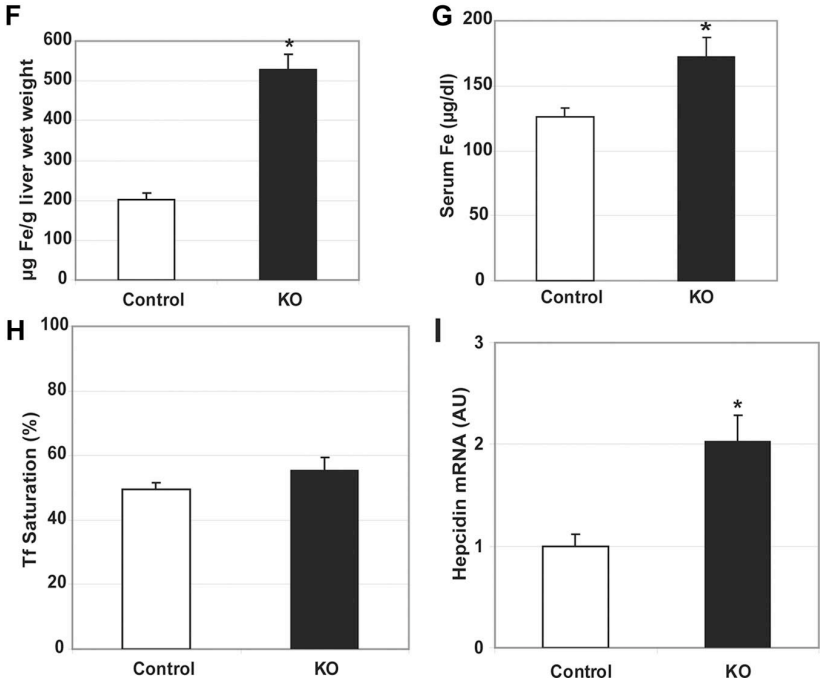

Figure 2. Iron overload in the absence of STAT5A/B. Iron content and hepcidin expression in control and *Stat5a/b*$^{f/f;\,TC}$ mice (A-E) and in mice that received a transplant of control or *Stat5a/b*$^{-/-}$ fetal liver cells (F-I). (A) Non–heme liver iron in adult and neonate female control and *Stat5a/b*$^{f/f;\,TC}$ mice. n = 5 neonates; n = 6 adults. (B,C) Serum iron (B) and transferrin saturation (C) in adult female control and *Stat5a/b*$^{f/f;\,TC}$ mice. n = 12 in each group. (D) Hepcidin mRNA expression in neonate and adult control and *Stat5a/b*$^{f/f;\,TC}$ mice (males and females). Hepcidin expression in control neonate and adult mice is set to 1. n = 9 in each group. (E) Perls Prussian blue iron staining of liver paraffin sections from adult female control and *Stat5a/b*$^{f/f;\,TC}$ mice. Original magnification, ×100 in top panel and ×200 in bottom panel. Non–heme iron is stained blue. (F) Non–heme liver iron. (G) Serum iron. (H) Serum transferrin saturation. (I) Hepcidin mRNA expression. Hepcidin expression in mice that received a transplant of control cells is set to 1. n = 5 in each group for all the measurements. *$P < .05$ compared with control samples. *P* values were determined by 2-tailed unpaired *t* test. Error bars represent SEM.

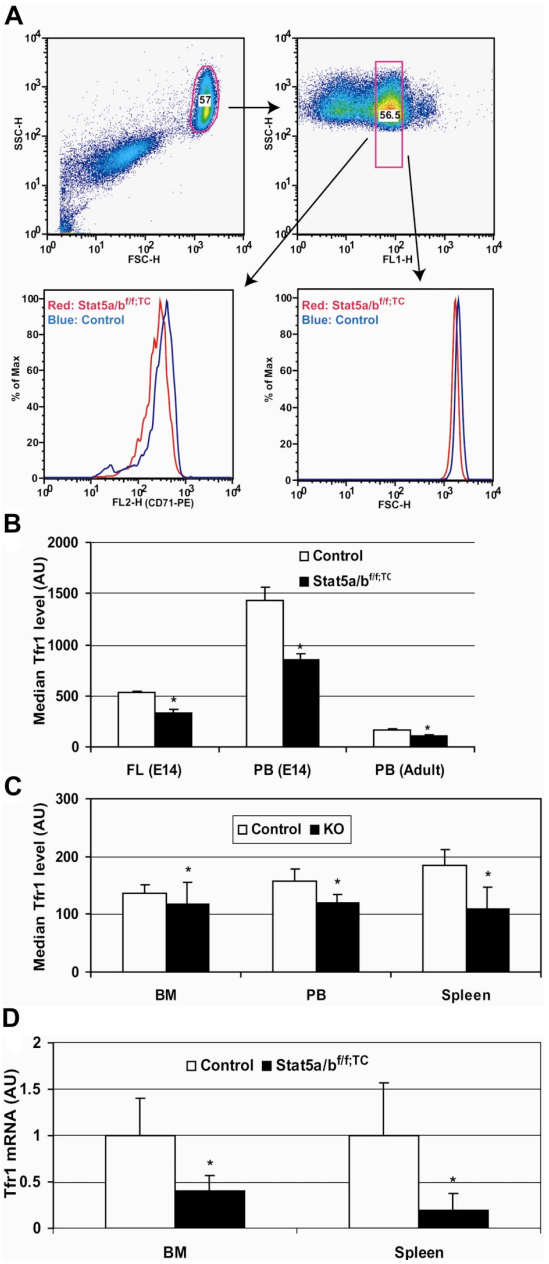

Figure 3. Decreased Tfr expression in the absence of STAT5A/B. Transferrin receptor expression in control and *Stat5a/b* mutant Ter119-positive cells and (A-C) transferrin receptor mRNA expression in *Stat5a/b*$^{f/f;\,TC}$ and control adult mice (D). (A,B) Gated Ter119-positive cells were analyzed for fluorescence of an α-CD71 (Tfr1) antibody in fetal liver and adult bone marrow and spleen cells. Peripheral blood data were generated by double staining with the α-CD71 antibody and thiazole orange dye, which stains RNA and can be used to isolate reticulocytes of a narrow age range as the amount of RNA changes significantly during maturation. (A) Representative data from 8 adult peripheral blood analyses. Top panels show the gate for thiazole orange–positive cells (right) in the whole red blood cell population (left panel). (B) Quantification of Tfr1 protein levels, expressed as the median measurements of α-CD71 fluorescence. E14 data were generated from *Stat5a/b*$^{-/-}$ embryos. n = 10 in each group. Adult data were generated from *Stat5a/b*$^{f/f;\,TC}$ mice. n = 6 for each group. (C) Quantification of Tfr1 protein levels in mice that received a transplant of control or *Stat5a/b*$^{-/-}$ fetal liver cells, expressed as the median measurements of α-CD71 fluorescence. n = 5 for each group. FL indicates fetal liver; PB, peripheral blood; and BM, bone marrow. *$P < .05$ compared with control mice. Error bars represent SEM. (D) Total RNA was extracted from Ter119-positive cells isolated from bone marrow and spleen. *Tfr1* expression levels in control mice are set to 1. n = 3 in control group; n = 4 in *Stat5a/b*$^{f/f;\,TC}$ group. *$P < .05$ compared with control mice. Error bars represent SEM.

Stat5a/b$^{-/-}$ fetal liver cells. Liver iron levels from mice that received a transplant of *Stat5a/b*$^{-/-}$ cells were increased more than 2.5-fold compared with controls (Figure 2F), and serum iron levels and transferrin saturation were also significantly increased (Figure 2G,H).

Hepcidin mRNA levels were analyzed in liver tissue from *Stat5a/b*$^{f/f;\,TC}$ and control adult and neonate mice by quantitative real-time PCR. Hepcidin mRNA levels were approximately 2.5-fold higher in mutant neonates than in wild-type controls, and approximately 1.9-fold higher in mutant adults than in wild-type controls (Figure 2D). Similarly, hepcidin levels in mice that received a transplant of *Stat5a/b*$^{-/-}$ fetal liver cells were elevated 2-fold over controls (Figure 2I).

Transferrin receptor expression in erythroid cells

Iron uptake into erythrocytes occurs by receptor-mediated endocytosis of iron transferrin bound to Tfr1. We assessed cell surface Tfr1 levels on similar populations of reticulocytes from control and *Stat5a/b*$^{f/f;\,TC}$ mice by FACS, using reticulocyte RNA content as a measure of cell maturity. We determined that Tfr1 levels were decreased by approximately 50% in adult mutant mice (Figure 3A,B). Tfr1 levels also were significantly reduced in fetal liver Ter119-positive cells from *Stat5a/b*$^{-/-}$ mice (Figure 3B). As determined from FACS analysis forward scatter, neonate and adult *Stat5a/b*$^{f/f;\,TC}$ Ter119-positive cells were 6% to 7% smaller than controls, and *Stat5a/b*$^{-/-}$ Ter119-positive cells were 23% smaller

Table 3. Microarray analysis of fetal liver Ter119-positive cells from *Stat5a/b*$^{-/-}$ or control E18.5 embryos

Gene symbol	Mean, KO	Mean, WT	Mean ratio, KO/WT	*P*
Socs3	67.50	601.83	0.11	.00
Stat5a	29.80	221.33	0.13	.01
Stat5b	110.03	571.53	0.19	.01
Pim1	4657.77	12268.10	0.38	.01
Cish	540.93	1209.23	0.45	.02
Hbb-bh1	10666.70	22056.97	0.48	.04
Osmr	111.93	176.20	0.64	.25
Bcl2l	11875.93	18033.90	0.66	.14
Osm	257.67	369.60	0.70	.04
Trf	12056.83	22319.70	0.54	.04
Trfr	2666.63	3803.30	0.70	.03
Bcl2l	2093.47	2570.73	0.81	.18
Hbb-y	57118.80	65485.93	0.87	.32
Hba-a1	60582.80	68668.43	0.88	.31
Ccnd1	1399.73	1561.93	0.90	.58
Actb	53338.57	58914.40	0.91	.33
Eraf	58985.63	64714.10	0.91	.36
Hbb-b2	43897.70	45628.30	0.96	.74
Ccnd3	12132.47	12562.27	0.97	.79
Pim2	646.43	659.43	0.98	.86
Pim3	749.00	739.33	1.01	.94
Hba-x	44065.57	42822.47	1.03	.93
Stat3	1292.90	1196.63	1.08	.13
Gapd	21993.63	20195.33	1.09	.39
Gbif-pending	269.13	236.60	1.14	.59
Stat1	766.13	660.93	1.16	.50
Epor	8875.87	7350.00	1.21	.14
Jak2	4147.47	3208.57	1.29	.13
Ireb2	911.00	917.77	0.99	.94

Biologic and technical triplicates were analyzed. Highlighted genes' expression levels differ significantly between mutant and control. Listed genes include those considered erythropoiesis-related genes. The entire data set is available in Table S1.

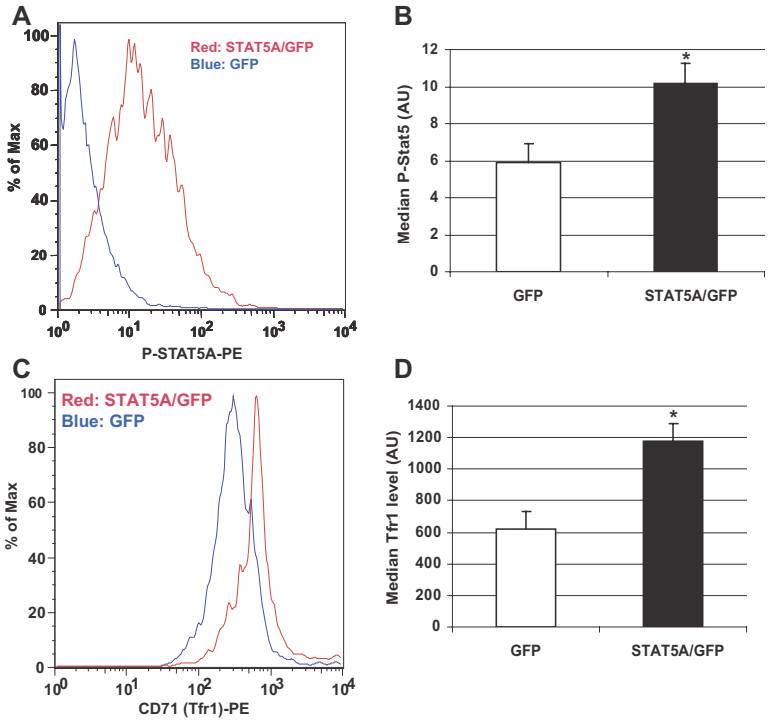

Figure 4. Transferrin receptor expression in murine erythroleukemia (MEL) cells transfected with a plasmid encoding constitutively active STAT5A. MEL cells were transfected with a plasmid encoding constitutively active STAT5A and GFP or GFP alone. (A,C) Histogram from FACS analyses of gated GFP-positive cells. (A) Phospho-STAT5A levels in MEL cells. (C) Transferrin receptor (CD71) expression in MEL cells. Quantification of phospho-STAT5A (B) and Tfr1 levels (D) in GFP- and STAT5A/GFP-transfected cells. Representative data are from 1 of 3 individual experiments. Error bars represent SEM. $*P < .05$ compared with GFP-transfected cells.

(data not shown). Gated Ter119-positive cells from lethally irradiated recipient mice that had received a transplant of *Stat5a/b*$^{-/-}$ cells also expressed significantly less Tfr1 (Figure 3C).

To investigate whether the reduction in cell surface Tfr1 was due to a change in transcriptional regulation, we isolated total RNA from *Stat5a/b*$^{-/-}$ and control fetal liver Ter119-positive cells and subjected it to microarray analyses (Document S1). This approach also allowed us to monitor the expression of other genes involved in iron metabolism and erythropoiesis. *Tfr1* mRNA levels were decreased by approximately 30% in *Stat5a/b*$^{-/-}$ erythroid cells, suggesting that the decrease in Tfr1 protein is due to reduced *Tfr1* mRNA. Real-time reverse-transcription (RT)–PCR showed *Tfr1* mRNA levels reduced by 60% in bone marrow and 80% in splenic cells from adult *Stat5a/b*$^{f/f;\,TC}$ mice (Figure 3D). As erythrocytes have a high demand for iron and obtain it only via transferrin and Tfr1,[2,19] this reduction in Tfr1 levels could cause iron-restricted erythropoiesis in the *Stat5a/b* mutant mice. Microarray analyses also

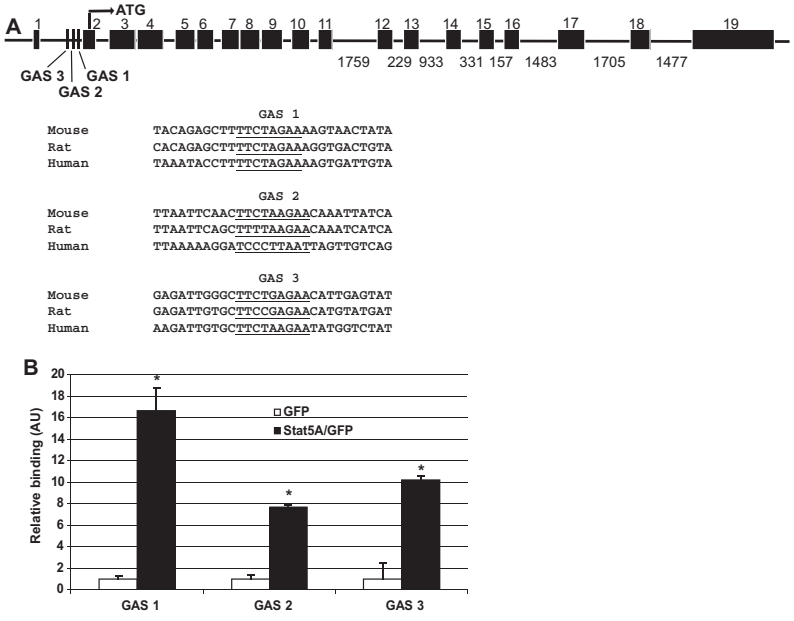

Figure 5. STAT5A/B binding sites in a putative *Tfr1* enhancer. (A) Putative STAT5A/B binding (GAS) sites within intron 1 of the *Tfr1* gene (underlined). Three conserved GAS sites were identified, with GAS 1 having the highest interspecies conservation. Sites are shown aligned with sequences from other species.[21] (B) Chromatin immunoprecipitation (ChIP) analysis of binding of active STAT5A to the putative GAS sites within intron 1 of *Tfr1*. Biologic and technical triplicates were performed. Error bars represent SEM. $*P < .05$ compared with GFP-transfected cells.

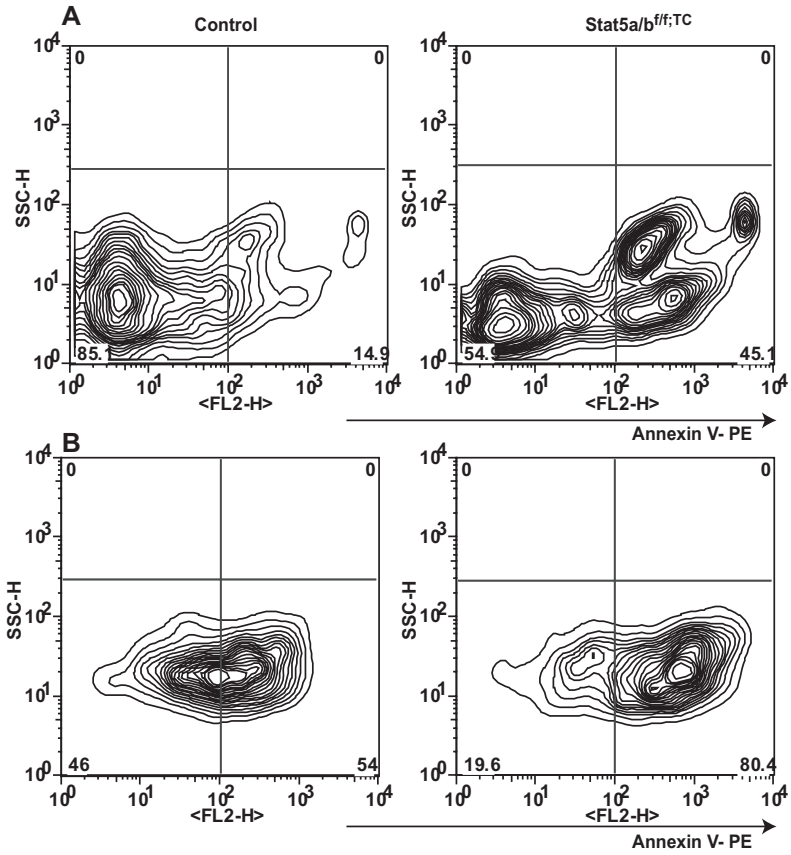

Figure 6. Apoptosis in *Stat5a/b*$^{f/f;\ TC}$ and control adult splenic erythroid cells. (A) Freshly isolated splenic Ter119-positive cells were analyzed by FACS using an apoptosis detection kit and Ter119 staining. (B) After 24 hours in culture with Epo, cells were subjected to the same analysis. The left panels are from control mice; the right panels are from *Stat5a/b*$^{f/f;\ TC}$ mice. Populations shown were gated as Ter119 positive and 7AAD negative. Representative profile from 1 of 3 individual experiments.

confirmed reduced expression of bona fide STAT5A/B target genes, such as *Socs3* and *Pim1* (Table 3;0).

Induction of Tfr1 expression by constitutively active STAT5A

The decreased amount of *Tfr1* mRNA and protein in *Stat5a/b*$^{f/f;\ TC}$ erythrocytes suggested that STAT5A/B regulates expression of the *Tfr1* gene. To investigate whether STAT5A/B activity leads to the induction of *Tfr1* gene transcription and protein expression, we transfected the murine erythroleukemia cell line MEL with a viral vector expressing a constitutively active STAT5A.[20] FACS analysis of cells 72 hours after transfection revealed activated STAT5A (Figure 4A,B) and a 2-fold increase in cell surface Tfr1 compared with GFP-transfected controls (Figure 4C,D). These analyses demonstrate that STAT5A induces Tfr1 levels in MEL cells.

Stat5 binds to GAS sites in the *Tfr1* gene

To investigate whether STAT5A/B directly induces *Tfr1* transcription, we searched for putative STAT5A/B binding sites (GAS sites) surrounding the *Tfr1* gene (http://www.ensembl.org).[21] We identified 3 GAS consensus sequences in the first intron of *Tfr1* (Figure 5A). STAT5A/B previously has been shown to induce transcription via intronic GAS sites in other genes.[17] Therefore, we hypothesized that STAT5A/B directly induces *Tfr1* transcription by binding to one or more of these putative GAS sites.

We used chromatin immunoprecipitation (ChIP) to determine whether STAT5A binds to any of the putative GAS sites. MEL cells were transfected with plasmids encoding constitutively active STAT5A or GFP as a control and STAT5A binding to GAS sites was analyzed. STAT5A binding was detected on all 3 GAS sites, and the most conserved GAS site (site 1) had a 16-fold enrichment compared with the GFP control (Figure 5B). Taken together, these data demonstrate that STAT5A binds to GAS sites in a putative *Tfr1* regulatory region and that STAT5A activity leads to increased *Tfr1* expression.

Increased apoptosis in the absence of STAT5A/B

Earlier studies have shown that erythroid cells expressing hypomorphic STAT5A/B undergo unscheduled apoptosis due to reduced levels of Bcl-x.[9,10] To further establish to what extent apoptosis contributed to the anemia observed in *Stat5a/b*$^{f/f;\ TC}$ mice, we analyzed the survival response of splenic Ter119-positive cells to Epo. Ter119-positive cells from mutant and control mice were cultured in the presence of Epo and cell death was determined using annexin V staining (Figure 6). At day 0, 10% of freshly isolated Ter119-positive cells from control mice and 42% from *Stat5a/b*$^{f/f;\ TC}$ mice were positive for annexin V. Twenty-four hours after initiating the culture, 53% of control cells and 78% of mutant cells were annexin V positive. The elevated cell death in the absence of STAT5A/B strongly supports the notion that STAT5A/B also controls Epo-mediated cell survival. Bcl-x levels in STAT5A/B-null Ter119-positive cells were only slightly reduced and the significance of this remains to be determined.

Discussion

Deletion of the *Stat5a/b* genes in HSCs and in the germ line results in microcytic, hypochromic anemia, and mutant mice display increased serum iron levels and liver iron deposition. In the absence of STAT5A/B, Tfr1 levels on erythroid precursors are reduced by 50%. Furthermore, STAT5A/B binds to GAS sites within the first intron of the *Tfr1* gene and induces *Tfr1* gene expression. Based on these data, we suggest that STAT5A/B controls erythropoiesis in part by regulating *Tfr1* expression, which in turn allows unimpeded iron acquisition by erythroid cells.

Stat5a/b$^{-/-}$ neonates display a hematocrit of 1.6 (16%) compared with 4.7 (47%) in controls. They die within hours after birth, which has precluded detailed studies of the in vivo function of STAT5A/B in adults.[8] To further understand the molecular basis of the erythropoietic defects, we deleted the *Stat5a/b* locus specifically in HSCs and endothelial cells using the Tie2-Cre transgene. Complete blood count analyses revealed that mutant mice were anemic (decreased red blood cell count, hemoglobin, and hematocrit), and had decreased mean corpuscular volume and mean corpuscular hemoglobin, indicating a microcytic, hypochromic anemia. The microcytic anemia was more profound in *Stat5a/b*$^{-/-}$ neonates than in *Stat5a/b*$^{f/f;\,TC}$ mice, suggesting that there might be additional defects from the whole body absence of STAT5A/B. *Stat5a/b*$^{-/-}$ neonates were smaller than control littermates or *Stat5a/b*$^{f/f;\,TC}$ mice. Possible explanations include more severe anemia, placental insufficiency, or a defect in IGF signaling.

Microcytic, hypochromic anemia is most commonly caused by insufficient iron acquisition by developing erythroid precursors. *Stat5a/b* mutant mice had increased serum iron levels and increased hepatocyte iron deposition, suggesting that the microcytic, hypochromic anemia was the result of insufficient erythroid iron utilization. The presence of abundant periportal hepatocyte iron further supported the hypothesis that excess unused iron had been removed from serum. Although some cells can use non–Tfr1-mediated mechanisms of acquiring iron, erythroid cells depend exclusively on Tfr1-mediated iron uptake.[2] *Tfr1*$^{-/-}$ mice display severe anemia and die before embryonic day 12.5. Since anemia occurred in animals with hematopoietic-specific inactivation of *Stat5a/b,* we hypothesized that there was a defect in iron transport into erythroid precursors. RNA expression and FACS analyses revealed a decrease in *Tfr1* mRNA and surface protein levels, respectively, on mutant erythroid cells. In addition, we found that active STAT5A stimulates expression of *Tfr1* and binds to GAS sites in the first intron of the *Tfr1* gene. Functional intronic GAS sites have been identified in other genes, such as the *IGF-1* gene, which is highly activated by STAT5A/B.[17] Given the known function of STAT5A/B as a transcriptional regulator, these data strongly suggest that STAT5A/B up-regulates *Tfr1* transcription. Erythroid cells must increase surface Tfr1 levels even as cellular iron content increases, because large amounts of iron are needed for hemoglobin production.[22,23] Therefore, although we cannot exclude posttranscriptional regulation of *Tfr1* mRNA stability by STAT5A/B, these data support a role for STAT5A/B in controlling *Tfr1* transcription.

To determine whether the phenotypic differences observed in *Stat5a/b* mutant mice compared with controls are autonomous to the hematopoietic lineage or due to changes in other tissues potentially affected by the loss of STAT5A/B, we transplanted *Stat5a/b*$^{-/-}$ fetal liver cells into lethally irradiated hosts. We found that mice that received a transplant of *Stat5a/b*$^{-/-}$ cells displayed a phenotype that mimicked that of *Stat5a/b*$^{f/f;\,TC}$ mice. These mice had microcytic, hypochromic anemia, increased liver iron, serum iron, and transferrin saturation and decreased erythroid Tfr1 levels. We conclude that loss of STAT5A/B in hematopoietic cells is sufficient to induce these phenotypes.

In addition to erythroid iron deficiency, globin chain imbalance can be a primary cause of microcytosis. We analyzed globin mRNA levels in *Stat5a/b*$^{-/-}$ fetal liver Ter119-positive cells and found that expression of all but one globin gene was unimpaired (Table 3). Steady-state levels of *Hbb-hb1* mRNA (encoding hemoglobin Z, beta-like embryonic chain) were reduced by 50%. We do not believe that decreased embryonic beta chain expression explains the microcytosis that we observed. Mutations in the gene encoding the divalent metal transporter 1 (DMT1) in humans also cause iron overload and hypochromic microcytic anemia.[24] Although DMT1 mRNA levels in *Stat5a/b*$^{f/f;\,TC}$ mice were reduced by approximately 60% (data not shown), we were unable to locate GAS sites within putative regulatory sequences, suggesting that the reduced expression was a secondary event. However, the absence of bona fide GAS sides does not rule out that the *Dmt1* gene is under the control of STAT5A/B.

Unlike the well-studied posttranscriptional regulation of *Tfr1* mRNA, transcriptional regulation of *Tfr1* remains less well characterized. It has been shown that various growth and differentiation factors can stimulate erythroid *Tfr1* transcription.[25] In this study, we identified STAT5A/B as critical for efficient expression of the *Tfr1* gene in erythroid precursors. STAT5A/B is considered a cytokine-inducible modulator and does not necessarily control basal levels of transcription. An accepted role of STAT5A/B is in the induction of target genes in hormone-responsive tissues to achieve high levels of specific mRNAs rapidly.[26-28] Similarly, Epo-induced stimulation of STAT5A/B activity would lead to the induction of erythroid *Tfr1* transcription, which would allow sufficient iron to enter erythrocyte precursors for hemoglobin synthesis.

Production of the iron-regulatory hormone hepcidin is modulated in response to changes in iron stores and erythroid demand. Accelerated or ineffective erythropoiesis induces an unknown signal, "the erythroid regulator," which leads to down-regulation of hepcidin expression in the liver, and consequently an increase in iron entering the system. Conversely, under conditions of iron overload, hepcidin expression is up-regulated by the "stores regulator" to prevent additional iron intake.[29] Under some circumstances, mice that are anemic but iron overloaded may have coexisting signals to both down-regulate and up-regulate hepcidin production. In most characterized cases of anemia coupled with iron overload, such as transferrin-deficient mice[19] and β-thalassemic mice,[30] the erythroid signal is dominant and hepcidin production is markedly reduced. Therefore, we had expected hepcidin expression to be reduced in *Stat5a/b*$^{f/f;\,TC}$ mice. However, hepcidin expression was slightly increased in these mice, suggesting that the stores regulator is the dominant signal. As the genetic defect in *Stat5a/b*$^{f/f;\,TC}$ mice is restricted to hematopoietic cells, we hypothesize that the stores regulator dominates due to a deficiency in production or signaling of the erythroid regulator.

Similar to *Stat5a/b*$^{f/f;\,TC}$ mice, *Tfr1*$^{+/-}$ mice exhibit decreased cell surface Tfr1 and have microcytic, hypochromic erythrocytes.[2] However, unlike *Stat5a/b*$^{f/f;\,TC}$ mice, which have fewer red blood cells than wild-type controls, *Tfr1*$^{+/-}$ mice have a compensatory induction of erythropoiesis and an increased red blood cell count.

Whereas *Stat5a/b*$^{f/f;\,TC}$ mice have decreased hemoglobin and hematocrit, *Tfr1*$^{+/-}$ mice display normal hemoglobin levels and hematocrits due to the increase in red blood cell number. It is an open question why *Tfr1*$^{+/-}$, but not *Stat5a/b*$^{f/f;\,TC}$, mice exhibit a compensatory increase in red blood cell production. In addition to decreased erythroid iron, *Tfr1*$^{+/-}$ mice have decreased hepatocyte iron due to the global reduction in *Tfr1* expression. This contrasts with *Stat5a/b*$^{f/f;\,TC}$ mice, which have a hematopoietic-specific reduction in *Tfr1* expression and have increased hepatocyte iron deposition.

In summary, this study provides evidence that STAT5A/B is an important transcriptional regulator of *Tfr1* in erythroid cells. Transcriptional regulation of *Tfr1* has not been fully characterized in these or other cells. It will be interesting to investigate the importance of STAT5A/B-driven *Tfr1* transcription in nonerythroid cell types and to compare how STAT5A/B activity is stimulated in each context.

Acknowledgments

The authors thank Susanne Pechhold for cell sorting and Ann Dean for providing MEL cells. We also thank Toshio Kitamura for providing the constitutively active Stat5A construct and Weiping Chen and Maggie Cam for microarray analysis.

This study was supported by the intramural research programs of NIDDK and NIAID, NIH, by NIH R01 HL51057 (N.C.A.) and NIH T32 HL07623 (S.K.M.).

Authorship

Contribution: B.-M.Z., S.K.M., R.N., J.L., G.W.R., N.C.A., and L.H. designed experiments; B.-M.Z., S.K.M., R.N., J.L., Y.C., C.M., A.K., and G.W.R. executed experiments; B.-M.Z., S.K.M., J.L., Y.C., and C.M. analyzed data; B.-M.Z., S.K.M., R.N., J.L., A.K., G.W.R., N.C.A., and L.H. interpreted data; and B.-M.Z., S.K.M., G.W.R., N.C.A., and L.H. wrote the paper.

Conflict-of-interest disclosure: The authors declare no competing financial interests.

Correspondence: Lothar Hennighausen or Bing-Mei Zhu, NIH/NIDDK, Bulding 8, Room 101, 8 Center Drive, Bethesda, MD 20892; e-mail: (L.H.) lotharh@mail.nih.gov or (B.-M.Z.) bingmei@mail.nih.gov.

References

1. Hentze MW, Muckenthaler MU, Andrews NC. Balancing acts: molecular control of mammalian iron metabolism. Cell. 2004;117:285-297.
2. Levy JE, Jin O, Fujiwara Y, Kuo F, Andrews NC. Transferrin receptor is necessary for development of erythrocytes and the nervous system. Nat Genet. 1999;21:396-399.
3. Andrews NC, Schmidt PJ. Iron homeostasis. Annu Rev Physiol. 2007;69:69-85.
4. Neubauer H, Cumano A, Muller M, Wu H, Huffstadt U, Pfeffer K. Jak2 deficiency defines an essential developmental checkpoint in definitive hematopoiesis. Cell. 1998;93:397-409.
5. Parganas E, Wang D, Stravopodis D, et al. Jak2 is essential for signaling through a variety of cytokine receptors. Cell. 1998;93:385-395.
6. Wu H, Liu X, Jaenisch R, Lodish HF. Generation of committed erythroid BFU-E and CFU-E progenitors does not require erythropoietin or the erythropoietin receptor. Cell. 1995;83:59-67.
7. Teglund S, McKay C, Schuetz E, et al. Stat5a and Stat5b proteins have essential and nonessential, or redundant, roles in cytokine responses. Cell. 1998;93:841-850.
8. Cui Y, Riedlinger G, Miyoshi K, et al. Inactivation of Stat5 in mouse mammary epithelium during pregnancy reveals distinct functions in cell proliferation, survival, and differentiation. Mol Cell Biol. 2004;24:8037-8047.
9. Socolovsky M, Fallon AE, Wang S, Brugnara C, Lodish HF. Fetal anemia and apoptosis of red cell progenitors in Stat5a-/-5b-/- mice: a direct role for Stat5 in Bcl-X(L) induction. Cell. 1999;98:181-191.
10. Socolovsky M, Nam H, Fleming MD, Haase VH, Brugnara C, Lodish HF. Ineffective erythropoiesis in Stat5a(-/-)5b(-/-) mice due to decreased survival of early erythroblasts. Blood. 2001;98:3261-3273.
11. Kisanuki YY, Hammer RE, Miyazaki J, Williams SC, Richardson JA, Yanagisawa M. Tie2-Cre transgenic mice: a new model for endothelial cell-lineage analysis in vivo. Dev Biol. 2001;230:230-242.
12. Sasaki A, Yasukawa H, Shouda T, Kitamura T, Dikic I, Yoshimura A. CIS3/SOCS-3 suppresses erythropoietin (EPO) signaling by binding the EPO receptor and JAK2. J Biol Chem. 2000;275:29338-29347.
13. Torrance JD, Bothwell TH. Methods in Hematology: Iron. New York, NY: Churchill Livingstone Press; 1980.
14. Nemeth E, Rivera S, Gabayan V, et al. IL-6 mediates hypoferremia of inflammation by inducing the synthesis of the iron regulatory hormone hepcidin. J Clin Invest. 2004;113:1271-1276.
15. National Center for Biotechnology Information. Gene Expression Omnibus. http://www.ncbi.nlm.nih.gov/geo/.
16. Morinobu A, Kanno Y, O'Shea JJ. Discrete roles for histone acetylation in human T helper 1 cell-specific gene expression. J Biol Chem. 2004;279:40640-40646.
17. Chia DJ, Ono M, Woelfle J, Schlesinger-Massart M, Jiang H, Rotwein P. Characterization of distinct Stat5b binding sites that mediate growth hormone-stimulated IGF-I gene transcription. J Biol Chem. 2006;281:3190-3197.
18. Wagner KU, Wall RJ, St-Onge L, et al. Cre-mediated gene deletion in the mammary gland. Nucleic Acids Res. 1997;25:4323-4330.
19. Trenor CC III, Campagna DR, Sellers VM, Andrews NC, Fleming MD. The molecular defect in hypotransferrinemic mice. Blood. 2000;96:1113-1118.
20. Onishi M, Nosaka T, Misawa K, et al. Identification and characterization of a constitutively active STAT5 mutant that promotes cell proliferation. Mol Cell Biol. 1998;18:3871-3879.
21. Wellcome Trust Sanger. Ensembl. http://www.ensembl.org.
22. Chan LN, Gerhardt EM. Transferrin receptor gene is hyperexpressed and transcriptionally regulated in differentiating erythroid cells. J Biol Chem. 1992;267:8254-8259.
23. Chan RY, Seiser C, Schulman HM, Kuhn LC, Ponka P. Regulation of transferrin receptor mRNA expression. Distinct regulatory features in erythroid cells. Eur J Biochem. 1994;220:683-692.
24. Pospisilova D, Mims MP, Nemeth E, Ganz T, Prchal JT. DMT1 mutation: response of anemia to darbepoetin administration and implications for iron homeostasis. Blood. 2006;108:404-405.
25. Lok CN, Loh TT. Regulation of transferrin function and expression: review and update. Biol Signals Recept. 1998;7:157-178.
26. Burdon T, Sankaran L, Wall RJ, Spencer M, Hennighausen L. Expression of a whey acidic protein transgene during mammary development: evidence for different mechanisms of regulation during pregnancy and lactation. J Biol Chem. 1991;266:6909-6914.
27. Pittius CW, Sankaran L, Topper YJ, Hennighausen L. Comparison of the regulation of the whey acidic protein gene with that of a hybrid gene containing the whey acidic protein gene promoter in transgenic mice. Mol Endocrinol. 1988;2:1027-1032.
28. Woelfle J, Chia DJ, Rotwein P. Mechanisms of growth hormone (GH) action: identification of conserved Stat5 binding sites that mediate GH-induced insulin-like growth factor-I gene activation. J Biol Chem. 2003;278:51261-51266.
29. Finch C. Regulators of iron balance in humans. Blood. 1994;84:1697-1702.
30. Adamsky K, Weizer O, Amariglio N, et al. Decreased hepcidin mRNA expression in thalassemic mice. Br J Haematol. 2004;124:123-124.